University of Alberta

Performance Evaluation and Pulse Design for Ultra-Wideband Communications

by

Bo Hu

A thesis submitted to the Faculty of Graduate Studies and Research in partial fulfillment of the requirements for the degree of **Doctor of Philosophy**.

Department of Electrical and Computer Engineering

Edmonton, Alberta

Spring 2006

Library and Archives Canada

Published Heritage Branch

395 Wellington Street
Ottawa ON K1A 0N4
Canada

Bibliothèque et Archives Canada

Direction du Patrimoine de l'édition

395, rue Wellington
Ottawa ON K1A 0N4
Canada

Your file Votre référence
ISBN: 0-494-13991-9
Our file Notre référence
ISBN: 0-494-13991-9

NOTICE:
The author has granted a non-exclusive license allowing Library and Archives Canada to reproduce, publish, archive, preserve, conserve, communicate to the public by telecommunication or on the Internet, loan, distribute and sell theses worldwide, for commercial or non-commercial purposes, in microform, paper, electronic and/or any other formats.

The author retains copyright ownership and moral rights in this thesis. Neither the thesis nor substantial extracts from it may be printed or otherwise reproduced without the author's permission.

AVIS:
L'auteur a accordé une licence non exclusive permettant à la Bibliothèque et Archives Canada de reproduire, publier, archiver, sauvegarder, conserver, transmettre au public par télécommunication ou par l'Internet, prêter, distribuer et vendre des thèses partout dans le monde, à des fins commerciales ou autres, sur support microforme, papier, électronique et/ou autres formats.

L'auteur conserve la propriété du droit d'auteur et des droits moraux qui protège cette thèse. Ni la thèse ni des extraits substantiels de celle-ci ne doivent être imprimés ou autrement reproduits sans son autorisation.

In compliance with the Canadian Privacy Act some supporting forms may have been removed from this thesis.

While these forms may be included in the document page count, their removal does not represent any loss of content from the thesis.

Conformément à la loi canadienne sur la protection de la vie privée, quelques formulaires secondaires ont été enlevés de cette thèse.

Bien que ces formulaires aient inclus dans la pagination, il n'y aura aucun contenu manquant.

Canada

To my family, who offered me endless love and support.

Abstract

Ultra-wideband (UWB) technology is being investigated in academy and industry as a good candidate for new generation communications. In general, the performance of UWB communications is limited by channel fading and interference from other systems or user signals. This thesis contributes to the accurate bit error rate (BER) performance analysis of UWB communication systems in different transmission scenarios. It also contributes to the system design of UWB communications, specifically on pulse shaping for UWB systems.

A time-hopping pulse position modulation (TH-PPM) system operating in multiple access interference is first considered. A tractable analytical expression for predicting the average BER is derived using a characteristic function method. The precise BER can be obtained for a system with an arbitrary number of users using arbitrary pulse shapes with modest computational complexity. Our results are used to assess the accuracy of the Gaussian approximation, which is widely used for BER estimation.

Similar analysis is then extended to different UWB modulation schemes. Tractable expressions are derived and used to compare the performances of these systems. Unlike some previous results obtained by using the Gaussian approximation, it is shown both analytically and numerically that different schemes have different capabilities for interference suppression.

Error analysis for UWB systems operating with narrowband orthogonal frequency division multiplexing (OFDM) signals is also studied. It is found that OFDM interference significantly worsens the performance of the desired UWB signal. Some methods are expected to suppress narrowband OFDM interference. In addition, the BER performances of different UWB systems in multipath fading scenarios are examined. A realistic fading channel model is considered and the properties of several receiver structures are thoroughly examined.

Pulse shapes for UWB communications are extensively investigated. Pulse shapes proposed for UWB communications are evaluated in light of frequency emission restrictions and the BER performances of systems using different pulses are accurately assessed. In addition, a novel pulse design paradigm is proposed to synthesize time-limited pulse shapes that meet a given frequency constraint. It is shown that the novel pulse design paradigm provides more flexibility in designing pulses for UWB communications.

Acknowledgements

My greatest debt is to my thesis supervisor Dr. Norman C. Beaulieu for his guidance, suggestion, encouragement and support. I am so grateful to him for leading me into this exciting research area. I will continue to be influenced by his rigorous scholarship, clarity in thinking, and professional integrity.

I would like to thank Dr. Sergio Benedetto from Politecnico di Torino for his willingness to serve as my external examiner. I am honoured to have him on my thesis examining committee. I would also like to thank Drs. Chintha Tellambura, Masoud Ardakani, Douglas P. Wiens and Jie Chen for serving on the committee. I would like to thank Ms. Sharon Walker and Ms. Sandra Abello for their kindness and help during my study.

I would also like to thank my labmates, particularly Dr. Julian Cheng and Dr. Zheng Du for their invaluable advice and numerous technical discussions throughout my thesis work.

This work is in part sponsored by an Alberta Ingenuity Studentship and a Graduate Scholarship from the Alberta Informatics Circle of Research Excellence (*i*CORE). This financial support is greatly appreciated.

Last, I would like to thank my husband, Bin Cheng, and my parents for their endless love, patience, understanding and support over all these years. This thesis is dedicated to them.

Contents

1 Introduction **1**

1.1 Introduction 1

1.2 UWB Communication Systems 2

1.3 UWB Modulation and Multiple Access Methods 5

1.3.1 Data Modulation Schemes 5

1.3.2 Multiple Access Methods 9

1.4 UWB Channel Model 12

1.5 Interference 15

1.5.1 Multiple Access Interference 17

1.5.2 Narrowband Interference 18

1.5.3 Intersymbol Interference 19

1.6 UWB Regulations 20

1.6.1 UWB regulations in USA 20

1.6.2 UWB regulations in Europe 20

1.7 Thesis outline and Contributions 23

2 Accurate Evaluation of Multiple Access Performance in TH-PPM and TH-BPSK UWB Systems **27**

2.1 Introduction 27

2.2 System Models 30

2.3 Approximation Methods 35

2.3.1 Analysis based on Gaussian Approximation 35
2.3.2 Analysis based on Gaussian Quadrature Rules 36
2.4 Analysis of TH-PPM system 37
2.4.1 Type-*A* TH-PPM 38
2.4.2 Type-*B* TH-PPM 42
2.5 Analysis of TH-BPSK system 43
2.6 Bit Error Probability 45
2.7 Numerical Results and Comparisons 47
2.8 Summary 61

3 Accurate Performance Evaluation of TH, DS and DS-IR UWB Systems in Multiple Access Interference 62
3.1 Introduction 62
3.2 System Models 64
3.3 Analysis of TH-PPM system 66
3.4 Analysis of TH-BPSK system 69
3.5 Analysis of DS-IR system 71
3.6 Analysis of DS-UWB system 74
3.6.1 Exact Decision Statistic 75
3.6.2 Simplified Decision Statistic 78
3.7 The Gaussian Approximation for TH and DS UWB systems 79
3.7.1 TH-UWB 80
3.7.2 DS-UWB 80
3.8 Numerical Results and Comparisons 82
3.9 Summary 94

4 Pulse Shapes and Design Paradigm for Ultra-Wideband Communication Systems 97
4.1 Introduction 97
4.2 Pulse shapes and power spectral densities 99

4.2.1 Gaussian Monocycles 100
4.2.2 Novel Pulses based on Prolate Spheroidal Functions (PS pulse) 106
4.2.3 Modified Hermite Polynomial Based Pulses (HP pulse) 107
4.3 Comparisons of Pulse Performances 108
4.4 Pulse Design Paradigm 114
4.4.1 Even Pulses 116
4.4.2 Odd Pulses 120
4.5 Pulse Examples and Discussion 121
4.6 Summary 132

5 Effects of Narrowband OFDM Interference on A UWB Communication System 134
5.1 Introduction 134
5.2 System Models 136
5.3 Interference Analysis 137
5.3.1 TH-PPM System 137
5.3.2 TH-BPSK system 141
5.3.3 DS-BPSK System 143
5.4 Bit Error Probability 145
5.5 Numerical Results and Comparisons 146
5.6 Summary 158

6 Modulation Schemes and Rake Receiver Structures for UWB Systems on an Realistic UWB Indoor Channel 159
6.1 Introduction 159
6.2 System Models 161
6.2.1 Fading Channel Model 161
6.2.2 Rake Receiver Structure 162
6.3 Bit Error Probability 164
6.4 Simulation Results and Comparisons 166

6.5 Summary 174

7 Conclusions and Suggestions for Future Work **176**

7.1 Conclusions 176

7.2 Suggestions for Future Research 179

References **182**

Vita **191**

List of Tables

1.1 Typical Parameters for the IEEE multipath fading model 15

1.2 FCC radiation limits for indoor and outdoor communications 20

1.3 ETSI limits for UWB indoor and outdoor communications 21

2.1 Parameters of the Example TH-PPM and TH-BPSK systems 48

3.1 Parameters of the Example TH, DS and DS-IR UWB systems 83

5.1 Parameters of the Example TH/DS UWB and OFDM systems 147

6.1 Parameters of the Example TH, DS and DS-IR UWB systems 167

List of Figures

1.1 The relationship between the power spectrums of narrowband and UWB systems (from [7]). 3

1.2 BPAM for "0" and "1" bits. 6

1.3 OOK for "0" and "1" bits. 7

1.4 PPM for "0" and "1" bits. 8

1.5 The relationship between the frame duration T_f and the pulse T_p (from [7]) 10

1.6 The pulse train structure with TH sequence (from [7]). 10

1.7 The repetition structure of an information bit. 11

1.8 The multipath fading model for UWB where multipath components arrive in clusters 14

1.9 Delay profiles of CM1 fading model with 100 channel realizations . . 16

1.10 FCC UWB emission Masks (from [7]) 21

1.11 UWB frequency emission limitations defined by ETSI (from [40]) . . 22

2.1 Autocorrelation functions of the 2^{nd}-order and 4^{th}-order Gaussian monocycles as a function of time. 33

2.2 The structure of UWB correlation receiver [7]. 34

2.3 Average BER of the TH-PPM UWB system versus SNR for a repetition code with $N_s = 2$, $N_s = 4$ and $N_s = 16$ assuming 7 asynchronous interferers. 50

2.4 Average BER of the TH-BPSK UWB system versus SNR for a repetition code with $N_s = 2$, $N_s = 4$ and $N_s = 16$ assuming 7 asynchronous interferers. 51
2.5 Average BER of the TH-PPM UWB system versus SNR for a repetition code with $N_s = 16$, $N_s = 50$ and $N_s = 100$. 52
2.6 Average BER of the TH-BPSK UWB system versus SNR for a repetition code with $N_s = 16$, $N_s = 50$ and $N_s = 100$. 53
2.7 Comparison of the type-A and type-B TH-PPM systems for a repetition code with $N_s = 2$ and $N_s = 4$ assuming 7 asynchronous interferers. 55
2.8 Comparison of the TH-PPM systems using different Gaussian monocycles for a repetition code with $N_s = 2$ and $N_s = 4$ assuming 7 asynchronous interferers. 57
2.9 Comparison of the TH-BPSK systems using different Gaussian monocycles for a repetition code with $N_s = 2$ and $N_s = 4$ assuming 7 asynchronous interferers. 58
2.10 Comparison of the TH-BPSK and TH-PPM systems for a repetition code with $N_s = 2$ and $N_s = 4$ assuming 7 asynchronous interferers. . . 59
2.11 Comparison of the TH-BPSK and TH-PPM systems for a repetition code with $N_s = 2$ and $N_s = 4$ assuming 50 asynchronous interferers. . 60

3.1 The average BER of the TH-PPM UWB system versus SNR for a repetition code with $N_s = 2$ and $N_s = 4$ assuming 7 asynchronous interferers. 84
3.2 The average BER of the TH-BPSK UWB system versus SNR for a repetition code with $N_s = 2$ and $N_s = 4$ assuming 7 asynchronous interferers. 85
3.3 The average BER versus SNR of the DS-IR BPSK system for a repetition code with $N_s = 2$ and $N_s = 4$ assuming 7 asynchronous interferers. 86

3.4 Comparison of the BER obtained from the exact analysis with the BER obtained from the simplified analysis for $N_c = 16$ and $N_c = 32$. . 87
3.5 The average BER of the DS-BPSK system for $N_c = 32$ and $N_c = 64$ assuming 7 asynchronous interferers. 88
3.6 Comparison of the TH-PPM, TH-BPSK and DS-BPSK systems with the same data rate assuming 7 asynchronous interferers. 90
3.7 Comparison of the TH-PPM, TH-BPSK and DS-BPSK systems with the same data rate assuming 15 asynchronous interferers. 91
3.8 Comparison of the TH-PPM, TH-BPSK and DS-BPSK systems with the same data rate for different numbers of users with SNR = 20 dB. 92
3.9 Comparison of the DS-IR BPSK and TH-BPSK assuming 7 asynchronous interferers. 93
3.10 Comparison of the DS-IR BPSK and DS-BPSK systems with the same date rate assuming 7 asynchronous interferers. 94

4.1 Magnitude of $C(f)$ for (a)$N_h = 8$, $T_c = 0.9ns$ and (b)$N_h = 50$, $T_c = 0.1ns$ 101
4.2 Power spectral density of (a) the 4^{th} order and (b) the 7^{th} order Gaussian monocycle and the FCC masks. 104
4.3 Power spectral density of (a) the 2^{nd} order and (b) the 3^{rd} order Gaussian monocycle and the FCC masks. 105
4.4 Power spectral densities of the 1^{st} order HP pulse with and without frequency shift together with the FCC masks. 108
4.5 The autocorrelation functions of different pulse shapes. 109
4.6 Comparison of indoor TH-PPM UWB systems using different pulses for a repetition code with $N_s = 2$ and $N_s = 4$ assuming 7 asynchronous interferers. 111

4.7 Comparison of outdoor TH-PPM UWB systems using different pulses for a repetition code with $N_s = 2$ and $N_s = 4$ assuming 7 asynchronous interferers. 112
4.8 Comparison of indoor TH-BPSK UWB systems using different pulses for a repetition code with $N_s = 2$ and $N_s = 4$ assuming 7 asynchronous interferers. 113
4.9 Comparison of outdoor TH-BPSK UWB systems using different pulses for a repetition code with $N_s = 2$ and $N_s = 4$ assuming 7 asynchronous interferers. 115
4.10 The power spectral density of the pulse $p_1^e(t)$ and (a) the FCC indoor spectral emission mask (b) the FCC outdoor spectral emission mask. 118
4.11 The power spectral densities of (a) the pulse $p_3^e(t)$ and (b) the pulse $p_4^e(t)$ and the FCC masks. 122
4.12 The power spectral density of the pulse $p_2^o(t)$ and (a) the FCC indoor spectral emission mask (b) the FCC outdoor spectral emission mask. 124
4.13 The pulse shapes and the autocorrelations of (a) $p_2^o(t)$, and (b) $p_4^e(t)$. 125
4.14 Pulse shapes of (a) $p_3^e(t)$ together with the 4^{th}-order Gaussian monocycle, and (b) $p_4^e(t)$ together with the 6^{th}-order Gaussian monocycle. . 127
4.15 Comparison of outdoor TH-PPM UWB systems using the novel even pulse $p_4^e(t)$, the odd pulse $p_2^o(t)$ and the 6^{th}-order Gaussian monocycle for a repetition code with $N_s = 2$ and $N_s = 4$ assuming 7 asynchronous interferers. 128
4.16 Power spectral densities of (a) the truncated 4^{th}-order and (b) the truncated 6^{th}-order Gaussian monocycles and the FCC masks. . . . 129
4.17 Power spectral densities of (a) the pulse $p_{in}^e(t)$ and (b) the pulse $p_{out}^e(t)$ together with the FCC masks and ETSI masks. 131

5.1 The average BER versus SNR of the TH-PPM UWB system operating with synchronous OFDM interference. 149

5.2 Comparison of the TH-PPM UWB system operating with synchronous and asynchronous OFDM interference. 150
5.3 The average BER versus SNR of the TH-BPSK UWB system operating with synchronous OFDM interference. 152
5.4 Comparison of the TH-BPSK UWB system operating with synchronous and asynchronous OFDM interference. 153
5.5 The average BER versus SNR of the DS-BPSK UWB system operating with synchronous and asynchronous OFDM interference. 155
5.6 Comparison of the TH-PPM, TH-BPSK and DS-BPSK systems with the same data rate operating in OFDM interference. 156
5.7 Comparison of the TH-PPM, TH-BPSK and DS-BPSK systems with the same data rate operating in OFDM interference and MAI. 157

6.1 The average BER of the TH-BPSK system in the presence of MAI for $N_s = 2$. 168
6.2 The average BER versus SNR of the TH-BPSK system in the presence of ISI and MAI for $N_s = 2$. 170
6.3 Comparison of single-user UWB systems in the presence of ISI with $N_s = 4$. 172
6.4 Comparison of multiple access UWB systems without ISI for $N_s = 2$. 173
6.5 Comparison of UWB systems in the presence of ISI and MAI with $N_s = 4$. 174

Acronyms

Acronyms	Definition
ARake	All-Rake
AWGN	Additive white Gaussian noise
BER	Bit error rate
BPSK	Binary phase shift keying
CDF	Cumulative distribution function
CDMA	Code division multiple access
CHF	Characteristic function
CLT	Central limit theorem
DC	Direct currrent
DS-CDMA	Direct sequence - code division multiple access
DS-IR	Direct sequence impulse radio
ETSI	European Telecommunications Standards Institute
FCC	Federal communications commission, USA
FDMA	Frequency division multiple access
FH	Frequency hopping
GA	Gaussian approximation
GPS	Global positioning system
GQR	Gaussian quadrature rule
GSM	Global system for mobile communications
HP	Hermite polynomial

IEEE	The Institute of Electrical and Electronics Engineers
IR	Impulse radio
ISI	Inter-symbol interference
LOS	Line-of-sight
MA	Multiple access
MAI	Multiple access interference
MRC	Maximum ratio combining
NLOS	None-line-of-sight
OFDM	Orthogonal frequency division multiplexing
OOK	On-off keying
PAM	Pulse amplitude modulatin
PDF	Probability density function
PPM	Pulse positioni modulation
PN	Pseudo-noise
PR	Pseudo random
PRake	Partial-Rake
PS	Prolate spheroidal
PSD	Power spectral density
PSK	Phase shift keying
PSM	Pulse shape modulation
QAM	Quadrature amplitude modulation
QoS	Quality of service
QPSK	Quadrature phase shift keying
RV	Random variable
S/H	Sample and hold
SIR	Signal-to-interference ratio
SINR	Signal-to-interference-plus-noise ratio
SNR	Signal-to-noise ratio
SRake	Selective-Rake

SS	Spread spectrum
SSMA	Spread spectrum multiple access
S-V	Saleh-Valenzuela
TDMA	Time division multiple access
TH	Time-hopping
TH-BPSK	Time-hopping binary phase shift keying
TH-PPM	Time-hopping pulse position modulation
UMTS	Universal mobile telephone service
UWB	Ultra-wideband
WCDMA	Wideband code division multiple access

List of Symbols

Symbol	Definition
A_k	channel attenuation
$c_j^{(k)}$	time-hopping sequence for the kth user
d_j	informatio bit
$\mathbf{E}[x]$	expectation of x
E_b	energy per bit
f_H	the upper 10 dB down point
f_L	the lower 10 dB down point
$f_x(x)$	PDF of x
$F_x(x)$	CDF of x
f_c	carrier frequency
$h(t)$	channel impulse response
I	interference
K	number of rays in a cluster
L	number of clusters
$n(t)$	noise signal
n	noise random variable
N	number of subcarriers
N_c	number of chips
N_h	number of hops
N_u	number of users

N_s	number of frames per information bit
N_0	noise power spectral density
$p(t)$	pulse waveform
$P[\cdot]$	probability function
p_e	average probability of bit error
$P_r\{S\}$	Probability of event S
$Q(\cdot)$	Q-function, the area under the tail of the Gaussian PDF
$R(x)$	autocorrelation function
r	decision statistic
$r(t)$	received signal
$s^{(k)}(t)$	signal for the kth user (k = 1, 2, 3...)
$sgn(\cdot)$	sign function
sinc(t)	sinc function
t	time (variable)
T_c	hop(chip) width
T_b	bit duration
T_f	frame duration
T_l	delay of the lth cluster
T_p	pulse duration
var$[x]$	variance of RV X
$w(t)$	pulse waveform
X	log-normal shadowing
$\alpha_{k,l}$	multipath gain coefficient for cluster l and ray k
$\beta_{k,l}$	fading associated with the kth ray of the lth cluster
Δf	subcarrier frequency spacing
δ	time shift
$\delta(\cdot)$	Dirac delta function
γ	ray decay factor
Γ	cluster decay factor

λ	ray arrival rate
Λ	cluster arrival rate
Ω_0	mean energy of the first ray of the first cluster
$\Phi_{ss}(f)$	PSD of the transmitted signal, $s(t)$
$\Phi_{ss}^{c}(f)$	continous part of PSD
$\Phi_{ss}^{d}(f)$	discrete part of PSD
$\Phi(\Omega)$	Characteristic function of RV x
σ_n^2	power of noise
τ_k	time shift
$\tau_{k,l}$	delay of the kth ray relative to the lth cluster
τ_p	time normalization factor
ξ_l	fading associated with the lth cluster

Chapter 1

Introduction

1.1 Introduction

Since the first wireless telegraph system telephone was invented by Marconi [1], usage of wireless services has experienced a dramatical growth. The number of global cellular subscribers has grown from 10 million in early 1990's to approximately 700 million nowadays. This cellular user population is projected to grow to 2 billion by 2007 [2]. Wireless communication devices are not just convenient communication tools, they are also becoming increasingly important in search and rescue operations, and extremely useful in many emergency situations.

With the rapid proliferation of wireless communications and wireless devices in the past several decades, the technology of wireless communication systems has grown enormously. Needless to say, the basic principle of the fast-growing technology is to provide higher bit rates and data services in addition to pure voice. Many technologies have been proposed to provide high-capacity and reliable wireless communications including code division multiple access (CDMA), orthogonal frequency division multiplexing (OFDM) and ultra-wideband (UWB). Techniques for generating UWB signals have been known for a long time [3]. UWB technology has dramatically changed in recent history. In the past 20 years, UWB has been used for radar, sensing, military

communications and other applications [4], [5]. A substantial change occurred in 2002, when the federal communications commission (FCC) issued a regulation that UWB can be used for data communications. Our research work will focus exclusively on the communications aspects of UWB signals. Currently, UWB technology is being investigated as a promising solution for high capacity wireless communications systems. The attractive features of UWB spread spectrum communications have motivated a growing interest in academic institutions as well as industrial. We will describe UWB communication systems in more detail in the next section.

1.2 UWB Communication Systems

The term "ultra-wideband" refers to electromagnetic signal waveforms that have instantaneous fractional bandwidths greater than 25% with respect to a center frequency. There are two other radar classes identified by signal fractional bandwidth: "narrowband", in which the fractional bandwidth is less than 1%, and "wideband" with a fractional bandwidth from 1% to 25% [6]. Ultra-wideband radio signals employ the transmission of extremely short pulses that spread the energy of the signal from near DC to a few gigahertz. In UWB systems, the wireless signal is intentionally spread over an extremely wide bandwidth, typically several gigahertz. The FCC defines UWB systems as radio systems having signal waveforms with fractional bandwidths greater than 25%, which is given by

$$\text{Fractional Bandwidth} = \frac{2(f_H - f_L)}{f_H + f_L} > 25\%$$

where f_H is the upper 10 dB down point and f_L is the lower 10 dB down point of the power spectrum of the transmitted signals. The relationship between the power spectrums of narrowband and UWB systems is shown in Fig. 1.1. Note that UWB system design is contrary to the usual practice of attempting to make the wireless signal occupy as little bandwidth as possible.

Also contrary to usual radio system practice, UWB radio does not use a radio

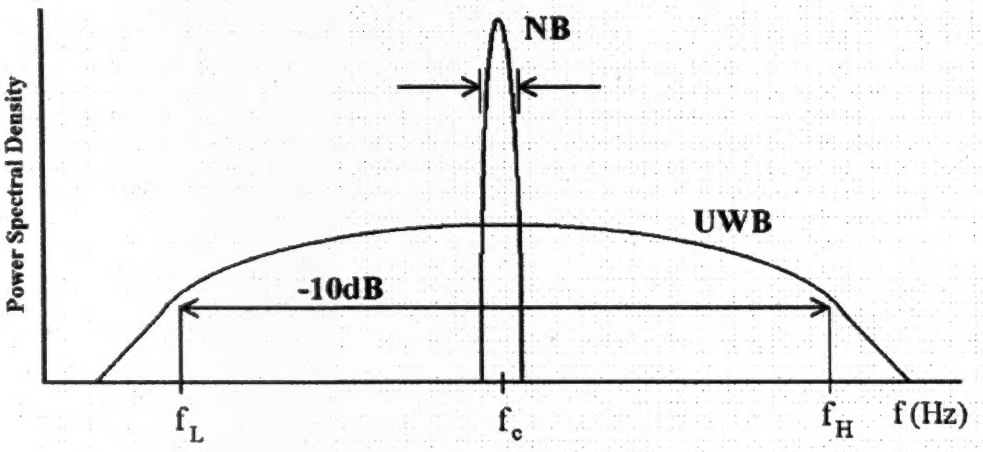

Fig. 1.1. The relationship between the power spectrums of narrowband and UWB systems (from [7]).

frequency carrier. Rather, extremely short duration electrical pulses (or impulses) are specially shaped to achieve the desired spectral emission characteristics without putting the electrical pulses on a radio frequency carrier. This great bandwidth and the property that UWB works in a carrierless manner distinguish UWB systems from conventional "narrowband"and carrier-based systems. The UWB signal will have a very small power spectral density per unit bandwidth (Hertz) because the signal energy is being spread over such a large bandwidth. Therefore, the UWB signal will appear basically as low power "noise" to other UWB users, and to other radio devices and systems. Thus, UWB can be used as a multiple access technique by several users, or as "tolerable" co-existing interference with other radio devices or systems. UWB signals can share frequency spectrum with narrowband and other UWB systems with proper design. Considering the proliferation of personal communications systems and demands on the available frequency spectrum, UWB technology is a good candidate for new generation communications. There are several motivations that drive the recent investigation on UWB wireless communications. First, fine spatial resolution,

low probability of interception and non-interfering signal waveforms are good features that make UWB appealing. The second is the increasing demand for cheap, low power, high bit rate portable wireless devices. UWB systems, with their much wider bandwidths, have much higher capacities and thus can be utilized in future high-capacity wireless systems.

UWB has a number of advantages such as

- Low power consumption
- Extremely high data rate performance
- Robustness to multipath fading
- Coexistence with existing narrowband systems
- Fine time resolution

Very small power spectral densities of UWB systems ensure only minimal mutual interference between UWB and other communication applications. The fine delay resolution properties make UWB radio a valuable candidate for communications in dense multipath environments and the ultra-wide bandwidth makes communications robust with respect to multipath fading. The high ratio of the transmitted signal bandwidth to the information signal bandwidth makes UWB technology attractive for multiple access applications. It is for the same reason that spread spectrum techniques are employed to provide multiple access for many users to share an available bandwidth. Applying a time-hopping (TH) sequence in UWB systems to eliminate catastrophic collisions is the original proposal for UWB multiple access communication systems [8] - [11]. Several modulation techniques have been proposed for UWB signals such as pulse position modulation (PPM) and a variety of pulse amplitude modulations (PAM's) including binary phase-shift keying (BPSK) and on-off keying (OOK) [12] and [13].

1.3 UWB Modulation and Multiple Access Methods

1.3.1 Data Modulation Schemes

Many possible modulation formats can be considered for UWB communications. The potential modulation schemes include antipodal and orthogonal schemes. The most common modulation schemes implemented and used in UWB transmission are described in the following sections.

1.3.1.1 Pulse Amplitude Modulation

The classical binary pulse amplitude modulation can be presented using two antipodal pulses as shown in Fig. 1.2. The transmitted binary modulated signal $s(t)$ can be represented as [13]

$$s(t) = d_j \cdot w(t) \tag{1.1}$$

where $w(t)$ is the pulse waveform, $j \in \{0, 1\}$ represents the transmitted information bit and

$$d_j = \begin{cases} -1 & j = 0 \\ 1 & j = 1. \end{cases} \tag{1.2}$$

1.3.1.2 On-Off Keying

The second modulation scheme is called on-off keying. Using the following definition of d_j

$$d_j = \begin{cases} 0 & j = 0 \\ 1 & j = 1 \end{cases}$$

the transmitted waveform $s(t)$ can be defined as (1.1) and plotted in Fig. 1.3. As seen, nothing will be transmitted in OOK when the information bit is "0".

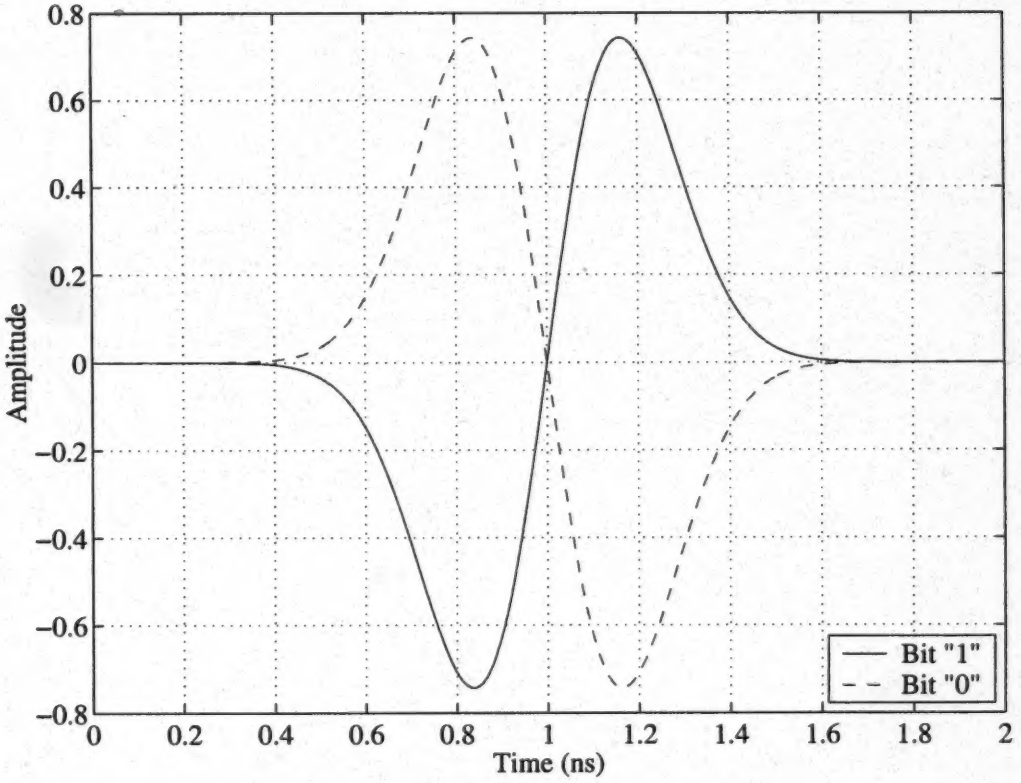

Fig. 1.2. BPAM for "0" and "1" bits.

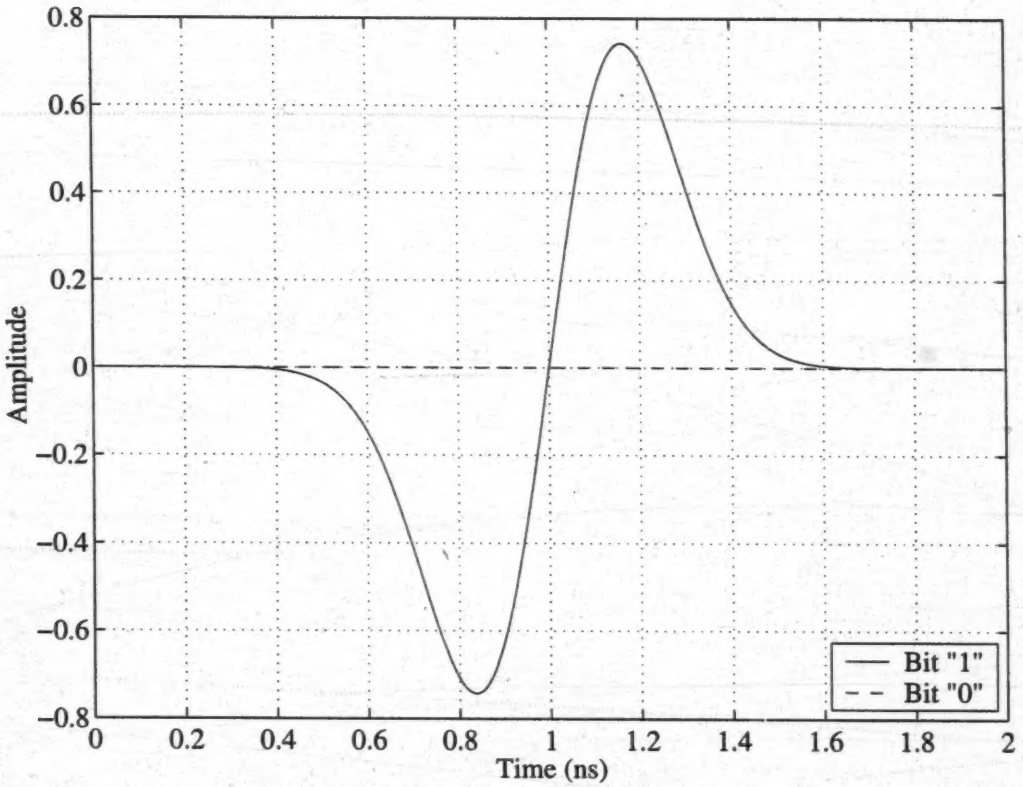

Fig. 1.3. OOK for "0" and "1" bits.

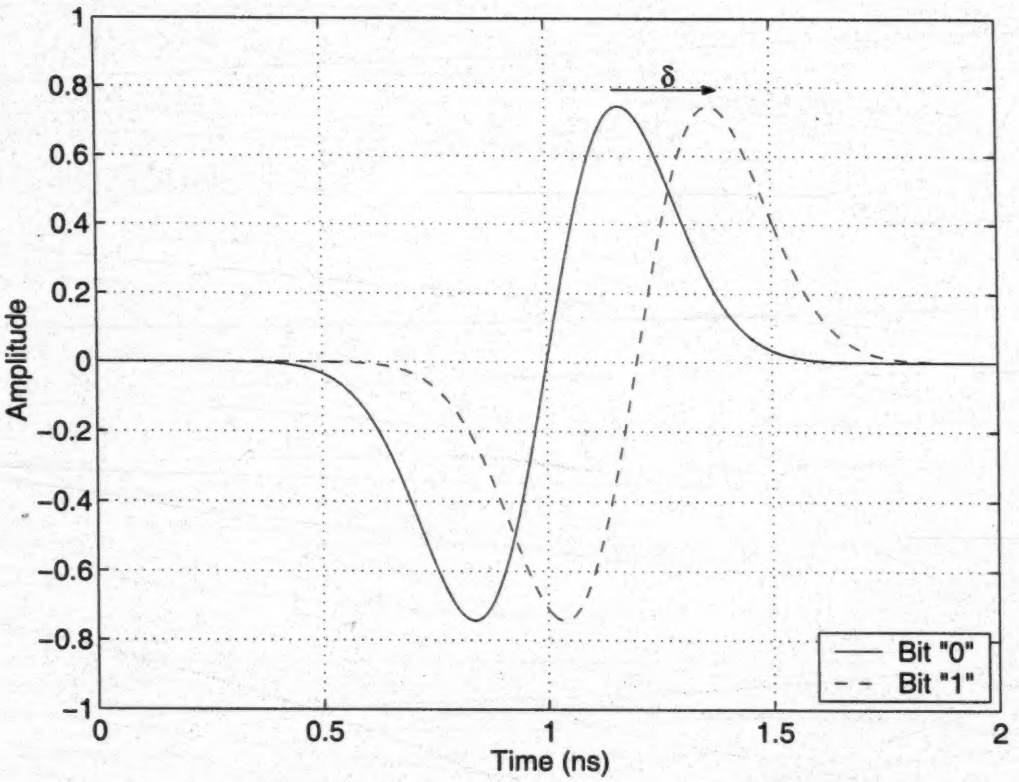

Fig. 1.4. PPM for "0" and "1" bits.

1.3.1.3 Pulse Position Modulation

In pulse position modulation, bit "0" is represented by a pulse originating at the time instant 0, while bit "1" is shifted in time by the amount of δ from 0 [14]. The signal can be expressed as

$$s(t) = w(t - \delta d_j)$$

where the information bit d_j can take values from $\{0, 1\}$ or $\{\pm 1\}$. Fig. 1.4 indicates a case of PPM in which data bit "1" is delayed by a time interval δ, and data bit "0" is sent at the nominal time.

The value of δ needs to be chosen carefully according to the autocorrelation func-

tion of the pulse. The autocorrelation function is defined as

$$R(x) = \int_{-\infty}^{+\infty} w(t)w(x-t)dt. \tag{1.3}$$

The behaviour of the autocorrelation provides a means of selecting the optimal value of δ for an additive white Gaussian noise (AWGN) channel case. It has been shown in [9] and [15] that the best BER performance achieves when δ makes the autocorrelation have the minimal value.

1.3.1.4 Pulse Shape Modulation

Pulse shape modulation (PSM) is based on the orthogonality of the pulse waveforms. In [16], pulse shape modulation was proposed to use different, orthogonal waveforms to represent bit "0" and "1". The transmitted signal can be written as

$$s(t) = (1-d_j)w^{(0)}(t) + d_j w^{(1)}(t) \tag{1.4}$$

where d_j is taking values from $\{0,1\}$, and $w^{(0)}(t)$, $w^{(1)}(t)$ represent two orthogonal pulse waveforms satisfying

$$R(x) = \int_{-\infty}^{+\infty} w^{(0)}(t)w^{(1)}(x-t)dt = 0. \tag{1.5}$$

1.3.2 Multiple Access Methods

In order to smooth the spectrum of a pulse train and make many users to share an available bandwidth, several spread spectrum techniques are applied.

1.3.2.1 TH-UWB

- *Uniform Pulse Train Spacing:* A pulse train of the form $s(t) = \sum_{j=-\infty}^{+\infty} w(t - jT_f)$ consists of pulses spaced T_f seconds apart in time. The *frame time* or *pulse repetition time* T_f typically may be a hundred to a thousand times the pulse width T_p, resulting in a signal with a very low duty cycle. Fig. 1.5 shows the relationship between T_f and T_p.

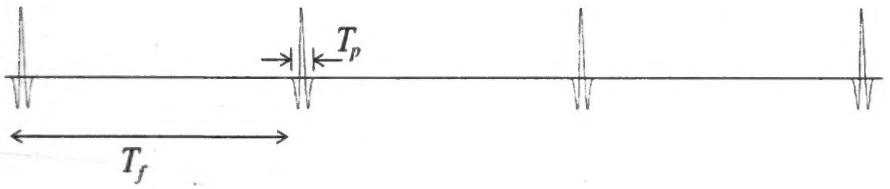

Fig. 1.5. The relationship between the frame duration T_f and the pulse T_p (from [7])

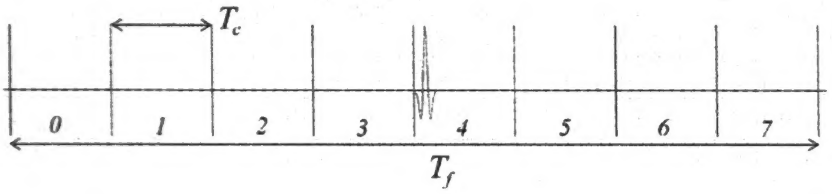

Fig. 1.6. The pulse train structure with TH sequence (from [7]).

- *Random/Pseudorandom TH:* As known, the spectrum of a pulse train contains strong spectral lines at the multiple of the pulse repetition frequency. These energy spikes may interfere with other communication systems at short Range. On the other hand, multiple access signals composed of uniformly spaced pulses are vulnerable to occasional *catastrophic collisions* in which a large number of pulses from two signals are received simultaneously. To spread the energy spikes all over the spectrum and to eliminate catastrophic collisions in multiple access applications, a randomizing technique using a distinct pulse-shift pattern $\{c_j\}$ called a *time-hopping sequence* was introduced [9]. With the hop width T_c, the TH sequence provides an additional time shift, $c_j T_c$, to each pulse in the pulse train. In each frame time, the pulse is pseudo-randomly positioned in time with a TH sequence as shown in Fig.1.6. The time hopping sequence randomizes the signal in both time and frequency domains [17].

- *Repetition Structure:* As defined in [14], the modulating data symbol is assumed to change only every N_s frames. Assuming that a new data symbol begins

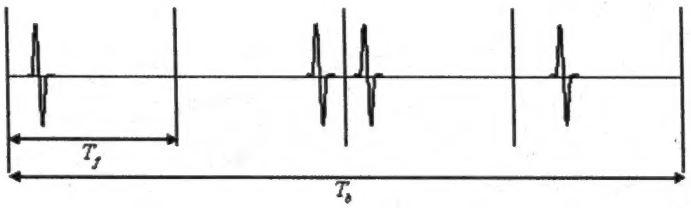

Fig. 1.7. The repetition structure of an information bit.

with pulse index $j = 0$, the index of the data symbol modulating pulse j is $\lfloor j/Ns \rfloor$. Fig. 1.7 shows this repetition structure. As we can see, the bit duration $T_b = N_s T_f$. The scheme can also be looked as using a repetition code with the code length of N_s.

1.3.2.2 Data Modulation with Time Hopping

In TH mode, the pulse transmission instant is defined by the pseudo-random (PR) code. An information bit is spread over multiple pulses to achieve a *processing gain* due to the repetition structure.

The information signal $s(t)$ for the kth user can be written as

$$s^{(k)}(t) = \sum_{m=-\infty}^{\infty} \sum_{j=0}^{N_s-1} w\left(t - mT_b - jT_f - c_j^{(k)} T_c\right) d_m^{(k)} \tag{1.6}$$

for PAM modulation,

$$s^{(k)}(t) = \sum_{m=-\infty}^{\infty} \sum_{j=0}^{N_s-1} w\left(t - mT_b - jT_f - c_j^{(k)} T_c - d_m^{(k)} \delta\right) \tag{1.7}$$

for PPM modulation, and

$$s^{(k)}(t) = \sum_{m=-\infty}^{\infty} \sum_{j=0}^{N_s-1} w_{d_m^{(k)}}\left(t - mT_b - jT_f - c_j^{(k)} T_c\right) \tag{1.8}$$

for PSM modulation.

1.3.2.3 Direct Sequence UWB

In direct-sequence (DS) UWB systems, a pseudo-random code is used to spread an information bit into multiple chips, as in conventional DS spread spectrum (SS) systems. In DS-UWB systems, the pulse waveform takes the role of the chip. The PAM or OOK information signal for the kth user, $s^{(k)}(t)$, can be written as

$$s^{(k)}(t) = \sum_{m=-\infty}^{\infty} \sum_{n=0}^{N_c-1} d_m^{(k)} c_n^{(k)} p(t - mT_b - nT_c) \tag{1.9}$$

where $\left\{c_n^{(k)}\right\}_{n=0}^{N_c-1}$ is the DS for the kth user, T_c is the chip width for DS-UWB systems and N_c is the number of chips per symbol.

Pseudo-random codes are used to separate users and to provide a processing gain. Unlike the TH code that is used to change the transmission instant in time-hopping systems, the DS code is used to change the pulse polarities in one information bit, which is similar to that in conventional CDMA systems.

1.4 UWB Channel Model

The channel model for UWB systems is very similar to the one for wideband systems such as CDMA. The time resolution of the channel is of the order of a nanosecond based on several GHz bandwidth of a UWB signal. The fundamental aspects of the multipath fading model for UWB systems include the delay spread, decay profiles and the number of paths. Various fading models have been presented based on significant data collection efforts [18], [19]. Several papers have investigated UWB systems using simplified multipath channels, such as a Rayleigh fading model. However, it is crucial to apply realistic channel models to get valid results. In this section, we pay attention to the IEEE UWB channel model.

The IEEE 802.15.1 Working group for Wireless Personal Area Networks, and its channel modeling subcommittee proposed a channel model for UWB systems in 2003 [18]. The multipath indoor fading model is a modified Saleh-Valenzuela model

(S-V) where multipath components arrive in clusters. The original S-V model was carried out by Saleh and Valenzuela in 1987 based on empirical measurements [20]. Due to the measured UWB indoor channel data, a lognormal distribution rather than a Rayleigh distribution is employed for the multipath gain magnitude. Independent fading is assumed for each cluster as well as each ray within the cluster. In the S-V model, both the cluster and ray arrival times are modeled by Poisson processes. The phase of the channel impulse response can be either 0 or π, and thus the model does not contain an imaginary component. A discrete multipath channel impulse was proposed by Foerster as [18]

$$h(t) = X \sum_{l=0}^{L} \sum_{k=0}^{K} \alpha_{k,l} \delta \left(t - T_l - \tau_{k,l} \right) \tag{1.10}$$

where $\alpha_{k,l}$ is the multipath gain coefficient for cluster l and ray k, T_l is the delay of the lth cluster, $\tau_{k,l}$ is the delay of the kth ray relative to the arrival time of the lth cluster, and X represents the log-normal shadowing. The number of clusters and rays in the multipath fading model is denoted as L and K, respectively, which are fixed for a given model.

Assuming that $\tau_{0,l} = 0$, the cluster arrival time distribution and the ray arrival time distribution can be presented as

$$p\left(T_l | T_{l-1}\right) = \Lambda \exp\left[-\Lambda \left(T_l - T_{l-1}\right)\right], \quad l > 0 \tag{1.11}$$

and

$$p\left(\tau_{k,l} \mid \tau_{k-1,l}\right) = \lambda \exp\left[-\lambda \left(\tau_{k,l} - \tau_{k-1,l}\right)\right], \quad k > 0 \tag{1.12}$$

respectively, where Λ is the cluster arrival rate and λ is the ray arrival rate, i.e. the arrival rate of path within each cluster. The relationship between clusters and rays can be shown in Fig. 1.8.

The channel coefficients are defined by

$$\alpha_{k,l} = p_{k,l} \xi_l \beta_{k,l} \tag{1.13}$$

$$|\xi_l \beta_{k,l}| = 10^{(\mu_{k,l} + n_1 + n_2)/20} \tag{1.14}$$

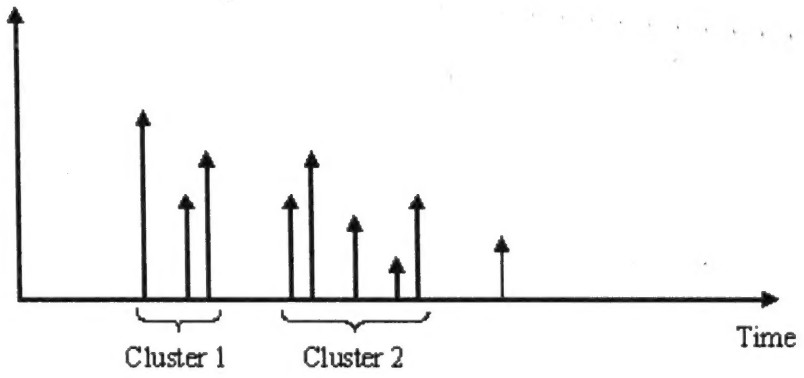

Fig. 1.8. The multipath fading model for UWB where multipath components arrive in clusters

where $p_{k,l}$ is taken from $\{-1, 1\}$ with equal probability to account for the signal polarity, ξ_l is the fading associated with the lth cluster, $\beta_{k,l}$ is the fading associated with the kth ray of the lth cluster, $n_1 \propto N(0, \sigma_1^2)$ and $n_2 \propto N(0, \sigma_2^2)$ are independent and correspond to the fading on each cluster and ray, respectively, and

$$E\left[|\xi_l \beta_{k,l}|^2\right] = \Omega_0 e^{-T_l/\Gamma} e^{-\tau_{k,l}/\gamma} \tag{1.15}$$

where Ω_0 is the mean energy of the first ray of the first cluster. $\mu_{k,l}$ is defined as [18]

$$\mu_{k,l} = \frac{10\ln(\Omega_0) - 10T_l/\Gamma - 10\tau_{k,l}/\gamma}{\ln(10)} - \frac{(\sigma_1^2 + \sigma_2^2)\ln(10)}{20}. \tag{1.16}$$

The log-normal shadowing is characterized as

$$20\log 10(X) \propto N\left(0, \sigma_x^2\right). \tag{1.17}$$

Based on the average distance between the transmitter and the receiver and whether there is a line-of-sight (LOS) component, four different channel implementations are suggested as follows:

- CM1: LOS model for 0-4m

TABLE 1.1

Typical Parameters for the IEEE multipath fading model

Parameters	CM1	CM2	CM3	CM4
Mean excess delay (ns)	5	9.9	15.9	30.1
RMS delay (ns)	5	8	15	25
Λ (1/ns)	0.0233	0.400	0.0667	0.0667
λ (1/ns)	2.5	0.5	2.1	2.1
Mean channel energy (dB)	-0.4	-0.5	0.0	0.3
Std channel energy (dB)	2.9	3.1	3.1	2.7

- CM2: NLOS model for 0-4m
- CM3: NLOS model for 4-10m
- CM4: NLOS model for more than 10m. This model presents an extreme NLOS multipath channel condition.

Table 1.1 contains typical parameters for four channel models mentioned above. As an example, Fig.1.9 shows the delay profiles of the IEEE modified S-V model. The average profiles are calculated from 100 independent channel realizations.

1.5 Interference

A desired wireless user signal is usually subject to the corruption of the interference from other wireless devices or user signals. As a result, the performance of a wireless system is limited dominately by interference rather than thermal noise. In this section, we describe several kinds of interference existing in UWB communications.

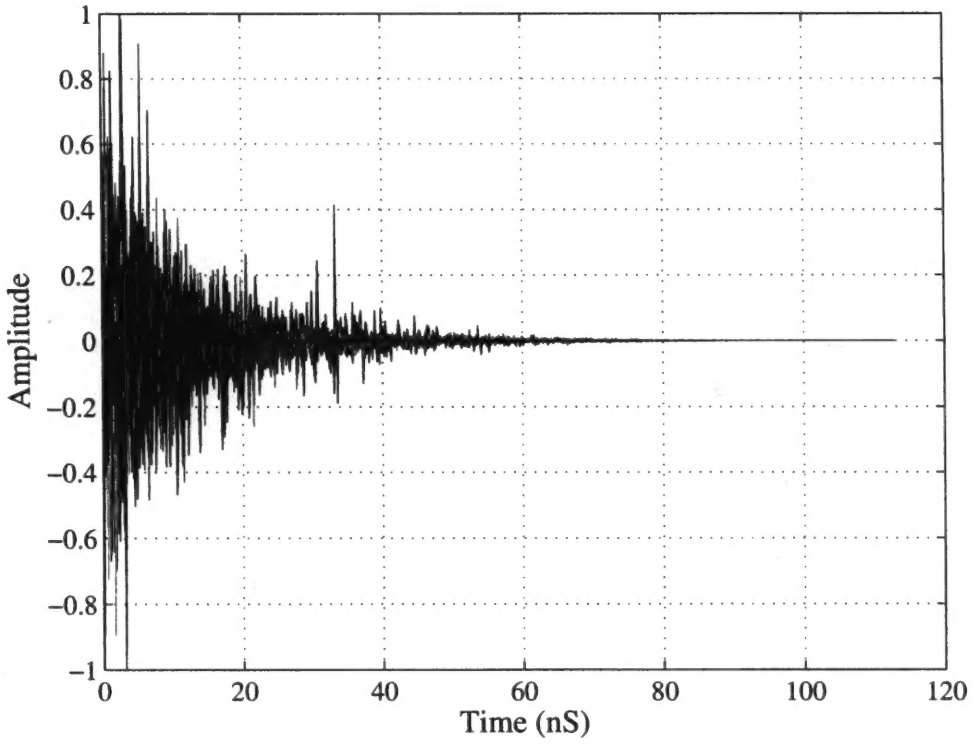

Fig. 1.9. Delay profiles of CM1 fading model with 100 channel realizations

1.5.1 Multiple Access Interference

The most challenging problem for wireless communication system design is to accommodate as more users as possible while maintaining required quality of service (QoS) with finite amount of radio spectrum. In order to accommodate increasing number of users, multiple access schemes are usually utilized to allow many mobile users to share limited frequency spectrum simultaneously. Frequency division multiple access (FDMA), time division multiple access (TDMA) and CDMA are the major techniques for multiple access applications. Each user is assigned to an individual channel in a frequency slot and in a time slot in FDMA and TDMA systems, respectively. In CDMA, user signals are spreaded by using pseudo-noise (PN) code sequences. In theory, FDMA, TDMA and CDMA techniques have the same capacity. However, in a cellular system, we may find that CDMA can potentially accommodate more users than either TDMA or FDMA, without requiring for precise time or frequency coordination among users [21]. Frequency-hopping (FH), time-hopping and direct-sequence are principal forms of CDMA. The FH-CDMA system achieves the bandwidth spreading by using the PN sequences to pseudo-randomly hop the carrier frequency in a large band, TH-CDMA uses PN sequences to pseudo-randomly hop the pulse waveform in a time slot, while DS-CDMA uses PN sequences to introduce rapid phase transitions into the carrier containing the information data.

This thesis deals with, in part, the system performance of TH and DS UWB communication systems. In these systems, multiple access interference (MAI) is caused by the simultaneous presence of multiple UWB user signals. MAI is modeled as the sum of other UWB user signals transmitting on the channel. These interfering signals are supposed to have the same basic signal characteristic as the desired user, but with different spreading codes.

The received signal $r(t)$ at the receiver can be written as

$$r(t) = s^{(1)}(t) * h^{(1)}(t) + i(t) + n(t) \tag{1.18}$$

where $s^{(1)}(t)$ is the desired user signal, $h^{(1)}(t)$ represents the impulse response of the

channel, $i(t)$ is interference from other users and $n(t)$ is Gaussian noise. If N_u users are transmitting information at the same time, $i(t)$ is defined as

$$i(t) = \sum_{k=2}^{N_u} s^{(k)}(t - \tau_k) * h^{(k)}(t) \tag{1.19}$$

where $\left\{h^{(k)}(t)\right\}_{k=2}^{N_u}$ are the impulse responses of the channel for interfering users, and $\{\tau_k\}_{k=2}^{N_u}$ are the time delays of the interfering users.

A conventional single-user matched filter receiver is used for data detection. The single-user matched filter is known to be sub-optimal for systems operating with interference, compared to the optimal multi-user receivers described in [22]. However, the system complexity of the optimal multi-user receiver increases exponentially with the number of users, which limits its application [23]. Compared to other sub-optimal multi-user receivers previously proposed [24], a single-user matched filter receiver doesn't require specific knowledge of the signature sequences of other users and exact timing offsets of all transmitters. Therefore, it is simple and economical.

1.5.2 Narrowband Interference

Narrowband interference in UWB communications is another important issue which needs to be carefully addressed. We define a narrowband signal as a signal of which bandwidth B_{narrow} satisfies the following relationship [13]

$$\frac{B_{narrow}}{B_{UWB}} < 10^{-3} \tag{1.20}$$

where B_{UWB} is the bandwidth of the UWB signal.

There are different types of narrowband interference, which can come from global system for mobile communications (GSM), universal mobile telephone service (UMTS), wideband CDMA (WCDMA), or global positioning system (GPS) wireless devices [25] - [33]. A multitone representation of the interfering signal is often utilized for analysis. The total interference is modeled as a finite sum of N_t sinusoidal waveforms,

given by

$$i_{narr}(t) = \sum_{n=1}^{N_t} A_n \sin(2\pi f_n t + \phi_n) \tag{1.21}$$

where A_n, f_n and ϕ_n is the amplitude, frequency and phase of the nth tone, respectively. In some literature [25], [26], the UMTS interference was also modeled as a bandlimited Gaussian noise.

OFDM systems may also introduce interference to UWB communications. Gaussian noise assumption was used for modeling the OFDM interference [34]. This thesis deals with the effects of the interfering OFDM signals on UWB systems.

1.5.3 Intersymbol Interference

Intersymbol interference (ISI) usually results from the smearing of the transmitted signal by channel and receiver filtering. Nonideal channel frequency response such as multipath fading causes the amplitude and delay distortion. As a result, a succession of pulses transmitted through the channel are smeared so that they overlap and are no longer distinguishable as well-defined pulses at the receiver end [35]. ISI represents the effect that energy from other symbols interferes with the reception of the desired symbol.

Given the expression for the transmitted UWB signal in (1.18), a coherent RAKE receiver is usually utilized [36]. The response of a RAKE receiver can be written as [37]

$$Z = Z_s + Z_{ISI} + Z_{MAI} + Z_N \tag{1.22}$$

where Z_s denotes the desired symbol component, Z_{ISI} represents intersymbol interference due to multipath fading, Z_{MAI} is MAI from all the other users and Z_N is due to AWGN.

TABLE 1.2

FCC radiation limits for indoor and outdoor communications

Frequency (MHz)	Indoor (dBm)	Outdoor (dBm)
960-1610	-75.3	-75.3
1610-1990	-53.3	-63.3
1990-3100	-51.3	-61.3
3100-10600	-41.3	-41.3
Above 10600	-51.3	-61.3

1.6 UWB Regulations

1.6.1 UWB regulations in USA

One of the important issues for UWB communications is frequency allocation. In 2002, the FCC proposed the first radiation limitations for UWB and permitted commercialization of UWB technology [38]. The FCC radiation limits are presented in Table 1.2 for indoor and outdoor data communications. Fig. 1.10 illustrates the FCC frequency emission masks for UWB communications.

1.6.2 UWB regulations in Europe

Similar discussion on frequency allocation and radio interference has emerged in Europe. European organizations have been influenced by the FCC regulations. Currently, the European Telecommunications Standards Institute (ETSI) is working on defining the standard for Europe [39]. The ETSI limits for indoor and outdoor UWB communications are defined in Table 1.3.

Fig. 1.11 shows the ETSI draft emission limits together with the FCC masks.

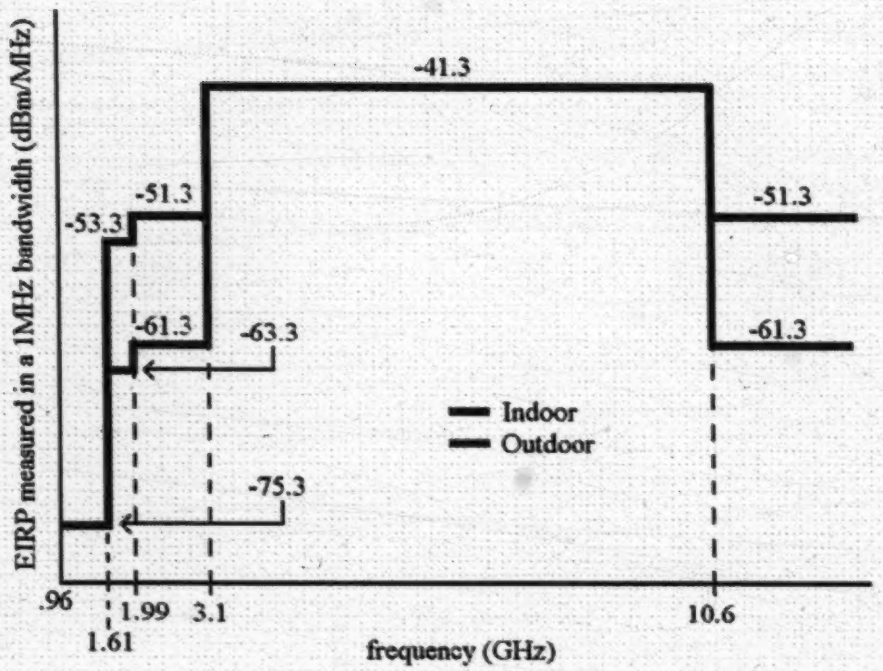

Fig. 1.10. FCC UWB emission Masks (from [7])

TABLE 1.3

ETSI limits for UWB indoor and outdoor communications

Frequency (GHz)	Indoor (dBm)	Outdoor (dBm)
$f < 3.1$	$-51.3 + 87\log(f/3.1)$	$-61.3 + 87\log(f/3.1)$
$3.1 < f < 10.6$	-41.3	-41.3
$f > 10.6$	$-51.3 + 87\log(f/3.1)$	$-61.3 + 87\log(f/3.1)$

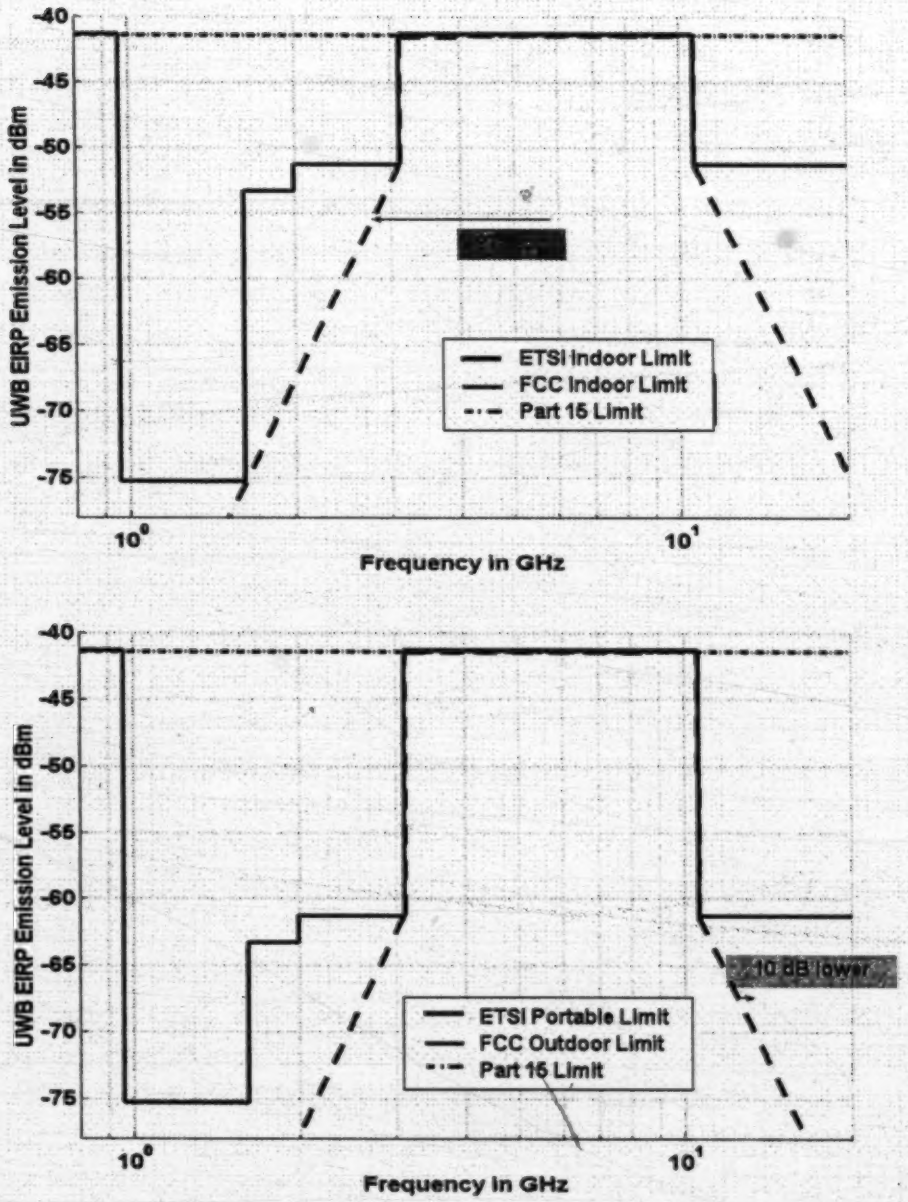

Fig. 1.11. UWB frequency emission limitations defined by ETSI (from [40])

1.7 Thesis outline and Contributions

This thesis consists of 5 major chapters. Each chapter corresponds to one or two major contributions. At the beginning of each chapter, we review some background and literature which are related to the subject of that chapter.

In Chapter 2, we first analyze the TH-PPM system in the presence of multiple access interference. Our goal is to provide a tractable analytical expression for calculating average bit error rate of the TH-PPM system without making any improper assumptions. Using rigorous probability arguments, we obtain the characteristic function (CHF) of the multiple access interference in TH-PPM systems. Based on the CHF, a double integral expression is provided and can be used for predicting the average BER of the TH-PPM system to any desired accuracy with modest computational complexity. Further, the expression for predicting the bit error rate of the TH-BPSK system is obtained. The analytical expressions are validated by Monte Carlo simulation and used to assess the accuracy of the Gaussian approximation (GA), a widely adopted method for estimating BER's. The Gaussian approximation is shown to be inaccurate for predicting BER's of UWB systems for medium and large signal-to-noise ratio (SNR) values. We also examine the sensitivity of the performance of the time-hopping modulation schemes to the system parameters through numerical examples. UWB systems using different Gaussian monocycles are examined. Further, TH-PPM and TH-BPSK are evaluated and compared through numerical examples. It is shown that the TH-BPSK system outperforms the TH-PPM system for all values of SNR.

In Chapter 3, we consider the error rate analysis of TH-UWB and DS-UWB communication systems. We first provide a unified framework for TH and DS UWB systems, in which different modulation schemes can be fairly compared. Employing this framework complicates the analysis of TH-UWB systems and makes it different from the analysis in Chapter 2. We then derive exact expressions for the probability of error for TH-PPM, TH-BPSK, DS-BPSK systems. Particularly, for DS-BPSK UWB systems, we also present a simple and accurate alternative analysis based on

the simplified receiver decision statistic. The simplified analytical method is shown to provide BER results essentially as accurate as the exact analysis and to require much less computational complexity. In addition, we consider a newly proposed DS impulse radio (DS-IR) modulation, which utilizes both a TH sequence and a DS sequence. The BER performance of this new scheme in MAI is extensively investigated and an accurate expression is derived. Relied on these analytical expressions, we accurately compare the BER's of TH-PPM, TH-BPSK, DS-BPSK and DS-IR BPSK systems for different system parameters. It is shown that DS-BPSK outperforms TH-BPSK for medium and large values of SNR, which contradicts some previous results obtained using the Gaussian approximation. Our results also indicate that DS-IR BPSK outperforms TH-BPSK. However, its performance is poorer than the performance of conventional DS-BPSK UWB systems, which cannot justify the use of the combination of TH and DS codes. Our evaluations, based on exact analyses of MAI in different modulation schemes, clearly indicate the actual BER performance difference among these well-know UWB systems and provide valuable criteria for practical applications.

In Chapter 4, we study the pulse shapes previously proposed for UWB communications and compare them to determine which provide the best performance. The performance measures considered are the bit error rate in MAI environments and compliance with the FCC spectral emission constraints. The Gaussian monocycles of higher orders and the prolate spheroidal function based pulses are found to meet the spectral emission masks without frequency shifting. Frequency shifting and bandpass filtering must be used for the modified Hermite polynomial based pulses to meet the spectral masks. The multiaccess (MA) average error rates of UWB systems using the different pulse shapes are examined and compared using exact analyses previously obtained. The Gaussian monocycles are shown to achieve performances as good as the prolate spheroidal function based pulses with the same effective bandwidths in numerical examples. The Gaussian monocycles outperform the modified Hermite polynomial based pulses for the system models considered. Some tradeoffs of these

pulses are also addressed in terms of the complexity of their implementations and the average bit error probabilities. Furthermore, we propose a novel paradigm to design time-limited pulse shapes for UWB communication systems. Pulses can be designed using the new paradigm that not only conform to spectral emission constraints, but also achieve good BER performance in MAI environments. Compared with previously proposed pulses, the novel pulses provide the same multiple access performance as the Gaussian monocycles yet have advantages over them in terms of power spectrum and spectral emission constraints.

In Chapter 5, the effects of narrowband interference, especially interference from OFDM signals, on UWB communications are investigated. The FCC frequency emission masks reduce the potential of UWB signals interfering to other co-existing wireless systems. However, the power spectral density (PSD) of conventional communications signals is much higher than that of UWB signals, the interference from other wireless applications to UWB systems becomes more severe and critical. In our work, we first analyze the OFDM narrowband interference to UWB systems. Closed-form expressions are derived for narrowband interference based on rigorous probability arguments. We examine the performance degradation of a UWB system in the presence of interference from OFDM signals. Several modulation schemes proposed for UWB communications are compared in terms of capability for interference suppression. The effects of system parameters on the BER performance are also addressed through numerical examples. Our results show that the narrowband interfering OFDM signal introduces more severe interference to UWB systems than the MAI and that the BER performance of these UWB systems will be significantly deteriorated by the interfering OFDM signal with higher power levels. Our comparisons indicate that TH-BPSK and DS-BPSK outperform TH-PPM for all values of SNR and the actual performance of TH-BPSK may be poorer than the actual performance of DS-BPSK depending on UWB system parameters.

In Chapter 6, we investigate the performance of different UWB systems in multipath fading scenarios. We first review analytical and semi-analytical methods utilized

for estimating the multipath performance of UWB applications and state some drawbacks of these methods. Then, we consider using different Rake receivers for reception. The IEEE 802.15.3a fading channel model is taken into account. Simulation is used for detecting data sequences. Our simulation results show that all-Rake receiver does not guarantee the best performance. On the contrary, selective-Rake receivers can achieve better performance than all-Rake when operating with intersymbol interference. In addition, the candidate modulation schemes are evaluated and compared according to the realistic fading model. Although some analytical and semi-analytical methods based on the Gaussian approximation provide the same BER estimates for several modulation schemes, our results show that the actual performance of these modulation schemes are different.

Chapter 7 concludes this thesis by outlining major findings. Some future work is also suggested.

Chapter 2

Accurate Evaluation of Multiple Access Performance in TH-PPM and TH-BPSK UWB Systems

2.1 Introduction

UWB technology is currently being investigated as a promising solution for high capacity wireless communications systems. The very small power spectral densities of UWB systems ensure only minimal mutual interference between UWB and other communication applications. The high ratio of the transmitted signal bandwidth to the information signal bandwidth makes UWB technology attractive for multiple access applications. A TH sequence is applied in UWB systems to eliminate catastrophic collisions in multiple access.

Time-hopping combined with pulse position modulation was originally proposed for UWB systems [9]. Studies of multiple access system performance for this modulation in terms of bit error rate were conducted in [14], [41]- [43]. A Gaussian approximation was used to estimate the BER in [14]. In the Gaussian approximation, a central limit theorem (CLT) is employed to approximate the sum of the multiple

access interference as an additive white Gaussian process. Thus, the receiver consists of a conventional single-user matched filter (correlation receiver) to detect the desired user signal. The variance of the MAI averaged over all random variables is used to calculate the SNR at the receiver output. The Gaussian approximation is widely used because it is easy to apply. However, it was shown in [44] that the Gaussian approximation significantly underestimates the BER of practical TH-PPM systems. The limitation of the Gaussian approximation has motivated researchers to search better analytical methods. In [45], Durisi *et al.* estimated BER's using a composite method. In this approach, a simulation-based, semi-analytical estimate is formed using results from a Gaussian quadrature rule (GQR) approximation of a definite integral. This approach can achieve more accurate BER estimation than CLT based approximation at the expense of much higher computational complexity. An exact BER calculation for asynchronous multiple access UWB systems is usually unwieldy. Our purpose is to provide an analytical method for calculating the average probability of bit error of UWB systems. In our work, we provide a new accurate and tractable method for calculating the BER of TH-PPM in the presence of multiple access interference based on a characteristic function technique [46], [47]. This technique can be used in the performance evaluation of TH-UWB systems without introducing any unrealistic assumptions. It gives the precise BER in the general case with very limited computational complexity [48].

Currently, TH-PPM and TH-BPSK UWB systems are often considered as alternatives for a given application, though the differences between the two systems lead to different performance characteristics. Analysis of multiple access scheme performance for TH-PPM UWB systems in terms of BER was reported in [14], [45], [48]. The performance of a PAM UWB system for an indoor wireless channel with multipath interference was investigated in [49] and [50]. Additionally, a performance analysis of antipodal TH-PAM systems, i.e. TH-BPSK systems, was described in [51]. The performances of TH-PPM and TH-BPSK UWB systems were compared in [52] based on the Gaussian approximation. Unfortunately, the unreliability of the Gaus-

sian approximation renders some previous comparisons less useful. A comparison of different UWB modulation schemes was also presented recently in [53]. The study in [53], however, assumes chip-synchronous systems, which is not realistic in practical UWB applications.

In this chapter, we analyze generic TH-PPM and TH-BPSK systems operating in multiple access interference. We provide expressions for the characteristic functions of the MAI in different modulation schemes. Exact average BER expressions for TH-PPM and TH-BPSK UWB systems in an additive white Gaussian noise environment are derived. The AWGN channel model is important in its own right for some UWB applications [14], [45], and is a necessary intermediate step for future work examining UWB on fading channel models. Numerical results obtained from our exact analysis are used to assess the accuracy of the Gaussian approximation. Our examples show the sensitivities of TH-PPM UWB systems to the pulse shape and the time shift parameter. We also compare the average bit error probabilities of these systems from a multiple access point of view. Accurate comparisons provide important and valuable criteria for choosing appropriate UWB modulation schemes in practical applications.

The remainder of this chapter is organized as follows. In Section 2.2, the TH-PPM and TH-BPSK UWB system models used in the evaluation are briefly described. Review of previous performance results for TH-PPM systems is provided in Section 2.3 for completeness. The exact expressions for the average probabilities of bit error are then derived for different systems in Sections 2.4, 2.5 and 2.6. In Section 2.7, the validity of the exact analysis is confirmed by simulation and the inaccuracy of the Gaussian approximation is proved using the analytical method. The performances of TH-PPM and TH-BPSK UWB systems using different pulse parameters are also evaluated. Moreover, comparisons of the BER's of the TH-PPM and TH-BPSK multiple-access systems with different system parameters are made. Finally, we summarize our chapter results in Section 2.8.

2.2 System Models

The asynchronous TH-PPM and TH-BPSK UWB systems are described in [14], [43] and [51]; our notation and terminology are consistent with those papers. A typical TH-PPM UWB signal takes the form

$$s^{(k)}(t,i) = \sqrt{\frac{E_b}{N_s}} \sum_{j=iN_s}^{(i+1)N_s-1} p\left(t - jT_f - c_j^{(k)}T_c - d_i^{(k)}\delta\right) \tag{2.1}$$

and a TH-BPSK UWB signal with antipodal data modulation is written as

$$s_{BPSK}^{(k)}(t,i) = \sqrt{\frac{E_b}{N_s}} \sum_{j=iN_s}^{(i+1)N_s-1} d_i^{(k)} p\left(t - jT_f - c_j^{(k)}T_c\right) \tag{2.2}$$

where t is time, $s^{(k)}(t,i)$ is the kth user's signal conveying the ith data bit, and $p(t)$ is the signal pulse with pulse width T_p, normalized so that $\int_{-\infty}^{+\infty} p^2(t)dt = 1$. The parameters employed in these UWB models are described as follows [14], [43], [51]:

- E_b is the bit energy common to all signals. $\sqrt{\frac{E_b}{N_s}}$ is a normalization factor.
- N_s is the number of pulses required to transmit a single data bit, called the length of the repetition code in [45].
- T_f is the time duration of a frame, and thus, the bit duration $T_b = N_s T_f$.
- T_c is the TH chip width and satisfies $N_h T_c \leq T_f$.
- $\{c_j^{(k)}\}$ represents the TH code for the kth source. It is pseudorandom with each element taking an integer in the range $0 \leq c_j^{(k)} < N_h$, where N_h is the number of hops.
- $d_i^{(k)}$ represents the ith binary data bit transmitted by the kth source and different bits are assumed to be equiprobable. In antipodal TH-BPSK UWB systems, $d_i^{(k)} \in \{1, -1\}$. In TH-PPM UWB systems, the data bits can conveniently be $\{0, 1\}$ or $\{1, -1\}$, as explained in the sequel.

- δ is the time shift associated with binary PPM.

In a UWB system, the choice of the pulse shape will strongly affect the choice of receiver bandwidth, the bit error rate performance and the performance in multipath propagation environments. A variety of pulse shapes has been proposed for UWB impulse radio systems including the Gaussian pulse, Gaussian monocycles and the Manchester monocycle [54]. The Gaussian pulse has the form [35]

$$p_0(t) = \exp\left[-2\pi\left(\frac{t}{\tau_p}\right)^2\right] \tag{2.3}$$

and its n^{th} derivative named the n^{th}-order Gaussian monocycle is [55]

$$p_n(t) = \mathcal{E}_n \frac{d^n}{dt^n} \exp\left[-2\pi\left(\frac{t}{\tau_p}\right)^2\right] \tag{2.4}$$

where τ_p represents a time normalization factor to keep $p_n(t)$ independent of a specific impulse duration and $\mathcal{E}_n$ is introduced to normalize the energy of the pulses $p_n(t)$. The most widely reported pulse in UWB systems is the 2^{nd}-order Gaussian monocycle [14], which is the second derivative of the Gaussian pulse given by

$$p(t) = \left[1 - 4\pi\left(\frac{t}{\tau_p}\right)^2\right] \exp\left[-2\pi\left(\frac{t}{\tau_p}\right)^2\right]. \tag{2.5}$$

The autocorrelation $R(x)$ of the Gaussian monocycle $p(t)$ in (2.5) is shown in Fig. 2.1 and is

$$R(x) = \left[1 - 4\pi\left(\frac{x}{\tau_p}\right)^2 + \frac{4\pi^2}{3}\left(\frac{x}{\tau_p}\right)^4\right] \exp\left[-\pi\left(\frac{x}{\tau_p}\right)^2\right]. \tag{2.6}$$

In this chapter, we restrict our performance analysis of time-hopping systems to the 2^{nd}-order Gaussian monocycle in (2.5). Some numerical results for the 4^{th}-order Gaussian monocycle are presented in Section 2.7 for comparison. The 4^{th}-order Gaussian monocycle has the form as

$$p_4(t) = \left[3 - 24\pi\left(\frac{t}{\tau_p}\right)^2 + 16\pi^2\left(\frac{t}{\tau_p}\right)^4\right] \exp\left[-2\pi\left(\frac{t}{\tau_p}\right)^2\right] \tag{2.7}$$

and the autocorrelation $R_4(x)$ of the 4^{th}-order Gaussian monocycle is given by

$$R_4(x) = \left[1 - 8\pi\left(\frac{x}{\tau_p}\right)^2 + 8\pi^2\left(\frac{x}{\tau_p}\right)^4 - \frac{32\pi^3}{15}\left(\frac{x}{\tau_p}\right)^6 + \frac{16\pi^4}{105}\left(\frac{x}{\tau_p}\right)^8\right]\exp\left[-\pi\left(\frac{x}{\tau_p}\right)^2\right]. \tag{2.8}$$

Our analytical method, however, can be applied to UWB systems using arbitrary pulse shapes.

Assuming N_u users are transmitting asynchronously on an AWGN channel, the received signal is

$$r(t) = \sum_{k=1}^{N_u} A_k s^{(k)}(t - \tau_k) + n(t) \tag{2.9}$$

where $n(t)$ is the additive noise with two-sided power spectral density $\frac{N_0}{2}$, $\{A_k\}_{k=1}^{N_u}$ represent the channel attenuation for all transmitted signals, and $\{\tau_k\}_{k=1}^{N_u}$ represent time shifts which account for user asynchronism for the N_u signals.

Consider using a conventional single-user matched filter or correlation receiver to coherently demodulate the desired user signal in an asynchronous system. The single-user UWB receiver is shown in Fig. 2.2 without RF hardware. Assume $s^{(1)}(t)$ to be the desired signal and $d_0^{(1)}$ to be transmitted. Without loss of generality, we will further assume $c_j^{(1)} = 0$, for all j [45]. All the other $N_u - 1$ signals are interference signals. Assuming perfect synchronization with the reference signal, the single-user correlation receiver computes the decision statistic

$$r = \sqrt{\frac{N_s}{E_b}} \sum_{j=0}^{N_s-1} \int_{jT_f}^{(j+1)T_f} r(t)v(t - \tau_1 - jT_f)dt \tag{2.10}$$

where $v(t)$ is the correlation template waveform, which takes different forms in the TH-PPM and TH-BPSK UWB systems correspondingly.

The receiver decision statistic in (2.10) can be rewritten as

$$r = S + I + n \tag{2.11}$$

where S represents the desired signal component, I is the multiple access interference from the $N_u - 1$ active users and the last term n is the component due to background noise.

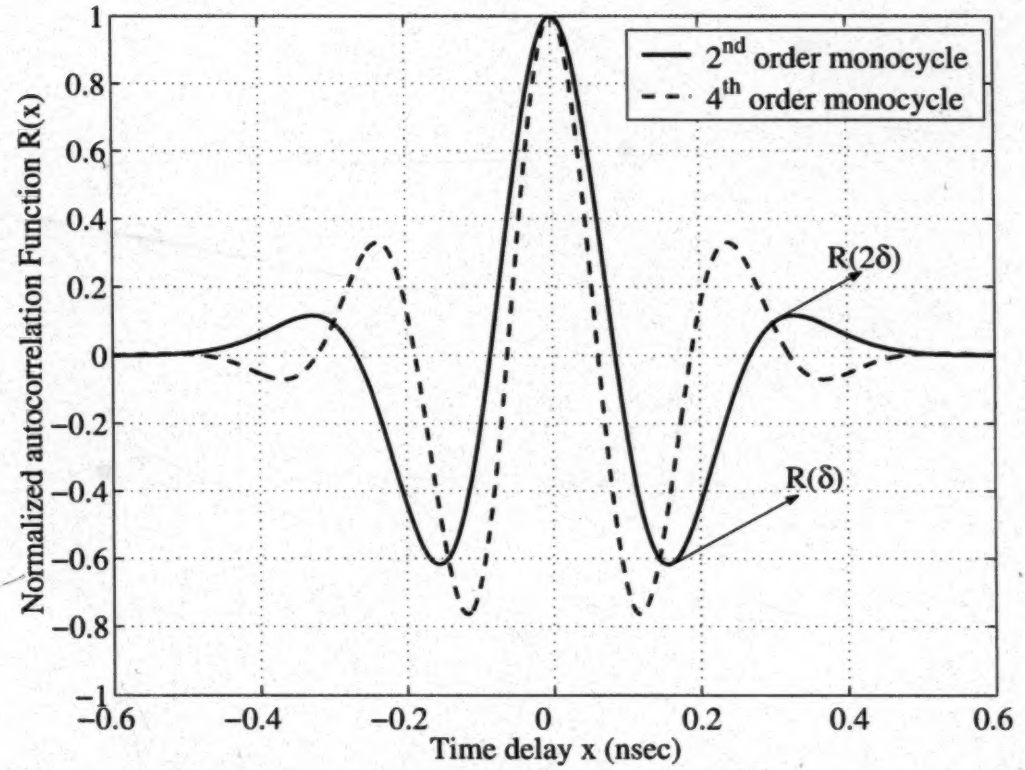

Fig. 2.1. Autocorrelation functions of the 2^{nd}-order and 4^{th}-order Gaussian monocycles as a function of time.

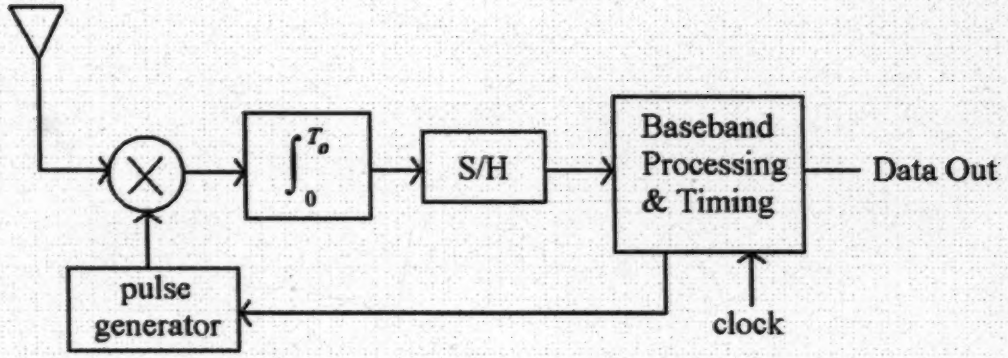

Fig. 2.2. The structure of UWB correlation receiver [7].

The mean of the noise term, n, can be obtained as

$$\begin{aligned}\mathbb{E}[n] &= \mathbb{E}\left[\sqrt{\frac{N_s}{E_b}}\sum_{j=0}^{N_s-1}\int_{jT_f}^{(j+1)T_f} n(t)v(t-\tau_1-jT_f)dt\right] \\ &= \sqrt{\frac{N_s}{E_b}}\sum_{j=0}^{N_s-1}\int_{jT_f}^{(j+1)T_f}\mathbb{E}\left[n(t)\right]v(t-\tau_1-jT_f)dt \\ &= 0 \end{aligned} \tag{2.12}$$

where $\mathbb{E}[\cdot]$ represents expectation, and the variance is

$$\begin{aligned}\mathrm{var}[n] &= \mathbb{E}\left[n^2\right] \\ &= \frac{N_s}{E_b}\sum_{i=0}^{N_s-1}\sum_{j=0}^{N_s-1}\int_{iT_f}^{(i+1)T_f}\int_{jT_f}^{(j+1)T_f}\mathbb{E}\left[n(s)n(t)\right]\mathbb{E}\left[v(s-\tau_1-iT_f)v(t-\tau_1-jT_f)\right]dtds \\ &= \frac{N_s}{E_b}\sum_{i=0}^{N_s-1}\sum_{j=0}^{N_s-1}\int_{iT_f}^{(i+1)T_f}\int_{jT_f}^{(j+1)T_f}\frac{N_0}{2}\delta(s-t)\mathbb{E}\left[v(s-\tau_1-iT_f)v(t-\tau_1-jT_f)\right]dtds \\ &= \frac{N_sN_0}{2E_b}\sum_{j=0}^{N_s-1}\int_{jT_f}^{(j+1)T_f}\mathbb{E}\left[v^2(t)\right]dt \\ &= \frac{N_s^2N_0}{2E_b}\int_{-\infty}^{\infty}v^2(t)dt \end{aligned} \tag{2.13}$$

where the last equation comes from the fact that the relationship between the frame width, T_f, and the pulse duration, T_p, satisfies $T_f >> T_p$.

In general, the exact analysis of I is unwieldy. Therefore, several approximation methods were ultilized to simplify the analysis of MAI.

2.3 Approximation Methods

2.3.1 Analysis based on Gaussian Approximation

The most widely adopted method in the analysis of MAI is the Gaussian approximation. In the Gaussian approximation, a central limit theorem is invoked to approximate the MAI as a Gaussian distributed random variable (RV), as the addtional background Gaussian noise.

In the Gaussian approximation, the variance of the MAI averaged over all operating conditions is used to calculate the equivalent noise power. MAI is expressed as

$$\begin{aligned} I &= \sqrt{\frac{N_s}{E_b}} \sum_{j=0}^{N_s-1} \int_{jT_f}^{(j+1)T_f} \sum_{k=2}^{N_u} A_k s^{(k)}(t-\tau_k) v(t-\tau_1-jT_f) dt \\ &= \sum_{k=2}^{N_u} A_k I^{(k)}. \end{aligned} \tag{2.14}$$

It has been shown in [14] that I has zero-mean, and its variance is given by

$$\begin{aligned} \mathrm{var}[I] &= \mathbb{E}[I^2] \\ &= \sum_{k=2}^{N_u} A_k^2 \mathbb{E}\left[\left(I^{(k)}\right)^2\right] \\ &= \frac{N_s}{T_f} \int_{-\infty}^{\infty} \left[\int_{-\infty}^{\infty} p(x-s)v(x)dx\right]^2 ds \sum_{k=2}^{N_u} A_k^2. \end{aligned} \tag{2.15}$$

Therefore, the average BER of the desired user is approximiated by

$$P_e \approx Q\left(\sqrt{\frac{S^2}{\sigma_n^2 + \mathrm{var}[I]}}\right) \tag{2.16}$$

where $Q(\cdot)$ is the Q-function defined as [35]

$$Q(x) = \frac{1}{\sqrt{2\pi}} \int_x^{\infty} e^{-t^2/2} dt, \;\; x \geq 0. \tag{2.17}$$

The Gaussian approximation is widely used because of its simplicity. In Section 2.7, we will assess the accurancy of the Gaussian approximation using the exact analysis which does not rely on CLT.

2.3.2 Analysis based on Gaussian Quadrature Rules

In [45], the bit error rates of TH-PPM systems in the presence of multiple access interference on an AWGN channel were evaluated based on Gaussian quadrature rules instead of the Gaussian approximation.

Using the decision statistic shown as (2.11) and conditioning on the MAI, the error probability of UWB in multiple access interference can be written as

$$P_e = \mathbb{E}_I \left[Q\left(\frac{S+I}{\sigma_n} \right) \right] \tag{2.18}$$

where $I = \sum_{k=2}^{N_u} A_k I^{(k)}$ is the MAI interference term. The exact computation of (2.18) requires the evaluation of the probability density function (pdf) of the MAI and the computation of the average by solving the associated integral.

It is known that the pdf of the MAI is difficult to obtain for TH-PPM systems. The GQR method was proposed as a more practical approach in [45]. According to the GQR technique, the integral of (2.18) can be computed in the following way:

$$\int_a^b g(x) f_X(x) dx = \sum_{i=1}^{N} w_i g(x_i) + E_N \tag{2.19}$$

where $\{x_i\}$ and $\{w_i\}$ are the abscissa and the weights associated to the quadrature rule, depending on the pdf $f_X(x)$ and the given interval of integration, and E_N is the truncation error. The knowledge of the first $2N-1$ moments of X is required to generate a GQR formula based on N points.

The first $2N-1$ moments of I in (2.18) can be evaluated with the consideration of the independence between random variables $I^{(k)}, \forall k$. Then, BER can be calculated from (2.18) (2.19) with the GQR technique using these moments. The evaluation of P_e was carried out in two steps:

- evaluation of the conditional probability $P_{e|\underline{\tau}}$ using the GQR technique previously described. $\underline{\tau} = (\tau_1, \ldots, \tau_{N_u})$ denotes the time shift vector of which each element accounts for user asynchronism as described in Section 2.1.1.

- computation of bit error rates P_e with a semi-analytic method. BER was obtained from $P_{e|\underline{\tau}}$ by averaging over 1000 realizations of the vector $\underline{\tau}$.

This composite approach, based on a GQR approximation of a definite integral, does not rely on CLT. However, the computational complexity of the GQR restricts the application of this method and the semi-analytical step using simulation is neither exact nor analytical.

2.4 Analysis of TH-PPM system

The performance analysis of the TH-PPM UWB system with multiple access interference must be based on the decision statistic used at the receiver. The original proposal for UWB pulse position modulation systems in [9] considers information bits $d_i^{(k)} \in \{0, 1\}$. In this modulation scheme, no additional time shift modulates the pulse $p(t)$ when the data bit is 0, and a time shift δ is added to $p(t)$ when the data bit is 1. This scheme is called a type-A TH-PPM UWB system in this paper. Reference [12] uses antipodal data bits $\{1, -1\}$ in the PPM system. In this case, the pulse train is modulated by delaying or advancing individual pulses in time according to a given reference. The pulse $p(t)$ is delayed by δ when the data bit is -1, and $p(t)$ is advanced by δ when the data bit is 1. This scheme, here called a type-B TH-PPM system, is also examined in this paper to make our analysis of TH-PPM systems complete. Corresponding to the different modulation schemes used in these two TH-PPM systems, different correlation template waveforms $v(t)$ are used.

2.4.1 Type-A TH-PPM

In this modulation scheme, the template waveform $v(t)$ has the form [14]

$$v(t) = p(t) - p(t - \delta). \tag{2.20}$$

Define the correlation of the template $v(t)$ with a time-shifted pulse $p(t)$ as

$$\tilde{R}(x) = \int_{-\infty}^{\infty} p(t - x)v(t)dt \tag{2.21}$$

and from (2.6), (2.20) and (2.21), we obtain

$$\tilde{R}(x) = R(x) - R(x - \delta). \tag{2.22}$$

Substituting (2.9) into (2.10) yields

$$r = S + I + n \tag{2.23}$$

where n is a Gaussian random variable with zero mean and variance

$$\begin{aligned}
\sigma_n^2 &= \mathbb{E}\left[n^2\right] \\
&= \frac{N_s^2 N_0}{2E_b} \int_{-\infty}^{\infty} v^2(t)dt \\
&= \frac{N_s^2 N_0}{E_b} [1 - R(-\delta)] \\
&= \frac{N_s^2 N_0}{E_b} \tilde{R}(0)
\end{aligned} \tag{2.24}$$

S is the contribution to the decision statistic r depending on user 1's useful signal bit $d_0^{(1)}$, given by

$$S = \pm A_1 N_s \tilde{R}(0) \tag{2.25}$$

and I is the total MAI due to all $N_u - 1$ interfering signals, given by

$$I = \sqrt{\frac{N_s}{E_b}} \sum_{k=2}^{N_u} \sum_{j=0}^{N_s-1} \int_{jT_f}^{(j+1)T_f} A_k s^{(k)}(t - \tau_k) v\left(t - \tau_1 - jT_f\right) dt. \tag{2.26}$$

We model the difference of time shifts for user asynchronism as [14, eqn. (55)]

$$\tau_k - \tau_1 = j_k T_f + \alpha_k, \quad -T_f/2 \leq \alpha_k < T_f/2 \tag{2.27}$$

where j_k is the value of the time difference $\tau_k - \tau_1$ rounded to the nearest frame time, and α_k is uniformly distributed on $[-T_f/2, T_f/2)$. [1]. Based on the assumption [14, eqn. (57)], which is rewritten as

$$N_h T_c < \frac{T_f}{2} - 2T_p \tag{2.28}$$

we then note that only one pulse from each interfering user in each frame contributes to the interference term. We can rewrite (2.26) in the form [14, eqn. (76)]

$$I = \sum_{k=2}^{N_u} \sum_{j=0}^{N_s-1} \int_{-\infty}^{\infty} A_k p\left(x - \alpha_k - c_j^{(k)} T_c - d^{(k)}_{\lfloor (j+j_k)/N_s \rfloor}\delta\right) v(x)dx. \tag{2.29}$$

Considering the interfering signal $d^{(k)}_{\lfloor (j+j_k)/N_s \rfloor}$ may change sign during the transmission time of $d_0^{(1)}$, we rewrite (2.29) as

$$I = \sum_{k=2}^{N_u} A_k \left[\sum_{j=0}^{\gamma_k - 1} \tilde{R}\left(\tilde{\Theta}_{0,j}^{(k)}\right) + \sum_{j=\gamma_k}^{N_s-1} \tilde{R}\left(\tilde{\Theta}_{1,j}^{(k)}\right)\right] \tag{2.30}$$

where

$$\tilde{\Theta}_{0,j}^{(k)} = \alpha_k + c_j^{(k)} T_c + d_0^{(k)}\delta \tag{2.31}$$

and

$$\tilde{\Theta}_{1,j}^{(k)} = \alpha_k + c_j^{(k)} T_c + d_1^{(k)}\delta. \tag{2.32}$$

$d_0^{(k)}$ and $d_1^{(k)}$ represent the two adjacent bits of the kth signal that overlap with the transmission time of $d_0^{(1)}$, and γ_k is uniform over $[0, N_s - 1]$ according to the definition of j_k in (2.27).

The probability density function of $\tilde{\Theta}_{0,j}^{(k)}$ conditioned on $d_0^{(k)}$ for a given α_k becomes

$$f_{\tilde{\Theta}_0|d,\alpha}\left(\tilde{\theta}|d_0^{(k)} = d, \alpha_k = \alpha\right) = \frac{1}{N_h} \sum_{h=0}^{N_h-1} \delta_D(\tilde{\theta} - hT_c - \delta d - \alpha) \tag{2.33}$$

[1] This assumption corresponds to the assumption made on $\alpha_{1,k}$ in [14, eqn. (55)], and is made for analytical simplicity.

where $\delta_D(\cdot)$ is the Dirac delta function. The CHF of $\tilde{R}(\tilde{\Theta}_{0,j}^{(k)})$ conditioned on $d_0^{(k)}$ and α_k can be written as

$$\begin{aligned}\Phi_{\tilde{R}_0|d,\alpha}(\omega) &= \mathbb{E}\left[e^{j\omega\tilde{R}_0}\middle| d_0^{(k)} = d, \alpha_k = \alpha\right] \\ &= \int_{-\infty}^{\infty} e^{j\omega\tilde{R}\left(\tilde{\Theta}_{0,j}^{(k)}\right)} f_{\tilde{\Theta}_0|d,\alpha}\left(\tilde{\theta} \mid d_0^{(k)} = d, \alpha_k = \alpha\right) d\tilde{\theta} \\ &= \frac{1}{N_h}\sum_{h=0}^{N_h-1} e^{j\omega\tilde{R}(\alpha+hT_c+\delta d)} \end{aligned} \tag{2.34}$$

where $\mathbb{E}[\cdot]$ denotes expectation. Further, we define $X^{(k)} = \sum_{j=0}^{\gamma_k-1}\tilde{R}\left(\tilde{\Theta}_{0,j}^{(k)}\right)$ and $Y^{(k)} = \sum_{j=\gamma_k}^{N_s-1}\tilde{R}\left(\tilde{\Theta}_{1,j}^{(k)}\right)$; then

$$\begin{aligned} I &= \sum_{k=2}^{N_u} A_k I^{(k)} \\ &= \sum_{k=2}^{N_u} A_k\left(X^{(k)} + Y^{(k)}\right). \end{aligned} \tag{2.35}$$

The conditional CHF of $X^{(k)}$ is obtained as

$$\begin{aligned}\Phi_{X^{(k)}|d,\alpha,\gamma}(\omega) &= \mathbb{E}\left[e^{j\omega\sum_{j=0}^{\gamma_k-1}\tilde{R}\left(\tilde{\Theta}_{0,j}^{(k)}\right)}\middle| d_0^{(k)} = d, \alpha_k = \alpha, \gamma_k = \gamma\right] \\ &= \prod_{j=0}^{\gamma-1}\Phi_{\tilde{R}_0|d,\alpha}(\omega) \\ &= \left(\frac{1}{N_h}\sum_{h=0}^{N_h-1} e^{j\omega\tilde{R}(\alpha+hT_c+\delta d)}\right)^{\gamma} \end{aligned} \tag{2.36}$$

where the second equality follows from the fact that $\tilde{R}\left(\tilde{\Theta}_{0,j}^{(k)}\right)$, $j = 0, ..., \gamma_k - 1$, are independent when conditioned on $d_0^{(k)}$ and α_k. We note that when N_hT_c is small compared to T_f (when N_hT_c is not very large compared to the pulse duration T_p), the assumption that the interference is independent in different frames of the bit is not rigorously correct and then (2.36) is an approximation. In the alternative, the analysis is valid under the assumption that the pseudorandom time-hopping sequence is random rather than deterministic. A similar assumption has been used in many

DS-CDMA system analyses [56]. Then, the CHF of $X^{(k)}$ conditioned on α_k and γ_k can be obtained using the theorem of total probability as

$$\begin{aligned}\Phi_{X^{(k)}|\alpha,\gamma}(\omega) &= \Phi_{X^{(k)}|0,\alpha,\gamma}(\omega)\Pr(d=0) + \Phi_{X^{(k)}|1,\alpha,\gamma}(\omega)\Pr(d=1) \\ &= \frac{1}{2N_h^{\gamma}}\left[\left(\sum_{h=0}^{N_h-1} e^{j\omega\tilde{R}(\alpha+hT_c)}\right)^{\gamma} + \left(\sum_{h=0}^{N_h-1} e^{j\omega\tilde{R}(\alpha+hT_c+\delta)}\right)^{\gamma}\right]. \end{aligned} \tag{2.37}$$

Similarly, the CHF of $Y^{(k)}$ conditioned on α_k and γ_k can be obtained as

$$\Phi_{Y^{(k)}|\alpha,\gamma}(\omega) = \frac{1}{2N_h^{N_s-\gamma}}\left[\left(\sum_{h=0}^{N_h-1} e^{j\omega\tilde{R}(\alpha+hT_c)}\right)^{N_s-\gamma} + \left(\sum_{h=0}^{N_h-1} e^{j\omega\tilde{R}(\alpha+hT_c+\delta)}\right)^{N_s-\gamma}\right]. \tag{2.38}$$

For given k, it can be shown that the RV's $X^{(k)}$ and $Y^{(k)}$ are independent, which results from the independence of the data bits (d_0 and d_1), and the independence of the chip sequences (with distinct chip index, j). Then, the CHF of $I^{(k)}$ conditioned on α_k and γ_k is given by

$$\Phi_{I^{(k)}|\alpha,\gamma}(\omega) = \Phi_{X^{(k)}|\alpha,\gamma}(\omega)\Phi_{Y^{(k)}|\alpha,\gamma}(\omega). \tag{2.39}$$

Considering the uniform distribution of γ_k, we obtain the CHF of $I^{(k)}$ conditioned on α_k as

$$\Phi_{I^{(k)}|\alpha}(\omega) = \frac{1}{N_s}\sum_{\gamma=0}^{N_s-1}\left[\Phi_{X^{(k)}|\alpha,\gamma}(\omega)\Phi_{Y^{(k)}|\alpha,\gamma}(\omega)\right]. \tag{2.40}$$

Averaging out α_k, we obtain the CHF of the kth interferer as

$$\Phi_{I^{(k)}}(\omega) = \frac{1}{T_f}\int_{-T_f/2}^{T_f/2}\Phi_{I^{(k)}|\alpha}(\omega)d\alpha. \tag{2.41}$$

Owing to the independence of the interfering components, the CHF of the total interference is

$$\Phi_I(\omega) = \prod_{k=2}^{N_u}\Phi_{I^{(k)}}(A_k\omega). \tag{2.42}$$

2.4.2 Type-B TH-PPM

If the antipodal data bits $d_i^{(k)}$ are used in TH-PPM systems, the correlator template waveform has to take the form

$$v(t) = p(t-\delta) - p(t+\delta) \tag{2.43}$$

which is modified from the original template waveform (2.20). Then, the correlation of $v(t)$ with a time shifted pulse $p(t)$ can be written as

$$\begin{aligned}\hat{R}(x) &= \int_{-\infty}^{\infty} p(t-x)v(t)dt \\ &= R(x-\delta) - R(x+\delta)\end{aligned} \tag{2.44}$$

where $R(x)$ is the autocorrelation function of $p(t)$ given in (2.6).

Following the same derivation as in Section A, we have the decision statistic

$$r_{anti} = S_{anti} + I_{anti} + n_{anti} \tag{2.45}$$

where n_{anti} is a Gaussian random variable with zero mean and variance

$$\begin{aligned}\sigma_{n_{anti}}^2 &= \frac{N_0 N_s^2}{2E_b}\int_{-\infty}^{\infty} v^2(t)dt \\ &= \frac{N_0 N_s^2}{E_b}[1 - R(2\delta)] \\ &= \frac{N_0 N_s^2}{E_b}\hat{R}(\delta)\end{aligned} \tag{2.46}$$

$S = d_0^{(1)} A_1 N_s \hat{R}(\delta)$ is a random variable depending on user 1's signal bit $d_0^{(1)}$, and I is given by

$$I = \sum_{k=2}^{N_u} A_k \left[\sum_{j=0}^{\gamma_k - 1} \hat{R}\left(\hat{\Theta}_{0,j}^{(k)}\right) + \sum_{j=\gamma_k}^{N_s-1} \hat{R}\left(\hat{\Theta}_{1,j}^{(k)}\right)\right] \tag{2.47}$$

where the definition of $\hat{\Theta}_{0,j}^{(k)}$ and $\hat{\Theta}_{1,j}^{(k)}$ is the same as in (2.31) and (2.32), respectively.

Similar to the analysis presented in Section A, we find the CHF of $I_{anti}^{(k)}$ conditioned

on α_k and γ_k,

$$\Phi_{I_{anti}^{(k)}|\alpha,\gamma}(\omega) = \frac{1}{4N_h^{N_s}} \left[\left(\sum_{h=0}^{N_h-1} e^{j\omega\hat{R}(\alpha+hT_c-\delta)} \right)^{\gamma} + \left(\sum_{h=0}^{N_h-1} e^{j\omega\hat{R}(\alpha+hT_c+\delta)} \right)^{\gamma} \right] \times \left[\left(\sum_{h=0}^{N_h-1} e^{j\omega\hat{R}(\alpha+hT_c-\delta)} \right)^{N_s-\gamma} + \left(\sum_{h=0}^{N_h-1} e^{j\omega\hat{R}(\alpha+hT_c+\delta)} \right)^{N_s-\gamma} \right] \quad (2.48)$$

and the CHF for $I_{anti}^{(k)}$ is

$$\Phi_{I_{anti}^{(k)}}(\omega) = \frac{1}{T_f N_s} \int_{-T_f/2}^{T_f/2} \sum_{\gamma=0}^{N_s-1} \Phi_{I_{anti}^{(k)}|\alpha,\gamma}(\omega) d\alpha. \quad (2.49)$$

The CHF of the total interference is again given by

$$\Phi_{I_{anti}}(\omega) = \prod_{k=2}^{N_u} \Phi_{I_{anti}^{(k)}}(A_k\omega). \quad (2.50)$$

2.5 Analysis of TH-BPSK system

The template waveform used in TH-BPSK systems is the pulse $p(t)$ [51]. The decision statistic r_{BPSK} is then

$$r_{BPSK} = S_{BPSK} + I_{BPSK} + n_{BPSK} \quad (2.51)$$

where n_{BPSK} is a Gaussian noise with zero mean and variance

$$\sigma^2_{n_{BPSK}} = \frac{N_0 N_s^2}{2E_b} \int_{-\infty}^{\infty} p^2(t) dt = \frac{N_0 N_s^2}{2E_b} \quad (2.52)$$

$S_{BPSK} = d_0^{(1)} A_1 N_s$ depends on user 1's useful signal bit $d_0^{(1)}$, and I_{BPSK} is the total MAI in the TH-BPSK UWB system, given by

$$I_{BPSK} = \sum_{k=2}^{N_u} A_k \left[\sum_{j=0}^{\gamma_k-1} d_0^{(k)} R\left(\Theta_j^{(k)}\right) + \sum_{j=\gamma_k}^{N_s-1} d_1^{(k)} R\left(\Theta_j^{(k)}\right) \right] \quad (2.53)$$

where $\Theta_j^{(k)} = \alpha_k + c_j^{(k)} T_c$. Similar to (2.33), the pdf of $\Theta_j^{(k)}$ conditioned on α_k is

$$f_{\Theta|\alpha}(\theta \mid \alpha_k = \alpha) = \frac{1}{N_h} \sum_{h=0}^{N_h-1} \delta_D(\theta - hT_c - \alpha). \tag{2.54}$$

Then, the CHF of $R\left(\Theta_j^{(k)}\right)$ conditioned on α_k can be written as

$$\begin{aligned}
\Phi_{R|\alpha}(\omega) &= \mathbb{E}\left[e^{j\omega R(\Theta_j^{(k)})} \middle| \alpha_k = \alpha\right] \\
&= \int_{-\infty}^{\infty} e^{j\omega R\left(\Theta_j^{(k)}\right)} f_{\Theta|\alpha}(\theta \mid \alpha_k = \alpha)\, d\theta \\
&= \frac{1}{N_h} \sum_{h=0}^{N_h-1} e^{j\omega R(\alpha + hT_c)}.
\end{aligned} \tag{2.55}$$

Define

$$\begin{aligned}
I_{BPSK} &= \sum_{k=2}^{N_u} A_k I_{BPSK}^{(k)} \\
&= \sum_{k=2}^{N_u} A_k \left[X_{BPSK}^{(k)} + Y_{BPSK}^{(k)}\right]
\end{aligned} \tag{2.56}$$

where

$$X_{BPSK}^{(k)} = \sum_{j=0}^{\gamma_k-1} d_0^{(k)} R\left(\Theta_j^{(k)}\right) \tag{2.57}$$

and

$$Y_{BPSK}^{(k)} = \sum_{j=\gamma_k}^{N_s-1} d_1^{(k)} R\left(\Theta_j^{(k)}\right). \tag{2.58}$$

The CHF of $X_{BPSK}^{(k)}$ conditioned on α_k and γ_k is obtained as

$$\Phi_{X^{(k)}|\alpha,\gamma} = \frac{1}{2N_h{}^{\gamma}} \left[\left(\sum_{h=0}^{N_h-1} e^{j\omega R(\alpha+hT_c)}\right)^{\gamma} + \left(\sum_{h=0}^{N_h-1} e^{-j\omega R(\alpha+hT_c)}\right)^{\gamma}\right] \tag{2.59}$$

and the conditional CHF of $Y_{BPSK}^{(k)}$ can be obtained similarly as

$$\Phi_{Y^{(k)}|\alpha,\gamma} = \frac{1}{2N_h{}^{N_s-\gamma}} \left[\left(\sum_{h=0}^{N_h-1} e^{j\omega R(\alpha+hT_c)}\right)^{N_s-\gamma} + \left(\sum_{h=0}^{N_h-1} e^{-j\omega R(\alpha+hT_c)}\right)^{N_s-\gamma}\right]. \tag{2.60}$$

Based on the conditional CHF's of $X_{BPSK}^{(k)}$ and $Y_{BPSK}^{(k)}$, the CHF of $I_{BPSK}^{(k)}$ conditioned on α_k and γ_k is given by

$$\Phi_{I_{BPSK}^{(k)}|\alpha,\gamma}(\omega) = \Phi_{X^{(k)}|\alpha,\gamma}(\omega)\Phi_{Y^{(k)}|\alpha,\gamma}(\omega). \tag{2.61}$$

Under the assumptions of uniformly distributed $\{\alpha_k\}_{k=2}^{N_u}$ and $\{\gamma_k\}_{k=2}^{N_u}$, we can obtain the CHF of $I_{BPSK}^{(k)}$, which is

$$\Phi_{I_{BPSK}^{(k)}}(\omega) = \frac{1}{T_f N_s}\int_{-T_f/2}^{T_f/2}\sum_{\gamma=0}^{N_s-1}\Phi_{X^{(k)}|\alpha,\gamma}(\omega)\Phi_{Y^{(k)}|\alpha,\gamma}(\omega)d\alpha. \tag{2.62}$$

Finally, the CHF of the total interference in the TH-BPSK system is given by

$$\Phi_{I_{BPSK}}(\omega) = \prod_{k=2}^{N_u}\Phi_{I_{BPSK}^{(k)}}(A_k\omega). \tag{2.63}$$

2.6 Bit Error Probability

In this section, we will determine expressions for the bit error probabilities of the TH-PPM and TH-BPSK UWB systems based on the previous analysis. The decision rule for the type-A TH-PPM system is [14]

$$\begin{aligned} r > 0 &\Rightarrow \text{“0”} \\ r \le 0 &\Rightarrow \text{“1”} \end{aligned}$$

and the decision rule for the antipodal type-B TH-PPM and TH-BPSK UWB systems is [51]

$$\begin{aligned} r > 0 &\Rightarrow \text{“1”} \\ r \le 0 &\Rightarrow \text{“-1”}. \end{aligned}$$

Owing to the symmetry of the MAI and the noise [14], the average probability of error for the type-A TH-PPM system is given by

$$\begin{aligned} P_e &= \Pr(r \le 0 \mid d = 0) \\ &= \Pr(A_1 N_s \tilde{R}(0) + I + n \le 0). \end{aligned} \tag{2.64}$$

and the BER for the type-B TH-PPM and TH-BPSK systems is

$$P_e = \Pr(r \leq 0 \mid d = 1). \tag{2.65}$$

Define $\Lambda = I + n$; then, using the independence of the MAI and the background noise, the CHF of Λ can be expressed as the product of the CHF of the interfering signals I and the CHF of the Gaussian noise as

$$\Phi_\Lambda(\omega) = \Phi_I(\omega)\Phi_n(\omega) \tag{2.66}$$

where $\Phi_n(\omega) = e^{\frac{-\sigma_n^2\omega^2}{2}}$ is the CHF for the noise term n and $\Phi_I(\omega)$ is the CHF of the total interference in the TH-PPM or TH-BPSK system.

Taking the inverse transform of the characteristic function [57, eqn. (3-23)], the cumulative density function (CDF) of Λ can be expressed as

$$F_\Lambda(\lambda) = \frac{1}{2} + \frac{1}{\pi}\int_0^\infty \frac{\sin(\lambda\omega)}{\omega}\Phi_\Lambda(\omega)d\omega \tag{2.67}$$

and the BER of the type-A TH-PPM is given by

$$\begin{aligned} P_e &= \Pr\left(I + n + A_1 N_s \tilde{R}(0) \leq 0\right) \\ &= 1 - F_\Lambda\left(A_1 N_s \tilde{R}(0)\right) \\ &= \frac{1}{2} - \frac{1}{\pi}\int_0^\infty \frac{\sin\left[A_1 N_s \tilde{R}(0)\omega\right]}{\omega}\Phi_I(\omega)e^{-\sigma_n^2\omega^2/2}d\omega. \end{aligned} \tag{2.68}$$

Then, the average probability of error for the desired user in the type-B TH-PPM and TH-BPSK UWB systems is obtained, respectively, as

$$\begin{aligned} P_{e_{anti}} &= \Pr\left(I + n + A_1 N_s \hat{R}(\delta) \leq 0\right) \\ &= 1 - F_\Lambda\left(A_1 N_s \hat{R}(\delta)\right) \\ &= \frac{1}{2} - \frac{1}{\pi}\int_0^\infty \frac{\sin\left[A_1 N_s \hat{R}(\delta)\omega\right]}{\omega}\Phi_{I_{anti}}(\omega)e^{-\sigma_{n_{anti}}^2\omega^2/2}d\omega \end{aligned} \tag{2.69}$$

and

$$\begin{aligned} P_{e_{BPSK}} &= \Pr\left(I + n + A_1 N_s \leq 0\right) \\ &= 1 - F_\Lambda\left(A_1 N_s\right) \\ &= \frac{1}{2} - \frac{1}{\pi}\int_0^\infty \frac{\sin(A_1 N_s \omega)}{\omega} \Phi_{I_{BPSK}}(\omega) e^{-\sigma_{n_{BPSK}}^2 \omega^2/2} d\omega. \end{aligned} \tag{2.70}$$

Note that (2.68), (2.69) and (2.70) are exact expressions for the average bit error probabilities of the TH-PPM and TH-BPSK UWB systems with $N_u - 1$ similar interferers having arbitrary energies.

2.7 Numerical Results and Comparisons

Examination of (2.68) and (2.41), (2.69) and (2.49), or (2.70) and (2.62) indicates that a double-integral calculation is need for computing the BER of TH-UWB systems. This double integration is performed numerically, but is not problematic. Our trials indicated that simple numerical integration techniques can be used to obtain the BER to any reasonable desired accuracy. All the numerical results in this paper were computed using the composite Simpson's rule. In addition, Monte Carlo simulation was used to validate our analytical derivations. We simulated the decision statistics including eqns. (2.23), (2.45) and (2.51) using Matlab. A large enough number of trials was used for each point to reduce the statistical scatter of the point to less than what can be discerned on a full size ($8\frac{1}{2} \times 11$ inch) plot. This number of trials is about 100 to 1000 times the inverse of the probability of error. Uniformly distributed RV's and Gaussian distributed RV's used in the simulation of the decision statistics were generated using random number generators provided by Matlab.

First, we compare the exact BER's of the TH-PPM and TH-BPSK UWB systems with results obtained from simulations and the Gaussian approximation. In addition, the performance of TH-PPM and TH-BPSK systems will be evaluated for different pulse parameters. Some comparisons between two different UWB modulation systems in terms of BER are presented as well. Most of the numerical results presented in

TABLE 2.1

Parameters of the Example TH-PPM and TH-BPSK systems

Parameter	Notation	2^{nd} and 4^{th} order monocycles
Time Normalization Factor	τ_p	0.2877 ns
Impulse Width	T_p	≈ 0.7 ns
Frame Width	T_f	50 (100) ns
PPM Delay	δ	0.15 ns
Chip Width	T_c	0.9 ns
Number of Users	N_u	8(50)
Number of Chips per Frame	N_h	8(50)
Repetition Code Length	N_s	2, 4, 16, 50 or 100

this paper are based on the analysis using the 2^{nd}-order Gaussian monocycle. Results for the 4^{th}-order monocycle are also provided here to show the effects of changing the pulse shape. The parameters of the example UWB systems are listed in Table 2.1 and follow [14] and [45].

Fig. 2.3 shows the accurate BER of the type-A TH-PPM system computed using the characteristic function method described in the previous section, as well as the BER's obtained by the Gaussian approximation and simulation. In our work, SNR is defined as $\frac{E_b}{N_0}$. As seen, the theoretical results and the simulation results are in excellent agreement. Fig. 2.3 also shows BER's obtained using the GA. It is seen that the GA is in good agreement with the exact analysis only for small SNR values, say SNR $\leq$ 6 dB. Furthermore, the GA fails to predict the error rate floor of the TH-PPM UWB system (caused by the interference) for large SNR values. Thus, the GA is not a reliable approximation. Indeed, when the SNR = 16 dB, the exact BER is 3.6×10^{-4} with $N_s = 2$, and the BER predicted from the GA is 2.6×10^{-9}, which underestimates the actual BER by over 5 orders of magnitude. Fig. 2.3 indicates

that the BER performance improves when the longer repetition code is used, as expected. Observe that the amount of the improvement can be less or more than the improvement predicted by the GA. For example, when the SNR = 9 dB, the amount of the improvement (between $N_s = 2$ and $N_s = 4$) due to the longer repetition code predicted by the GA is less than the actual improvement; when the SNR = 16 dB, the amount of improvement predicted by the GA is more than the actual improvement.

Fig. 2.4 shows the accurate BER results for the TH-BPSK system and the BER obtained from the GA and simulation as well. We observe, from our numerical results, that the BER estimates based on the GA also underestimate the accurate BER of the TH-BPSK system for medium and large SNR values. Similar to the results seen in Fig. 2.4, Fig. 2.4 shows that the GA fails to predict the error rate floor caused by the interference and that the GA can underestimate or overestimate the improvement obtained by using a longer repetition code.

In order to assess the accuracy of the GA at high values of N_s, we also provide numerical results for TH-UWB systems with $N_s = 16$, 50 and 100 shown in Figs. 2.5 and 2.6. Fig. 2.5 shows the accurate BER results for the TH-PPM system and the BER obtained from the GA for $N_s = 16$, 50 and 100. It is seen that the GA improves for the longer repetition codes in the sense that it is accurate for a wider range of values of SNR. For example, while the GA is highly accurate only for SNR $\leq$ 6 dB when $N_s = 2$, it is highly accurate for SNR $\leq$ 10 dB when $N_s = 100$. Nonetheless, the Gaussian approximiation still underestimates the BER's of TH-PPM systems at larger values of N_s. Similar behavior is also observed for the BER's of the TH-BPSK system with different values of N_s as indicated in Fig. 2.6. In the GA, the BER's are obtained by modeling the total MAI as a Gaussian distributed RV. In fact, we can show that the MAI is not Gaussian distributed. For small values of SNR, the background Gaussian noise n is dominant in the term $\Lambda = I + n$, and then Λ can be approximated as a Gaussian distributed RV. Therefore, the GA can provide good BER estimates for small SNR. On the other hand, when SNR is large, the interference I is dominant in the term Λ, and Λ cannot be approximated as a Gaussian distributed RV.

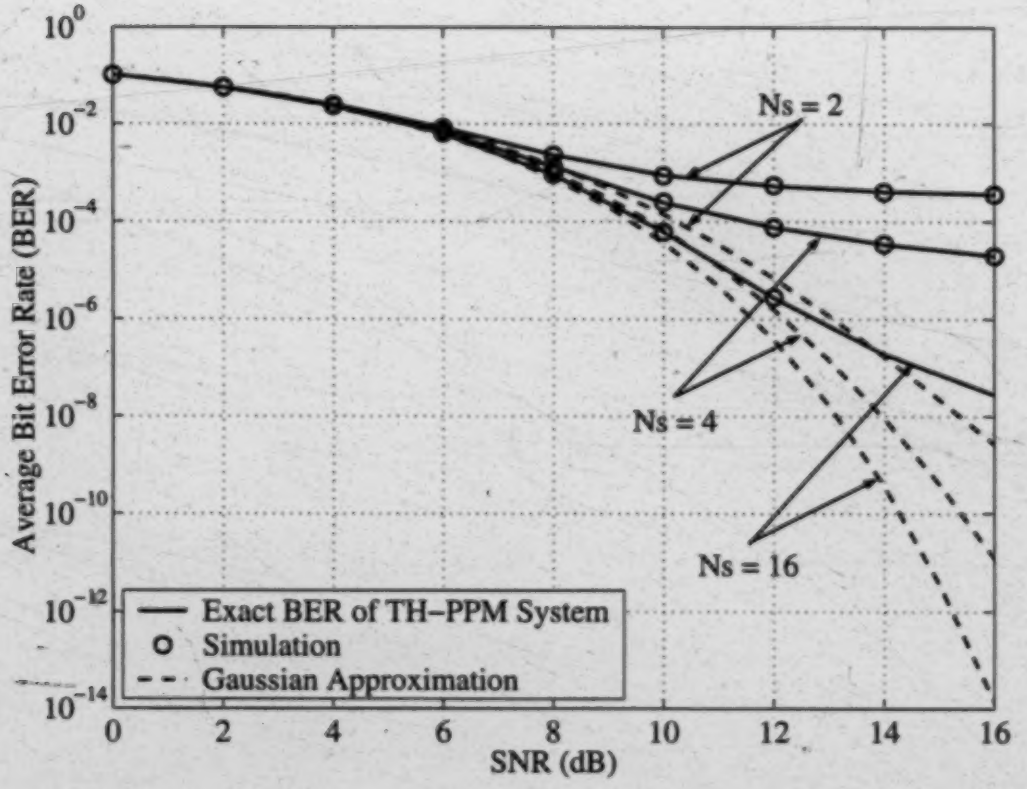

Fig. 2.3. Average BER of the TH-PPM UWB system versus SNR for a repetition code with $N_s = 2$, $N_s = 4$ and $N_s = 16$ assuming 7 asynchronous interferers.

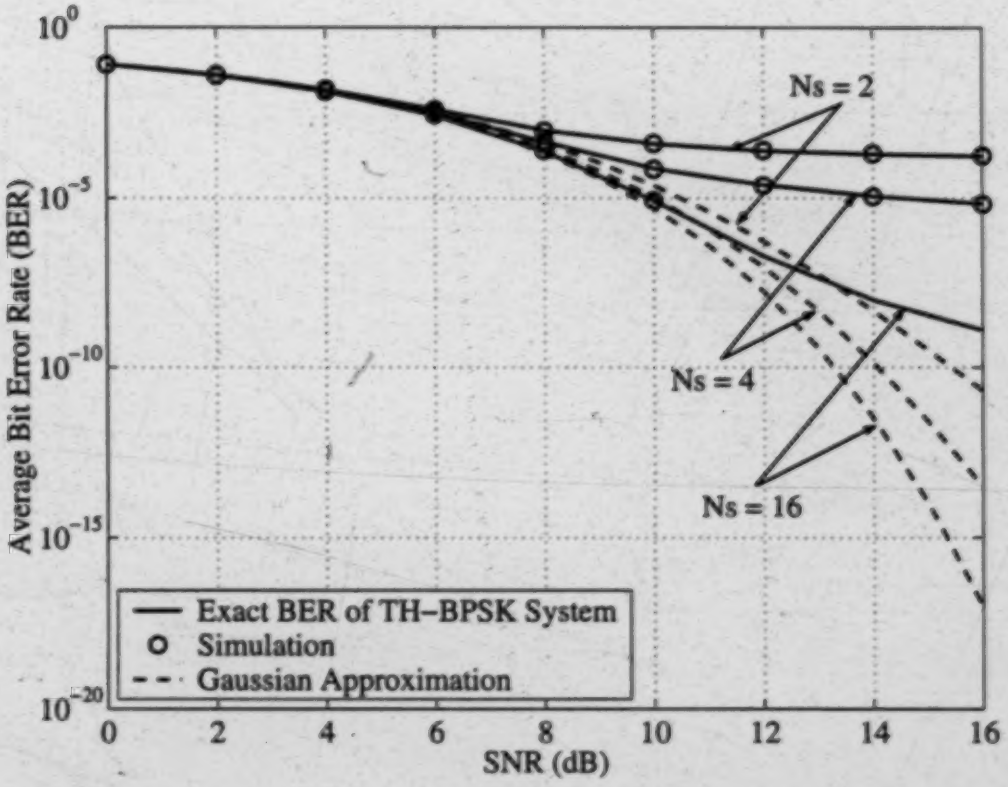

Fig. 2.4. Average BER of the TH-BPSK UWB system versus SNR for a repetition code with $N_s = 2$, $N_s = 4$ and $N_s = 16$ assuming 7 asynchronous interferers.

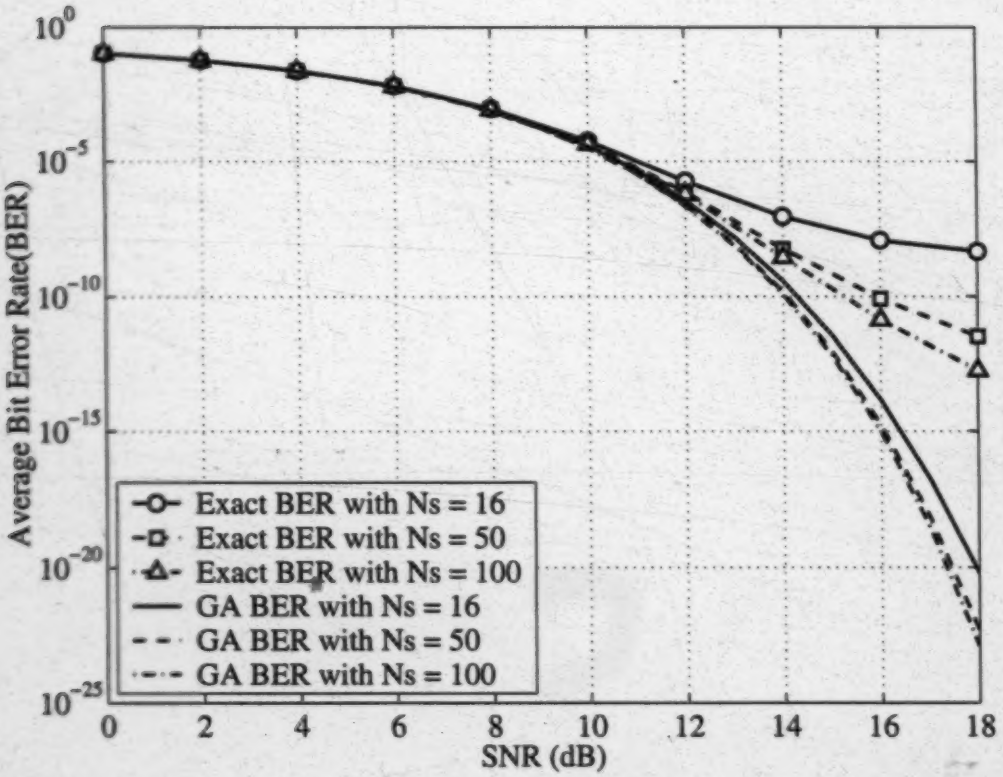
Average Bit Error Rate(BER)
SNR (dB)
Exact BER with Ns = 16
Exact BER with Ns = 50
Exact BER with Ns = 100
GA BER with Ns = 16
GA BER with Ns = 50
GA BER with Ns = 100

Fig. 2.5. Average BER of the TH-PPM UWB system versus SNR for a repetition code with $N_s = 16$, $N_s = 50$ and $N_s = 100$.

Thus, the GA fails to predict the actual BER's for large values of SNR as indicated in Figs. 2.3 -2.6.

In Fig. 2.7, the performances of the type-A TH-PPM and type-B TH-PPM are compared. The solid lines denote the average BER's of the type-A TH-PPM system and the dashed lines denote the BER's of the type-B system all with the same system parameters. Observe that the type-A TH-PPM system performs better for all SNR values. This can be explained by comparing the correlation functions $\tilde{R}(0)$ and $\hat{R}(\delta)$, which are given in (2.22) and (2.44), respectively. Considering the autocorrelation function $R(x)$ of the 2^{nd}-order Gaussian monocycle shown in Fig. 2.1, we note that

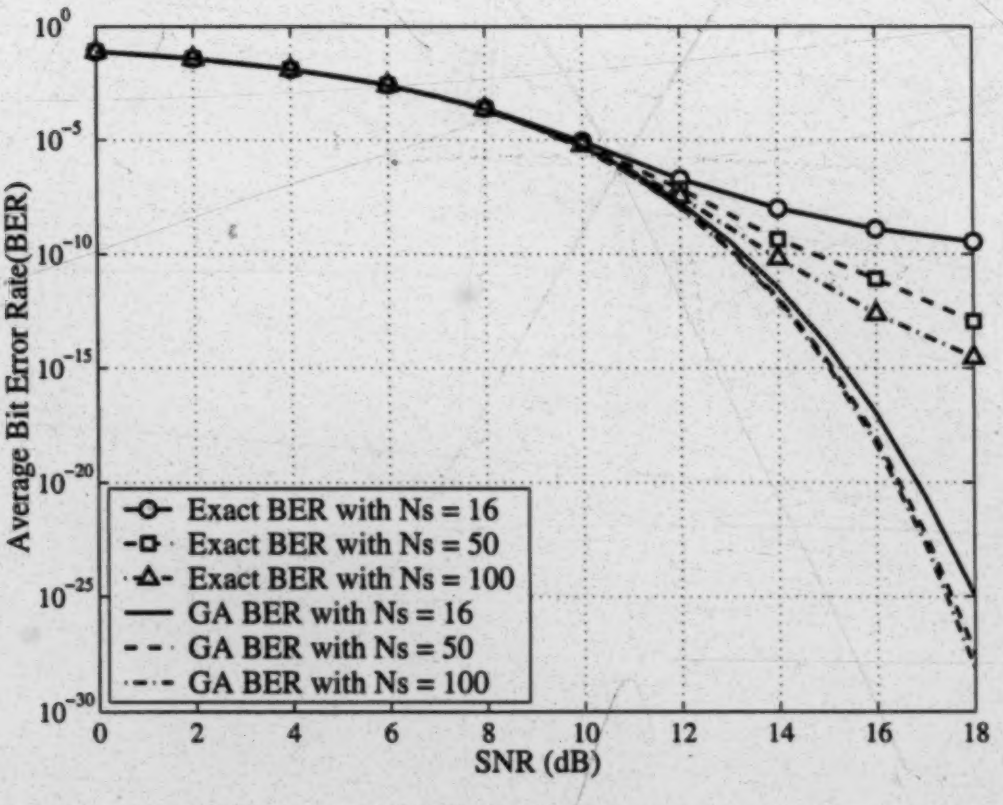
Average Bit Error Rate(BER)
SNR (dB)
Exact BER with Ns = 16
Exact BER with Ns = 50
Exact BER with Ns = 100
GA BER with Ns = 16
GA BER with Ns = 50
GA BER with Ns = 100

Fig. 2.6. Average BER of the TH-BPSK UWB system versus SNR for a repetition code with $N_s = 16$, $N_s = 50$ and $N_s = 100$.

$R(\delta)$ is less than $R(2\delta)$ for $\delta = 0.15$ ns, and then $\tilde{R}(0)$ is significantly greater than $\hat{R}(\delta)$, which leads to a smaller BER in the type-A TH-PPM system (compare (2.68) with (2.69)). On the other hand, if δ is chosen to satisfy $R(\delta) > R(2\delta)$, then type-B TH-PPM will outperform type-A TH-PPM. Fig. 2.7 also shows the BER's of the type-B system using a different time shift δ^{new}, denoted by squares. We choose $\delta^{new} = \frac{1}{2}\delta$ for this type-B TH-PPM system. In this case, $\tilde{R}(0)$ equals $\hat{R}(\delta^{new})$ and we expect the performance of the type-B TH-PPM system with $\delta^{new} = 0.075$ ns to be almost the same as the performance of the type-A system with $\delta = 0.15$ ns. This expected performance is confirmed by the results seen in Fig. 2.7. That means type-A and type-B TH-PPM can be used as alternatives with similar performances for a given application by making suitable choices of the time shift δ.

The results in Fig. 2.7 indicate that the time shift δ directly affects the performance of TH-PPM systems. Define the optimal value of δ that minimizes $R(\delta)$ as

$$\delta_{opt} = argument\ of\ \left\{ \underset{\delta}{minimum}\ R(\delta) \right\} \tag{2.71}$$

where $R(\cdot)$ is the autocorrelation function of the pulse $p(t)$ (assumed to be the 2^{nd}-order Gaussian monocycle in this paper). It is clear that the type-A TH-PPM systems will achieve the best performance when $\delta = \delta_{opt}$ and the type-B TH-PPM systems will achieve the best performance when $\delta = \frac{\delta_{opt}}{2}$. From (2.6), we also know that δ_{opt} is determined by the pulse shape $p(t)$ and the pulse width normalization factor τ_p. Due to the sensitivity of the TH-PPM UWB system to the choice of the time shift, a suitable value of δ should be chosen according to the specific pulse shape and pulse width employed in a particular UWB application.

The impact of the pulse shape on the average BER's of the TH-PPM UWB system for different Gaussian monocycles and different pulse widths is examined in Fig. 2.8. The optimal time shift δ is chosen for each pulse. The dotted lines with triangle markers denote the BER's of the TH-PPM system using the 2^{nd}-order Gaussian monocycle with original parameters as given in Table 2.1. The dashed lines with star markers denote the BER's of the TH-PPM system for the 2^{nd}-order monocycle with

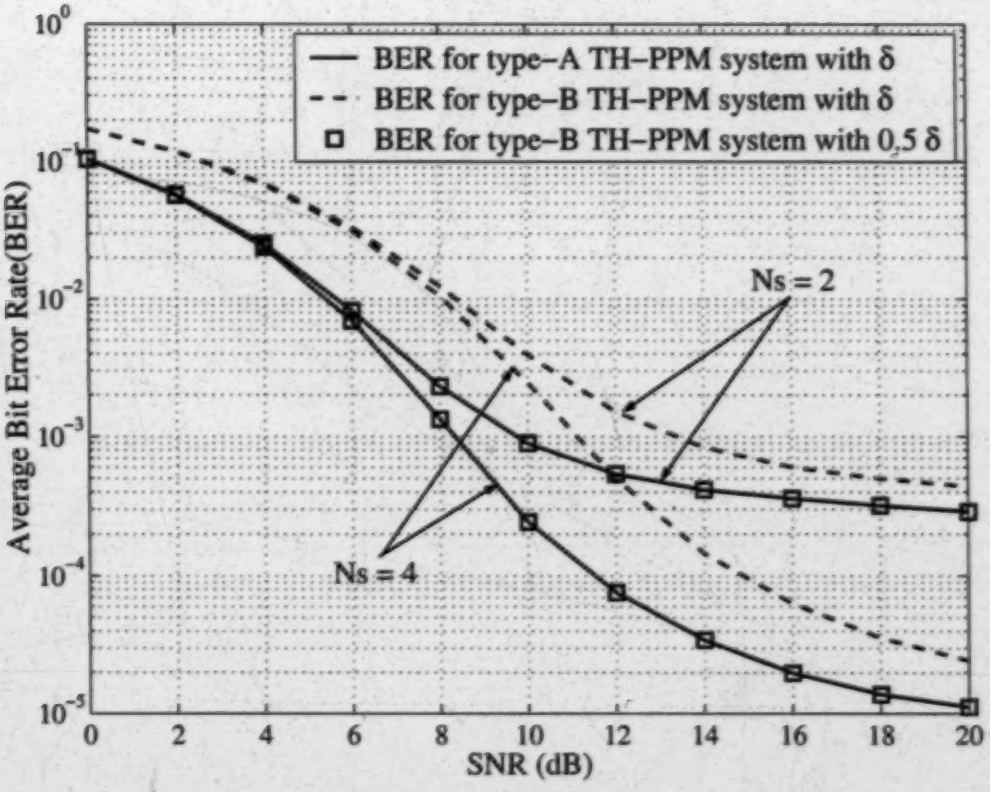

Fig. 2.7. Comparison of the type-A and type-B TH-PPM systems for a repetition code with $N_s = 2$ and $N_s = 4$ assuming 7 asynchronous interferers.

larger τ_p, corresponding to a larger pulse width. We observe that the performance using the 2^{nd}-order monocycle with smaller τ_p is better than the performance using the same order monocycle with larger τ_p, for all SNR values. When τ_p is fixed, the 4^{th}-order Gaussian monocycle outperforms the 2^{nd}-order monocycle as indicated by the solid lines with circle markers. Hence, it seems that the higher-order Gaussian monocycle can provide lower multiple access bit error rates when the pulse width is fixed, and that the same order monocycle with smaller pulse width provides lower bit error rates. These results can be explained by comparing the autocorrelation functions of the Gaussian monocycles. Our observations are consistent with those reported in [55], obtained from a SNR analysis (i.e., not an accurate BER analysis) using a Gaussian approximation.

The performance of the TH-BPSK UWB system for different Gaussian monocycles and pulse widths is presented in Fig. 2.9. When τ_p is fixed, unlike the TH-PPM system, the TH-BPSK system shows almost the same bit error rates for Gaussian monocycles with different orders except for large values of SNR, where the performance of the higher-order Gaussian monocycle is slightly better than the performance of the lower-order Gaussian monocycle with the same τ_p. However, Gaussian monocycles of the same order, but with smaller pulse widths also provide lower bit error rates as in the TH-PPM system. This behaviour results directly from the features of the autocorrelation functions of different monocycles shown in Fig. 2.1.

Fig. 2.10 shows the performance of the TH-BPSK and TH-PPM UWB systems with the 2^{nd}-order Gaussian monocycle assuming 7 asynchronous interferers. We observe that the TH-BPSK system outperforms the TH-PPM system for all values of SNR. Note that our observation is consistent with the findings in [53], which states that the TH-BPSK system with antipodal modulation yields better performance than the TH-PPM UWB system. The conclusion in [53] was reached according to analysis based on chip-synchronous systems, which is a special case of MAI environments. Here the same conclusion is reached but for chip-asynchronous systems, which are more common in practical applications.

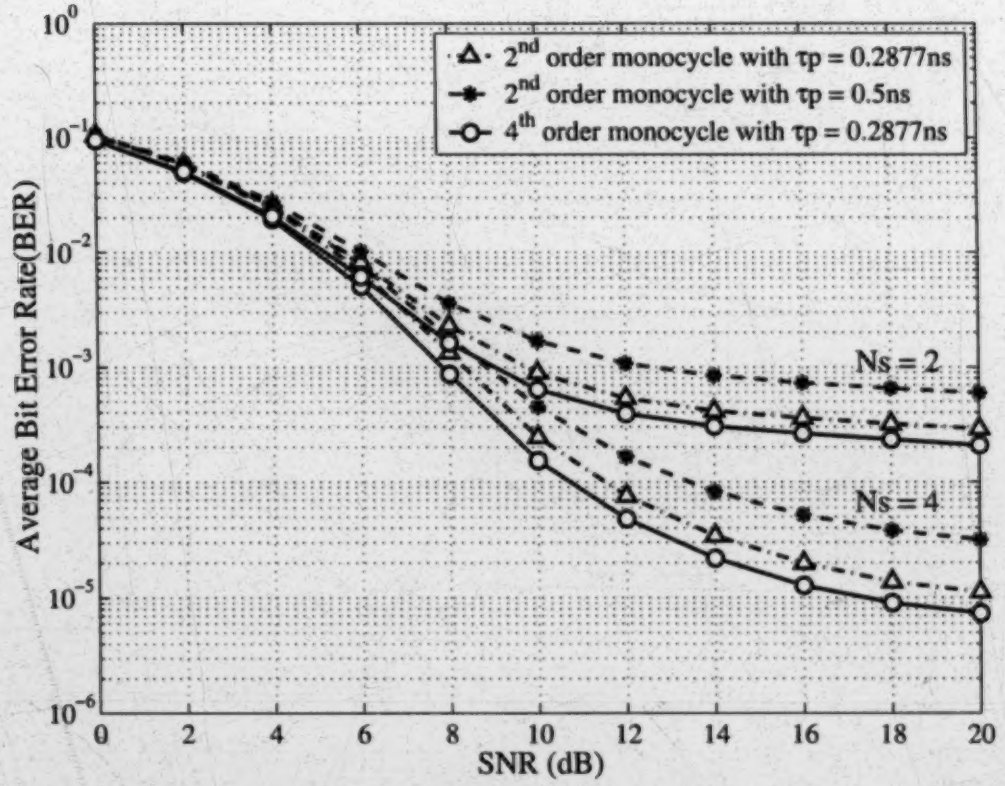

Fig. 2.8. Comparison of the TH-PPM systems using different Gaussian monocycles for a repetition code with $N_s = 2$ and $N_s = 4$ assuming 7 asynchronous interferers.

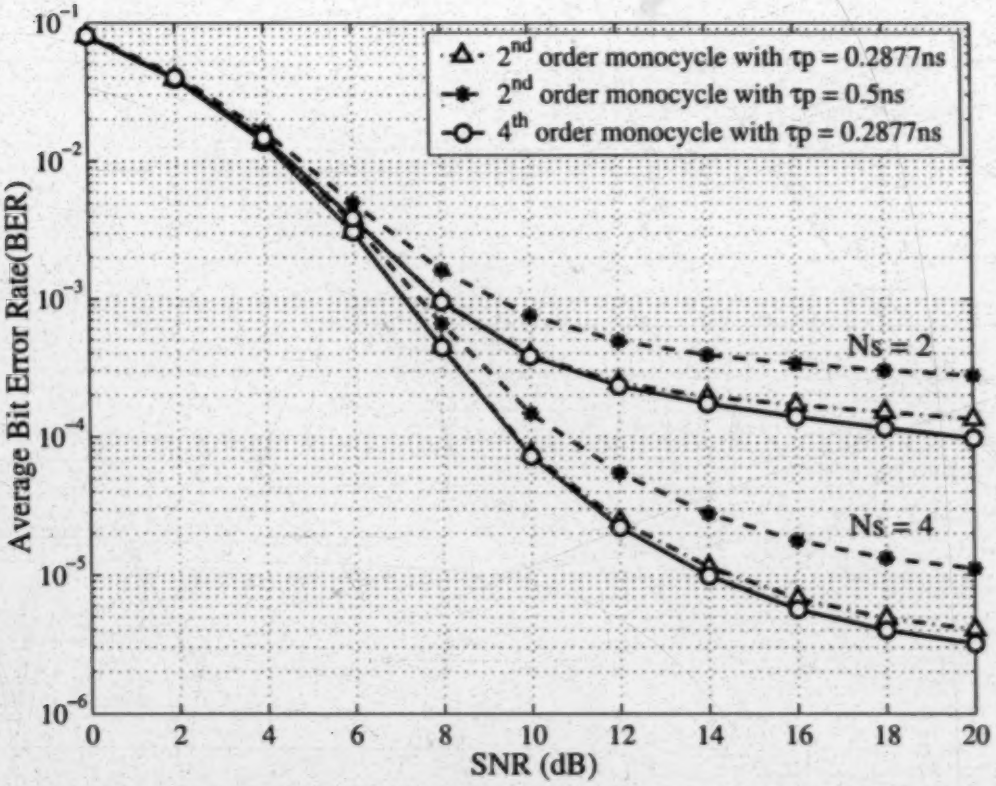

Fig. 2.9. Comparison of the TH-BPSK systems using different Gaussian monocycles for a repetition code with $N_s = 2$ and $N_s = 4$ assuming 7 asynchronous interferers.

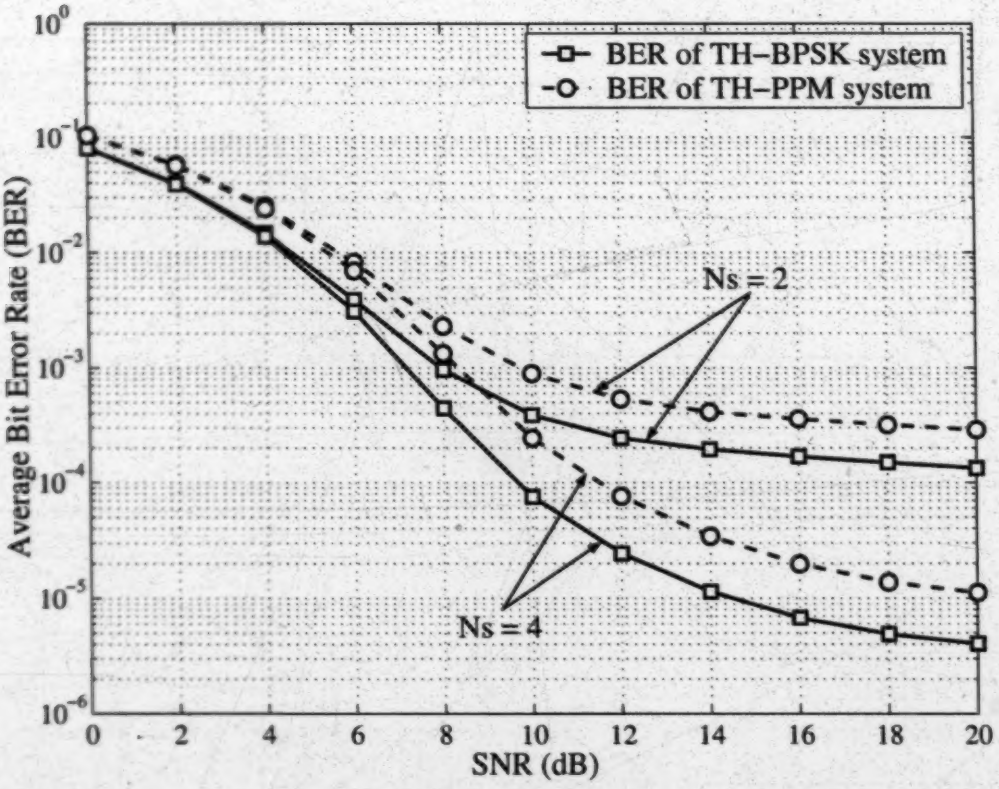

Fig. 2.10. Comparison of the TH-BPSK and TH-PPM systems for a repetition code with $N_s = 2$ and $N_s = 4$ assuming 7 asynchronous interferers.

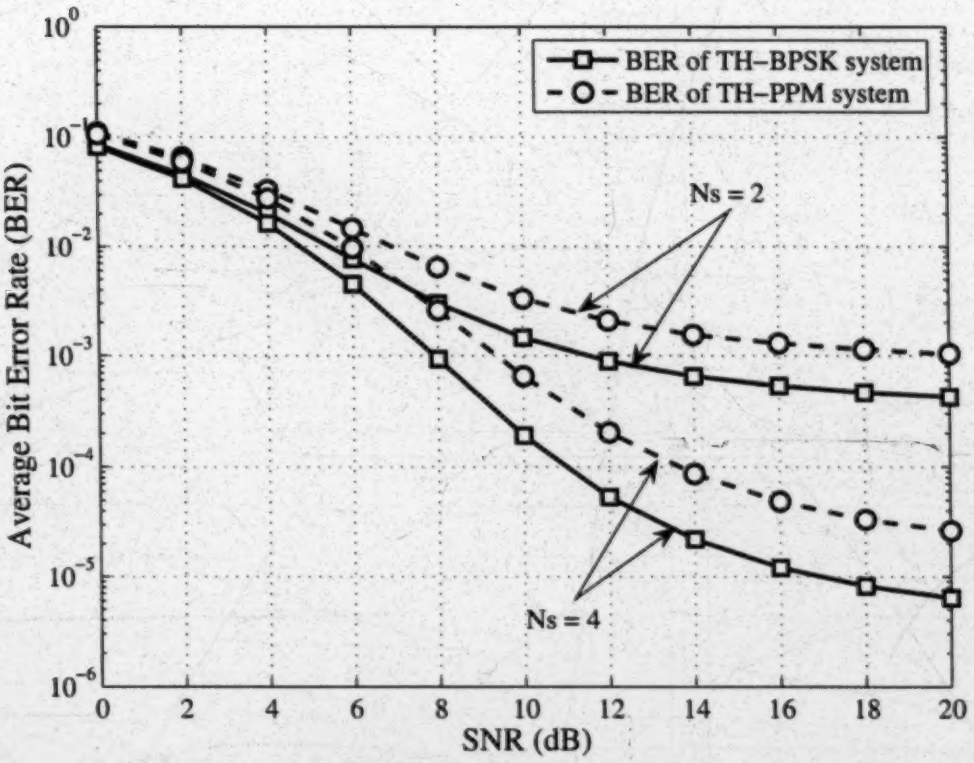

Fig. 2.11. Comparison of the TH-BPSK and TH-PPM systems for a repetition code with $N_s = 2$ and $N_s = 4$ assuming 50 asynchronous interferers.

2.8 Summary

In this chapter, we have derived accurate, analytical expressions for the average probability of bit error of TH-PPM and TH-BPSK UWB systems . Compared with other methods used in the performance analysis of UWB systems, our analysis provides a powerful tool for calculating BER's to any desired accuracy with very low complexity. Our precise analysis indicates that the GA substantially overestimates the performance of UWB systems at large values of SNR. The CHF method can be used as a reliable method in the performance evaluation of TH-PPM and TH-BPSK UWB systems for arbitrary values of SNR.

Our analytical method can also be applied to UWB systems using arbitrary pulse shapes. The effects of pulse shape and the corresponding pulse parameters on the performances of TH-PPM and TH-BPSK systems have been briefly examined using the precise analysis. An example indicated that the optimal value of the time shift δ associated with the binary TH-PPM system should be chosen to ensure the best performance of the TH-PPM system for a given pulse shape used in a practical application. Examples also indicated that among Gaussian monocycles of the same order those with a smaller pulse width have better multiple access performance. In general, higher-order Gaussian monocycles have better performances than lower-order Gaussian monocycles for a fixed pulse width. Our comparisons of the performances of TH-PPM and TH-BPSK UWB systems, as measured by the average probability of bit error, showed that the TH-BPSK system outperforms the TH-PPM system for all values of SNR. This analytical result confirms the results obtained in past work by other authors using approximate analyses. The evaluation of different UWB systems based on our precise analysis provides reliable information for choosing suitable modulation schemes in the design of UWB systems.

Chapter 3

Accurate Performance Evaluation of TH, DS and DS-IR UWB Systems in Multiple Access Interference

3.1 Introduction

As we have mentioned in Chapters 1, TH sequence was introduced to smooth the spectrum of the transmitted signal and to eliminate catastrophic collisions in multiple access UWB communication systems. It is well-known that DS-SS has the ability to combat interference, increase system capacity and improve quality of service. Therefore, DS-SS has been widely adopted in CDMA systems. As a candidate technique for multiple access UWB systems, DS-UWB is also worthy of investigation with the consideration of its advantages.

Some studies on TH-UWB and DS-UWB systems have been done by other researchers, including multi-user performance analysis of TH-PPM [14], TH-BPSK [51], DS-UWB systems [58], and a performance comparison of TH-UWB with DS-

UWB [52]. However, the performance analyses were conducted based on a Gaussian approximation for the interference term in their works. In [44], the authors used simulation to demonstrate the inaccuracy of the Gaussian approximation for TH-PPM systems. Recently, [59] provided an analytical method for estimating BER's for TH-PPM systems. However, multiple integrations are required to obtain the BER, involving significant computational complexity if the number of interferers is large. It has also been shown that the Gaussian approximation can significantly underestimate the BER of TH-UWB systems [15], rendering these results [14] - [52] less useful. A performance comparison of different UWB modulation schemes was also presented in [53] and [60] using two approximate approaches, a semi-analytical approach and a Gaussian approximation. More recently, reference [15] has studied the multiple access performance of time-hopping UWB systems including PPM and BPSK modulation schemes based on exact analysis of the multiple access interference. Such an exact analysis is not available for comparing TH-UWB and DS-UWB systems.

Except for TH-UWB and DS-UWB systems, a new UWB radio system design, called direct-sequence impulse radio, was proposed in [61]. Unlike TH-UWB that only employs a time-hopping code or DS-UWB that only employs a direct spreading sequence, the DS-IR design in [61] employs both direct-sequence spreading and time-hopping codes. The performance of the DS-IR BPSK UWB system is compared to the original TH-BPSK UWB system using simulation in [61]. However, [61] does not provide a performance comparison of the new DS-IR system with the conventional DS-UWB system. Thus, it has not been established that the complexity incurred by using the combination of TH and DS codes is justified. Specifically, the DS-IR system must outperform the simpler DS-UWB system or the implementation of the former is not warranted.

In this chapter, we provide a unified framework for TH, DS and DS-IR UWB systems, in which different modulation schemes can be fairly compared. Employing this unified framework complicates the analysis of TH-UWB systems and makes it different from the previous analysis in Chapter 2. In the sequel, we derive expressions

for the probability of error for TH-PPM, TH-BPSK, DS-BPSK and DS-IR BPSK UWB systems in AWGN. A simple and accurate alternative method is also provided for calculating the BER of the DS-BPSK system. We further use our analytical results to evaluate and compare these systems. The comparisons, based on the exact analysis of multiple access interference, clearly indicate the actual BER performance difference among these well-known UWB systems in AWGN and provide important and valuable criteria for choosing appropriate UWB modulation schemes in practical applications.

This chapter is organized as follows. In Section 3.2, the TH-PPM, TH-BPSK, DS-BPSK and DS-IR UWB system models used in our work are briefly described in a unified framework. An exact analysis for the multiple access interference is then provided for each system in Sections 3.3-3.6. Then, the Gaussian approximation for time-hopping and direct-sequence schemes is reviewed in Section 3.7 in order to clarify mistakes in previous works and to make this chapter self-contained. In Section3.8 , the validity of the exact analysis is confirmed by simulation and the inaccuracy of the Gaussian approximation is shown. In addition, design comparisons of the BER's of TH-PPM, TH-BPSK and DS-BPSK with different system parameters are made. Finally, we summarize major findings of this chapter in Section 3.9.

3.2 System Models

The asynchronous TH-PPM, TH-BPSK, DS-BPSK and DS-IR BPSK UWB systems are described in previous studies [14], [58] and [61]. Here we use the same notation and terminology and introduce a unified framework for these schemes. In this framework, a TH-PPM UWB signal takes the form

$$s_{PPM}^{(k)}(t) = \sqrt{\frac{E_b}{N_s}} \sum_{j=-\infty}^{+\infty} p\left(t - jT_f - c_j^{(k)} T_c - d_{\lfloor j/N_s \rfloor}^{(k)} \delta\right) \tag{3.1}$$

a DS-BPSK UWB signal has the form

$$s_{DS}^{(k)}(t) = \sqrt{\frac{E_b}{N_c}} \sum_{j=-\infty}^{\infty} \sum_{n=0}^{N_c-1} d_j^{(k)} b_n^{(k)} p(t - jT_f - nT_c) \tag{3.2}$$

and TH-BPSK and DS-IR BPSK signals can be written as [61]

$$s_{TH/DS-IR}^{(k)}(t) = \sqrt{\frac{E_b}{N_s}} \sum_{j=-\infty}^{\infty} d_{\lfloor j/N_s \rfloor}^{(k)} b_j^{(k)} p\left(t - jT_f - c_j^{(k)} T_c\right) \tag{3.3}$$

where t is time, $s^{(k)}(t)$ is the kth user's signal, and $p(t)$ is a chip waveform, which can take arbitrary time-limited pulse shapes proposed specifically for UWB communication systems, and is normalized to satisfy $\int_{-\infty}^{+\infty} p^2(t)dt = 1$. The notations and parameters employed in these UWB models are [71]:

- N_s is the number of pulses used to transmit a single information bit in TH or DS-IR UWB systems. N_c is the number of chips per information bit in DS-BPSK systems.
- In (3.1) and (3.3), the sequence $\left\{c_j^{(k)}\right\}$ represents the TH code for the kth source; it is pseudorandom with each element taking an integer value in the range $0 \le c_j^{(k)} < N_h$, where N_h is the number of hops.
- For DS-BPSK UWB signals shown in (3.2) and DS-IR signals given in (3.3), $\left\{b_{n/j}^{(k)}\right\}$ represents the spreading signature sequence, of which each element is assumed to take values from $\{\pm 1\}$ with equal probability. For TH-BPSK signals, $\left\{b_j^{(k)}\right\} = 1$ for all j.
- T_f is the time duration of a frame. T_c is the hop width in TH/DS-IR systems satisfying $N_h T_c = T_f$, while it is the chip duration in DS-UWB systems satisfying $N_c T_c = T_f$. Note that we assume $N_h T_c = T_f$ in order to fairly compare the performances of TH-UWB and DS-UWB systems. This assumption is different from the corresponding assumption made in [14], [15] and leads to different analysis.

- In TH/DS-IR systems, the bit duration $T_b = N_s T_f$, while $T_b = T_f = N_c T_c$ in DS systems.
- $d_j^{(k)}$ represents the jth binary data bit transmitted by the kth source. In TH-PPM UWB systems, the data bits can conveniently be $\{0, 1\}$. In TH/DS-IR BPSK and DS-BPSK UWB systems, $d_j^{(k)} \in \{1, -1\}$.

Assuming N_u users are transmitting asynchronously on an AWGN channel, the received signal is

$$r(t) = \sum_{k=1}^{N_u} A_k s^{(k)}(t - \tau_k) + n(t) \tag{3.4}$$

where $s^{(k)}(t)$ can be the TH-PPM, TH/DS-IR BPSK or DS-BPSK signal, $n(t)$ is additive noise with two-sided power spectral density $\frac{N_0}{2}$, common to all systems, $\{A_k\}_{k=1}^{N_u}$ represent the channel gains for all transmitted signals, and $\{\tau_k\}_{k=1}^{N_u}$ represent time shifts which account for user asynchronisms. Without loss of generality, we assume $\tau_1 = 0$ [45], [56]. Following a widely-adopted assumption on τ_k for DS-CDMA systems, we further assume $\{\tau_k\}_{k=2}^{N_u}$ are uniformly distributed on a bit duration $[0, T_b)$ as in [56].

3.3 Analysis of TH-PPM system

For the TH-PPM system, we still define the correlation of the template $v(t) = p(t) - p(t - \delta)$ with a time-shifted pulse $p(t)$ as

$$\tilde{R}(x) = R(x) - R(x - \delta) \tag{3.5}$$

where $R(x)$ is the autocorrelation of the UWB pulse waveform $p(t)$ as in Chapter 2.

Assuming perfect synchronization with the reference signal, the decision statistic of the single-user correlation receiver is obtained as

$$\begin{aligned} r &= \sum_{m=0}^{N_s-1} \int_{mT_f}^{(m+1)T_f} r(t) v(t - mT_f) dt \\ &= S + I + n \end{aligned} \tag{3.6}$$

where n is a Gaussian random variable (RV) with zero mean and variance $\sigma_n^2 = N_0 N_s \tilde{R}(0)$, $S = \pm A_1 \sqrt{E_b N_s} \tilde{R}(0)$ is the contribution to the decision statistic r depending on user 1's useful signal bit $d_0^{(1)}$, and I is the total MAI, given by

$$I = \sqrt{\frac{E_b}{N_s}} \sum_{k=2}^{N_u} A_k I^{(k)} \tag{3.7}$$

where

$$I^{(k)} = \sum_{m=0}^{N_s-1} \sum_{j=-\infty}^{+\infty} \tilde{R}\left(c_j^{(k)} T_c + \delta d_{\lfloor j/N_s \rfloor}^{(k)} + \tau_k - (m-j)T_f\right). \tag{3.8}$$

If we define

$$\tilde{\Theta}_j^{(k)} = c_j^{(k)} T_c + \delta d_{\lfloor j/N_s \rfloor}^{(k)} + \tau_k \tag{3.9}$$

then, $I^{(k)}$ can be written as

$$I^{(k)} = \sum_{m=0}^{N_s-1} \sum_{j=-\infty}^{+\infty} \tilde{R}\left(\tilde{\Theta}_j^{(k)} - (m-j)T_f\right). \tag{3.10}$$

Note that $N_h T_c = T_f$ is assumed in the TH-UWB systems considered; this assumption is different from the assumption [14, eqn. (57)], rewritten as

$$N_h T_c < T_f/2 - 2T_p \tag{3.11}$$

where T_p is the pulse duration of $p(t)$. We note that our present model assumes that there is more than one pulse from each interfering user in each frame contributing to the interference term. In this case, the expression for the MAI is more complicated than the expression presented in [48], and therefore necessitates a different analysis.

Owing to the uniform distribution of τ_k on $[0, N_s T_f)$, the auxiliary RV $\tilde{\Theta}_j^{(k)}$ satisfies

$$\tilde{\Theta}_j^{(k)} \in [0, (N_h - 1)T_c + \delta + N_s T_f). \tag{3.12}$$

Similar to the analysis presented in [45], the summation over j in (3.10) only includes $N_s + 1$ contributing terms and $I^{(k)}$ is written as

$$\begin{aligned} I^{(k)} &= \sum_{m=0}^{N_s-1} \sum_{j=m-N_s}^{m} \tilde{R}\left(\tilde{\Theta}_j^{(k)} - (m-j)T_f\right) \\ &= \sum_{m=0}^{N_s-1} \sum_{i=0}^{N_s} \tilde{R}\left(\tilde{\Theta}_{m-i}^{(k)} - iT_f\right) \end{aligned} \tag{3.13}$$

where the second equality comes from replacing $m-j$ with i. Considering that the two adjacent bits of the kth signal, $d_{-1}^{(k)}$ and $d_0^{(k)}$, contribute to the interference, we can rewrite (3.13) as

$$I^{(k)} = \underbrace{\sum_{l=1}^{N_s}\sum_{j=l}^{N_s}\tilde{R}\left(\tilde{\Theta}_{-l}^{(k)} - jT_f\right)}_{X^{(k)}} + \underbrace{\sum_{l=0}^{N_s-1}\sum_{j=0}^{N_s-l-1}\tilde{R}\left(\tilde{\Theta}_{l}^{(k)} - jT_f\right)}_{Y^{(k)}} \tag{3.14}$$

where $X^{(k)}$ denotes the interference component coming from the information bit $d_{-1}^{(k)}$, and $Y^{(k)}$ denotes the interference component from $d_0^{(k)}$. For a given τ_k, it can be shown that RV's $X^{(k)}$ and $Y^{(k)}$ are independent, which results from the independence of the chip sequences (with distinct chip index, $\left\{c_l^{(k)}\right\}_{l=-N_s}^{-1}$ in $X^{(k)}$ and $\left\{c_l^{(k)}\right\}_{l=0}^{N_s-1}$ in $Y^{(k)}$) and the independence of the data bits ($d_{-1}^{(k)}$ in $X^{(k)}$ and $d_0^{(k)}$ in $Y^{(k)}$).

According to the random time-hopping sequence assumption, the PDF of $\left\{\tilde{\Theta}_l^{(k)}\right\}_{l=0}^{N_s-1}$ conditioned on $d_0^{(k)}$ and τ_k can be obtained as

$$f_{\tilde{\Theta}|d,\tau}\left(\tilde{\theta}\middle|d_0^{(k)}=d,\tau_k=\tau\right) = \frac{1}{N_h}\sum_{h=0}^{N_h-1}\delta_D(\tilde{\theta} - hT_c - \delta d - \tau). \tag{3.15}$$

Then, the characteristic function of $Y^{(k)}$ conditioned on $d_0^{(k)}$ and τ_k is expressed as

$$\begin{aligned}
\Phi_{Y|d,\tau}(\omega) &= \mathbf{E}\left[e^{j\omega\sum_{l=0}^{N_s-1}\sum_{j=0}^{N_s-l-1}\tilde{R}\left(\tilde{\Theta}_l^{(k)}-jT_f\right)}\middle|d_0^{(k)}=d,\tau_k=\tau\right] \\
&= \prod_{l=0}^{N_s-1}\mathbf{E}\left[e^{j\omega\sum_{j=0}^{N_s-l-1}\tilde{R}\left(\tilde{\Theta}_l^{(k)}-jT_f\right)}\middle|d_0^{(k)}=d,\tau_k=\tau\right] \\
&= \prod_{l=0}^{N_s-1}\int_{-\infty}^{\infty}\left[\prod_{j=0}^{N_s-l-1}e^{j\omega\tilde{R}\left(\tilde{\Theta}_l^{(k)}-jT_f\right)}\right] f_{\tilde{\Theta}|d,\tau}\left(\tilde{\theta}\middle|d_0^{(k)}=d,\tau_k=\tau\right)d\tilde{\theta} \\
&= \frac{1}{N_h^{N_s}}\prod_{l=0}^{N_s-1}\left[\sum_{h=0}^{N_h-1}\prod_{j=0}^{N_s-l-1}e^{j\omega\tilde{R}(hT_c+\delta d+\tau-jT_f)}\right]
\end{aligned} \tag{3.16}$$

where the second equality in (3.16) follows from the fact that $\left\{\sum_{j=0}^{N_s-l-1}\tilde{R}\left(\tilde{\Theta}_l^{(k)}-jT_f\right)\right\}_{l=0}^{N_s-1}$ are independent when conditioned on $d_0^{(k)}$ and τ_k. The CHF of $Y^{(k)}$ conditioned on τ_k can be obtained using the theorem of total probability as

$$\Phi_{Y|\tau}(\omega) = \Phi_{Y|d=0,\tau}(\omega)\Pr(d=0) + \Phi_{Y|d=1,\tau}(\omega)\Pr(d=1). \tag{3.17}$$

Similarly, the CHF of $X^{(k)}$ conditioned on $d_{-1}^{(k)}$ and τ_k is expressed as

$$\Phi_{X|d,\tau}(\omega) = \prod_{l=1}^{N_s} \mathbf{E}\left[e^{j\omega\sum_{j=l}^{N_s} R\left(\hat{\Theta}_{-1}^{(k)} - jT_f\right)} \middle| d_{-1}^{(k)} = d, \tau_k = \tau\right]$$
$$= \frac{1}{N_h^{N_s}} \prod_{l=1}^{N_s} \left[\sum_{h=0}^{N_h-1} \prod_{j=l}^{N_s} e^{j\omega\hat{R}(hT_c + \delta d + \tau - jT_f)}\right] \tag{3.18}$$

and the CHF of $X^{(k)}$ conditioned on τ_k is given by

$$\Phi_{X|\tau}(\omega) = \Phi_{X|d=0,\tau}(\omega)\Pr(d=0) + \Phi_{X|d=1,\tau}(\omega)\Pr(d=1). \tag{3.19}$$

Considering the independence of $X^{(k)}$ and $Y^{(k)}$ when conditioned on τ_k, we obtain the conditional CHF of $I^{(k)}$ as

$$\Phi_{I^{(k)}|\tau}(\omega) = \Phi_{X|\tau}(\omega)\Phi_{Y|\tau}(\omega). \tag{3.20}$$

Averaging out τ_k, we obtain the CHF of $I^{(k)}$ as

$$\Phi_{I^{(k)}}(\omega) = \frac{1}{N_s T_f}\int_0^{N_s T_f} \Phi_{I^{(k)}|\tau} d\tau. \tag{3.21}$$

Owing to the independence of the interference components, the CHF of the total interference is given by

$$\Phi_I(\omega) = \prod_{k=2}^{N_u} \Phi_{I^{(k)}}\left(A_k\sqrt{\frac{E_b}{N_s}}\omega\right). \tag{3.22}$$

3.4 Analysis of TH-BPSK system

The template waveform used in TH-BPSK systems is the pulse $p(t)$ [51]. The decision statistic r_{BPSK} is then

$$r_{BPSK} = S_{BPSK} + I_{BPSK} + n_{BPSK} \tag{3.23}$$

where n_{BPSK} is a Gaussian noise process with zero mean and variance $\sigma^2_{n_{BPSK}} = \frac{N_0 N_s}{2}$, $S_{BPSK} = A_1\sqrt{E_b N_s}d_0^{(1)}$ depends on user 1's useful signal bit $d_0^{(1)}$, and I_{BPSK} is the total MAI in the TH-BPSK UWB system, given by

$$I_{BPSK} = \sqrt{\frac{E_b}{N_s}}\sum_{k=2}^{N_u} A_k I_{BPSK}^{(k)} \tag{3.24}$$

where

$$I_{BPSK}^{(k)} = \sum_{m=0}^{N_s-1} \sum_{j=-\infty}^{+\infty} d_{\lfloor j/N_s \rfloor}^{(k)} R\left(c_j^{(k)} T_c + \tau_k - (m-j)T_f\right). \tag{3.25}$$

We also define

$$\Theta_j^{(k)} = c_j^{(k)} T_c + \tau_k. \tag{3.26}$$

Similar to the analysis described in Section III, the kth user interference can be simplified as

$$\begin{aligned} I_{BPSK}^{(k)} &= \sum_{m=0}^{N_s-1} \sum_{i=0}^{N_s} d_{\lfloor (m-i)/N_s \rfloor}^{(k)} R\left(\Theta_{m-i}^{(k)} - iT_f\right) \\ &= \underbrace{\sum_{l=1}^{N_s} \sum_{j=l}^{N_s} d_{-1}^{(k)} R\left(\Theta_{-l}^{(k)} - jT_f\right)}_{X_{BPSK}^{(k)}} + \underbrace{\sum_{l=0}^{N_s-1} \sum_{j=0}^{N_s-l-1} d_0^{(k)} R\left(\Theta_l^{(k)} - jT_f\right)}_{Y_{BPSK}^{(k)}}. \end{aligned} \tag{3.27}$$

Based on the PDF of $\Theta_j^{(k)}$ conditioned on τ_k, which is given by

$$f_{\Theta|\tau}(\theta \mid \tau_k = \tau) = \frac{1}{N_h} \sum_{h=0}^{N_h-1} \delta_D(\theta - hT_c - \tau) \tag{3.28}$$

the CHF of $X_{BPSK}^{(k)}$ conditioned on $d_{-1}^{(k)}$ and τ_k can be written as

$$\begin{aligned} \Phi_{X|d,\tau}(\omega) &= \mathbb{E}\left[e^{j\omega \sum_{l=1}^{N_s} \sum_{j=l}^{N_s} d_{-1}^{(k)} R\left(\Theta_{-l}^{(k)} - jT_f\right)} \middle| d_{-1}^{(k)} = d, \tau_k = \tau\right] \\ &= \frac{1}{N_h^{N_s}} \prod_{l=1}^{N_s} \left[\sum_{h=0}^{N_h-1} \prod_{j=l}^{N_s} e^{j\omega d R(hT_c + \tau - jT_f)}\right] \end{aligned} \tag{3.29}$$

and the conditional CHF of $Y_{BPSK}^{(k)}$ can be expressed as

$$\Phi_{Y|d,\tau}(\omega) = \frac{1}{N_h^{N_s}} \prod_{l=0}^{N_s-1} \left[\sum_{h=0}^{N_h-1} \prod_{j=0}^{N_s-l-1} e^{j\omega d R(hT_c + \tau - jT_f)}\right]. \tag{3.30}$$

Then, the CHF of $X_{BPSK}^{(k)}$ and $Y_{BPSK}^{(k)}$ conditioned on τ_k can be obtained, respectively, as

$$\Phi_{X|\tau}(\omega) = \Phi_{X|d=-1,\tau}(\omega)\Pr(d=-1) + \Phi_{X|d=1,\tau}(\omega)\Pr(d=1) \tag{3.31}$$

and

$$\Phi_{Y|\tau}(\omega) = \Phi_{Y|d=-1,\tau}(\omega)\Pr(d=-1) + \Phi_{Y|d=1,\tau}(\omega)\Pr(d=1). \tag{3.32}$$

Considering the independence of $X_{BPSK}^{(k)}$ and $Y_{BPSK}^{(k)}$ when conditioned on τ_k and averaging the conditional CHF of $I_{BPSK}^{(k)}$ in terms of the uniform distribution of τ_k, we can obtain the CHF of $I_{BPSK}^{(k)}$ as

$$\Phi_{I_{BPSK}^{(k)}} = \frac{1}{N_s T_f} \int_0^{N_s T_f} \Phi_{X|\tau} \Phi_{Y|\tau} d\tau \tag{3.33}$$

and the CHF of the total interference in the TH-BPSK system is given by

$$\Phi_{I_{BPSK}}(\omega) = \prod_{k=2}^{N_u} \Phi_{I_{BPSK}^{(k)}} \left(A_k \sqrt{\frac{E_b}{N_s}} \omega \right). \tag{3.34}$$

3.5 Analysis of DS-IR system

The decision statistic for the DS-IR system is obtained as [63]

$$\begin{aligned} r_{DS-IR} &= \sum_{m=0}^{N_s-1} \int_{mT_f}^{(m+1)T_f} r(t) b_m^{(1)} p(t - jT_f - c_j^{(k)} T_c) dt \\ &= S_{DS-IR} + I_{DS-IR} + n_{DS-IR} \end{aligned} \tag{3.35}$$

where n_{DS-IR} is a Gaussian noise process with zero mean and variance $\sigma^2_{n_{DS-IR}} = \frac{N_0 N_s}{2}$, $S_{DS-IR} = A_1 \sqrt{E_b N_s} d_0^{(1)}$ depends on user 1's useful signal bit $d_0^{(1)}$, and I_{DS-IR} is the total MAI in the DS-IR BPSK UWB system, given by

$$I_{DS-IR} = \sqrt{\frac{E_b}{N_s}} \sum_{k=2}^{N_u} A_k I_{DS-IR}^{(k)} \tag{3.36}$$

where

$$I_{DS-IR}^{(k)} = \sum_{m=0}^{N_s-1} \sum_{j=-\infty}^{+\infty} d_{\lfloor j/N_s \rfloor}^{(k)} b_j^{(k)} b_m^{(1)} R\left(c_j^{(k)} T_c + \tau_k - (m-j) T_f \right). \tag{3.37}$$

Owing to the distribution of $c_j^{(k)} T_c + \tau_k$, the kth user interference can be simplified

as

$$I_{DS-IR}^{(k)} = \sum_{m=0}^{N_s-1} \sum_{j=m-N_s}^{m} d_{\lfloor j/N_s \rfloor}^{(k)} b_j^{(k)} b_m^{(1)} R\left(c_j^{(k)} T_c + \tau_k - (m-j)T_f\right)$$
$$= \sum_{m=0}^{N_s-1} \sum_{i=0}^{N_s} d_{\lfloor (m-i)/N_s \rfloor}^{(k)} b_{m-i}^{(k)} b_m^{(1)} R\left(c_{m-i}^{(k)} T_c + \tau_k - iT_f\right) \tag{3.38}$$

where the second equality comes from replacing $m-j$ with i. Considering that the two adjacent bits of the kth signal, $d_{-1}^{(k)}$ and $d_0^{(k)}$, contribute to the interference, we can rewrite (3.38) as

$$I_{DS-IR}^{(k)} = X^{(k)} + Y^{(k)} \tag{3.39}$$

where

$$X^{(k)} = \sum_{l=1}^{N_s} \sum_{j=l}^{N_s} d_{-1}^{(k)} b_{-l}^{(k)} b_{j-l}^{(1)} R\left(c_{-l}^{(k)} T_c + \tau_k - jT_f\right) \tag{3.40}$$

$$Y^{(k)} = \sum_{l=0}^{N_s-1} \sum_{j=0}^{N_s-l-1} d_0^{(k)} b_l^{(k)} b_{j+l}^{(1)} R\left(c_l^{(k)} T_c + \tau_k - jT_f\right). \tag{3.41}$$

For a given τ_k, it can be shown that RV's $X^{(k)}$ and $Y^{(k)}$ are independent when conditioned on $\left\{b_m^{(1)}\right\}_{m=0}^{N_s-1}$, which results from the independence of the chip sequences (with distinct chip index, $\left\{b_l^{(k)}, c_l^{(k)}\right\}_{l=-N_s}^{-1}$ in $X^{(k)}$ and $\left\{b_l^{(k)}, c_l^{(k)}\right\}_{l=0}^{N_s-1}$ in $Y^{(k)}$), and the independence of the data bits ($d_{-1}^{(k)}$ in $X^{(k)}$ and $d_0^{(k)}$ in $Y^{(k)}$).

In order to simplify the notation, we further define

$$X_l^{(k)} = d_{-1}^{(k)} b_{-l}^{(k)} \sum_{j=l}^{N_s} b_{j-l}^{(1)} R\left(c_{-l}^{(k)} T_c + T_c - jT_f\right). \tag{3.42}$$

Considering the Bernoulli distribution of $b_{-l}^{(k)}$, we can write the CHF of $X_l^{(k)}$ conditioned on $d_{-1}^{(k)}$, $\left\{b_m^{(1)}\right\}_{m=0}^{N_s-1}$, $c_{-l}^{(k)}$ and τ_k as

$$\Phi_{X_l|d,b_{j-l},c_{-l}^{(k)},\tau}(\omega) = \mathbb{E}\left[e^{j\omega X_l^{(k)}} \middle| d_{-1}^{(k)} = d, b_{j-l}^{(1)} = b_{j-l}, c_{-l}^{(k)} = c_{-l}, \tau_k = \tau\right]$$
$$= \cos\left[\omega d \sum_{j=l}^{N_s} b_{j-l} R\left(c_{-l} T_c + \tau - jT_f\right)\right]. \tag{3.43}$$

Based on the PDF of $c_{-l}^{(k)}$, which is given by

$$f_c(x) = \frac{1}{N_h} \sum_{h=0}^{N_h-1} \delta_D(x - hT_c) \tag{3.44}$$

the conditional CHF of $X_l^{(k)}$ can be written as

$$\Phi_{X_l|d,b_{j-l},\tau}(\omega) = \frac{1}{N_h} \sum_{h=0}^{N_h-1} \cos\left[\omega d \sum_{j=l}^{N_s} b_{j-l} R(hT_c + \tau - jT_f)\right]. \tag{3.45}$$

Considering the independence of $\left\{c_{-l}^{(k)}\right\}_{l=1}^{N_s}$, we obtain the CHF of $X^{(k)}$ conditioned on $d_{-1}^{(k)}$, $\left\{b_m^{(1)}\right\}_{m=0}^{N_s-1}$, and τ_k as

$$\Phi_{X|d,b_{j-l},\tau}(\omega) = \prod_{l=1}^{N_s} \Phi_{X_l|d,b_{j-l},\tau}(\omega). \tag{3.46}$$

Averaging out the information bit $d_{-1}^{(k)}$, the CHF of $X^{(k)}$ conditioned on $\left\{b_m^{(1)}\right\}_{m=0}^{N_s-1}$ and τ_k can be obtained as

$$\Phi_{X|b_{j-l},\tau}(\omega) = \frac{1}{N_h^{N_s}} \prod_{l=1}^{N_s} \left\{ \sum_{h=0}^{N_h-1} \cos\left[\omega \sum_{j=l}^{N_s} b_{j-l} R(hT_c + \tau - jT_f)\right] \right\}. \tag{3.47}$$

Similarly, we can calculate the CHF of $Y^{(k)}$ conditioned on $\left\{b_m^{(1)}\right\}_{m=0}^{N_s-1}$ and τ_k as

$$\Phi_{Y|b_{j+l},\tau}(\omega) = \frac{1}{N_h^{N_s}} \prod_{l=0}^{N_s-1} \left\{ \sum_{h=0}^{N_h-1} \cos\left[\omega \sum_{j=0}^{N_s-l-1} b_{j+l} R(hT_c + \tau - jT_f)\right] \right\}. \tag{3.48}$$

Considering the independence of $X^{(k)}$ and $Y^{(k)}$ when conditioned on τ_k and $\left\{b_m^{(1)}\right\}_{m=0}^{N_s-1}$ and averaging the conditional CHF of $I_{DS-IR}^{(k)}$ in terms of the uniform distribution of τ_k, we can obtain the CHF of $I_{DS-IR}^{(k)}$ conditioned on $\left\{b_m^{(1)}\right\}_{m=0}^{N_s-1}$ as

$$\begin{aligned}
\Phi_{I_{DS-IR}^{(k)}|\mathbf{b}}(\omega) &= \mathbb{E}\left[e^{j\omega I_{DS-IR}^{(k)}} \mid \left\{b_m^{(1)}\right\}_{m=0}^{N_s-1} = \mathbf{b}\right] \\
&= \frac{1}{N_s T_f} \int_0^{N_s T_f} \Phi_{X|b_{j-l},\tau}(\omega) \Phi_{Y|b_{j+l},\tau}(\omega) d\tau.
\end{aligned} \tag{3.49}$$

By averaging the conditional CHF of $I_{DS-IR}^{(k)}$ according to User 1's spreading sequence, $\mathbf{b}$, the CHF of $I_{DS-IR}^{(k)}$ can be obtained. Finally, the CHF of the total interference can be obtained.

3.6 Analysis of DS-UWB system

Under the assumption of perfect synchronization for the reference signal $s_{DS}^{(1)}$, the correlation receiver computes the decision statistic as [58]

$$r_{DS} = \sum_{m=0}^{N_c-1} \int_0^{T_f} r(t) b_m^{(1)} p(t - mT_c) dt. \tag{3.50}$$

The decision statistic can be written as

$$r_{DS} = S_{DS} + I_{DS} + n_{DS} \tag{3.51}$$

where S_{DS} is the contribution to the decision statistic r depending on user 1's information bit $d_0^{(1)}$, expressed as

$$S_{DS} = A_1 \sqrt{E_b N_c} d_0^{(1)} \tag{3.52}$$

n_{DS} is a Gaussian RV with zero mean and variance $\sigma_{n_{DS}}^2 = \frac{N_0 N_c}{2}$, and I_{DS} is the total MAI, given by

$$I_{DS} = \sqrt{\frac{E_b}{N_c}} \sum_{k=2}^{N_u} A_k \sum_{m=0}^{N_c-1} \int_0^{T_f} s^{(k)}(t - \tau_k) b_m^{(1)} p(t - mT_c)\, dt. \tag{3.53}$$

Define the spreading signal for the kth user, $b^{(k)}(t)$, as [56]

$$b^{(k)}(t) = \sum_{n=-\infty}^{+\infty} b_n^{(k)} p(t - nT_c). \tag{3.54}$$

Then, the partial cross-correlation functions between $b^{(k)}(t)$ and $b^{(1)}(t)$ can also be defined as

$$R_{k,1}(\tau) = \int_0^{\tau} b^{(k)}(t - \tau) b^{(1)}(t) dt \tag{3.55}$$

and

$$\hat{R}_{k,1}(\tau) = \int_{\tau}^{T_f} b^{(k)}(t - \tau) b^{(1)}(t) dt. \tag{3.56}$$

Therefore, the MAI term can be written as

$$I_{DS} = \sqrt{\frac{E_b}{N_c}} \sum_{k=2}^{N_u} A_k W_k \tag{3.57}$$

where

$$W_k = d_{-1}^{(k)} R_{k,1}(\tau_k) + d_0^{(k)} \hat{R}_{k,1}(\tau_k). \tag{3.58}$$

There are two ways to analyze W_k. The most common one was provided in [56]. More recently, a simplified version of W_k was obtained in [64] based on an assumption of approximate independence. We will derive BER expressions for DS-UWB systems using both the precise and approximate approaches to analyzing W_k. The precise analysis follows closely the part of the analysis published in [56] that derives the characteristic function of the interference. Reference [56], however, considered DS-CDMA systems. The approximate analysis follows that in [64], also for DS-CDMA systems, but is applied here to obtain solutions for DS-UWB systems.

3.6.1 Exact Decision Statistic

We define the partial autocorrelation functions of the chip waveform as

$$R_w(s) = \int_0^s w(t)w(t + T_c - s)dt, \;\; 0 \le s \le T_c \tag{3.59}$$

$$\hat{R}_w(s) = \int_s^{T_c} w(t)w(t - s)dt, \;\; 0 \le s \le T_c \tag{3.60}$$

and zero elsewhere. The time delay τ_k can be modeled as

$$\tau_k = \gamma_k T_c + \alpha_k \tag{3.61}$$

where $\gamma_k = \lfloor \tau_k / T_c \rfloor$ and α_k is a random variable uniformly distributed over $[0, T_c)$, which accounts for the fractional chip displacement of the kth user relative to the first user.

Further, we define auxiliary RV's $Z_j^{(k)}$, $j = 0, 1, \ldots, N_c$ as

$$Z_j^{(k)} = \begin{cases} d_{-1}^{(k)} b_{j-\gamma_k+N_c}^{(k)} b_j^{(1)} & j = 0, \ldots, \gamma_k - 1 \\ d_0^{(k)} b_{j-\gamma_k}^{(k)} b_j^{(1)} & j = \gamma_k, \ldots, N_c - 2 \\ d_0^{(k)} b_{N_c-\gamma_k-1}^{(k)} b_{N_c-1}^{(1)} & j = N_c - 1 \\ d_{-1}^{(k)} b_{N_c-\gamma_k-1}^{(k)} b_0^{(1)} & j = N_c. \end{cases} \tag{3.62}$$

Then, W_k can be simplified as [56, eqn. (19)]

$$W_k = P_k R_w(\alpha_k) + Q_k \hat{R}_w(\alpha_k) + X_k \left[\hat{R}_w(\alpha_k) + R_w(\alpha_k)\right] + Y_k \left[\hat{R}_w(\alpha_k) - R_w(\alpha_k)\right] \tag{3.63}$$

where the RV's X_k, Y_k, P_k and Q_k are defined as

$$X_k = \sum_{j \in \mathcal{A}} Z_j^{(k)} \tag{3.64}$$

$$Y_k = \sum_{j \in \mathcal{B}} Z_j^{(k)} \tag{3.65}$$

$$P_k = Z_{N_c}^{(k)} \tag{3.66}$$

$$Q_k = Z_{N_c-1}^{(k)} \tag{3.67}$$

where $\mathcal{A}$ denotes the set of all integers in $[0, N_c - 2]$ satisfying $b_j^{(1)} b_{j+1}^{(1)} = 1$ and $\mathcal{B}$ denotes the set of all integers in $[0, N_c - 2]$ satisfying $b_j^{(1)} b_{j+1}^{(1)} = -1$. According to previous analysis, P_k and Q_k are symmetric Bernoulli RV's and X_k is the sum of A independent symmetric Bernoulli RV's, where A denotes the cardinality of the set $\mathcal{A}$. Y_k is the sum of B independent symmetric Bernoulli RV's, where B denotes the cardinality of the set $\mathcal{B}$.

Define the discrete aperiodic autocorrelation function of the first user's signature sequence as

$$D_1(1) = \sum_{j=0}^{N_c-2} b_j^{(1)} b_{j+1}^{(1)}. \tag{3.68}$$

Note that

$$A = \frac{N_c - 1 + D_1(1)}{2} \tag{3.69}$$

and

$$B = \frac{N_c - 1 - D_1(1)}{2}. \tag{3.70}$$

Thus, the RV's X_k and Y_k depend on the first user's signature sequence only through the parameter $D_1(1)$. It has been shown that P_k, Q_k, X_k and Y_k conditioned on $D_1(1)$ are independent and the $N_u - 1$ MAI terms conditioned on $D_1(1)$ are also independent.

The PDF of X_k and Y_k is given, respectively, by

$$p_{X_k}(j) = \binom{A}{\frac{j+A}{2}} 2^{-A}, \quad j = -A, -A+2, \cdots, A-2, A \tag{3.71}$$

and

$$p_{Y_k}(j) = \binom{B}{\frac{j+B}{2}} 2^{-B}, \quad j = -B, -B+2, \cdots, B-2, B. \tag{3.72}$$

Based on the PDF's of P_k, Q_k, X_k and Y_k, the CHF of W_k conditioned on α_k and $D_1(1)$ can be obtained as

$$\Phi_{W_k|\alpha,D_1}(\omega) = \cos[\omega \hat{R}_w(\alpha)] \cdot \cos[\omega R_w(\alpha)] \cdot \cos^A[\omega f(\alpha)] \cdot \cos^B[\omega g(\alpha)] \tag{3.73}$$

where

$$f(\alpha) = \hat{R}_w(\alpha) + R_w(\alpha) \tag{3.74}$$

and

$$g(\alpha) = \hat{R}_w(\alpha) - R_w(\alpha). \tag{3.75}$$

Averaging out α_k, the CHF of W_k conditioned on $D_1(1)$ is expressed by

$$\Phi_{W_k|D_1}(\omega) = \frac{1}{T_c} \int_0^{T_c} \Phi_{W_k|\alpha,D_1}(\omega) d\alpha. \tag{3.76}$$

Considering the independence of the $N_u - 1$ MAI terms when conditioned on $D_1(1)$, we obtain the conditional CHF of the total interference I as

$$\Phi_{I|D_1}(\omega) = \prod_{k=2}^{N_u} \Phi_{W_k|C_1}\left(A_k \sqrt{\frac{E_b}{N_c}} \omega\right). \tag{3.77}$$

The PDF of the RV $D_1(1)$ is given by

$$p_{D_1}(i) = \binom{N_c - 1}{i} 2^{1-N_c}, \quad i = 0, 1, \cdots, N_c - 1 \tag{3.78}$$

and $p_{D_1}(i) = 0$, otherwise. Expressing A and B in terms of $D_1(1)$ and averaging over the PDF of $D_1(1)$, we can obtain the characteristic function of the total MUI, I, as

$$\Phi_I(\omega) = 2^{1-N_c} \sum_{i=0}^{N_c-1} \binom{N_c - 1}{i} \prod_{k=2}^{N_u} \left[B\left(A_k \sqrt{\frac{E_b}{N_c}} \omega, i\right) + B\left(A_k \sqrt{\frac{E_b}{N_c}} \omega, i+1\right) \right] \tag{3.79}$$

where

$$B(\omega, i) = \frac{1}{2T_c} \int_0^{T_c} \cos^i[\omega f(\alpha)] \cdot \cos^{N_c - i}[\omega g(\alpha)] \, d\alpha. \tag{3.80}$$

3.6.2 Simplified Decision Statistic

Although the expression of W_k in (3.58) provides an exact analysis for calculating the BER of DS-UWB systems, the computation complexity increases greatly when the number of chips per symbol, N_c, increases. Here we introduce a simple alternative method based on a simplified decision statistic.

It has been proved in [64] that the RV W_k can be further simplified to

$$W_k = \Gamma_k \hat{R}_w(\alpha_k) + \Delta_k R_w(\alpha_k) \tag{3.81}$$

where

$$\Gamma_k = \sum_{j=0}^{N_c-1} Z_j^{(k)} \tag{3.82}$$

and

$$\Delta_k = \sum_{j=0}^{N_c-2} Z_j^{(k)} c_j^{(1)} c_{j+1}^{(1)} + Z_{N_c}^{(k)} \tag{3.83}$$

where $\{Z_j^{(k)}\}_{j=0}^{N_c-1}$ follow the definition at (3.62), and are independently and identically distributed (i.i.d) symmetric Bernoulli RV's.

Therefore, the PDF of Γ_k and Δ_k can be obtained as

$$p_{\Gamma_k}(j) = p_{\Delta_k}(j) = \binom{N_c}{\frac{j+N_c}{2}} 2^{-N_c} \quad j = -N_c, 2-N_c, \cdots, N_c-2, N_c. \tag{3.84}$$

Additionally, Γ_k and Δ_k can be shown to be independent. Based on the PDF's of Γ_k and Δ_k , the CHF of W_k conditioned on α_k is given by

$$\begin{aligned}
\Phi_{W_k|\alpha}(\omega) &= \mathbb{E}\left[e^{j\omega W_k} \mid \alpha_k = \alpha\right] \\
&= \mathbb{E}\left[e^{j\omega\Gamma_k \hat{R}_w(\alpha_k)} \mid \alpha_k = \alpha\right] \mathbb{E}\left[e^{j\omega\Delta_k R_w(\alpha_k)} \mid \alpha_k = \alpha\right] \\
&= \left\{\cos[\omega \hat{R}_w(\alpha)] \cdot \cos\left[\omega R_w(\alpha)\right]\right\}^{N_c}.
\end{aligned} \tag{3.85}$$

Considering the uniform distribution of α_k, we can express the CHF of W_k as

$$\Phi_{W_k}(\omega) = \frac{1}{T_c} \int_0^{T_c} \left\{\cos[\omega \hat{R}_w(\alpha)] \cdot \cos\left[\omega R_w(\alpha)\right]\right\}^{N_c} d\alpha. \tag{3.86}$$

In general, W_k and W_{k+1} are dependent because of the single-user receiver correlates them. If one assumes that $\{W_k\}_{k=2}^{N_u}$ are independent for different users, we can obtain the CHF of the total MAI as

$$\Phi_I(\omega) = \prod_{k=2}^{N_u} \Phi_{W_k}\left(A_k\sqrt{\frac{E_b}{N_c}}\omega\right). \tag{3.87}$$

Note that the CHF in (3.87) is an approximation because different W_k are assumed independent. Based on the simplified decision statistic W_k, the CHF of the interference can be easily obtained without averaging over $D_1(1)$. Compared with the exact expression in (3.79), the computational complexity of (3.87) decreases significantly. In Section 3.8, it will be shown by numerical examples that this approximate expression can provide BER estimates essentially as accurate as the exact analysis previously described.

3.7 The Gaussian Approximation for TH and DS UWB systems

In this section, we provide the expressions for the Gaussian approximations for TH, DS and DS-IR UWB systems in order to clarify some mistakes in previous work and to enable the reader to use this chapter as a stand-alone reference. Corresponding to the different modulation schemes used, different expressions for the Gaussian approximation are obtained.

3.7.1 TH-UWB

For TH/DS-IR UWB systems, the variance of the total interference can be written as

$$\begin{aligned}\text{var}[I] &= \mathbb{E}\left[\left(\sqrt{\frac{E_b}{N_s}}\sum_{k=2}^{N_u} A_k I^{(k)}\right)^2\right] \\ &= E_b\sigma_a^2\sum_{k=2}^{N_u} A_k^2 \end{aligned} \tag{3.88}$$

where var[·] denotes the variance and the parameter σ_a^2 is defined as [14, eqn. (79)]

$$\sigma_a^2 = \frac{1}{T_f}\int_{-\infty}^{\infty}\left[\int_{-\infty}^{\infty} p(x-s)v(x)dx\right]^2 ds \tag{3.89}$$

where $v(t)$ takes different forms for the TH-PPM and TH/DS-IR BPSK systems correspondingly. Therefore, the expression for signal-to-interference-plus-noise ratio (SINR) in TH/DS-IR UWB systems is

$$\text{SINR}(N_u) = \frac{S^2}{\sigma_n^2 + E_b\sigma_a^2\sum_{k=2}^{N_u} A_k^2} \tag{3.90}$$

where σ_n^2 is the variance of the noise component.

3.7.2 DS-UWB

For DS-BPSK UWB systems, there are two methods for calculating the variance of the total interference. The first one is the standard Gaussian approximation adopted in CDMA systems, given by

$$\begin{aligned}\text{var}\left[I_{DS}\right] &= \mathbb{E}\left[\left(\sqrt{\frac{E_b}{N_c}}\sum_{k=2}^{N_u} A_k W_k\right)^2\right] \\ &= \frac{E_b}{N_c}\sum_{k=2}^{N_u} A_k^2\mathbb{E}\left[W_k^2\right] \end{aligned} \tag{3.91}$$

where $\mathbb{E}\left[W_k^2\right]$ can be obtained by averaging $\mathbb{E}[W_k^2|\alpha_k = \alpha]$ in terms of the distribution of α_k as

$$\begin{aligned}\mathbb{E}\left[W_k^2\right] &= \frac{1}{T_c}\int_0^{T_c} \mathbb{E}[W_k^2|\alpha_k = \alpha]d\alpha \\ &= \frac{1}{T_c}\int_0^{T_c} \left[\mathbb{E}\left[\Gamma_k^2\right]\hat{R}_p^2(\alpha) + \mathbb{E}\left[\Delta_k^2\right]R_p^2(\alpha)\right]d\alpha \\ &= \frac{N_c}{T_c}\int_0^{T_c} \left[\hat{R}_p^2(\alpha) + R_p^2(\alpha)\right]d\alpha \end{aligned} \tag{3.92}$$

where the last equality comes from the fact that the variance of Γ_k and Δ_k in (3.81) is N_c. Substituting (3.92) into (3.91) yields

$$\text{var}\left[I_{DS}\right] = \frac{E_b}{T_c}\left(\int_0^{T_c}\left[\hat{R}_p^2(\alpha) + R_p^2(\alpha)\right]d\alpha\right)\sum_{k=2}^{N_u} A_k^2. \tag{3.93}$$

Another method for calculating the variance of the MAI in the DS-BPSK UWB system can be obtained similar to the method used for the Gaussian approximation for TH-UWB as [58]

$$\text{var}[I_{DS}] = E_b\sigma_{a_{DS}}^2\sum_{k=2}^{N_u} A_k^2 \tag{3.94}$$

where $\sigma_{a_{DS}}^2$ is expressed as

$$\sigma_{a_{DS}}^2 = \frac{1}{T_c}\int_{-\infty}^{\infty}\left[\int_{-\infty}^{\infty} p(x-s)p(x)dx\right]^2 ds. \tag{3.95}$$

Note that (3.95) is a corrected version of [58, eqn. (16)], in which the authors misused the frame duration T_f instead of the chip width T_c. Comparing (3.93) with (3.94) and considering the definitions of $\hat{R}_p(\alpha)$ and $R_p(\alpha)$, we can see (3.93) is equivalent to (3.94), which further supports that our expressions for the Gaussian approximation for DS-BPSK are correct. Therefore, the SINR in DS-BPSK UWB systems is written as

$$\text{SINR}_{DS}(N_u) = \frac{S_{DS}^2}{\sigma_{n_{DS}}^2 + E_b\sigma_{a_{DS}}^2\sum_{k=2}^{N_u} A_k^2}. \tag{3.96}$$

We define SNR as $\frac{E_b}{N_0}$, common to TH-PPM, TH/DS-IR BPSK and DS-BPSK systems. In order to fairly compare the performances of TH, DS and DS-IR UWB

systems, we further assume that the same data rate $R_b = \frac{1}{T_b}$ is used for all systems, which requires $N_c = N_s N_h$. Thus, T_f used in TH/DS-IR systems equals $N_h T_c$ and T_f used in DS systems equals $N_s N_h T_c$, related to the length of the repetition code, N_s, in TH/DS-IR UWB systems. Based on the normalization, we can see that the SINR of the TH/DS-IR BPSK system in (3.90) is exactly the same as the SINR of the DS-BPSK system in (3.96), which further means that these three systems would achieve the same BER performance when predicted by the Gaussian approximation. This conclusion is consistent with the result reported in [52]. However, in the next section, we will show that this result is not rigorously true and does not reveal the true relationship between the performances of TH-BPSK, DS-BPSK and DS-IR BPSK systems.

3.8 Numerical Results and Comparisons

It is seen that a double-integral calculation is needed for precisely computing the BER of TH-UWB systems, while a single-integral calculation is required for computing the BER using the Gaussian approximation. The parameters of the example UWB systems are listed in Table 3.1. In our numerical examples, we restrict our calculation of the BER for TH, DS and DS-IR systems to the 2^{nd}-order Gaussian monocycle. We consider UWB applications for indoor communications, which requires high-speed data transmission. $N_s = 2, 4$ and 8 are used in our examples to achieve high data rates and low BER's of UWB systems operating with limited number of users. Our analysis, however, can be applied to UWB systems using arbitrary pulse shapes with different values of N_s.

First, we compare the exact BER's of the TH, DS and DS-IR UWB systems with results obtained from simulations and the Gaussian approximation. Fig. 3.1 shows the accurate BER's of the TH-PPM system computed using the exact analysis described in the previous section, as well as the BER's obtained from the Gaussian approximation and simulation. Several observations can be made. As shown, the

TABLE 3.1

Parameters of the Example TH, DS and DS-IR UWB systems

Parameter	Notation	2^{nd}-order monocycle
Time Normalization Factor	τ_p	0.2877 ns
Frame Width	T_f	14.4 ns for TH, 28.8/57.6 ns for DS
Bit Duration	T_b	28.8/57.6/115.2 ns
PPM Delay	δ	0.15 ns
Chip Width	T_c	0.9 ns
Number of Users	N_u	8, 16
Number of Hops per Frame	N_h	16
Repetition Code Length	N_s	2, 4, 8
Number of Chips per Frame	N_c	32, 64, 128

exact BER results and the simulation results are in excellent agreement for all SNR values. It is seen that the GA is in good agreement with the exact analysis only for small SNR values, say SNR $\leq$ 6 dB. The Gaussian approximation fails to predict the error rate floor of the TH-PPM UWB system (caused by the interference) for large SNR values. Indeed, when the SNR = 20 dB, the exact BER is 4.4×10^{-5} with $N_s = 4$, and the BER predicted from the Gaussian approximation is 4.15×10^{-9}, which underestimates the actual BER by over 5 orders of magnitude. Furthermore, Fig. 3.1 indicates that the BER performance improves when the longer repetition code is used, as expected. We observe that the amount of the improvement can be less or more than the improvement predicted by the GA. For example, when the SNR = 9 dB, the amount of the improvement due to use of the longer repetition code predicted by the GA is less than the actual improvement; when the SNR = 20 dB, the amount of improvement predicted by the GA is more than the actual improvement. Therefore, the Gaussian approximation is not a reliable method for predicting BER's

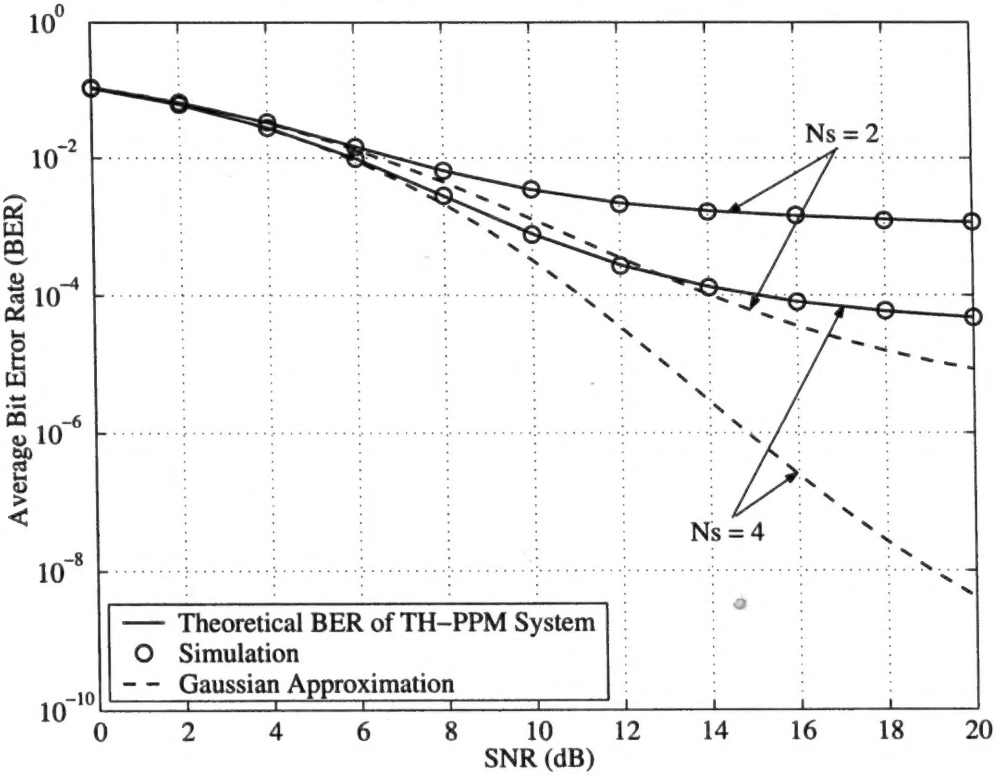

Fig. 3.1. The average BER of the TH-PPM UWB system versus SNR for a repetition code with $N_s = 2$ and $N_s = 4$ assuming 7 asynchronous interferers.

for TH-PPM systems.

Figs. 3.2 and 3.3 show the BER results for the TH-BPSK and DS-IR BPSK system. Similar observations and conclusions can be drawn. The Gaussian approximation again overestimates the bit error rate performance of TH-BPSK system for medium and large SNR values and can underestimate or overestimate the improvement obtained by using a longer repetition code.

In Fig. 3.4, the BER's of the DS-UWB system obtained using the exact decision statistic are plotted together with the BER's obtained using the simplified decision statistic. As shown, the results from the exact analysis agree extremely well with

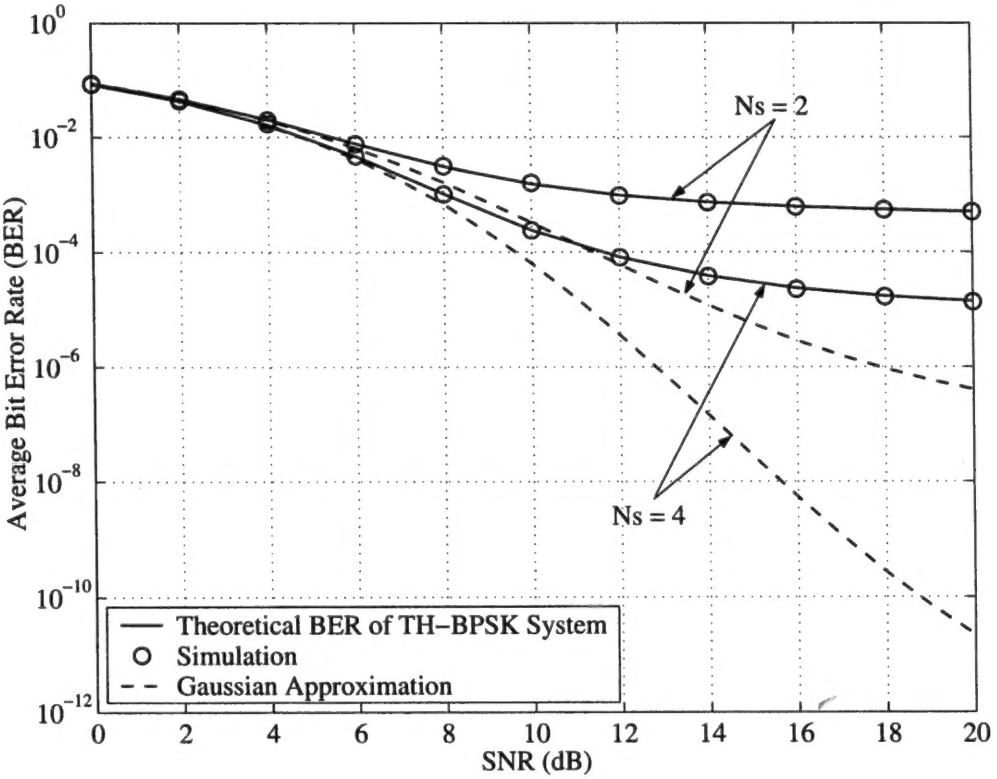

Fig. 3.2. The average BER of the TH-BPSK UWB system versus SNR for a repetition code with $N_s = 2$ and $N_s = 4$ assuming 7 asynchronous interferers.

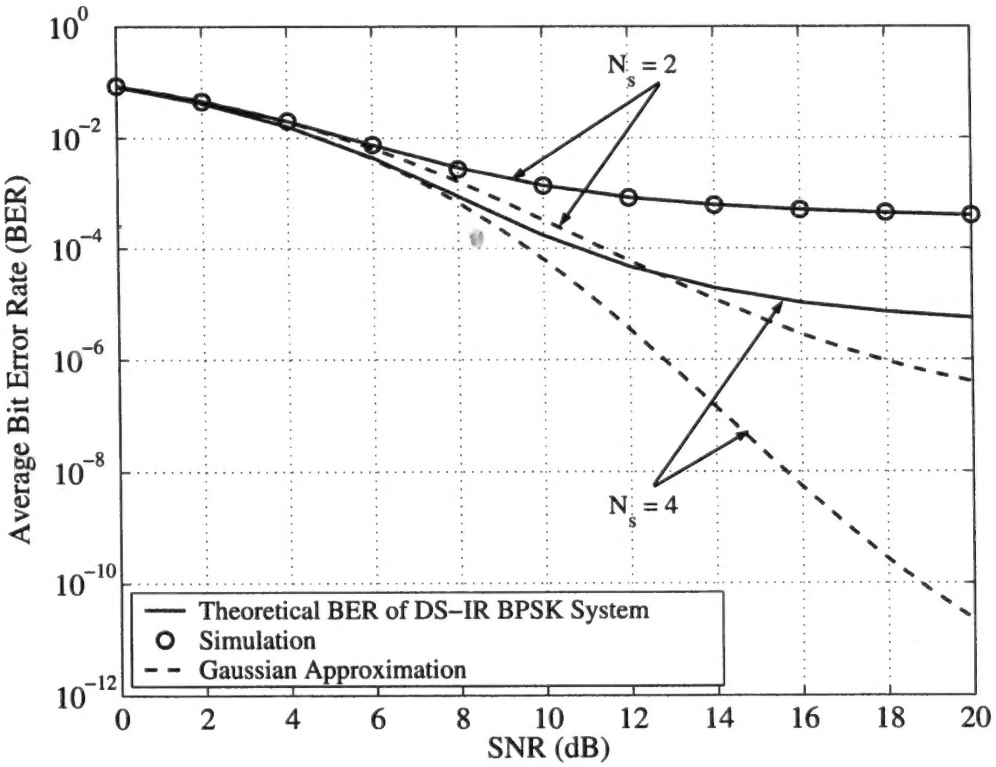

Fig. 3.3. The average BER versus SNR of the DS-IR BPSK system for a repetition code with $N_s = 2$ and $N_s = 4$ assuming 7 asynchronous interferers.

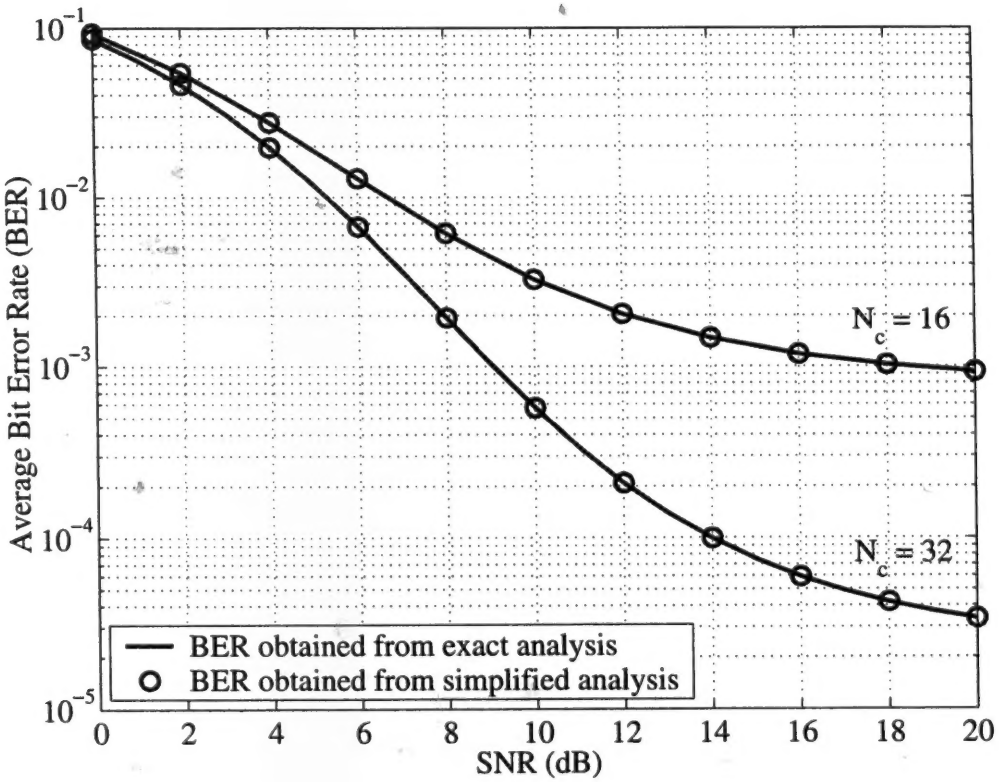

Fig. 3.4. Comparison of the BER obtained from the exact analysis with the BER obtained from the simplified analysis for $N_c = 16$ and $N_c = 32$.

the BER's obtained from the simplified analysis. Compared with the exact analysis, the simplified analytical method provides BER results essentially as accurate as the exact analysis and requires much less computational complexity. Therefore, the simplified method can be used as an very good alternative for precisely calculating the probability of error of DS-UWB systems.

Fig. 3.5 shows the performance of the DS-BPSK UWB system with the 2^{nd}-order Gaussian monocycle assuming 7 asynchronous interferers. We observe, from our numerical results, that the Gaussian approximation also underestimates the BER's for the DS-BPSK UWB system for large SNR values and fails to predict the error

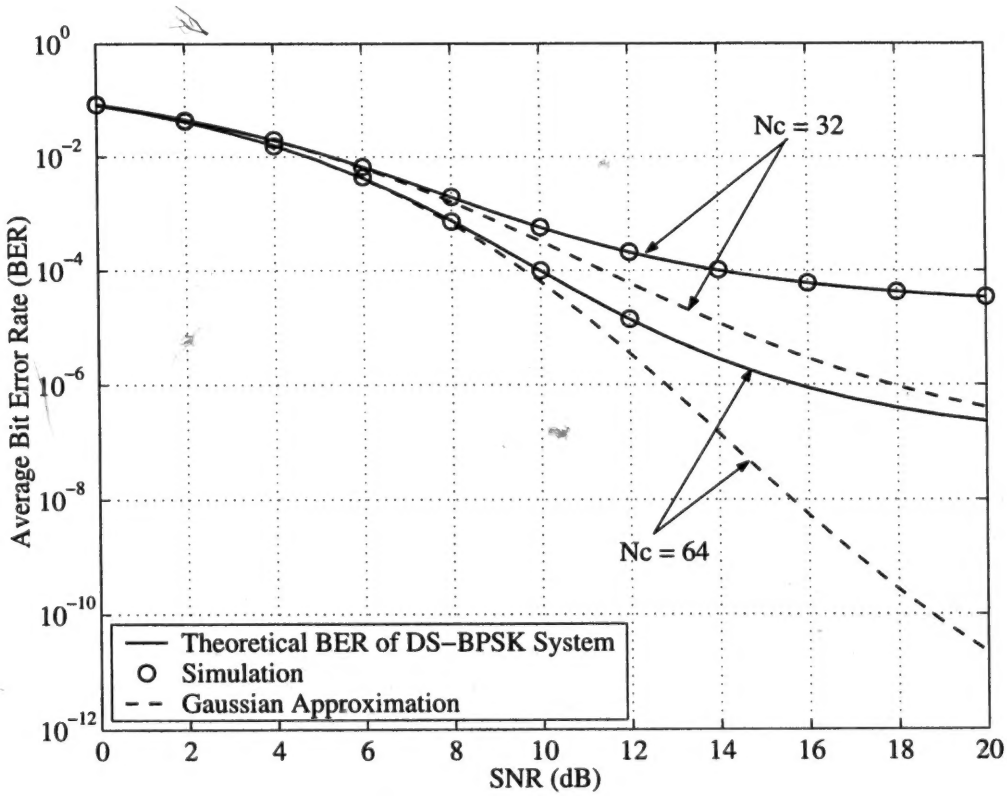

Fig. 3.5. The average BER of the DS-BPSK system for $N_c = 32$ and $N_c = 64$ assuming 7 asynchronous interferers.

rate floor caused by multi-user interference in the DS-UWB system. Compared with the Gaussian approximation, our exact analysis for TH, DS and DS-IR UWB systems provides accurate BER estimates for all values of SNR; it can be used for accurately comparing TH, DS and DS-IR UWB systems.

In Fig. 3.6, the bit error rates of TH-PPM, TH-BPSK and DS-BPSK assuming 7 asynchronous interferers are compared. We observe that the TH-BPSK system outperforms the TH-PPM system for all values of SNR. The TH-BPSK system provides similar performance to the DS-BPSK system for small SNR values, say SNR $\leq$ 4 dB. Unlike the result reported in [52] obtained using the Gaussian approximation,

which states that the TH-BPSK achieves the same multiple access performance as the DS-BPSK system, the actual performance of the DS-BPSK system is better than the actual performance of the TH-BPSK system for medium and large SNR values. As seen, DS-BPSK significantly outperforms TH-PPM for all SNR values, and the BER's of DS-BPSK with $N_c = 32$ are smaller than the BER's of TH-PPM with $N_s = 4$, even though the data rate of the TH-PPM system is half of the data rate of the DS-BPSK system.

Fig. 3.7 shows the performances of time-hopping and direct-sequence UWB systems assuming 15 asynchronous interferers. When more interfering users exist, the bit error rate performance of each system is worse than its performance with fewer interfering users, as expected. Our numerical examples indicate that TH-BPSK and DS-BPSK outperform TH-PPM for all SNR values and DS-BPSK outperforms TH-BPSK for medium and large SNR values. However, the performance gap between TH-BPSK and DS-BPSK systems for larger numbers of users is not as big as the gap for small numbers of users.

In order to show the validity of the Gaussian approximation for large numbers of users, we compare the BER's of TH/DS-UWB systems with different numbers of users in Fig. 3.8. As we can see, the Gaussian approximation still significantly underestimates the BER's of TH-PPM and TH-BPSK systems, even for large number of users, say $N_u = 100$. On the other hand, as the number of users increases, the Gaussian approximation for the DS-BPSK system is more accurate for estimating the BER's. Specifically, when $N_u = 100$, the BER of the DS-BPSK system obtained from the Gaussian approximation is very close to the BER obtained from the exact analysis. Although the Gaussian approximation predicts the same BER's for DS-BPSK as for TH-BPSK, DS-BPSK achieves much better performance than TH-BPSK even for a large number of users. This observation can be explained by considering the structures of TH/DS-BPSK systems and the central limit theorem.

Fig. 3.9 shows the performance comparison of TH-BPSK and DS-IR BPSK for $N_s = 2$, 4 and 8. As shown, the DS-IR BPSK system provides very similar perfor-

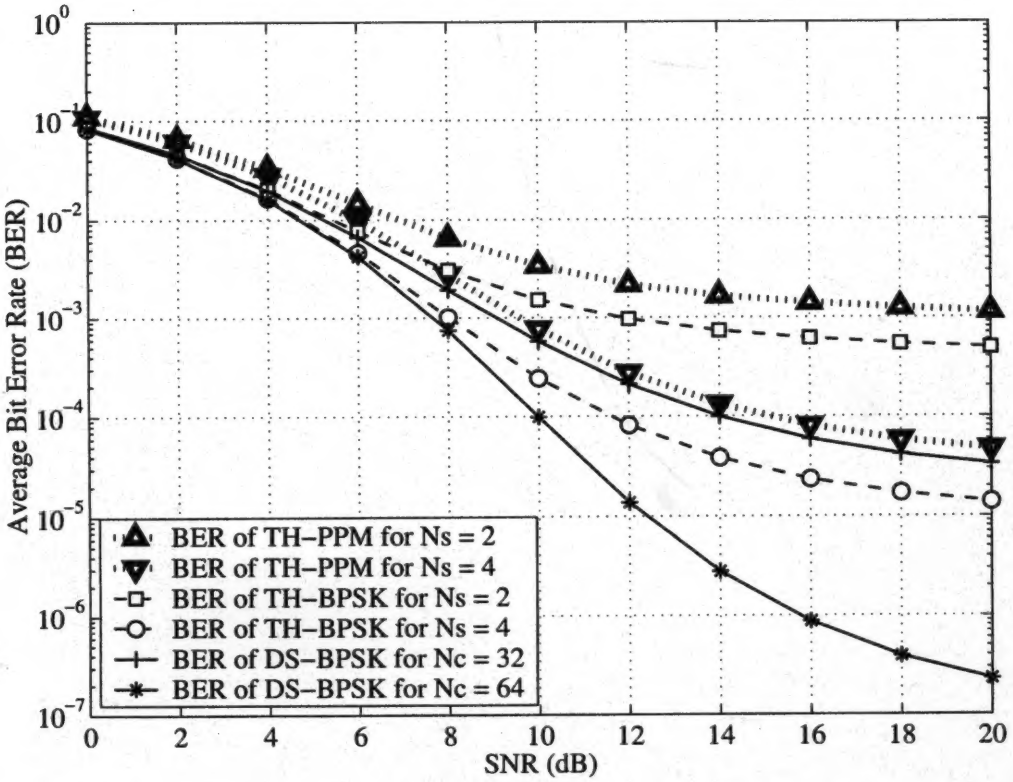
Average Bit Error Rate (BER)
SNR (dB)
BER of TH–PPM for Ns = 2
BER of TH–PPM for Ns = 4
BER of TH–BPSK for Ns = 2
BER of TH–BPSK for Ns = 4
BER of DS–BPSK for Nc = 32
BER of DS–BPSK for Nc = 64

Fig. 3.6. Comparison of the TH-PPM, TH-BPSK and DS-BPSK systems with the same data rate assuming 7 asynchronous interferers.

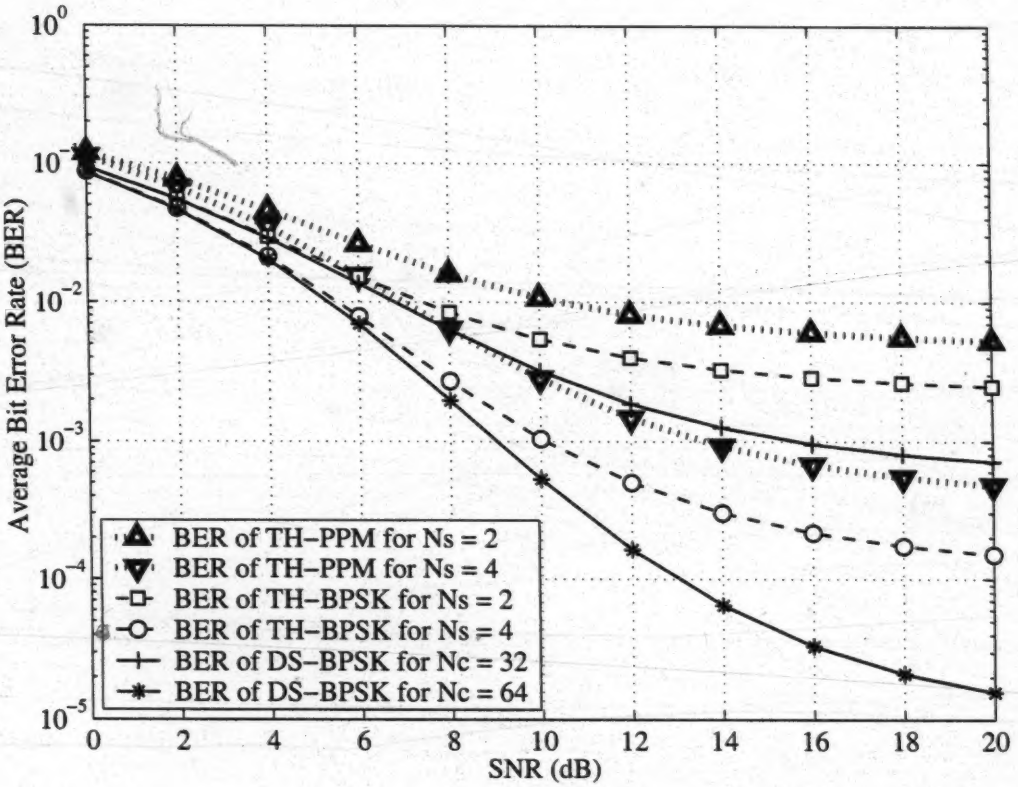
Average Bit Error Rate (BER)
SNR (dB)
BER of TH–PPM for Ns = 2
BER of TH–PPM for Ns = 4
BER of TH–BPSK for Ns = 2
BER of TH–BPSK for Ns = 4
BER of DS–BPSK for Nc = 32
BER of DS–BPSK for Nc = 64

Fig. 3.7. Comparison of the TH-PPM, TH-BPSK and DS-BPSK systems with the same data rate assuming 15 asynchronous interferers.

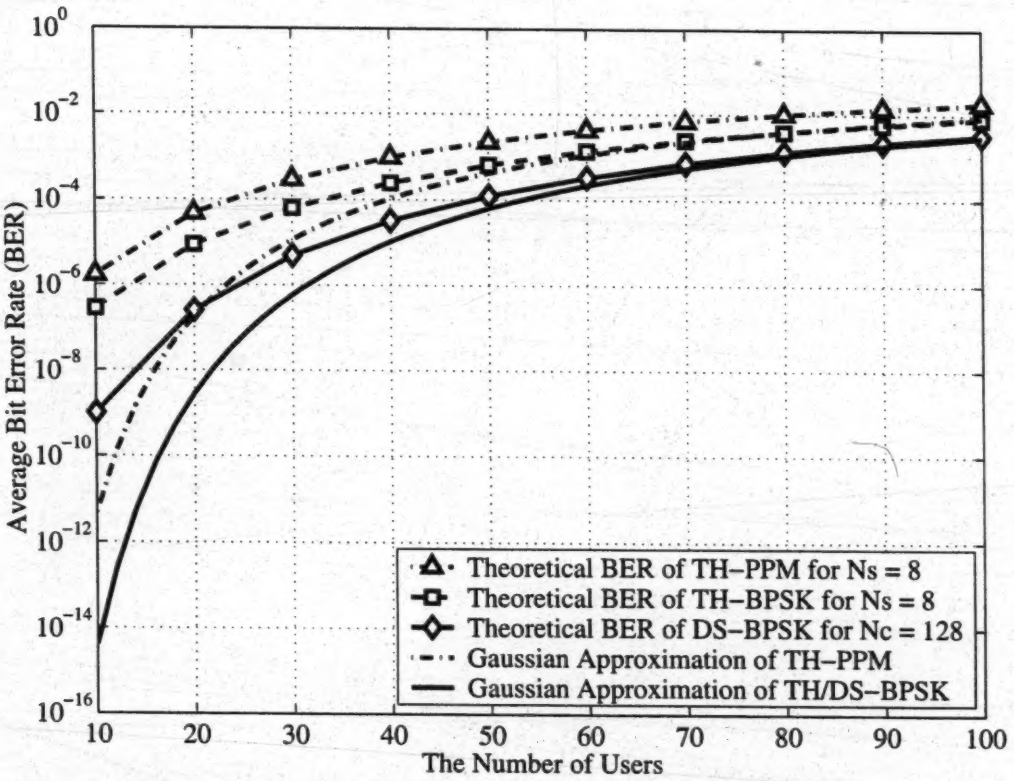
Average Bit Error Rate (BER)
The Number of Users
Theoretical BER of TH–PPM for Ns = 8
Theoretical BER of TH–BPSK for Ns = 8
Theoretical BER of DS–BPSK for Nc = 128
Gaussian Approximation of TH–PPM
Gaussian Approximation of TH/DS–BPSK

Fig. 3.8. Comparison of the TH-PPM, TH-BPSK and DS-BPSK systems with the same data rate for different numbers of users with SNR = 20 dB.

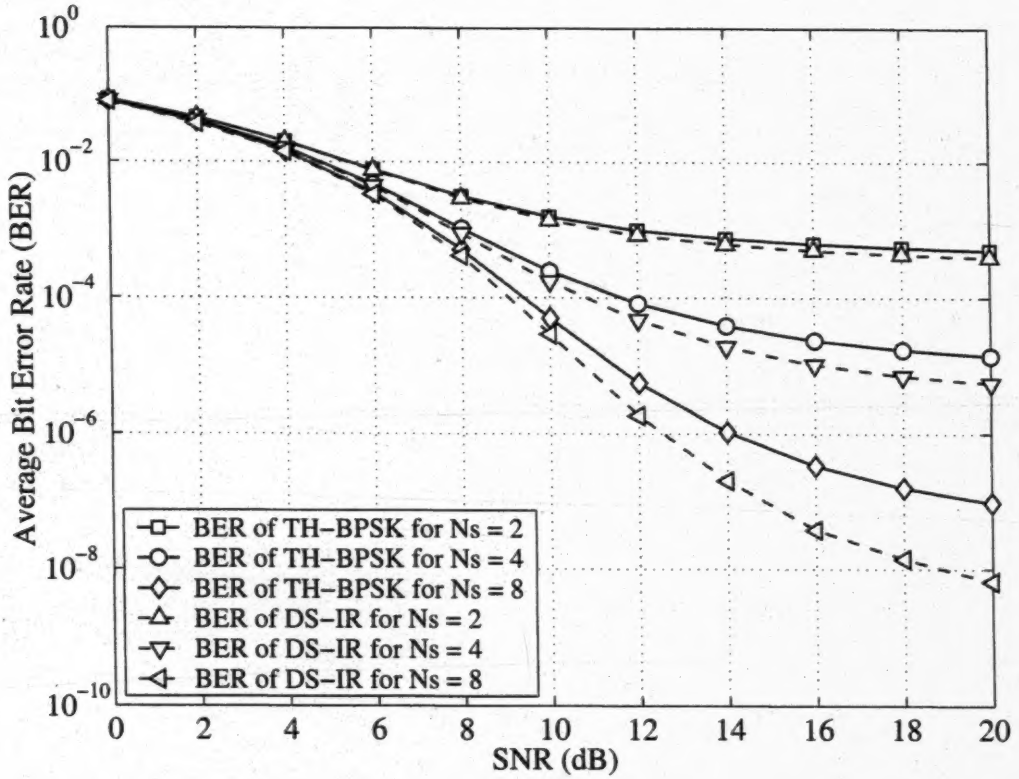
Average Bit Error Rate (BER)
SNR (dB)
BER of TH–BPSK for Ns = 2
BER of TH–BPSK for Ns = 4
BER of TH–BPSK for Ns = 8
BER of DS–IR for Ns = 2
BER of DS–IR for Ns = 4
BER of DS–IR for Ns = 8

Fig. 3.9. Comparison of the DS-IR BPSK and TH-BPSK assuming 7 asynchronous interferers.

mance to the TH-BPSK system for small SNR values, say SNR $\leq$ 6 dB. DS-IR slightly outperforms TH-BPSK for medium and large SNR values when $N_s = 2$. When the value of N_s increases, the performance improvement by adding direct-sequence to the original time-hopping UWB system becomes larger. The performance difference between DS-IR BPSK and TH-BPSK for $N_s = 4$ is greater than the difference for $N_s = 2$, and again better for $N_s = 8$.

In Fig. 3.10, the bit error rates of DS-BPSK and DS-IR BPSK assuming 7 asynchronous interferers are compared. We observe from Fig. 3.10 that although the DS-BPSK system achieves the same multiple access performance as DS-IR systems

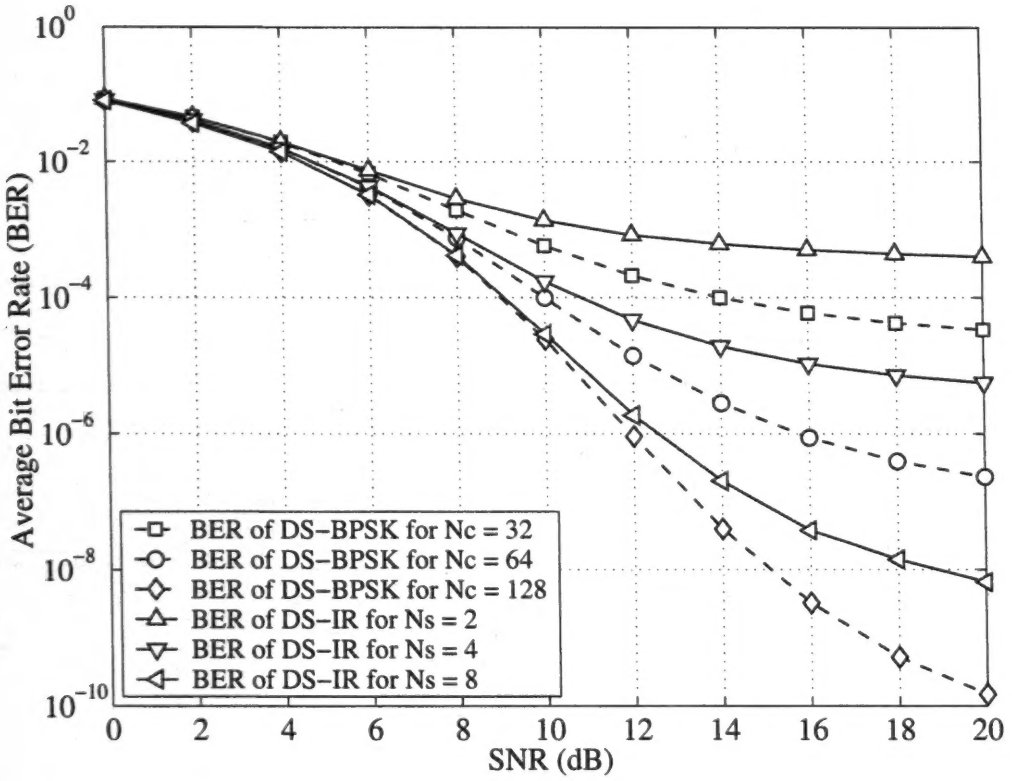
Average Bit Error Rate (BER)
SNR (dB)
BER of DS–BPSK for Nc = 32
BER of DS–BPSK for Nc = 64
BER of DS–BPSK for Nc = 128
BER of DS–IR for Ns = 2
BER of DS–IR for Ns = 4
BER of DS–IR for Ns = 8

Fig. 3.10. Comparison of the DS-IR BPSK and DS-BPSK systems with the same date rate assuming 7 asynchronous interferers.

for small SNR values, it significantly outperforms DS-IR for medium and large SNR values. Noteworthy, the error floors of DS-IR are almost 10 times and 25 times the error floors of DS-BPSK for $N_s = 2$ and $N_s = 4$, repectively.

3.9 Summary

In this chapter, we have derived accurate, analytical expressions for the average probability of bit error of TH-PPM, TH-BPSK, DS-BPSK and DS-IR BPSK UWB systems in a unified framework. Our precise analysis indicates that the Gaussian approxima-

tion for these UWB modulation schemes substantially overestimates the performance at large values of SNR. Compared with other methods used in the performance analysis of UWB systems, our analysis provides a powerful tool for calculating BER's to any desired accuracy with low complexity. The analytical method proposed can be used as a reliable analytical tool in the performance evaluation of time-hopping and direct-sequence UWB systems for arbitrary values of SNR and arbitrary pulse waveforms.

Our comparisons of the performances of time-hopping and direct-sequence UWB systems in the presence of multiple access interference, as measured by the average probability of bit error, showed that the TH-BPSK system outperforms the TH-PPM system for all values of SNR. In contrast to the previous result obtained using the Gaussian approximation, our numerical examples obtained using the exact analysis show that the actual performance of the DS-BPSK system is better than the actual performance of the TH-BPSK system for medium and large SNR values. However, when the values of SNR are small, the TH-BPSK and DS-BPSK achieve almost the same BER's for the same system load. As the number of users increases, the Gaussian approximation still overestimates the BER's of TH-UWB systems, however, it provides more accurate BER estimates for the DS-BPSK system.

In addition, our comparisons of the performances of DS-BPSK, TH-BPSK and DS-IR BPSK UWB systems in the presence of multiple access interference showed that the DS-IR BPSK system outperforms the TH-BPSK system for medium and large values of SNR, though the performance difference is small when the value of N_s is small. The performance of DS-IR, however, is poorer than the performance of the DS-BPSK system for medium and large SNR values. On the other hand, when the values of SNR are small, TH-BPSK, DS-IR and DS-BPSK achieve almost the same BER's. Although TH-UWB was the original proposal for multiple access UWB systems, DS-UWB system is superior to the TH-UWB system in terms of the multiple access error rate performance. In particular, we can conclude that the DS-BPSK system is the best choice among these TH, DS and DS-IR systems, under consideration of the

multiple access performances and the complexity of the implementations. The newly proposed DS-IR system, with its more complicated transceiver design and poorer bit error rate performance, does not compete well with the DS-BPSK system for multiple access UWB communications.

Chapter 4

Pulse Shapes and Design Paradigm for Ultra-Wideband Communication Systems

4.1 Introduction

Unlike conventional wireless communications systems that are carrier-based, a UWB system transmits the information without translating it to a higher carrier frequency, and so UWB is called carrier-less impulse radio. This carrier-less technique will greatly reduce the complexity and cost of the transceiver. In a UWB system, the choice of the impulse (pulse shape) will strongly affect the design of filters, the choice of receiver bandwidth, the bit error rate performance in general, and the performance in multipath propagation environments. Impulse radio signals in UWB systems utilize the extremely broad bandwidth for transmission and coexist with other radio applications in the same frequency spectrum. It is desirable for UWB signals to spread the energy as widely in frequency as possible to minimize the power spectral density and hence the potential for interference to other user systems. A variety of pulse shapes has been proposed for UWB impulse radio systems including the Gaussian

monocycles and the Manchester monocycle, which are designed to approach an ideal transmission power spectrum and to avoid having a DC component. There are two motivatives that make an investigation into pulse-shaping for UWB communication systems timely. First, the FCC has recently introduced restrictions that the UWB systems must operate with their -10 dB bandwidth within the frequency 3.1-10.6 GHz for indoor communications and their -20 dB bandwidth within 3.1-10.6 GHz for outdoor communications [38]. These new frequency bandwidth constraints motivate an evaluation of the pulses previously proposed for UWB systems. Second, accurate assessment of the BER performance of UWB systems has heretofore been complicated or intractable. Recently, reference [15] has provided an efficient and exact method that now permits accurate and tractable computation of UWB system BER's.

A set of Gaussian monocycles was the original proposal for UWB communications systems and has been widely adopted in the investigation of UWB applications. An orthogonal pulse set based on modified Hermite polynomials was introduced in [16]. More recently, a novel pulse design algorithm utilizing the concepts of prolate spheroidal functions was proposed in [65]. In this chapter, we first analyze and evaluate pulses proposed for UWB systems in light of the FCC frequency emission restrictions. We find that some do not meet the FCC requirements. For the pulses that can (possibly with frequency translations) meet the FCC masks, we examine and compare the average bit error probabilities of time-hopping UWB systems using the different pulses based on the exact performance analysis method newly published in [15].

The new frequency bandwidth constraint motivates not only an evaluation of the pulses previously proposed for UWB systems, but also the design of novel pulses. As a result, we propose a new paradigm to design pulse shapes for UWB communication systems in this chapter. The pulses generated from our paradigm are limited to time so as to reduce the interference, while meeting the FCC bandwidth regulations without complicated implementation. It is important to recognize that the transmitter antenna may not have a flat spectral response over the full bandwidth of the trans-

mitted signal. Our results then apply, as do also the results in [16], [55], and [65], to the overall response. That is, the cascade of the antenna filter characteristic and the transmitter pulse-shaping filters should be designed so as to realize the pulse shapes derived here. In the alternative, the antenna filter characteristic can be compensated by a pre-emphasis network at the transmitter.

The remaining content of this chapter is organized as follows. In Section 4.2, pulse shapes previously proposed for UWB systems are described and the power spectral densities of these pulse shapes are examined for compliance with the FCC frequency emission regulations. The error rate performances of these pulse shapes are then evaluated and compared in Section 4.3 . In Section 4.4, we describe our novel pulse design paradigm. Some pulse examples and discussion are provided in Section 4.5. Finally, Section 4.6 summarizes the chapter results.

4.2 Pulse shapes and power spectral densities

The spectral emission constraints specified by government regulatory agencies are formulated as relative amplitude frequency spectral masks that the UWB system must meet. Thus, it is the transmitted UWB system signal that must meet the spectral mask. Note that the spectrum of the transmitted signal will not, in general, be the same as the spectrum of the pulse used for the pulse-shaping. In general, the transmitted spectrum will depend on the modulation scheme used.

The power spectral density of the transmitted signal, $s(t)$, for TH-PPM systems is [66]

$$\Phi_{ss}(f) = \Phi_{ss}^{c}(f) + \Phi_{ss}^{d}(f) \tag{4.1}$$

where $\Phi_{ss}^{c}(f)$ denotes the continuous part of the PSD, given by

$$\Phi_{ss}^{c}(f) = \frac{1}{T_f}|P(f)|^2 \left\{ 1 - \left| \frac{1}{N_h} \sum_{h=0}^{N_h-1} e^{j2\pi f h T_c} \right|^2 \left| \frac{1}{2}\left(1 + e^{j2\pi f \delta}\right) \right|^2 \right\} \tag{4.2}$$

and $\Phi_{ss}^{d}(f)$ is the discrete part of the PSD, given by

$$\Phi_{ss}^{d}(f) = \frac{1}{T_f^2}|P(f)|^2 \left|\frac{1}{N_h}\sum_{h=0}^{N_h-1} e^{j2\pi fhT_c}\right|^2 \left|\frac{1}{2}\left(1+e^{j2\pi f\delta}\right)\right|^2 \sum_{k=-\infty}^{\infty} \delta_D\left(f-\frac{k}{T_f}\right). \quad (4.3)$$

The average PSD of the transmitted signal in TH-BPSK systems is [12], [66]

$$\Phi_{ss_{BPSK}}(f) = \frac{1}{T_f}|P(f)|^2. \quad (4.4)$$

Define

$$C(f) = 1 - \left|\frac{1}{N_h}\sum_{h=0}^{N_h-1} e^{-j2\pi fhT_c}\right|^2 \left|\frac{1}{2}\left(1+e^{j2\pi f\delta}\right)\right|^2 \quad (4.5)$$

then rewrite (4.2) and (4.3) into

$$\Phi_{ss}^{c}(f) = \frac{1}{T_f}|P(f)|^2 C(f) \quad (4.6)$$

and

$$\Phi_{ss}^{d}(f) = \frac{1}{T_f^2}|P(f)|^2\left[1-C(f)\right]\sum_{k=-\infty}^{\infty} \delta_D\left(f-\frac{k}{T_f}\right) \quad (4.7)$$

respectively. It can be proved that $0 \leq |C(f)| \leq 1$; Fig. 4.1 illustrates $C(f)$ for some different values of N_h and T_c. Thus, the envelope of the transmitted UWB system spectrum equals a scaling of the power spectrum of the shaping pulse as shown in eqns. (4.4), (4.6) and (4.7). Therefore, the PSD of the pulse shape is used in studies to determine whether the UWB system spectrum meets the frequency emission mask [65].

Now we introduce several types of pulses proposed for ultra-wideband communications systems and examine the power spectral densities of these pulses for compliance with the FCC UWB masks.

4.2.1 Gaussian Monocycles

The Gaussian pulse has the form

$$p_0(t) = \exp\left[-2\pi\left(\frac{t}{\tau_p}\right)^2\right] \quad (4.8)$$

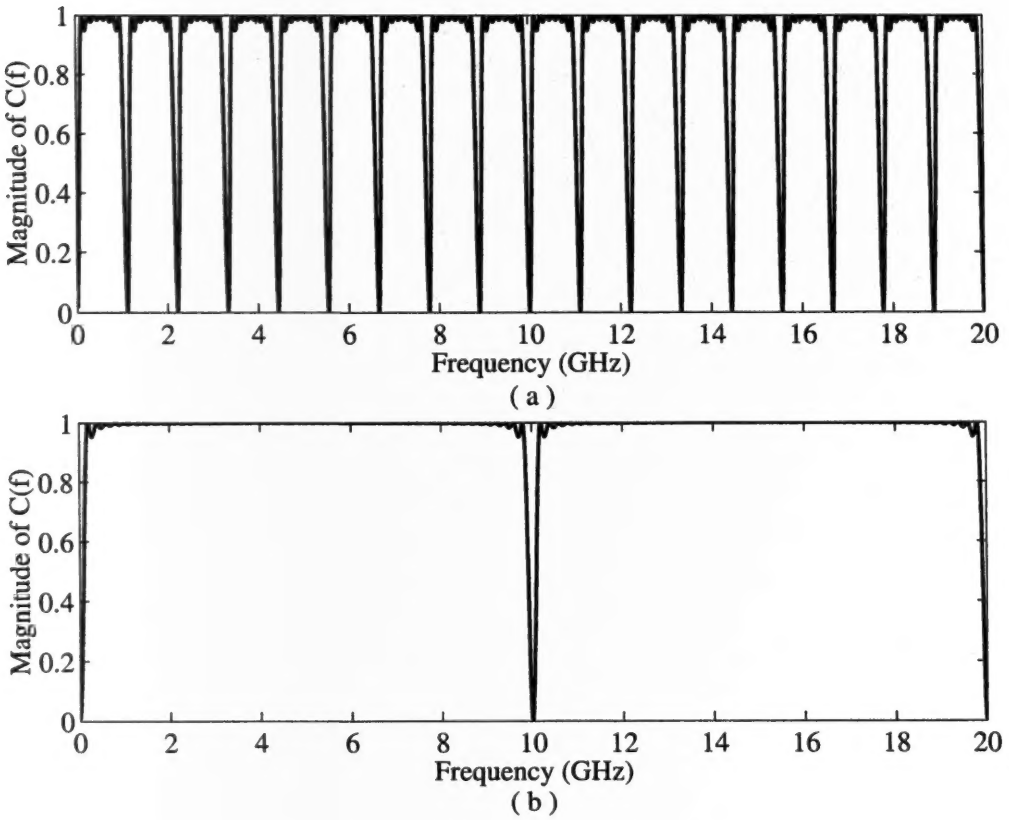

Fig. 4.1. Magnitude of $C(f)$ for (a)$N_h = 8$, $T_c = 0.9ns$ and (b)$N_h = 50$, $T_c = 0.1ns$

and its n^{th} derivative named the n^{th} order Gaussian monocycle is [55]

$$p_n(t) = \mathcal{E}_n \frac{d^n}{dt^n} \exp\left[-2\pi \left(\frac{t}{\tau_p}\right)^2\right] \tag{4.9}$$

where τ_p represents a bandwidth scaling factor and $\mathcal{E}_n$ is introduced to normalize the energy of the pulses $p_n(t)$. The most widely reported pulse in the UWB literature is the 2^{nd} order Gaussian monocycle [14], which is the second derivative of the Gaussian pulse given by

$$p_2(t) = \left[1 - 4\pi \left(\frac{t}{\tau_p}\right)^2\right] \exp\left[-2\pi \left(\frac{t}{\tau_p}\right)^2\right]. \tag{4.10}$$

The autocorrelation $R_2(x)$ of the 2^{nd} order Gaussian monocycle $p_2(t)$ in (4.10) is

$$R_2(x) = \left[1 - 4\pi \left(\frac{x}{\tau_p}\right)^2 + \frac{4\pi^2}{3}\left(\frac{x}{\tau_p}\right)^4\right] \exp\left[-\pi \left(\frac{x}{\tau_p}\right)^2\right]. \tag{4.11}$$

In order to analyze the spectral behaviour of Gaussian monocycles, Fourier transforms of these monocycles are calculated. As known, the Fourier transform of the Gaussian pulse is given by

$$\mathcal{F}\left[\exp\left(-2\pi \left(\frac{t}{\tau_p}\right)^2\right)\right] = \frac{\tau_p}{\sqrt{2}} \exp\left[-\frac{\pi(f\tau_p)^2}{2}\right] \tag{4.12}$$

The Fourier transforms of the derivatives of the Gaussian pulse can be obtained using the following property

$$\mathcal{F}\left[\frac{d^n}{dt^n} p_0(t)\right] = (j2\pi f)^n \mathcal{F}\left[p_0(t)\right]. \tag{4.13}$$

The power spectral density of the Gaussian monocycle can also be obtained by taking the Fourier transform of the autocorrelation function of the monocycle. The

autocorrelations of high-order Gaussian monocycles are given by

$$R_3(x) = \left[1 - 6\pi\left(\frac{x}{\tau_p}\right)^2 + 4\pi^2\left(\frac{x}{\tau_p}\right)^4 - \frac{8\pi^3}{15}\left(\frac{x}{\tau_p}\right)^6\right]\exp\left[-\pi\left(\frac{x}{\tau_p}\right)^2\right] \tag{4.14}$$

$$R_4(x) = \left[1 - 8\pi\left(\frac{x}{\tau_p}\right)^2 + 8\pi^2\left(\frac{x}{\tau_p}\right)^4 - \frac{32\pi^3}{15}\left(\frac{x}{\tau_p}\right)^6 + \frac{16\pi^4}{105}\left(\frac{x}{\tau_p}\right)^8\right]\exp\left[-\pi\left(\frac{x}{\tau_p}\right)^2\right] \tag{4.15}$$

$$R_5(x) = \left[1 - 10\pi\left(\frac{x}{\tau_p}\right)^2 + \frac{40\pi^2}{3}\left(\frac{x}{\tau_p}\right)^4 - \frac{16\pi^3}{3}\left(\frac{x}{\tau_p}\right)^6 + \frac{16\pi^4}{21}\left(\frac{x}{\tau_p}\right)^8 - \frac{32\pi^5}{945}\left(\frac{x}{\tau_p}\right)^{10}\right]\exp\left[-\pi\left(\frac{x}{\tau_p}\right)^2\right]. \tag{4.16}$$

The center frequency and the -10 (-20) dB bandwidth of the spectrum (the bandwidth measured between the 10 (20) dB down points of the spectrum) are determined by the scaling factor τ_p in (4.11). Checking the power spectral densities of the Gaussian monocycles for compliance with the FCC frequency masks for indoor and outdoor communications, we found that the PSD's of the 2^{nd} and 3^{rd} order Gaussian monocycles cannot meet the FCC masks unless a frequency translation is implemented. However, with suitable values of τ_p, the PSD's of the Gaussian monocycles with order higher than 3 can meet the frequency restriction for indoor UWB communications. Moreover, the Gaussian monocycles with order higher than 5 can fit their -20 dB bandwidth within the frequency 3.1 - 10.6 GHz for some values of τ_p without any frequency shift, and thus can be utilized in UWB systems for outdoor communications. As examples of pulses that comply with the FCC specifications, the power spectral densities of the 4^{th} order and the 7^{th} order Gaussian monocycles are shown in Fig. 4.2 together with the FCC frequency masks. Fig. 4.3 illustrates that the 2^{nd} and 3^{rd} order Gaussian monocycles cannot meet the spectral masks. In our attempts to make the pulse spectra meet the masks, we found that compressing the spectra by adjusting the scaling factor could not be done because changing the scaling factor also changes the center frequency in such a way that the spectra fails to meet the mask.

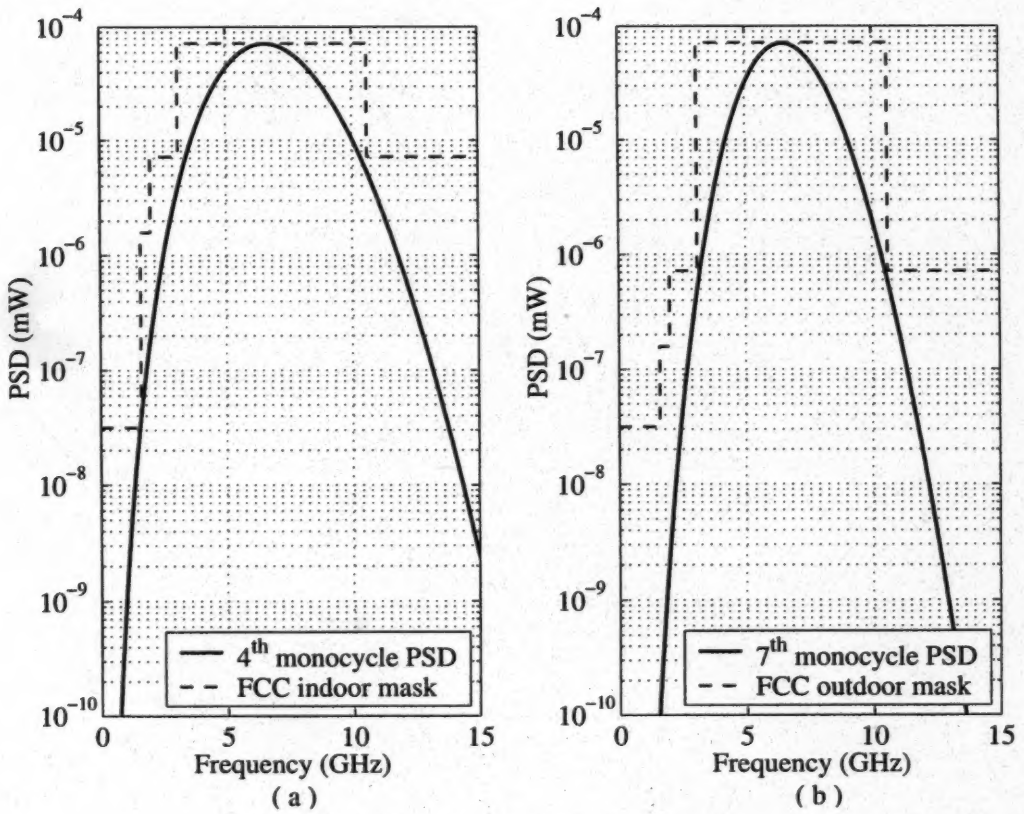

Fig. 4.2. Power spectral density of (a) the 4^{th} order and (b) the 7^{th} order Gaussian monocycle and the FCC masks.

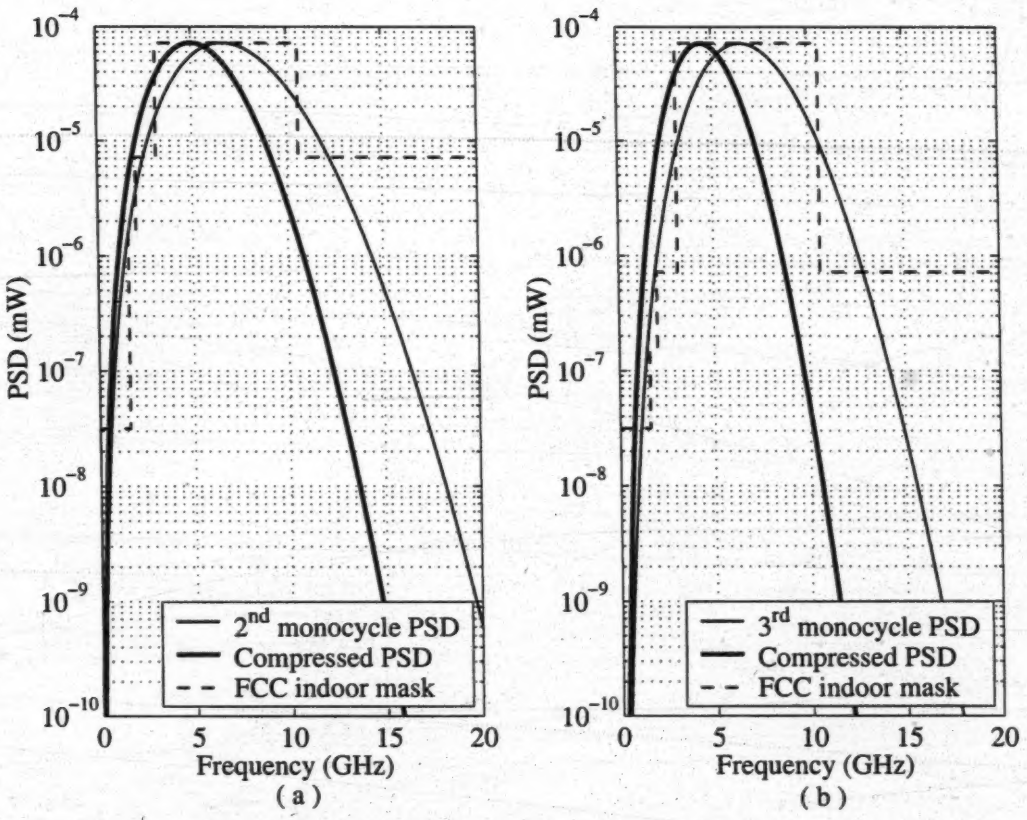

Fig. 4.3. Power spectral density of (a) the 2^{nd} order and (b) the 3^{rd} order Gaussian monocycle and the FCC masks.

4.2.2 Novel Pulses based on Prolate Spheroidal Functions (PS pulse)

In [65], a novel pulse design algorithm was proposed based on the prolate spheroidal functions. It can be used to numerically generate pulses whose power spectrums fit the desired frequency mask. We briefly review this algorithm here in order to make our evaluation and comparisons of different pulse-shaping self contained. Only needed material is summarized.

A designed pulse signal $w(t)$ that meets the desired frequency mask satisfies the form in [65, eqn.(3)] as

$$\lambda w(t) = \int_{T_m/2}^{T_m/2} w(\tau)h(t-\tau)d\tau \tag{4.17}$$

where T_m is the pulse width and $h(t)$ is the impulse response of the bandpass filter. Rather than solving (4.17) directly, [65] introduced a numerical solution based on the discretization of (4.17). By using N samples per pulse width T_m, (4.17) can be written in a vector form as

$$\lambda \underbrace{\begin{bmatrix} w\left[-\frac{N}{2}\right] \\ \vdots \\ w[0] \\ \vdots \\ w\left[\frac{N}{2}\right] \end{bmatrix}}_{w} = \underbrace{\begin{bmatrix} h[0] & \cdots & h[-N] \\ \vdots & \vdots & \vdots \\ h[\frac{N}{2}] & \cdots & h\left[-\frac{N}{2}\right] \\ \vdots & \vdots & \vdots \\ h[N] & \cdots & h[0] \end{bmatrix}}_{H} \times \underbrace{\begin{bmatrix} w\left[-\frac{N}{2}\right] \\ \vdots \\ w[0] \\ \vdots \\ w\left[\frac{N}{2}\right] \end{bmatrix}}_{w} \tag{4.18}$$

where H is a Toeplitz matrix and w is an eigenvector of H. Applying the theory of prolate spheroidal wave functions, eigenvectors corresponding to large eigenvalues are chosen for designing pulses (for maximum energy capture). Then, considering the FCC frequency masks, the ideal bandpass filter $h(t)$ is chosen to operate between $f_L = 3.1$ GHz and $f_U = 10.6$ GHz, which has the form

$$h(t) = 2f_U\text{sinc}(2f_U t) - 2f_L\text{sinc}(2f_L t). \tag{4.19}$$

Two eigenvectors corresponding to the two largest eigenvalues for $N = 64$ and $T_m = 1$ ns were obtained in [65] using eigenvalue decomposition. These two eigenvectors were used to numerically form the desired pulses $w_1(t)$ and $w_2(t)$. It was shown in [65] that the power spectrums of $w_1(t)$ and $w_2(t)$ meet the FCC frequency masks.

As mentioned in [65], the pulse width T_m has a significant effect on the design of the pulses. Decreasing T_m, we can design a pulse whose -10 (-20) dB bandwidth is exactly fitted into the specified bandwidth of 3.1 - 10.6 GHz. However, the PSD of the pulse generated has large sidelobes, which can produce strong adjacent channel interference, undesirable in some applications.

4.2.3 Modified Hermite Polynomial Based Pulses (HP pulse)

A set of orthogonal pulses based on the Hermite polynomials was proposed for ultra-wideband communications in [16]. Using modified Hermite polynomial functions, a set of orthogonal pulses with almost invariant pulse width can be obtained.

The modified Hermite polynomial based pulse shapes are given by

$$\begin{aligned} h_n(t) &= e^{-\frac{t^2}{4}} h_{e_n}(t) \\ &= (-1)^n e^{\frac{t^2}{4}} \frac{d^n}{dt^n} \left(e^{-\frac{t^2}{2}} \right) \end{aligned} \tag{4.20}$$

where $h_{e_n}(t)$ are the Hermite polynomials given in [68, eqn. (6.23)] as

$$\begin{aligned} h_{e_0}(t) &= 1 \\ h_{e_2}(t) &= t^2 - 1 \\ h_{e_4}(t) &= t^4 - 6t^2 + 3. \end{aligned} \tag{4.21}$$

Examining the PSD's of the HP pulses of different orders, we note that the pulses of even orders have a DC component. Further, a frequency shift is necessary for the HP pulses of order 0 and 1 to meet the FCC spectral masks as shown in Fig. 4.4. HP pulses with order higher than 1 have multiple large sidelobes, which have to be removed using bandpass filters. Therefore, several operations are required for HP

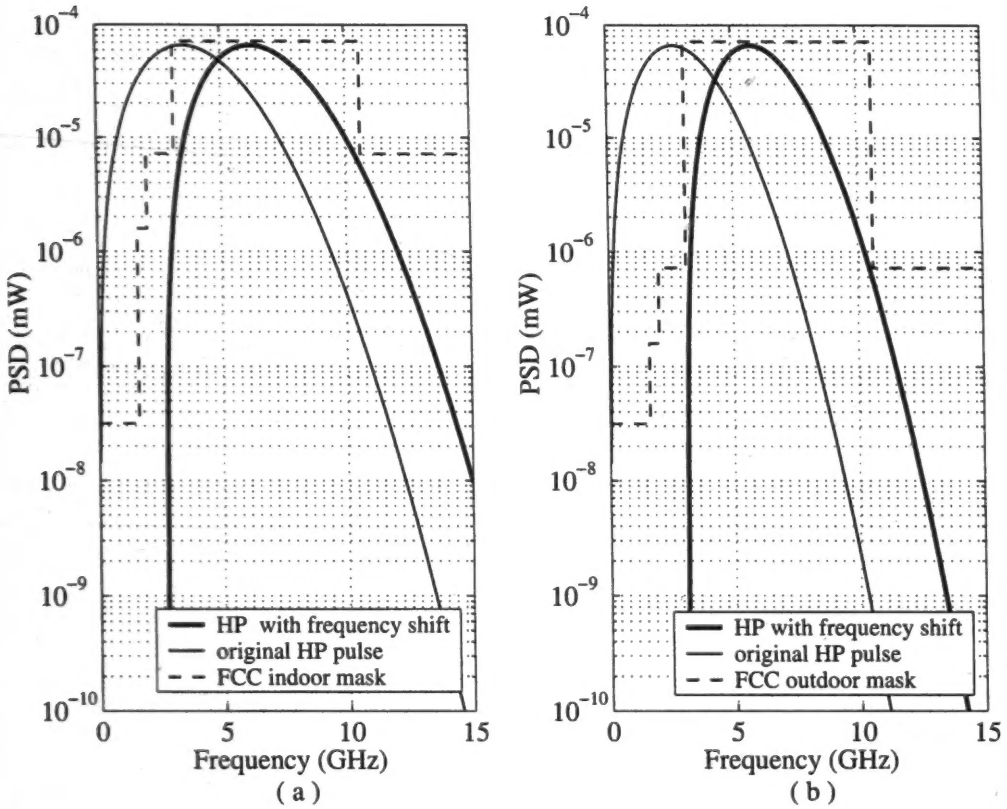

Fig. 4.4. Power spectral densities of the 1^{st} order HP pulse with and without frequency shift together with the FCC masks.

pulses to meet the FCC UWB masks, which greatly increases the complexity of their implementation.

4.3 Comparisons of Pulse Performances

In TH-PPM UWB systems, the time shift δ will strongly affect the bit error rate performance [9], [15]. The optimal choice of δ for a given received signal in TH-PPM

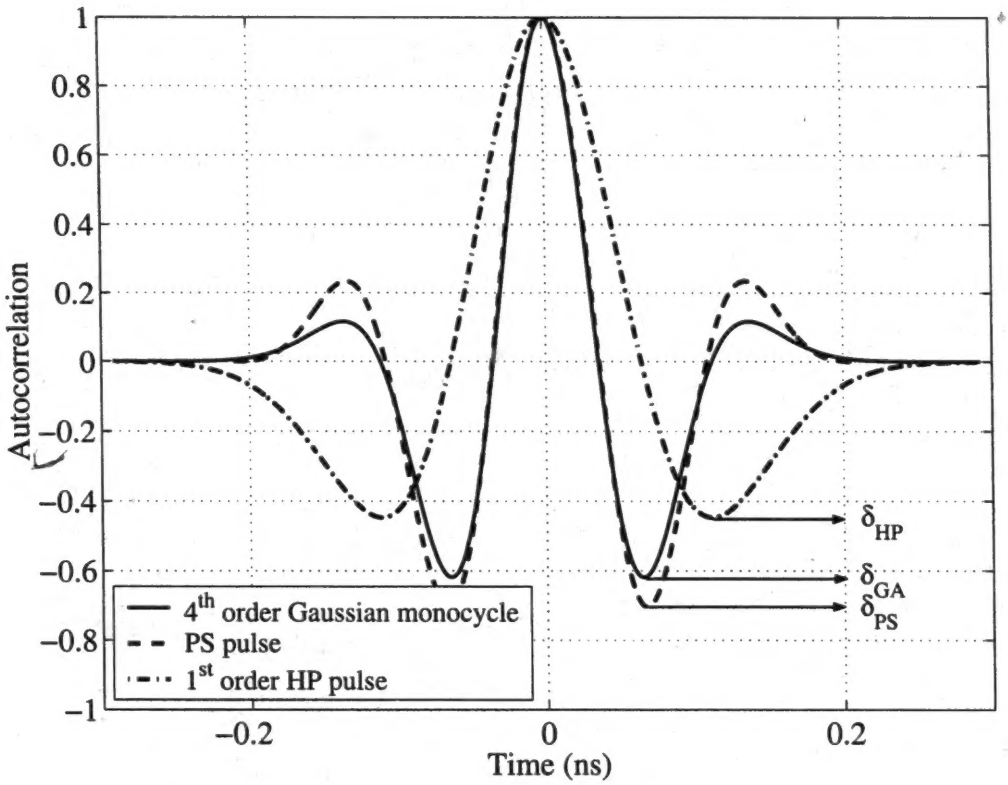

Fig. 4.5. The autocorrelation functions of different pulse shapes.

systems is given in [15] as

$$\delta_{opt} = argument\ of\ \left\{ \underset{\delta}{minimum}\ R(\delta) \right\} \tag{4.22}$$

where $R(\cdot)$ is the autocorrelation function of the pulse $p(t)$. In the comparisons of the Gaussian monocycle, the PS pulse and the HP pulse, the optimal time shift δ is chosen for each pulse shown in Fig. 4.5.

Although the pulses $w_1(t)$ and $w_2(t)$ numerically generated in [65] were reported to be orthogonal, it is clear from [65, Fig. 4] that the cross-correlation between $w_1(t)$ and $w_2(t)$ is zero only at the sampling instants and the values of the cross-correlation at other times are very large. Therefore, these two pulses cannot be assigned to

different users in asynchronous multi-user UWB systems. Note that asynchronous implementations are more common in practical multiple access environments.

If each user can be assigned a unique HP pulse orthogonal to all other users' pulses, the error rate in perfect transmission conditions will be zero in the absence of thermal noise. As shown in [69], the HP pulses with high orders are susceptible to timing jitter and noise so that possibly only a limited number of the orthogonal HP pulses can be used in practical UWB applications. Here, we examine the performance of UWB systems using a single HP pulse for all users. The 1^{st} order HP pulse is chosen to avoid multiple spectral sidelobes and a DC component. A frequency shift has to be added to this pulse to make it meet the FCC indoor and outdoor masks as seen in Fig. 4.4.

We first compare the performance of asynchronous indoor TH-PPM UWB systems using the 4^{th} order Gaussian monocycle, as well as the PS pulse and the 1^{st} order HP pulse. The 4^{th} order Gaussian monocycle is chosen to meet the FCC indoor mask without need for a frequency shift. All the pulses have the same -10 dB bandwidth, which satisfies the FCC indoor mask. In this case, we regenerate the PS pulse following the same method introduced in [65] with $T_m = 0.23$ ns. Fig. 4.6 shows the bit error rate of TH-PPM systems with different pulses. The BER curves are presented as a function of SNR. Note that the square symbols denote the results for the PS pulse; these results are almost coincident with the results for the Gaussian monocycle which are indicated by solid lines. (The same symbol notations are used in Figs. 4.7-4.9 as well). It is seen that the 4^{th} order Gaussian monocycle achieves virtually the same performance as the PS pulse for different lengths of the repetition code, N_s. The Gaussian monocycle outperforms the HP pulse for all values of SNR.

In Fig. 4.7, the performance of asynchronous outdoor TH-PPM UWB systems using the 6^{th} order Gaussian monocycle, the PS pulse and the 1^{st} order HP pulse are compared. The 6^{th} order Gaussian monocycle is used to meet the FCC outdoor mask without a frequency shift. Similarly, the same -20 dB bandwidth is chosen for all pulses. As seen, for all values of SNR, the multiple access performance of the

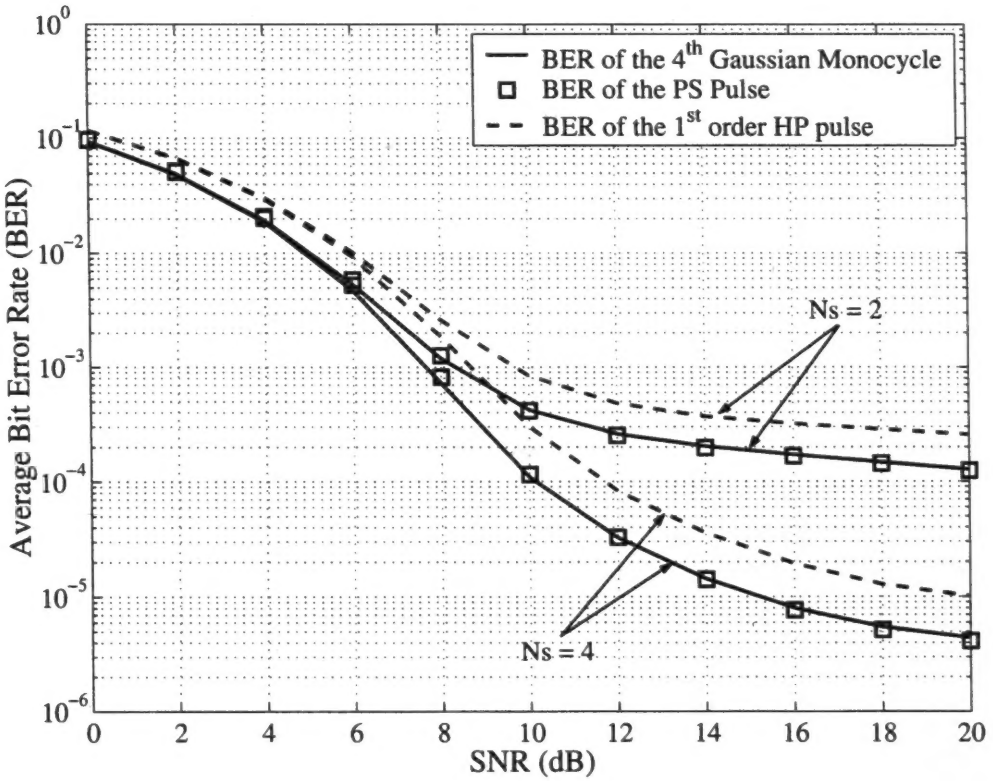

Fig. 4.6. Comparison of indoor TH-PPM UWB systems using different pulses for a repetition code with $N_s = 2$ and $N_s = 4$ assuming 7 asynchronous interferers.

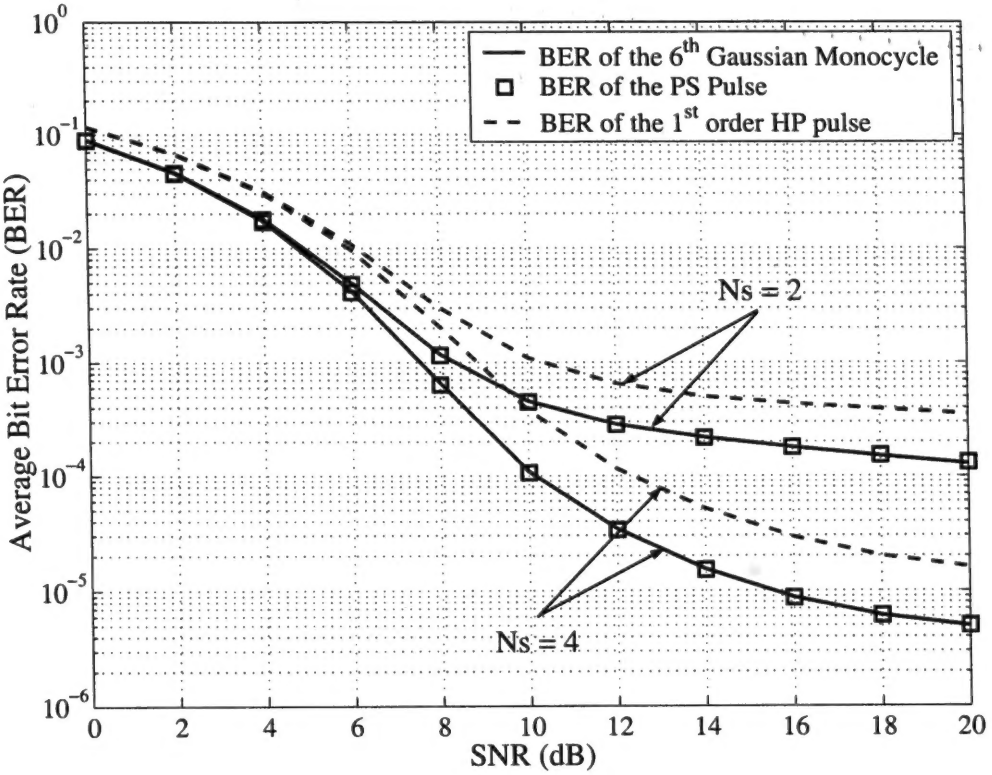

Fig. 4.7. Comparison of outdoor TH-PPM UWB systems using different pulses for a repetition code with $N_s = 2$ and $N_s = 4$ assuming 7 asynchronous interferers.

6^{th} order Gaussian monocycle is as good as the performance of the PS pulse. After a frequency shift to meet the spectral mask, the HP pulse performs worse than the Gaussian monocycle for the system model considered.

Fig. 4.8 shows the performance of indoor TH-BPSK systems with the 4^{th} order Gaussian monocycle, the PS pulse and the 1^{st} order HP pulse. We observe, from our numerical results, that the BER's of the Gaussian monocycle are almost the same as the BER's of the PS pulse. It is also seen that the performance of the Gaussian monocycle is better than the performance of the HP pulse for large SNR, say SNR $\geq$ 12 dB. Unlike in the TH-PPM system, the HP pulse shows similar performance with

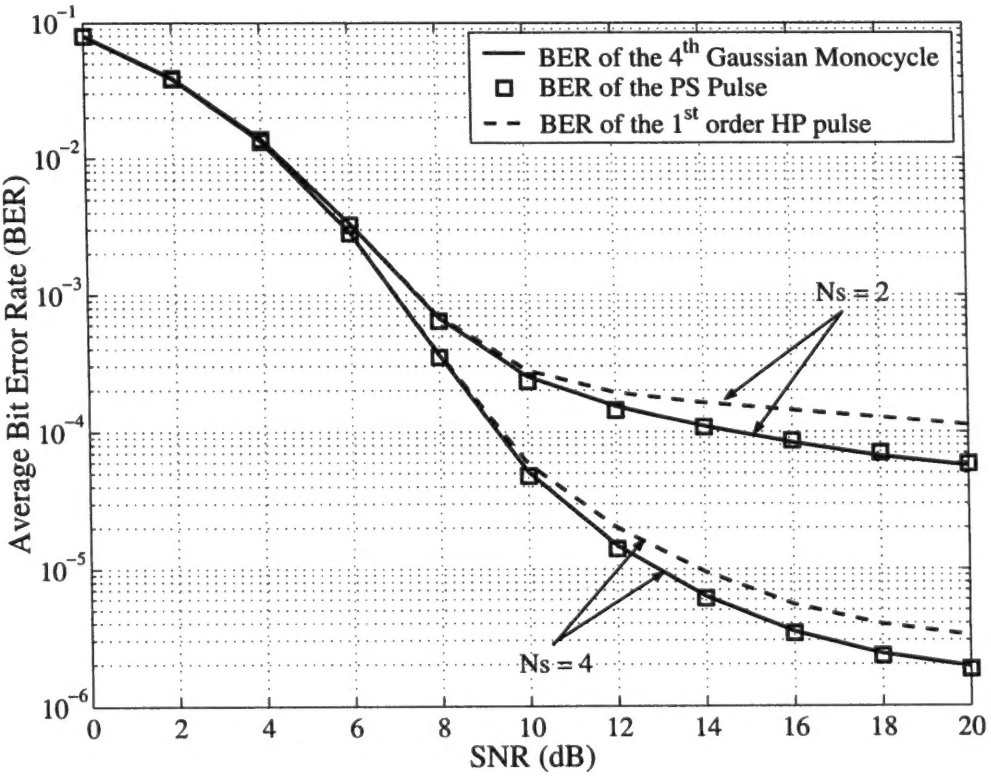

Fig. 4.8. Comparison of indoor TH-BPSK UWB systems using different pulses for a repetition code with $N_s = 2$ and $N_s = 4$ assuming 7 asynchronous interferers.

the Gaussian monocycle for small values of SNR in the TH-BPSK system. This can be explained by comparing the autocorrelation of the Gaussian monocycle and the autocorrelation of the HP pulse shown in Fig. 5. We note that the minimum value of the autocorrelation of the Gaussian monocycle is less than the minimum value of the autocorrelation of the HP pulse, which leads to a larger value of $\tilde{R}(0) = R(0) - R(\delta)$ for the Gaussian monocycle in the TH-PPM system. Considering the decision statistic given in (2.23), we have a larger decision threshold for the TH-PPM system using the Gaussian monocycle. Therefore, the Gaussian monocycle achieves better BER performance than the HP pulse in the TH-PPM system.

A comparison of the performances of outdoor TH-BPSK systems using the 6^{th} order Gaussian monocycle, the PS pulse and the 1^{st} order HP pulse is given in Fig. 4.9 for $N_s = 2$ and $N_s = 4$. As shown, the Gaussian monocycle provides performance as good as the PS pulse for all values of SNR. The Gaussian monocycle outperforms the HP pulse for large values of SNR as expected. Comparing the results in Fig. 4.8 with the results in Fig. 4.9, one sees that the performance difference between the Gaussian monocycle and the HP pulse in the TH-PPM system is much more than the performance difference between these two pulses in the TH-BPSK system. This can also be explained by considering the autocorrelations of the different pulses and the decision thresholds of the different systems. Although the minimum values of these pulses are different, the decision thresholds of the TH-BPSK system using different pulses are the same with the decision statistic provided in (2.51). The difference of the minimum values of the autocorrelations for the Gaussian monocycle and the HP pulse will not affect the decision threshold of the TH-BPSK system. Therefore, the performance difference between the Gaussian monocycle and the HP pulse in the TH-BPSK system is not as large as that in the TH-PPM system. Hence, the autocorrelation function for a specific pulse shape can be used as a guide for choosing a modulation scheme in a practical UWB application.

4.4 Pulse Design Paradigm

In this section, we give a design paradigm for the construction of pulse shapes that can be used to design pulses to fit a given spectral emission mask. The design procedure can accommodate frequency masks of arbitrary shapes and frequency rolloff rates. Our design procedure will be illustrated using the FCC masks specified for indoor and outdoor UWB communications. The discussion will consider pulses having even symmetry and pulses having odd symmetry separately, as there are some differences in the construction of the former from the construction of the latter. Note that the envelope of a transmitted TH-PPM signal (which contains spectral lines) and the

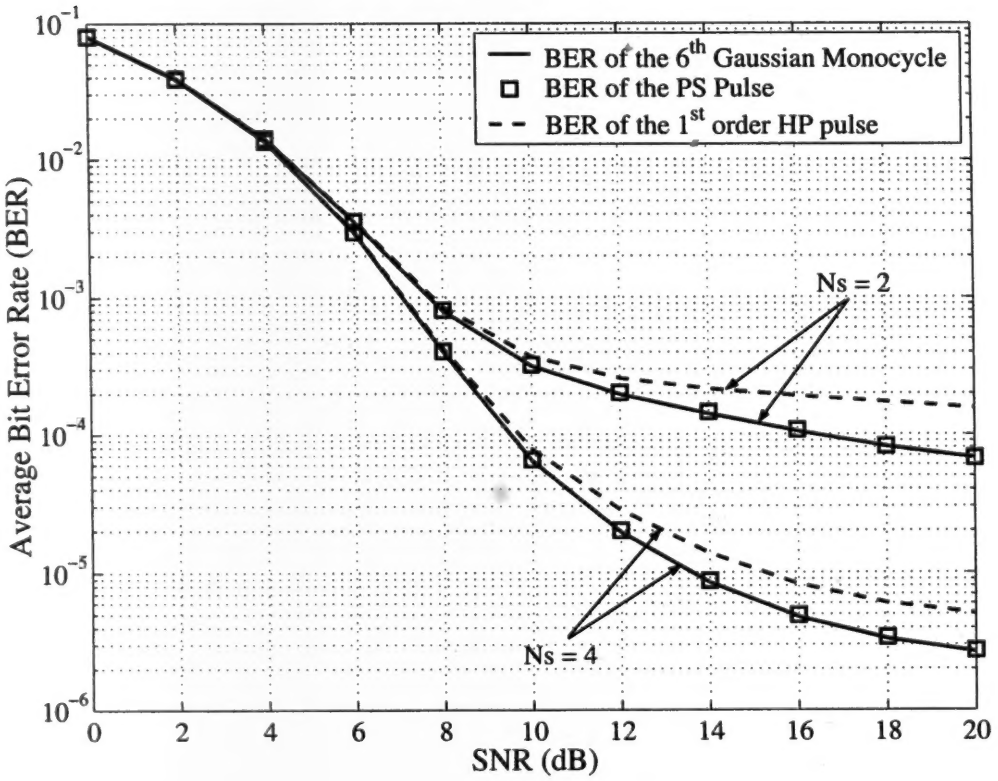

Fig. 4.9. Comparison of outdoor TH-BPSK UWB systems using different pulses for a repetition code with $N_s = 2$ and $N_s = 4$ assuming 7 asynchronous interferers.

envelope of a TH-BPSK signal equal a scaling of the power spectrum of the shaping pulse shown as eqns. (4.4)-(4.7). Therefore, the pulse PSD is used in applying the spectral mask.

4.4.1 Even Pulses

For a given frequency mask, we first determine a center frequency, f_c, for this mask. The choice of a "center" frequency is usually obvious for a given mask. For example, Fig. 4.10 (a) and Fig. 4.10 (b) show the FCC indoor and outdoor mask, respectively. The chosen "center" frequency is indicated in both figures. A candidate pulse can be obtained by windowing the cosine function $f(t) = \cos(2\pi f_c t)$ according to

$$p(t) = f(t) \times w\left(\frac{t}{\tau}\right) \tag{4.23}$$

where $p(t)$ is a time-limited pulse and $w\left(\frac{t}{\tau}\right)$ is a window function. The parameter τ determines the time duration of the window, and thus the pulse duration of $p(t)$.

Many choices of $w(t)$ can be used for windowing the cosine function $f(t)$. Consider the simplest window, a rectangular window. The window function has the form

$$w_1(x) = \begin{cases} 1 & |x| < \frac{1}{2} \\ \frac{1}{2} & |x| = \frac{1}{2} \\ 0 & |x| > \frac{1}{2}. \end{cases} \tag{4.24}$$

Applying this rectangular window in (4.23), the cosine function $f(t)$ is truncated at time $-\frac{\tau}{2}$, $\frac{\tau}{2}$, and the pulse $p(t)$ obtained is time-limited to pulse duration τ. The spectrum of the rectangular window $w_1(t/\tau)$ can be obtained by taking the Fourier transform of (4.24), and is given by

$$W_1(f) = \tau \text{sinc}(f\tau) \tag{4.25}$$

where the sinc$(\cdot)$ function is defined as

$$\text{sinc}(x) = \begin{cases} \frac{\sin(\pi x)}{\pi x} & \text{if } x \neq 0 \\ 1 & \text{if } x = 0. \end{cases} \tag{4.26}$$

We denote the pulse obtained from (4.23) as $p_1^e(t)$ when the rectangular window $w_1(t/\tau)$ is used. Then, the frequency spectrum of $p_1^e(t)$ is given by the convolution of the frequency spectra of $f(t)$ and $w_1(t/\tau)$ as

$$\begin{aligned} P_1^e(f) &= \frac{1}{2}[\delta(f-f_c)+\delta(f+f_c)] * W_1(f) \\ &= \frac{\tau}{2}\{\text{sinc}[\tau(f-f_c)]+\text{sinc}[\tau(f+f_c)]\}. \end{aligned} \tag{4.27}$$

where $*$ denotes the convolution operation.

Two issues must be dealt with. First, our task is to design a pulse whose pulse spectrum $P_n^e(f)$ meets the desired frequency mask. Second, desirable pulse shapes for UWB communication systems do not have a DC component [14]. In the case of even pulses, this requirement complicates the choice of the window function $w(t/\tau)$. Our design procedure will circumvent this difficulty. When the rectangular window (4.24) is used, the pulse $p_1^e(t)$ has zero DC component if and only if

$$\tau f_c = k,\ k = 1, 2, \ldots\ . \tag{4.28}$$

Consistent with the objective of spectral spreading (and making the pulse impulse-like), $k = 1$ is chosen. Fig. 4.10 (a) and Fig. 4.10 (b) show $P_1^e(f)$ for this choice. Observe that the spectrum does not meet the masks.

More generally, now consider the window $w_n(t/\tau)$ generated by convolving the rectangular windows $w_1(t/\tau)$, defined as

$$w_n\left(\frac{t}{\tau}\right) = \underbrace{w_1\left(\frac{t}{\tau}\right) * w_1\left(\frac{t}{\tau}\right) * \cdots * w_1\left(\frac{t}{\tau}\right)}_{n} \tag{4.29}$$

where n denotes the number of rectangular windows convolved. For example, $w_2(t/\tau)$ is a triangular window with length 2τ and $w_3(t/\tau)$ is a window composed of concatenated quadratic sections and having length 3τ. The window $w_n(t/\tau)$, having window width $n\tau$, is a concatenation of $n+1$ polynomial splines, each of order $n-1$, given by

$$w_n\left(\frac{t}{\tau}\right) = \sum_{m=0}^{n} \frac{n\left[\frac{t}{\tau} - \left(\frac{n}{2} - m\right)\right]^{n-1}(-1)^{n-m}}{m!(n-m)!} \cdot U\left[\frac{t}{\tau} - \left(\frac{n}{2} - m\right)\right] \tag{4.30}$$

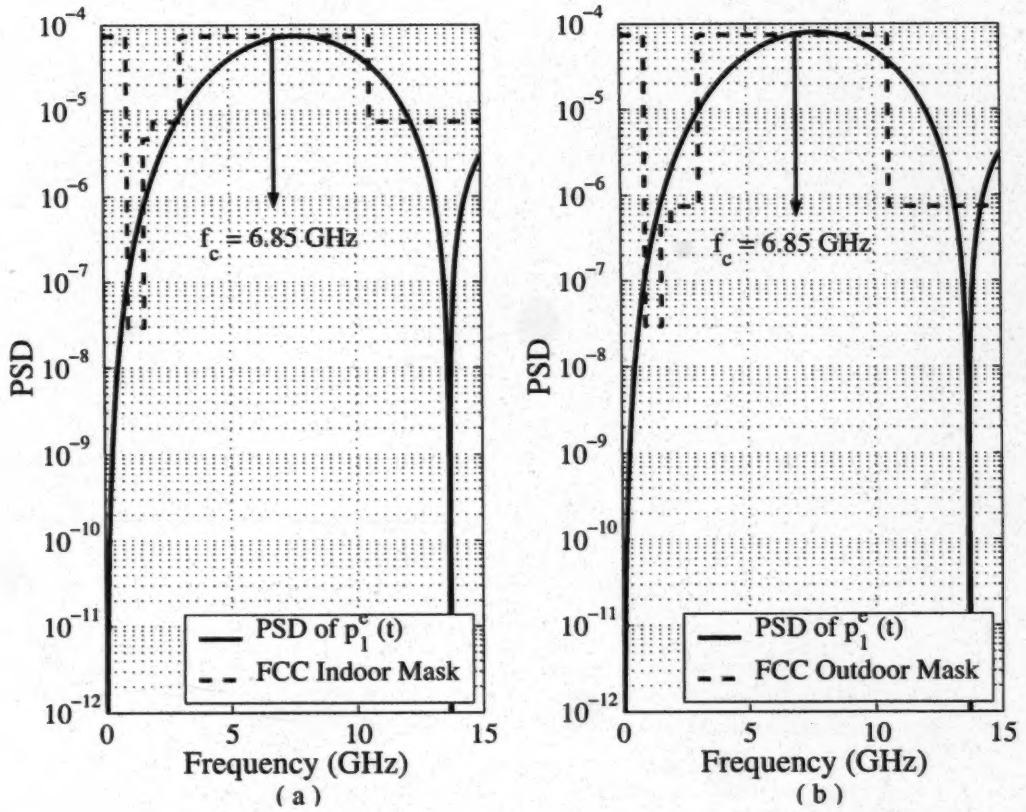

Fig. 4.10. The power spectral density of the pulse $p_1^e(t)$ and (a) the FCC indoor spectral emission mask (b) the FCC outdoor spectral emission mask.

where $U[\cdot]$ denotes the unit step function. If the window $w_n(t/\tau)$ is used in (4.23), the pulse $p_n^e(t)$ obtained has pulse duration, $n\tau$. The frequency spectrum of $w_n(t/\tau)$, denoted by $W_n(f)$, is given by

$$\begin{aligned} W_n(f) &= W_1^n(f) \\ &= \tau^n \text{sinc}^n(f\tau), \quad n = 1, 2, 3, \ldots . \end{aligned} \tag{4.31}$$

Therefore, the spectrum of the pulse $p_n^e(t)$, denoted by $P_n^e(f)$, can be obtained as

$$\begin{aligned} P_n^e(f) &= \frac{1}{2}[\delta(f - f_c) + \delta(f + f_c)] * W_n(f) \\ &= \frac{\tau^n}{2} \left\{ \text{sinc}^n \left[\tau(f - f_c)\right] + \text{sinc}^n \left[\tau(f + f_c)\right] \right\}, \quad n = 1, 2, 3, \ldots . \end{aligned} \tag{4.32}$$

The corresponding time function is

$$\begin{aligned} p_n^e(t) &= \cos(2\pi f_c t) \times w_n\left(\frac{t}{\tau}\right) \\ &= \sum_{m=0}^{n} \frac{n(-1)^{n-m} \left[\frac{t}{\tau} - \left(\frac{n}{2} - m\right)\right]^{n-1} \cos(2\pi f_c t)}{m!(n-m)!} \cdot U\left[\frac{t}{\tau} - \left(\frac{n}{2} - m\right)\right]. \end{aligned} \tag{4.33}$$

Observe from (4.32) that the pulse spectrum remains centered at f_c and that as n increases the relative amplitudes of the sidelobes decreases. Further, the width of the main lobe also becomes narrower as n increases. Thus, increasing the value of n is a device enabling adjustment of the pulse spectrum to fit inside the spectral emission mask. In fact, note that the spectrum given in (4.32) provides two degrees of freedom, τ and n, for a given center frequency, f_c. These two parameters are used to adjust the pulse shape and pulse duration in the time domain, while ensuring that the pulse spectrum meets the emission constraints in the frequency domain. Furthermore, it is clear that the DC component of $p_n^e(t)$ is zero for all values of n if it is zero for $n = 1$. Thus, once τ is chosen to satisfy (4.28), n can be varied freely and the DC component will be zero. A set of novel pulses can be generated by adjusting suitable combinations of the values of τ and n to approach the desired power spectrum.

4.4.2 Odd Pulses

Rather than using a cosine function, we can also use a sine function $f(t) = \sin(2\pi f_c t)$ in (4.23). Similar to (4.32), the frequency spectrum of the odd pulse $p_n^o(t)$ obtained from (4.23) using a sine function is given by

$$\begin{aligned} P_n^o(f) &= \frac{1}{2j}[\delta(f - f_c) - \delta(f + f_c)] * W_n(f) \\ &= \frac{\tau^n}{2j}\left\{\text{sinc}^n\left[\tau(f - f_c)\right] - \text{sinc}^n\left[\tau(f + f_c)\right]\right\}, \quad n = 1, 2, 3, \ldots \end{aligned} \tag{4.34}$$

and

$$\begin{aligned} p_n^o(t) &= \sin(2\pi f_c t) \times w_n\left(\frac{t}{\tau}\right) \\ &= \sum_{m=0}^{n} \frac{n(-1)^{n-m}\left[\frac{t}{\tau} - \left(\frac{n}{2} - m\right)\right]^{n-1} \sin(2\pi f_c t)}{m!(n-m)!} \cdot U\left[\frac{t}{\tau} - \left(\frac{n}{2} - m\right)\right]. \end{aligned} \tag{4.35}$$

One sees that the pulse spectrum $P_n^o(0)$ in (4.34) equals 0 for any value of τ (this also follows because the pulse has odd symmetry). Therefore, arbitrary values of τ can be chosen to synthesize pulse shapes to meet a given frequency mask in the case of pulses having odd symmetry.

We conclude this section by reflecting upon the family of windows given in (4.30). The application of this family of time-limited functions for windowing seems novel. In addition to the rectangular window based family, we have examined the application of Hamming and Hanning windows, well-known in digital signal processing theory. The minimum width required for these to obtain a zero DC component for the even pulses is twice the minimum required width of the rectangular window, that is, $2\tau_0$. Importantly, the Hamming and Hanning windowed pulses with the minimum width $2\tau_0$ do not meet the FCC emission masks. One can construct a family of windows based on convolving the Hamming (Hanning) window with itself, similarly to the construction of the family of windows in (4.30) which was based on the rectangular window. However, the n-order Hamming-based and Hanning-based windows have width $2n\tau_0$, whereas the n-order rectangular-based window has width $n\tau_0$. Hence,

there is additional freedom for the rectangular-based windows since all the windows with width $n\tau_0$ where n is odd are candidates for synthesis in the design paradigm. The second-order pulses obtained using the Hamming-based and Hanning-based windows do meet the indoor mask but the corresponding pulses have width $4\tau_0$ in contrast to the rectangular-based windowed pulse of order 3, which satisfies the indoor mask but yields a pulse of width $3\tau_0$. A longer pulse duration is undesirable in multiple access environments because it leads to greater multiple access interference. We utilize the rectangular-based windows in our subsequent study of pulse design in this paper. In general, other window families can be derived using repeated convolution of a chosen basic window shape according to the principles of our design paradigm.

4.5 Pulse Examples and Discussion

In this section, examples are provided to show how to design a pulse for a specific frequency mask. Given the FCC frequency constraint for UWB communication systems described in Section I, the center frequency f_c is set to be 6.85 GHz as shown in Fig. 4.10 (the midpoint of the range 3.1 - 10.6 GHz). Adjusting the parameters τ and n simultaneously, we can obtain many pulse shapes that meet the FCC indoor and outdoor masks. Considering the pulse duration is $n\tau$, we will choose the value of $n\tau$ as small as possible to achieve good multiple access performance. The desired indoor even pulse with the smallest duration is obtained with τ_0 and $n = 3$, denoted by $p_3^e(t)$. This pulse can fit its -10dB bandwidth within the frequency 3.1 - 10.6 GHz without any frequency shift, and thus can be utilized in UWB systems for indoor communications. Using the same method, the pulse $p_4^e(t)$ with τ_0 and $n = 4$ meets the frequency regulation for UWB outdoor communications. As examples of pulses that comply with the FCC specifications, the power spectral densities of the pulses $p_3^e(t)$ and $p_4^e(t)$, which meet the FCC indoor and outdoor masks, respectively, are shown in Fig. 4.11 together with the FCC masks.

Similarly, a set of pulse shapes based on a sine function $\sin(2\pi f_c t)$ can also be

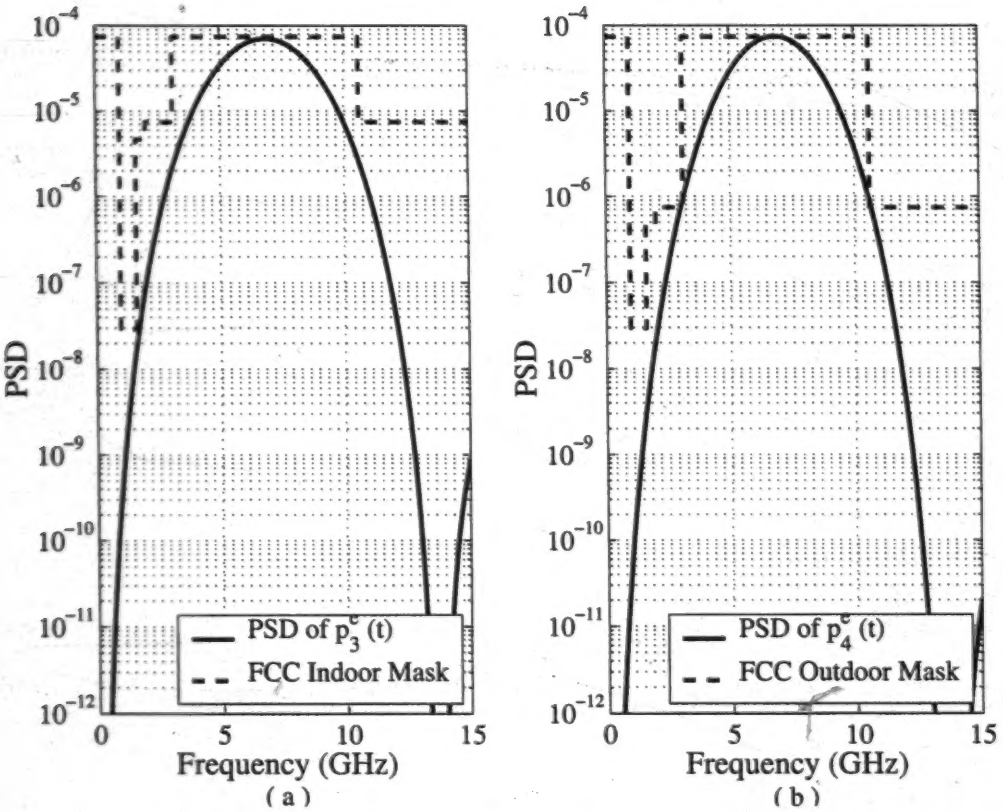

Fig. 4.11. The power spectral densities of (a) the pulse $p_3^e(t)$ and (b) the pulse $p_4^e(t)$ and the FCC masks.

generated by setting suitable parameters τ and n in (4.34). We first try values of τ smaller than τ_0; then the value of n has to be increased correspondingly. In this case, the pulse durations of the obtained odd pulses that meet the FCC indoor and outdoor mask are larger than the pulse widths of $p_3^e(t)$ and $p_4^e(t)$, respectively. On the other hand, when τ is chosen larger than τ_0, the desired odd pulse with the smallest pulse duration is obtained with $\tau = 1.38\tau_0$ and $n = 2$, denoted by $p_2^o(t)$. This pulse is shown to meet the FCC UWB frequency emission indoor mask. Additionally, $p_2^o(t)$ can also fit its -20dB bandwidth within the frequency 3.1 -10.6 GHz without any frequency shift, and thus can meet the FCC frequency emission outdoor mask. The power spectral density of the pulse $p_2^o(t)$, which meets the FCC indoor and outdoor masks, is shown in Fig. 4.12 together with the FCC frequency masks.

In order to compare the odd pulse $p_2^o(t)$ and the even pulse $p_4^e(t)$ that both comply with the outdoor frequency emission mask, the pulse shapes of $p_2^o(t)$ and $p_4^e(t)$ are shown in Fig. 4.13 (a) and the autocorrelations of these two pulses are plotted in Fig. 4.13 (b). Although the odd pulse $p_2^o(t)$ and the even pulse $p_4^e(t)$ show different pulse shapes and pulse duration, it is seen that the autocorrelation of $p_2^o(t)$ is almost the same as the autocorrelation of $p_4^e(t)$, which leads to very similar multiple access error rate performance for these two pulses, as will be seen later.

Results in [70] show that the BER's of these pulses are graphically coincident for practical conditions. It was shown in [70] that the higher-order Gaussian monocycles can meet the FCC frequency masks without frequency shift. Specifically, the 4^{th}-order and the 6^{th}-order Gaussian monocycles were utilized in [70] to meet the FCC frequency emission indoor and outdoor masks, respectively. Additionally, the results in [70] show that the Gaussian monocycles achieve performance as good as the prolate spheroidal function based pulses [65] and outperform the modified Hermite polynomial based pulses [16] for the same effective bandwidths. In Fig. 4.14, the pulse shapes $p_3^e(t)$ and $p_4^e(t)$ are shown together with the 4^{th}-order and the 6^{th}-order Gaussian monocycles. Comparing the novel even pulses with the Gaussian monocycles, one sees that the shapes of our novel pulses are surprisingly similar to those of the Gaussian monocycles.

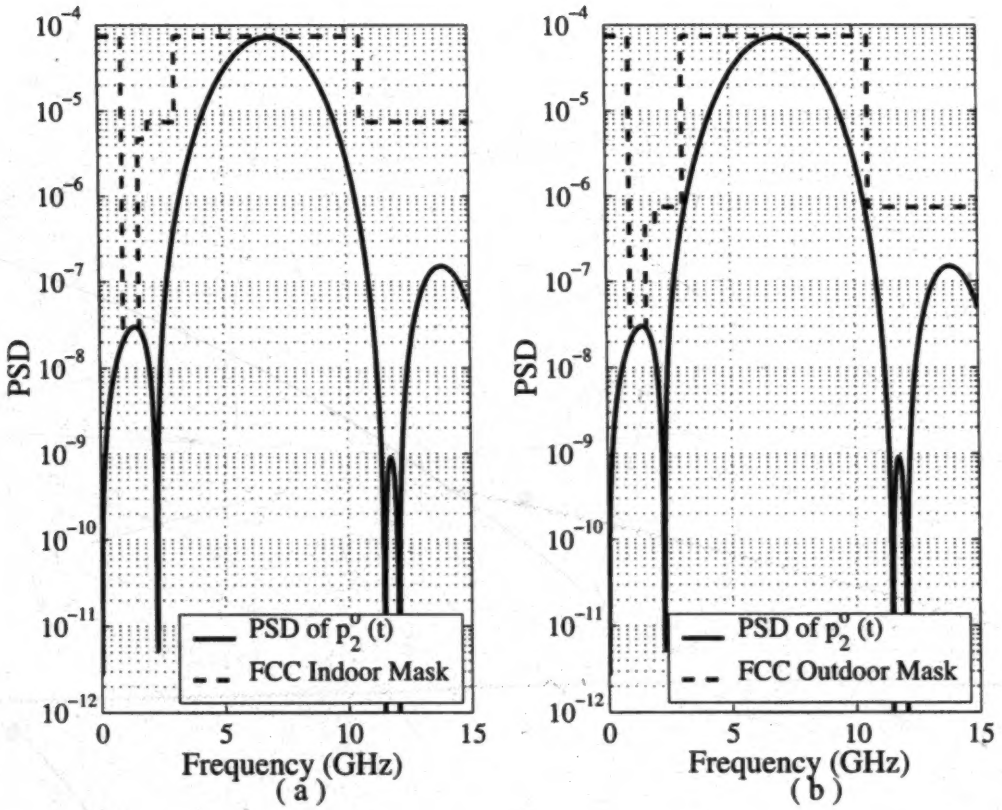

Fig. 4.12. The power spectral density of the pulse $p_2^o(t)$ and (a) the FCC indoor spectral emission mask (b) the FCC outdoor spectral emission mask.

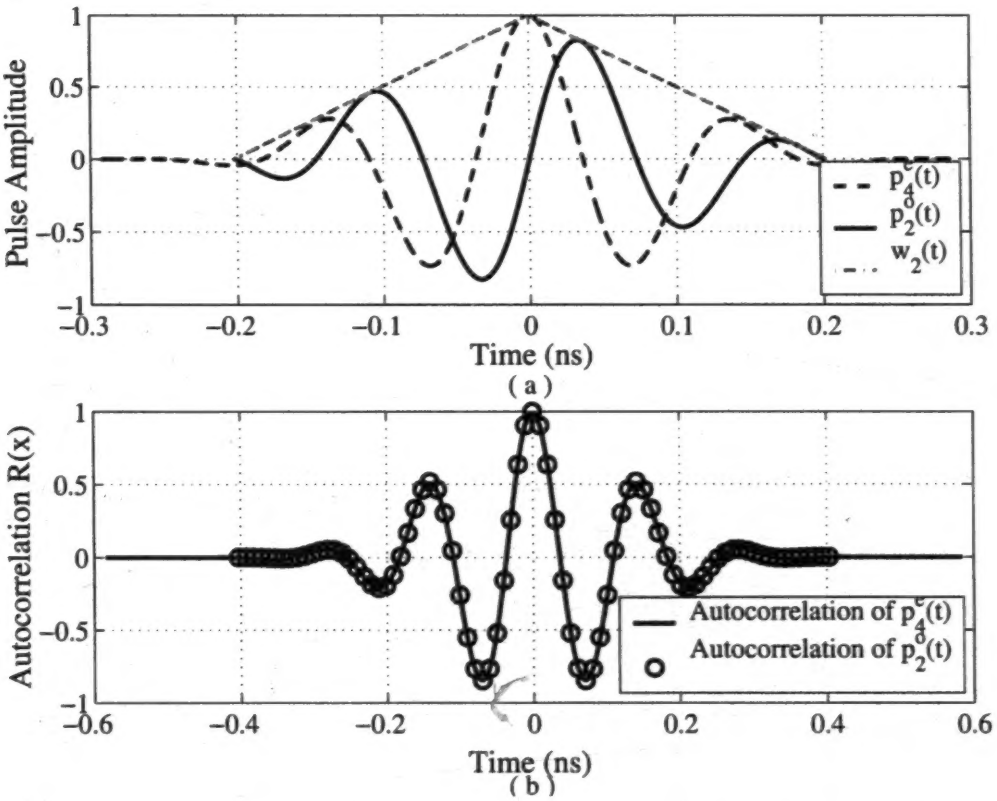

Fig. 4.13. The pulse shapes and the autocorrelations of (a) $p_2^o(t)$, and (b) $p_4^e(t)$.

An important difference, however, is that the Gaussian monocycles have pulse tails of infinitely long duration. Note that our pulses are strictly time-limited.

Considering the similarity between the novel even pulses and the Gaussian monocycles, we expect that the multiple access performance of time-hopping UWB systems using the novel pulses to be almost the same as the performance of UWB systems using the Gaussian monocycles for the same effective bandwidths. This expected performance is confirmed by our numerical results based on the exact analysis of time-hopping UWB systems published in [15]. For example, a comparison of the performance of outdoor TH-PPM systems using the novel pulse $p_4^e(t)$ and the 6^{th}-order Gaussian monocycle is given in Fig. 4.15 for $N_s = 2$ and $N_s = 4$. SNR in this figure is defined as E_b/N_0, in which E_b is the energy of the information bit and N_0 is the PSD of AWGN. It is seen that the pulses $p_4^e(t)$ and $p_2^o(t)$ provide BER performances indistinguishable from the performance of the 6^{th}-order Gaussian monocycle with the same effective bandwidth for all values of SNR. Considering the comparative performances of the Gaussian monocycles, the prolate spheroidal function based pulses and the modified Hermite polynomial based pulses reported in [48], it is clear that the novel pulse achieves almost the same multiple access performance as the prolate spheroidal function based pulse and outperforms the modified Hermite polynomial based pulse for the same effective bandwidth.

The original, ideal Gaussian monocycles were used in performance comparisons of the novel pulses and the Gaussian monocycles. As we know, the original Gaussian monocycle has infinite duration pulse tails, though the values of the tails are very small. These infinite-time Gaussian monocycles have to be truncated using some window in practical communication systems. One might then ask whether our previous conclusions, based on infinite duration Gaussian monocycles are affected. To study this question, we use windows with the same width as the window used in the novel pulse design to truncate the Gaussian monocycle. Then, the truncated Gaussian monocycle has the same pulse duration as the novel pulse. For example, the 4^{th}-order Gaussian monocyle is truncated by a window with length $3\tau_0$ and the 6^{th}-order Gaus-

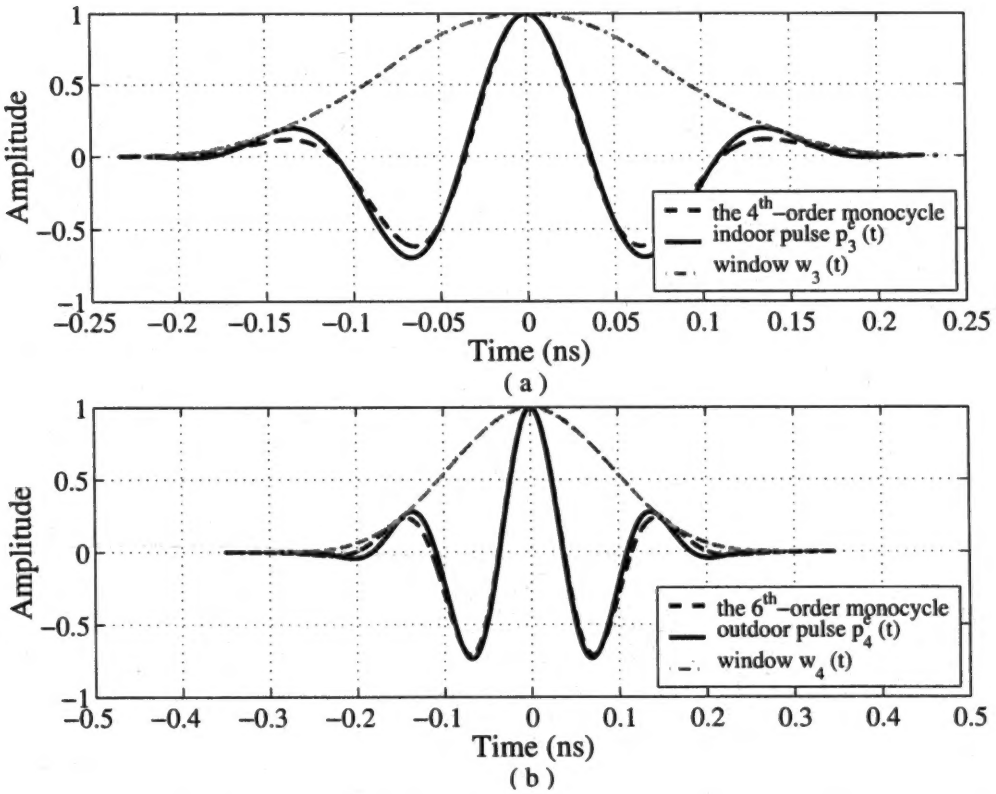

Fig. 4.14. Pulse shapes of (a) $p_3^e(t)$ together with the 4^{th}-order Gaussian monocycle, and (b) $p_4^e(t)$ together with the 6^{th}-order Gaussian monocycle.

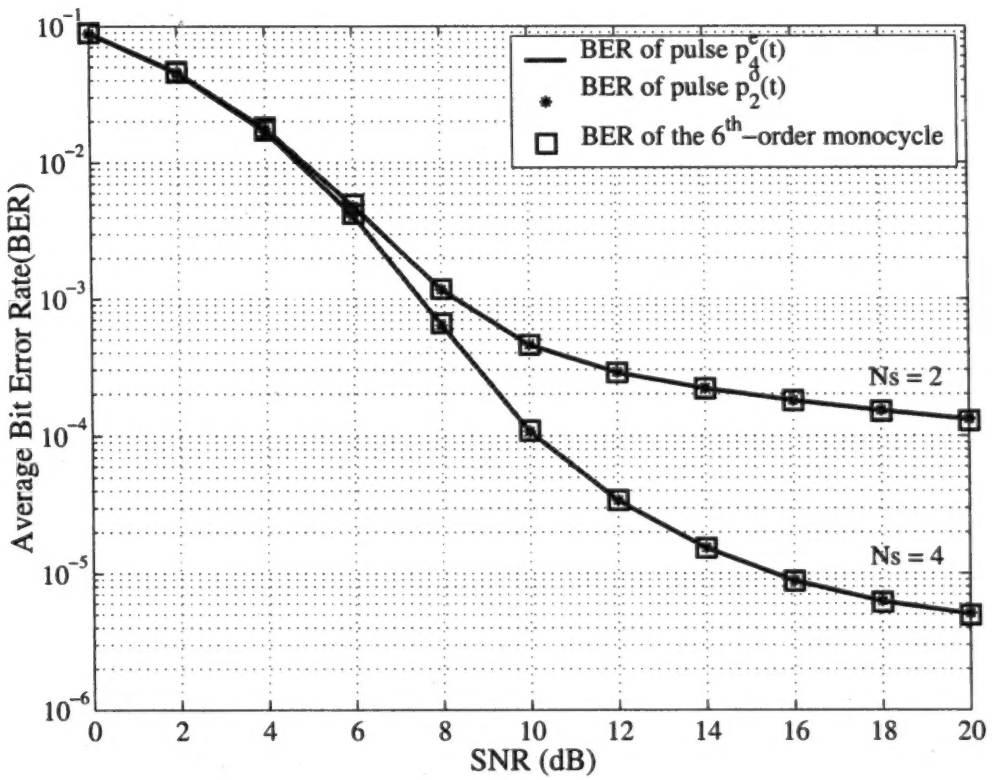

Fig. 4.15. Comparison of outdoor TH-PPM UWB systems using the novel even pulse $p_4^e(t)$, the odd pulse $p_2^o(t)$ and the 6^{th}-order Gaussian monocycle for a repetition code with $N_s = 2$ and $N_s = 4$ assuming 7 asynchronous interferers.

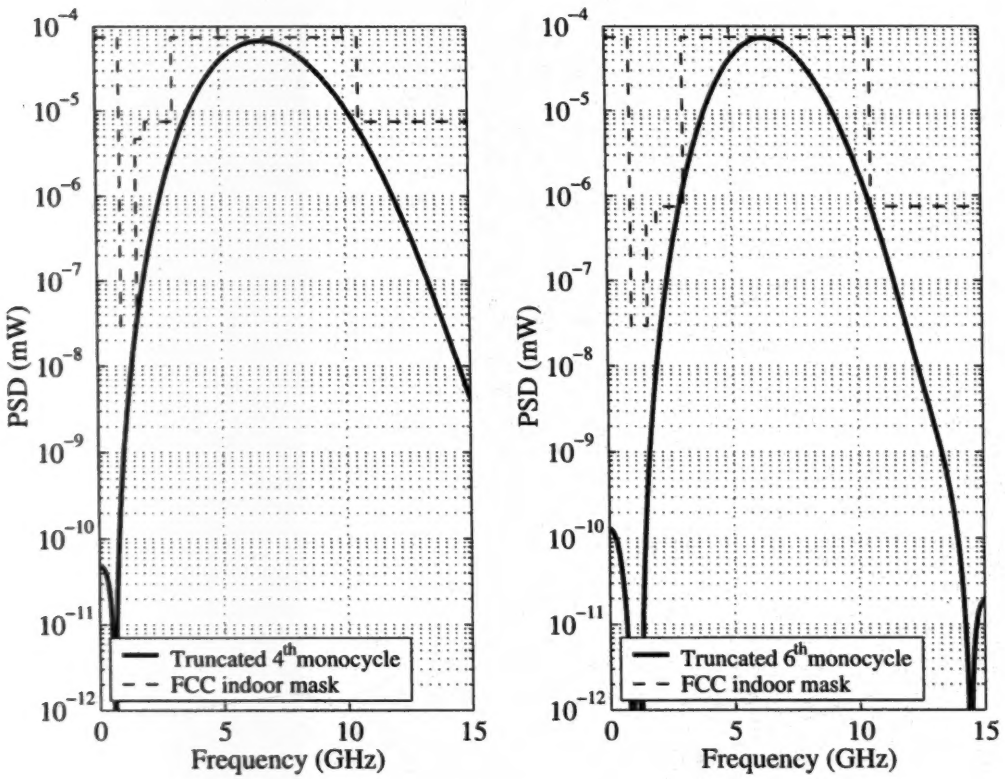

Fig. 4.16. Power spectral densities of (a) the truncated 4^{th}-order and (b) the truncated 6^{th}-order Gaussian monocycles and the FCC masks.

sian monocycle is truncated by a window with length $4\tau_0$, for the indoor and outdoor frequency masks, respectively. We found that our conclusions are unaltered by any judicious windowing of the Gaussian monocycles. The performances of the truncated monocycles are virtually the same as the performances of the original monocycles. A small DC component is introduced for some choices of window functions, but this component is well below the spectral mask constraint. Fig. 4.16 shows the power spectral densities of the 4^{th}-order and 6^{th}-order truncated Gaussian monocycles.

The novel pulses are preferable to the Gaussian monocycles, the Hermite polynomial based pulses and the prolate spheroidal function based pulses in the following

senses. Regarding the Gaussian monocycles and the modified Hermite polynomial function based pulses, the center frequency and the -10 (-20) dB bandwidth of the pulse spectrum are determined by the scaling factor τ_p, used to set the pulse width, and a frequency shift is required for the Gaussian monocycle with some values of τ_p to ensure the pulse spectrum meets the FCC masks. This results in less flexibility in changing data rates in an implementation. Unlike these two types of pulses whose center frequencies cannot be set manually, the spectral center frequency of our novel pulses, f_c, can be modified to meet a specific frequency emission regulation. In the design of the prolate spheroidal function based pulses in [65], the bandpass filter will be determined in terms of the FCC frequency mask. Then only the pulse width T_m can be adjusted to make the pulse shape fit the desired mask. In other words, for a given mask, only one parameter, T_m, of the prolate spheroidal function based pulses can be adjusted to ensure the spectrum meets the frequency constraint. Our algorithm, however, provides two degrees of freedoms, τ and n, for a given frequency mask. Actually, for any frequency emission restriction, we first set the center frequency, f_c. Then other two parameters, τ and n, are used to shape the pulse and adjust the spectrum of the pulse. It is clear that our pulse design method provides more freedom than other pulse design methods previously proposed. Therefore, it is much more convenient to design a pulse that meets a frequency spectral emission mask using our method and many more pulses can be obtained by setting suitable combinations of values of τ and n. Our UWB pulse design approach provides an effective and flexible tool for designing pulses satisfying arbitrary UWB frequency emission masks, and as such can be used to design UWB pulses that meet European and Japanese UWB frequency regulations. The ETSI recently proposed the UWB emission limits for indoor and portable communication systems in Europe, which align with the respective FCC masks [39] but are more restrictive than the respective FCC masks. Fig. 4.17 shows the power spectral densities of $p_3^e(t)$ and $p_4^e(t)$ complying with the ETSI masks. As seen, our novel pulses can also meet the ETSI UWB spectral emission constraints, and thus can be used for European UWB communication systems.

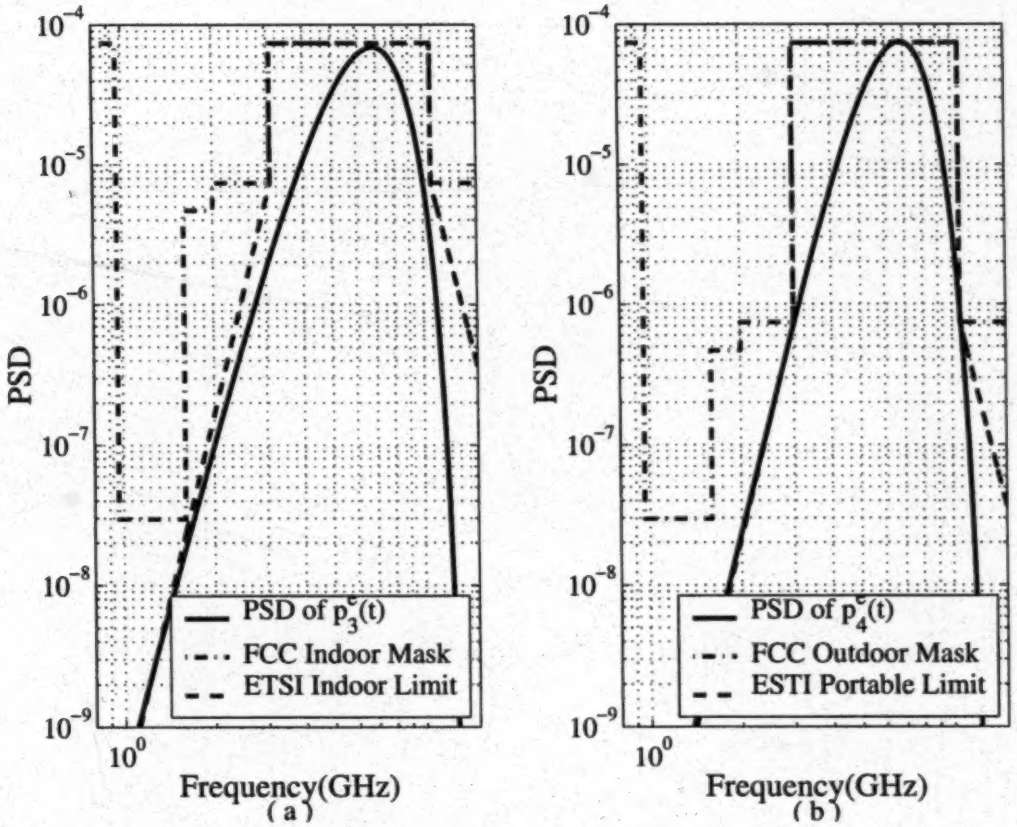

Fig. 4.17. Power spectral densities of (a) the pulse $p_{in}^{e}(t)$ and (b) the pulse $p_{out}^{e}(t)$ together with the FCC masks and ETSI masks.

4.6 Summary

In this chapter, different pulse shapes recently proposed for UWB communications systems were examined and evaluated in terms of the FCC frequency masks and their multiple access BER performances. We found that the Gaussian monocycles of higher orders can meet FCC masks without frequency shifting and provide performance as good as the PS pulse introduced in [65] for both TH-PPM and TH-BPSK UWB systems. However, the center frequency and the bandwidth are both determined by the scaling factor, τ_p, used to set the pulse width, and a frequency shift is required for the Gaussian monocycle with some values of τ_p to ensure the pulse spectrum meets the FCC masks. This results in less flexibility in changing data rates in an implementation.

The PS pulses generated using eigenvectors can meet FCC masks without frequency shift. The PS pulse, however, has no closed-form expression and has to be generated numerically. Thus, the PS pulses are more difficult to implement compared with the Gaussian monocycles. Additionally, decreasing the pulse width T_m increases the amplitude of the dominant sidelobe in the PSD, which causes strong adjacent channel interference in some applications.

Compared with the Gaussian monocycle and the PS pulse, the HP pulse needs frequency shifts and bandpass filters to meet FCC masks, thus requiring much more complicated implementation. Moreover, the multiple access performance of a single HP pulse is worse than the performance of the other two pulses when all pulses are constrained to meet the FCC spectral emission requirements.

Further, a novel pulse design paradigm has been proposed for UWB communication systems in this chapter. Using our paradigm, many pulses that meet the FCC UWB spectral masks can be obtained by adjusting the pulse parameters. The novel pulses generated are time-limited so as to reduce the interference and simplify implementation. It has been shown that the novel pulses have similar shapes to the Gaussian monocycles and achieve multiple access performance as good as the ideal

Gaussian monocycles and the prolate spheroidal function based pulses. However, the ideal Gaussian monocycles have to be truncated which leads to a small DC component in the truncated Gaussian monocycles. Unlike the prolate spheroidal function based pulse, which has to be generated numerically, our novel pulse has a closed-form expression. Compared with all pulse design algorithms previously proposed, our paradigm provides more freedoms for adjusting the pulse spectrum to meet the FCC UWB mask and many more novel pulses can be obtained using this design paradigm. Additionally, our method provides more flexibility in designing pulses to fit any other possible UWB spectral emission constraint.

Chapter 5

Effects of Narrowband OFDM Interference on A UWB Communication System

5.1 Introduction

FCC has introduced restrictions that the UWB system must operate within the frequency 3.1-10.6 GHz with an emission limit of -41 dBm/MHz for communications [38]. This specification on the PSD of UWB effectively reduces the potential for interference to other co-existing wireless user systems. Since the power spectral density of conventional communication signals is much higher than that of UWB signals, the interference from other wireless application to UWB systems becomes more severe and critical. Therefore, the performance of UWB signals in the presence of interference from other communication systems in the same frequency band must be carefully investigated before implementing commercial applications. Specifically, IEEE 802.11a systems operate around 5 GHz, which overlap the band of UWB signals regulated by the FCC, and will bring significant interference to UWB systems.

Some studies on UWB systems in the presence of different types of interference

have been done by other researchers. In [25] and [26], the performance of UWB with interference from the UMTS band was studied using simulation. The UMTS interference was modeled as a bandlimited Gaussian white noise. A study of UWB communications in the presence of jamming was presented in [28], in which the performance of a single-user UWB system with a jamming signal was analyzed and closed-form expressions for the jamming resistance of TH-PPM utilizing rectangular pulse-shaping were reported. The jamming signal used in [28] was also assumed to be a passband Gaussian noise. In addition, the in-band interference was modeled as a cosinusoidal tone in [33]. All these results were obtained using simplified models of real interference. Despite the practical reality for a IEEE 802.11a signal, i.e., an OFDM signal, to introduce significant interference to UWB systems, there is little literature on it. Recently, an expression for calculating the interference from OFDM signals to TH-PPM UWB systems was developed in [34], and, then, a semi-analytical method using simulation was applied to obtain the average BER of a single-user UWB signal corrupted by synchronous OFDM interference. This work was conducted using a Gaussian approximation for the interference.

In our work, we provide an analysis for the performance of different UWB systems in the presence of OFDM interference. Particularly, PPM and BPSK using time-hopping or direct-sequence are considered. A closed-form expression for the interference can be obtained without using bandlimited Gaussian assumption or approximation, for UWB systems employing pulse-shaping for which the inverse Fourier transform exists. In the sequel, we derive expressions for the probability of error in TH-PPM, TH-BPSK and DS-BPSK UWB systems and compare the performances of these modulation schemes operating in OFDM interference. In addition, based on previous analyses on multiple access interference, performance comparisons of the different modulation schemes operating in narrowband interference and multiple access interference are also made. The comprehensive comparisons clearly indicate the capability for suppressing interference of different UWB systems.

The organizations of this chapter is as follows. In Section 5.2, the time-hopping

and direct-sequence UWB system models used in our work are briefly described. Closed form expressions and the corresponding analysis of the OFDM interference is then derived for each system in Section 5.3. The average probabilities of bit error for these systems are provided in Section 5.4. In Section 5.5, our analysis is validated by simulation and used to evaluate the performance of UWB systems operating in interference for different system parameters. Moreover, comparions of the BER's of TH-UWB and DS-UWB systems in the presence of IEEE 802.11a interference are made. Finally, the major results are summarized in Section 5.6.

5.2 System Models

The asynchronous TH-PPM, TH-BPSK and DS-BPSK UWB systems are described in Chapter 3. We use the same notation and terminology there. A TH-PPM UWB signal takes the form

$$s_{PPM}^{(k)}(t) = \sqrt{\frac{E_b}{N_s}} \sum_{j=-\infty}^{+\infty} p\left(t - jT_f - c_j^{(k)} T_c - d_{\lfloor j/N_s \rfloor}^{(k)} \delta\right) \tag{5.1}$$

a TH-BPSK UWB signal is written as

$$s_{BPSK}^{(k)}(t) = \sqrt{\frac{E_b}{N_s}} \sum_{j=-\infty}^{+\infty} d_{\lfloor j/N_s \rfloor}^{(k)} p\left(t - jT_f - c_j^{(k)} T_c\right) \tag{5.2}$$

and a DS-BPSK UWB signal has the form

$$s_{DS}^{(k)}(t) = \sqrt{\frac{E_b}{N_c}} \sum_{j=-\infty}^{\infty} \sum_{n=0}^{N_c-1} d_j^{(k)} c_n^{(k)} p(t - jT_f - nT_c) \tag{5.3}$$

where $s^{(k)}(t)$ is the kth user's signal, and $p(t)$ is the signal pulse with pulse width T_p, normalized to have unit energy. The notations and parameters in these UWB models are described as in Chapter 3.

Assuming N_u users are transmitting on an AWGN channel in the presence of the interference from the IEEE 802.11a system, the received signal, $r(t)$, at the UWB

receiver is written as

$$r(t) = \sum_{k=1}^{N_u} A_k s^{(k)}(t - \tau_k) + A_i I(t - \tau_i) + n(t) \tag{5.4}$$

where $n(t)$ is additive noise with two-sided power spectral density $\frac{N_0}{2}$, $\{A_k\}_{k=1}^{N_u}$ represent the received amplitudes for all transmitted UWB signals, and $\{\tau_k\}_{k=1}^{N_u}$ represent time shifts for N_u UWB signals. Additionally, A_i and τ_i represents the received amplitude and the time shift of the narrowband interfering signal $I(t)$, respectively. Considering an analysis of the MAI has been provided in Chapter 3, we only use related results obtained in [71] for our numerical examples in Section 5.5.

In the present chapter, we focus on the investigation of the interference from the IEEE 802.11a system employing OFDM. We assume that the symbol duration of the OFDM signal, T, is much greater than the symbol duration of the UWB system, which is common in practical systems, and rectangular pulse shaping is used for the OFDM signal. Therefore, phase transitions in the OFDM signal can be neglected and one symbol of the transmitted OFDM signal has the form

$$I_{OFDM}(t) = \frac{1}{\sqrt{N}} \sum_{n=0}^{N-1} a_n e^{j2\pi(n\Delta f + f_c)t}, \qquad t \leq T \tag{5.5}$$

where N is the number of subcarriers in the OFDM signal, Δf represents the subcarrier frequency spacing, f_c is the carrier frequency, and a_n is the transmitted OFDM data symbol, which can represent BPSK, QPSK or some quadrature amplitude modulation (QAM) signaling.

5.3 Interference Analysis

5.3.1 TH-PPM System

Define the correlation of the template $v(t)$ in the TH-PPM system with a time-shifted pulse $p(t)$ as

$$\tilde{R}(x) = \int_{-\infty}^{\infty} p(t - x)v(t)dt = R(x) - R(x - \delta) \tag{5.6}$$

where $R(x)$ is the autocorrelation of the UWB pulse waveform $p(t)$.

Consider $s^{(1)}_{PPM}(t)$ to be the desired signal and $d^{(1)}_0$ to be the transmitted information bit. Without loss of generality, we assume $\tau_1 = 0$. Assuming perfect synchronization with the reference signal, the decision statistic of the correlation receiver is obtained as

$$r = S_{PPM} + I_{PPM} + I_{OFDM} + n_{PPM} \tag{5.7}$$

where n_{PPM} is a Gaussian random variable with zero mean and variance $\sigma_n^2 = N_0 N_s \tilde{R}(0)$, $S_{PPM} = \pm A_1 \sqrt{E_b N_s} \tilde{R}(0)$ is signal component depending on user 1's signal bit $d^{(1)}_0$, I_{PPM} is the total MAI due to all $N_u - 1$ interfering signals described in [71], and I_{OFDM} is the interference from the OFDM signal, given by

$$\begin{aligned} I_{OFDM} &= A_i \sum_{m=0}^{N_s-1} \mathbf{Re}\left\{ \int_{mT_f}^{(m+1)T_f} I_{OFDM}(t-\tau_i)\, v\left(t - mT_f - c^{(1)}_m T_c\right) dt \right\} \\ &= \frac{A_i}{\sqrt{N}} \sum_{m=0}^{N_s-1} \sum_{n=0}^{N-1} \mathbf{Re}\left\{ a_n e^{j2\pi(n\Delta f + f_c)(mT_f + c^{(1)}_k T_c - \tau_i)} \int_0^{T_f} e^{j2\pi(n\Delta f + f_c)x} v(x) dx \right\} \end{aligned} \tag{5.8}$$

where $\mathbf{Re}\{X\}$ is the real part of X.

Defining $\omega_n = 2\pi(n\Delta f + f_c)$ and substituting the form of $v(t)$ into (5.8) yields [34]

$$\begin{aligned} I_{OFDM} &= \frac{A_i}{\sqrt{N}} \sum_{m=0}^{N_s-1} \sum_{n=0}^{N-1} \mathbf{Re}\left\{ a_n (1 - e^{j\omega_n \delta}) e^{j\omega_n (mT_f + c^{(1)}_m T_c - \tau_i)} \int_0^{T_f} e^{j\omega_n x} p(x) dx \right\} \\ &= \frac{A_i}{\sqrt{N}} \sum_{m=0}^{N_s-1} \sum_{n=0}^{N-1} \mathbf{Re}\left\{ a_n (1 - e^{j\omega_n \delta}) e^{j\omega_n (mT_f + c^{(1)}_m T_c + \frac{T_p}{2} - \tau_i)} \int_{-T_p/2}^{T_p/2} e^{j\omega_n z} p_s(z) dz \right\} \end{aligned} \tag{5.9}$$

where $p_s(z)$ has identical shape as $p(x)$ with pulse width T_p, but is symmetric about $z = 0$, which comes from left shifting the pulse $p(x)$. Defining

$$\mathcal{F}(\omega_n) = \int_{-T_p/2}^{T_p/2} e^{j\omega_n z} p_s(z) dz \tag{5.10}$$

and considering the pulse $p_s(z)$ is limited on $[-\frac{T_p}{2}, \frac{T_p}{2}]$, we can approximate the integral $\mathcal{F}(\omega_n)$ by changing the integration interval to $(-\infty, \infty)$. Then $\mathcal{F}(\omega_n)$ can be

interpreted as the inverse Fourier transform of $p_s(z)$. Based on this interpretation, we can conclude that the interference from the OFDM signal, I_{OFDM}, has a closed-form expression as long as the inverse Fourier transform of the pulse $p_s(z)$ exists.

In this paper, we restrict our analysis of UWB systems to the 2^{nd}-order Gaussian monocycle, given by

$$p_s(z) = \epsilon \left[1 - 4\pi \left(\frac{z}{\tau_p}\right)^2\right] \exp\left[-2\pi \left(\frac{z}{\tau_p}\right)^2\right] \tag{5.11}$$

where τ_p represents a time normalization factor and ϵ is introduced to normalize the energy of the pulses, $p_s(z)$. Our analytical method, however, can be generalized to UWB systems using other pulse shapes provided their inverse Fourier transforms exist. In fact, similar results for higher-order Gaussian monocycles can be obtained using the same analysis described in the sequel.

For the 2^{nd}-order Gaussian monocycle, $\epsilon = \frac{8}{3\tau_p}$ for a given τ_p. The integral $\mathcal{F}(\omega_n)$ can be written as

$$\mathcal{F}(\omega_n) = \frac{8}{3\tau_p}\left[\int_{-\infty}^{\infty} e^{-2\pi\left(\frac{z}{\tau_p}\right)^2} e^{j\omega_n z} dz - 4\pi \int_{-\infty}^{\infty} \left(\frac{z}{\tau_p}\right)^2 e^{-2\pi\left(\frac{z}{\tau_p}\right)^2} e^{j\omega_n z} dz\right] \tag{5.12}$$

where the two integrals can be solved as

$$\int_{-\infty}^{\infty} e^{-2\pi\left(\frac{z}{\tau_p}\right)^2} e^{j\omega_n z} dz = \frac{\tau_p}{\sqrt{2}} \exp\left(-\frac{\tau_p^2 \omega_n^2}{8\pi}\right) \tag{5.13}$$

$$\int_{-\infty}^{\infty} \left(\frac{z}{\tau_p}\right)^2 e^{-2\pi\left(\frac{z}{\tau_p}\right)^2} e^{j\omega_n z} dz = \frac{\tau_p}{4\pi\sqrt{2}} \exp\left(-\frac{\tau_p^2 \omega_n^2}{8\pi}\right)\left(1 - \frac{\tau_p^2 \omega_n^2}{4\pi}\right). \tag{5.14}$$

Thus, $\mathcal{F}(\omega_n)$ is given by

$$\mathcal{F}(\omega_n) = \frac{2\tau_p^2}{3\pi\sqrt{2}} \omega_n^2 e^{-\frac{\tau_p^2 \omega_n^2}{8\pi}}. \tag{5.15}$$

Therefore, I_{OFDM} has a closed-form expression as

$$\begin{aligned} I_{OFDM} &= \frac{2A_I \tau_p^2}{3\pi\sqrt{2N}} \sum_{m=0}^{N_s-1} \sum_{n=0}^{N-1} a_n \omega_n^2 e^{-\frac{\tau_p^2 \omega_n^2}{8\pi}} \mathbf{Re}\left\{\left(1 - e^{j\omega_n \delta}\right) e^{j\omega_n\left(mT_f + c_m^{(1)} T_c + \frac{T_p}{2} - \tau_i\right)}\right\} \\ &= \frac{4A_I \tau_p^2}{3\pi\sqrt{2N}} \sum_{m=0}^{N_s-1} \sum_{n=0}^{N-1} \omega_n^2 e^{-\frac{\tau_p^2 \omega_n^2}{8\pi}} I_{m,n} \end{aligned} \tag{5.16}$$

where $I_{m,n}$ is defined as

$$I_{m,n} = a_n \sin\left[\omega_n\left(mT_f + c_m^{(1)}T_c + \frac{T_p+\delta}{2} - \tau_i\right)\right]\sin\left(\frac{\omega_n\delta}{2}\right) \tag{5.17}$$

for BPSK signaling, where a_n takes $\{\pm 1\}$ with equal probability. Similarly, the expression for $I_{m,n}$ can be obtained for QPSK signaling as

$$\begin{aligned} I_{m,n} =& a_n^I \sin\left[\omega_n\left(mT_f + c_m^{(1)}T_c + \frac{T_p+\delta}{2} - \tau_i\right)\right]\sin\left(\frac{\omega_n\delta}{2}\right) + \\ & a_n^Q \cos\left[\omega_n\left(mT_f + c_m^{(1)}T_c + \frac{T_p+\delta}{2} - \tau_i\right)\right]\sin\left(\frac{\omega_n\delta}{2}\right) \end{aligned} \tag{5.18}$$

in which a_n^I and a_n^Q represents the in-phase and quadrature part of the data symbol a_n, respectively, having values chosen from $\{\pm 1\}$ independently. As seen, $I_{m,n}$ for OFDM QPSK signaling can be regarded as the sum of two independent BPSK signals. Therefore, the analysis of BPSK signaling in the sequel can be easily extended to QPSK constellations.

It is seen that the interference I_{OFDM} is a RV depending on a_n, $c_m^{(1)}$, and the time shift of the OFDM signal,τ_i. Considering the uniform distribution of the BPSK symbol a_n, we can calculate the CHF of $I_{m,n}$ conditioned on $c_m^{(1)}$ and τ_i as

$$\begin{aligned} \Phi_{I_{m,n}|c,\tau}(\Omega) &= \mathbb{E}\left[e^{j\Omega I_{k,n}} \mid c_m^{(1)} = c, \tau_i = \tau\right] \\ &= \cos\left\{\sin\left[\omega_n\left(mT_f + cT_c + \frac{T_p+\delta}{2} - \tau\right)\right]\sin\left(\frac{\omega_n\delta}{2}\right)\Omega\right\}. \end{aligned} \tag{5.19}$$

We define

$$I_m = \sum_{n=0}^{N-1} \omega_n^2 e^{-\frac{\tau_p^2\omega_n^2}{8\pi}} I_{m,n} \tag{5.20}$$

and assume $\{a_n\}_{n=0}^{N-1}$ are independent. Then, the conditional CHF of I_m is

$$\Phi_{I_m|c,\tau}(\Omega) = \prod_{n=0}^{N-1} \Phi_{I_{m,n}|c,\tau}\left(\omega_n^2 e^{-\frac{\tau_p^2\omega_n^2}{8\pi}}\Omega\right). \tag{5.21}$$

Using the uniform distribution of $c_m^{(1)}$ on $[0, N_h - 1]$, we can express the CHF of I_k conditioned on τ_i as

$$\Phi_{I_n|\tau}(\Omega) = \frac{1}{N_h}\sum_{c=0}^{N_h-1} \Phi_{I_m|c,\tau}(\Omega). \tag{5.22}$$

Owing to the independence of $\left\{c_m^{(1)}\right\}_{m=0}^{N_s-1}$, the CHF of the OFDM interference, I_{OFDM}, when conditioned on τ_i is

$$\begin{aligned}\Phi_{I_{OFDM}|\tau}(\Omega) &= \mathbb{E}\left\{e^{j\Omega I_{OFDM}} \mid \tau_i = \tau\right\} \\ &= \prod_{m=0}^{N_s-1} \Phi_{I_m|\tau}\left(\frac{4A_i\tau_p^2}{3\pi\sqrt{2N}}\Omega\right). \end{aligned} \tag{5.23}$$

Note that (5.23) is a closed-form expression for the CHF of I_{OFDM} when the interfering OFDM signal is synchronized to the desired UWB signal, i.e., $\tau_i = 0$. When the OFDM signal is not transmitted simultaneously with the reference UWB signal, $s_{PPM}^{(1)}(t)$, the conditional CHF of I_{OFDM} needs to be averaged over τ_i. Without loss of generality, assume that the time shift τ_i is uniformly distributed on a bit duration of the UWB signal, $[0, N_sT_f)$. Then, the CHF of I_{OFDM} in the asynchronous scenario is given by

$$\Phi_{I_{OFDM}}(\Omega) = \frac{1}{N_sT_f}\int_0^{N_sT_f} \Phi_{I_{OFDM}|\tau}(\Omega). \tag{5.24}$$

5.3.2 TH-BPSK system

The decision statistic r_{BPSK} in TH-BPSK systems is given by

$$r_{BPSK} = S_{BPSK} + I_{BPSK} + I_{OFDM} + n_{BPSK} \tag{5.25}$$

where n_{BPSK} is a Gaussian noise with variance $\sigma_{n_{BPSK}}^2 = \frac{N_0N_s}{2}$, $S_{BPSK} = A_1d_0^{(1)}\sqrt{E_bN_s}$ is the signal contribution to the decision statistic r_{BPSK}, I_{BPSK} is the MAI and I_{OFDM} is the narrowband interference from the OFDM signal given by

$$I_{OFDM} = \frac{A_i}{\sqrt{N}}\sum_{m=0}^{N_s-1}\sum_{n=0}^{N-1}\mathbf{Re}\left\{a_ne^{j2\pi(n\Delta f+f_c)(mT_f+c_m^{(1)}T_c-\tau_i)}\int_0^{T_f} e^{j2\pi(n\Delta f+f_c)x}p(x)dx\right\}. \tag{5.26}$$

Utilizing the same definitions of ω_n, $p_s(z)$ and $\mathcal{F}(\omega_n)$ as those used in Section III, we can write the interference I_{OFDM} in the TH-BPSK system as

$$I_{OFDM} = \frac{A_i}{\sqrt{N}} \sum_{m=0}^{N_s-1} \sum_{n=0}^{N-1} \mathbf{Re}\left\{ a_n e^{j\omega_n (mT_f + c_m^{(1)} T_c + \frac{T_p}{2} - \tau_i)} \int_{-\frac{T_p}{2}}^{\frac{T_p}{2}} e^{j2\pi(n\Delta f + f_c)z} p_s(z) dz \right\}$$
$$= \frac{A_i}{\sqrt{N}} \sum_{m=0}^{N_s-1} \sum_{n=0}^{N-1} \mathbf{Re}\left\{ a_n e^{j\omega_n (mT_f + c_m^{(1)} T_c + \frac{T_p}{2} - \tau_i)} \mathcal{F}(\omega_n) \right\}. \quad (5.27)$$

For the 2^{nd}-order Gaussian monocycle, we can also obtain a closed-form expression for I_{OFDM} as

$$I_{OFDM} = \frac{2A_i\tau_p^2}{3\pi\sqrt{2N}} \sum_{m=0}^{N_s-1} \sum_{n=0}^{N-1} a_n \omega_n^2 e^{-\frac{\tau_p^2\omega_n^2}{8\pi}} \mathbf{Re}\left\{ e^{j\omega_n \left(mT_f + c_m^{(1)} T_c + \frac{T_p}{2} - \tau_i\right)} \right\}$$
$$= \frac{2A_i\tau_p^2}{3\pi\sqrt{2N}} \sum_{m=0}^{N_s-1} \sum_{n=0}^{N-1} \omega_n^2 e^{-\frac{\tau_p^2\omega_n^2}{8\pi}} I_{m,n} \quad (5.28)$$

where $I_{m,n}$ is expressed as

$$I_{m,n} = a_n \cos\left[\omega_n \left(mT_f + c_m^{(1)} T_c + \frac{T_p}{2} - \tau_i\right)\right] \quad (5.29)$$

for BPSK signaling, or as

$$I_{m,n} = a_n^I \cos\left[\omega_n \left(mT_f + c_m^{(1)} T_c + \frac{T_p}{2} - \tau_i\right)\right] -$$
$$a_n^Q \sin\left[\omega_n \left(mT_f + c_m^{(1)} T_c + \frac{T_p}{2} - \tau_i\right)\right] \quad (5.30)$$

for QPSK signaling.

Following similar steps as in Section 5.3, we can obtain the CHF of $I_{m,n}$ conditioned on $c_m^{(1)}$ and τ_i as

$$\Phi_{I_{m,n}|c,\tau}(\Omega) = \mathbb{E}\left[e^{j\Omega I_{m,n}} \mid c_m^{(1)} = c, \tau_i = \tau\right]$$
$$= \cos\left\{\Omega \cos\left[\omega_n \left(mT_f + cT_c + \frac{T_p}{2} - \tau\right)\right]\right\}. \quad (5.31)$$

Then, the conditional CHF of $I_m = \sum_{n=0}^{N-1} \omega_n^2 e^{-\frac{\tau_p^2\omega_n^2}{8\pi}} I_{m,n}$ can be expressed using the independence of a_n as

$$\Phi_{I_m|c,\tau}(\Omega) = \prod_{n=0}^{N-1} \Phi_{I_{m,n}|c,\tau}\left(\omega_n^2 e^{-\frac{\tau_p^2\omega_n^2}{8\pi}} \Omega\right). \quad (5.32)$$

Further, the CHF of I_{OFDM} conditioned on τ_i as

$$\Phi_{I_{OFDM}|\tau}(\Omega) = \frac{1}{N_h^{N_s}} \prod_{m=0}^{N_s-1} \sum_{c=0}^{N_h-1} \prod_{n=0}^{N-1} \cos\left\{ \frac{2A_i\tau_p^2\omega_n^2}{3\pi\sqrt{2N}} e^{-\frac{\tau_p^2\omega_n^2}{8\pi}} \cos\left[\omega_n\left(kT_f + cT_c + \frac{T_p}{2} - \tau\right)\right]\Omega \right\} \tag{5.33}$$

thus, the CHF of the interference I_{OFDM} in the TH-BPSK system is calculated by averaging τ_i as

$$\Phi_{I_{OFDM}}(\Omega) = \frac{1}{N_sT_f} \int_0^{N_sT_f} \Phi_{I_{OFDM}|\tau}(\Omega). \tag{5.34}$$

5.3.3 DS-BPSK System

Under the assumption of perfect synchronization for the reference signal $s_{DS}^{()}$, the correlation receiver computes the decision statistic for the DS-BPSK system as

$$r_{DS} = \sum_{m=0}^{N_c-1} \int_0^{T_c} r(t)c_m^{(1)}p(t - mT_c)dt. \tag{5.35}$$

The signal component in the decision statistic can be written as

$$r_{DS} = S_{DS} + I_{DS} + I_{OFDM} + n_{DS} \tag{5.36}$$

where S_{DS} is the contribution to the decision statistic r_{DS} depending on user 1's information bit $d_0^{(1)}$, expressed as

$$S_{DS} = A_1\sqrt{E_bN_c}d_0^{(1)} \tag{5.37}$$

n_{DS} is the noise component with zero mean and variance $\sigma_{n_{DS}}^2 = \frac{N_0N_c}{2}$, I_{DS} is the total MAI, and I_{OFDM} is the interference to the DS-BPSK UWB system from the OFDM signal, expressed as

$$\begin{aligned} I_{OFDM} &= \frac{A_i}{\sqrt{N}} \sum_{m=0}^{N_c-1} c_m^{(1)} \mathbf{Re}\left\{ \int_0^{T_b} \sum_{n=0}^{N-1} a_n e^{j2\pi(n\Delta f + f_c)(t-\tau_i)} p(t - mT_c)dt \right\} \\ &= \frac{A_i}{\sqrt{N}} \sum_{m=0}^{N_c-1} c_m^{(1)} \sum_{n=0}^{N-1} \mathbf{Re}\left\{ a_n e^{j2\pi(n\Delta f + f_c)(mT_c - \tau_i)} \int_0^{T_c} e^{j2\pi(n\Delta f + f_c)x} p(x)dx \right\} \\ &= \frac{A_i}{\sqrt{N}} \sum_{m=0}^{N_c-1} c_m^{(1)} \sum_{n=0}^{N-1} \mathbf{Re}\left\{ a_n e^{j\omega_n(mT_c + \frac{T_p}{2} - \tau_i)} \mathcal{F}(\omega_n) \right\}. \end{aligned} \tag{5.38}$$

We can further simplify the interference I as

$$I_{OFDM} = \frac{2A_i\tau_p^2}{3\pi\sqrt{2N}} \sum_{m=0}^{N_c-1} c_m^{(1)} \sum_{n=0}^{N-1} \omega_n^2 e^{-\frac{\tau_p^2\omega_n^2}{8\pi}} I_{m,n} \tag{5.39}$$

where

$$I_{m,n} = a_n \cos\left[\omega_n\left(mT_c + \frac{T_p}{2} - \tau_i\right)\right]. \tag{5.40}$$

Then, the CHF of $I_{m,n}$ conditioned on τ_i is given by

$$\Phi_{I_{m,n}|\tau}(\Omega) = \cos\left\{\Omega\cos\left[\omega_n\left(mT_c + \frac{T_p}{2} - \tau\right)\right]\right\} \tag{5.41}$$

and the CHF of $I_m = c_m^{(1)} \sum_{n=0}^{N-1} \omega_n^2 e^{-\frac{\tau_p^2\omega_n^2}{8\pi}} I_{m,n}$ conditioned on τ_i and $c_m^{(1)}$ can be obtained as

$$\begin{aligned}\Phi_{I_m|c,\tau}(\Omega) &= \mathbf{E}\left[e^{j\Omega I_m} \mid c_m^{(1)} = c, \tau_i = \tau\right]. \\ &= \prod_{n=0}^{N-1} \cos\left\{c\omega_n^2 e^{-\frac{\tau_p^2\omega_n^2}{8\pi}} \Omega\cos\left[\omega_n\left(mT_c + \frac{T_p}{2} - \tau\right)\right]\right\}.\end{aligned} \tag{5.42}$$

In DS-BPSK UWB systems, $c_m^{(1)}$ is assumed to take values $\{\pm 1\}$ with equal probability. Therefore, the CHF of I_m conditioned on τ_i can be computed as

$$\begin{aligned}\Phi_{I_m|\tau}(\Omega) &= \frac{1}{2}\left[\Phi_{I_m|-1,\tau}(\Omega) + \Phi_{I_m|1,\tau}(\Omega)\right] \\ &= \prod_{n=0}^{N-1} \cos\left\{\omega_n^2 e^{-\frac{\tau_p^2\omega_n^2}{8\pi}} \cos\left[\omega_n\left(mT_c + \frac{T_p}{2} - \tau\right)\right]\Omega\right\}\end{aligned} \tag{5.43}$$

where the second equality comes from the even symmetry of the cosine function.

Finally, using the independence of $c_m^{(1)}$ and averaging $\Phi_{I_m|\tau}(\Omega)$ over the uniform distribution of τ_i, we obtain the CHF of the total interference I_{OFDM} as

$$\begin{aligned}\Phi_{I_{OFDM}}(\Omega) = \frac{1}{N_cT_c} \prod_{m=0}^{N_c-1} \prod_{n=0}^{N-1} \int_0^{N_cT_c} \cos\Bigg\{&\frac{2A_I\tau_p^2\omega_n^2}{3\pi\sqrt{2N}} e^{-\frac{\tau_p^2\omega_n^2}{8\pi}} \times \\ &\cos\left[\omega_n\left(mT_c + \frac{T_p}{2} - \tau\right)\right]\Omega\Bigg\}\, d\tau.\end{aligned} \tag{5.44}$$

Also note that the integrand in (5.44) is an analytical expression for the interference I_{OFDM} when the OFDM interfering signal is transmitted synchronously with $s_{DS}^{(1)}(t)$, which indicates a special case in UWB transmission.

5.4 Bit Error Probability

In this section, the expressions for the bit error probabilities of the TH-UWB and DS-UWB systems in the presence of interference will be determined based on previous analysis. It is seen from previous sections that the interference I_{OFDM} is symmetric because its CHF is real. Owing to the symmetry of the OFDM interference, the MAI and the noise, the average probability of error for the TH-PPM system is given by

$$P_e = \Pr(-A_1\sqrt{E_bN_s}\tilde{R}(0) + I_{OFDM} + I_{PPM} + n_{PPM} > 0) \tag{5.45}$$

the BER for the TH-BPSK systems is

$$P_e = \Pr(A_1\sqrt{E_bN_s} + I_{OFDM} + I_{BPSK} + n_{BPSK} < 0) \tag{5.46}$$

and the BER of the DS-BPSK systems is expressed as

$$P_e = \Pr(A_1\sqrt{E_bN_c} + I_{OFDM} + I_{DS} + n_{DS} < 0). \tag{5.47}$$

Define $\Lambda = I_{OFDM} + I + n$; then, using the independence of interference and the background noise, the CHF of Λ can be expressed as

$$\Phi_\Lambda(\Omega) = \Phi_{I_{OFDM}}(\Omega)\Phi_I(\Omega)\Phi_n(\Omega) \tag{5.48}$$

where $\Phi_n(\Omega) = e^{\frac{-\sigma_n^2\omega^2}{2}}$ is the CHF for the noise term n, $\Phi_{I_{OFDM}}(\Omega)$ and $\Phi_I(\Omega)$ is the CHF of the interference from the OFDM signal and the MAI from $N_u - 1$ interfering UWB signals, respectively, in the TH or DS UWB system.

Considering the relationship between the CDF and the CHF of a RV [57, eq. (3-23)], we can express the BER of the TH-PPM system as

$$\begin{aligned} P_e &= 1 - F_\Lambda\left(A_1\sqrt{E_bN_s}\tilde{R}(0)\right) \\ &= \frac{1}{2} - \frac{1}{\pi}\int_0^\infty \frac{\sin(A_1\sqrt{E_bN_s}\tilde{R}(0)\Omega)}{\Omega}\Phi_{I_{OFDM}}(\Omega)\Phi_I(\Omega)e^{\frac{-\sigma_n^2\Omega^2}{2}}d\Omega \end{aligned} \tag{5.49}$$

where $F_\Lambda(\cdot)$ represents the CDF of Λ. Then, the average probability of error for the desired user in the TH-BPSK and DS-BPSK UWB systems is obtained, respectively,

as

$$P_{e_{BPSK}} = \frac{1}{2} - \frac{1}{\pi}\int_0^\infty \frac{\sin(A_1\sqrt{E_bN_s}\Omega)}{\Omega}\Phi_{I_{OFDM}}(\Omega)\Phi_{I_{BPSK}}(\Omega)e^{\frac{-\sigma^2_{n_{BPSK}}\Omega^2}{2}}d\Omega \quad (5.50)$$

and

$$P_{e_{DS}} = \frac{1}{2} - \frac{1}{\pi}\int_0^\infty \frac{\sin(A_1\sqrt{E_bN_c}\Omega)}{\Omega}\Phi_{I_{OFDM}}(\Omega)\Phi_{I_{DS}}(\Omega)e^{\frac{-\sigma^2_{n_{DS}}\Omega^2}{2}}d\Omega. \quad (5.51)$$

5.5 Numerical Results and Comparisons

In this section, we use our accurate analytical results to study the average BER performance of TH-UWB and DS-UWB systems in the presence of IEEE 802.11a OFDM interference. From the previous sections, it is seen that a double-integral calculation is required for precisely computing the BER of TH and DS UWB systems operating in asynchronous interference, while a single-integral calculation is required for computing the BER of UWB systems with synchronous interference. These integrations are performed numerically. Monte Carlo simulation was used to validate our analytical derivations. The parameters of the example UWB systems and the OFDM system are listed in Table 5.1 following [34], [71].

First, we compare the analytical BER's of the TH-UWB and DS-UWB systems with results obtained from simulations and the Gaussian approximation. The BER's of the UWB system operating in OFDM interference are plotted to show the effect of narrowband interference and further used to characterize OFDM interference in UWB systems. Additionally, the performance of the UWB system in the presence of narrowband interference and MAI as well will be shown using the numerical examples. Therefore, we can comprehensively compare the anti-interference capability of the different UWB modulation schemes so as to draw some general conclusions, regarding the effects of narrowband interference and multiple access interference on the transmission of UWB signals.

Fig. 5.1 shows the BER of the TH-PPM system computed using our analysis described in the previous section, as well as some test BER's obtained by simulation and

TABLE 5.1

Parameters of the Example TH/DS UWB and OFDM systems

Parameter	Notation	2^{nd}-order monocycles
Time Normalization Factor	τ_p	0.16 ns
Impulse Width	T_p	$\approx$ 0.5 ns
Frame Width	T_f	14.4 ns
PPM Delay	δ	0.0864 ns
Chip Width	T_c	0.9 ns
Number of Users	N_u	8
Number of Chips per Frame	N_h	16
Repetition Code Length	N_s	2, 4, 8
Number of Chips per Frame	N_c	32, 64, 128
The number of subcarriers	N	52
The carrier frequency	f_c	5.22 GHz
The subcarrier frequency spacing	Δf	0.3125 MHz

the Gaussian approximation. The BER curves are presented as a function of SNR, E_b/N_0, with $N_s = 2$, 4 and 8. In this figure, only synchronous OFDM interference is considered. As seen, the theoretical results obtained from the analytical expression and the test simulation results are in excellent agreement. It is also seen that the Gaussian approximation is in good agreement with the theoretical analysis for small and medium SNR values, say SNR $\leq$ 10 dB, when $N_s = 2$. However, the Gaussian approximation slightly underestimates the BER's for larger SNR values when A_i/A_1 is 3 dB or -3 dB, and by an order of magnitude when A_i/A_1 is 0 dB and the SNR is 16 dB. We observe that the BER estimates obtained from the Gaussian approximation are almost the same for $N_s = 2$, 4 and 8. Unlike the analytical result, which indicates that the actual performance for $N_s = 4$ is better than the actual performance for $N_s = 2$, and again better for $N_s = 8$, the Gaussian approximation fails to predict the BER performance improvement achieved by using a longer repetition code. Thus, the Gaussian approximation is not a precise approximation for the parameters given in our examples. On the other hand, we note that the BER curves obtained from the analytical expression become increasingly closer to the BER curves obtained from the Gaussian approximation as the length of the repetition code N_s increases. This observation can be explained as follows. Considering the expression for the OFDM interference in (5.15), we can see that more interfering terms will contribute to I_{OFDM} when N_s increases. Owing to the near independence between these terms, the total interference I_{OFDM} can be well approximated as a Gaussian RV following the central limit theorem for large values of N_s. It appears that the Gaussian approximation is valid for estimating the BER of the TH-PPM system operating with OFDM interference for large values of N_s, but it underestimates the BER's for large values of SNR and small values of N_s. Compared with the Gaussian approximation, our precise analysis provides accurate BER estimates for arbitrary values of N_s and SNR with reasonable computational complexity. In order to assess the effect of interference, BER curves for different values of signal-to-interference power ratio (SIR) are also plotted in Fig. 5.1. It is seen that the error probability performance of the TH-PPM

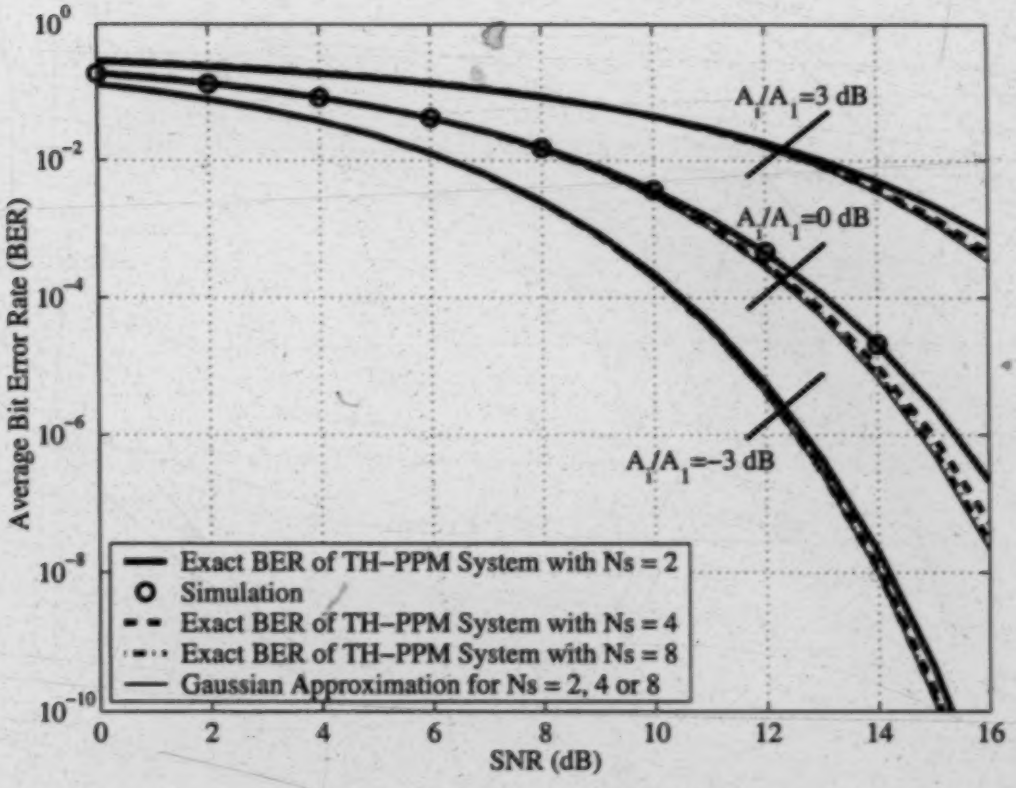
Average Bit Error Rate (BER)
SNR (dB)
A_i/A_1=3 dB
A_i/A_1=0 dB
A_i/A_1=-3 dB
Exact BER of TH-PPM System with Ns = 2
Simulation
Exact BER of TH-PPM System with Ns = 4
Exact BER of TH-PPM System with Ns = 8
Gaussian Approximation for Ns = 2, 4 or 8

Fig. 5.1. The average BER versus SNR of the TH-PPM UWB system operating with synchronous OFDM interference.

system will be significantly deteriorated by stronger interfering OFDM signals.

In Fig. 5.2, the performances of the TH-PPM system in the presence of synchronous and asynchronous OFDM interference are compared. Asynchronous interference introduces more degradation to the BER of the TH-PPM system than synchronous interference, although the difference is small.

Fig. 5.3 shows analytical BER results for the TH-BPSK system and BER's obtained from the Gaussian approximation and test simulation results as well. Similar to the results seen in Fig. 5.1, the Gaussian approximation also slightly underestimates the BER's of the TH-BPSK system for values of SNR more than 10 dB but by more

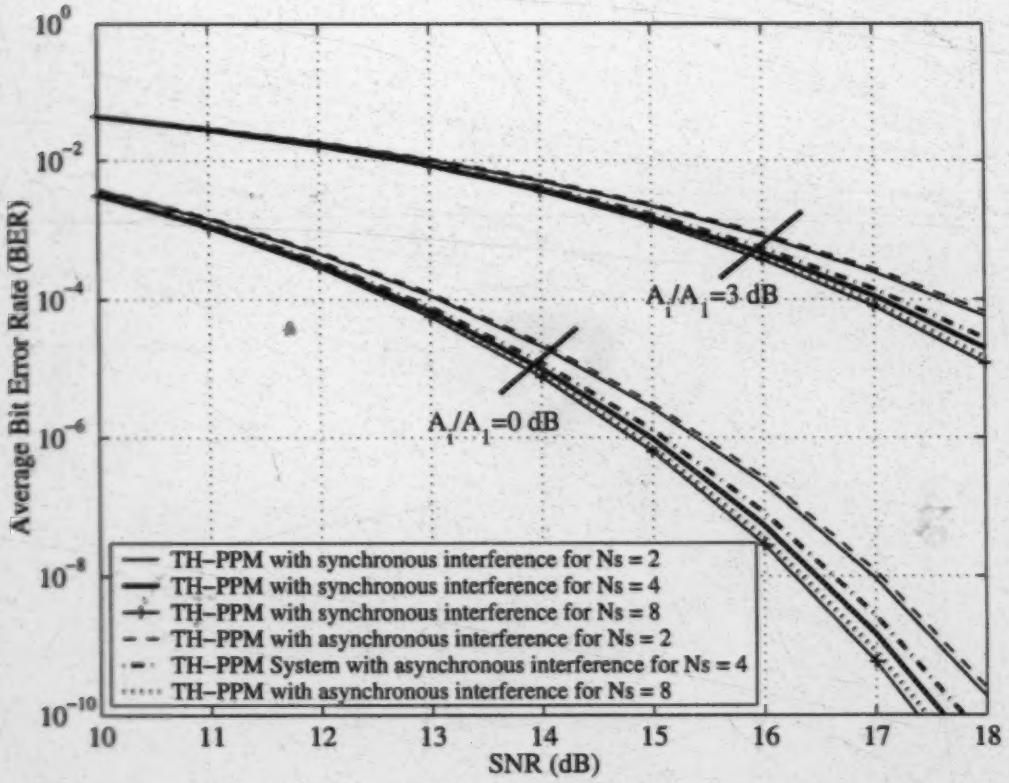
Average Bit Error Rate (BER)
SNR (dB)
A_i/A_i=3 dB
A_i/A_i=0 dB
TH–PPM with synchronous interference for Ns = 2
TH–PPM with synchronous interference for Ns = 4
TH–PPM with synchronous interference for Ns = 8
TH–PPM with asynchronous interference for Ns = 2
TH–PPM System with asynchronous interference for Ns = 4
TH–PPM with asynchronous interference for Ns = 8

Fig. 5.2. Comparison of the TH-PPM UWB system operating with synchronous and asynchronous OFDM interference.

than an order of magnitude when $N_s = 2$, SNR = 16 dB and A_i/A_1= 0 dB. Again, the Gaussian approximation cannot predict accurately the performance improvement obtained by using a longer repetition code as indicated by our analysis, but when the value of N_s increases, the Gaussian approximation will provide good BER estimates for the TH-BPSK system for the reasons explained previously. The performances of the TH-BPSK UWB system operating in synchronous and asynchronous interference are compared in Fig. 5.4. As seen, the asynchronous interfering signal causes more interference and results in a little larger BER's. Similar to the behaviour seen in Fig. 5.2, the BER's in synchronous and asynchronous interference are close to each other.

Fig. 5.5 shows the performance of the DS-BPSK UWB system in the presence of narrowband OFDM interference. In order to fairly compare the BER performance of DS-UWB systems, we assume that the same data rate $R_b = \frac{1}{T_b}$ is used for all TH and DS systems, which requires $N_c = N_s N_h$ [71]. Based on the normalization, we can also plot the BER versus SNR for the DS-BPSK system. The Gaussian approximation almost provides the same BER estimates for different values of N_s. However, unlike the results seen in Figs. 5.1 and 5.3, the Gaussian approximation is in excellent agreement with the theoretical analysis for all values of SNR. Note that the BER's, for any given value of SNR, in synchronous and asynchronous interference are virtually equal, even for different values of N_s. All these behaviours can be explained using a CLT. Checking the expression for I_{OFDM} in (5.39) for the DS-UWB system, we note that many more terms than the case in TH-UWB systems contribute to the total interference when we use $N_c = N_s N_h$ to normalize the DS-UWB system. In this case, the OFDM interference more closely approximates a Gaussian distributed RV and the Gaussian approximation is highly accurate for estimating the BER. As long as the value of N_c is large enough to make the interference AWGN-like, the BER performance will no longer be improved by using a longer repetition code or affected by having synchronization between the interfering signal and the desired UWB signal. These results corroborate the observations obtained from Figs. 5.1, 5.2 and Figs. 5.3,

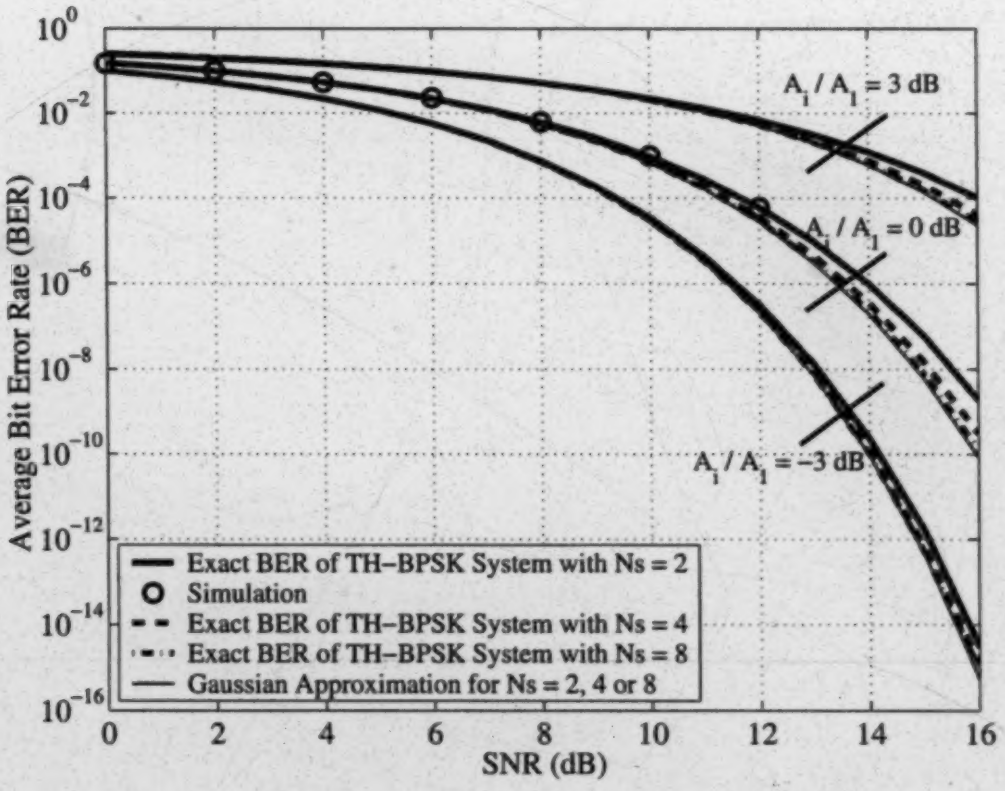
Average Bit Error Rate (BER)
SNR (dB)
$A_i / A_1 = 3$ dB
$A_i / A_1 = 0$ dB
$A_i / A_1 = -3$ dB
Exact BER of TH–BPSK System with Ns = 2
Simulation
Exact BER of TH–BPSK System with Ns = 4
Exact BER of TH–BPSK System with Ns = 8
Gaussian Approximation for Ns = 2, 4 or 8

Fig. 5.3. The average BER versus SNR of the TH-BPSK UWB system operating with synchronous OFDM interference.

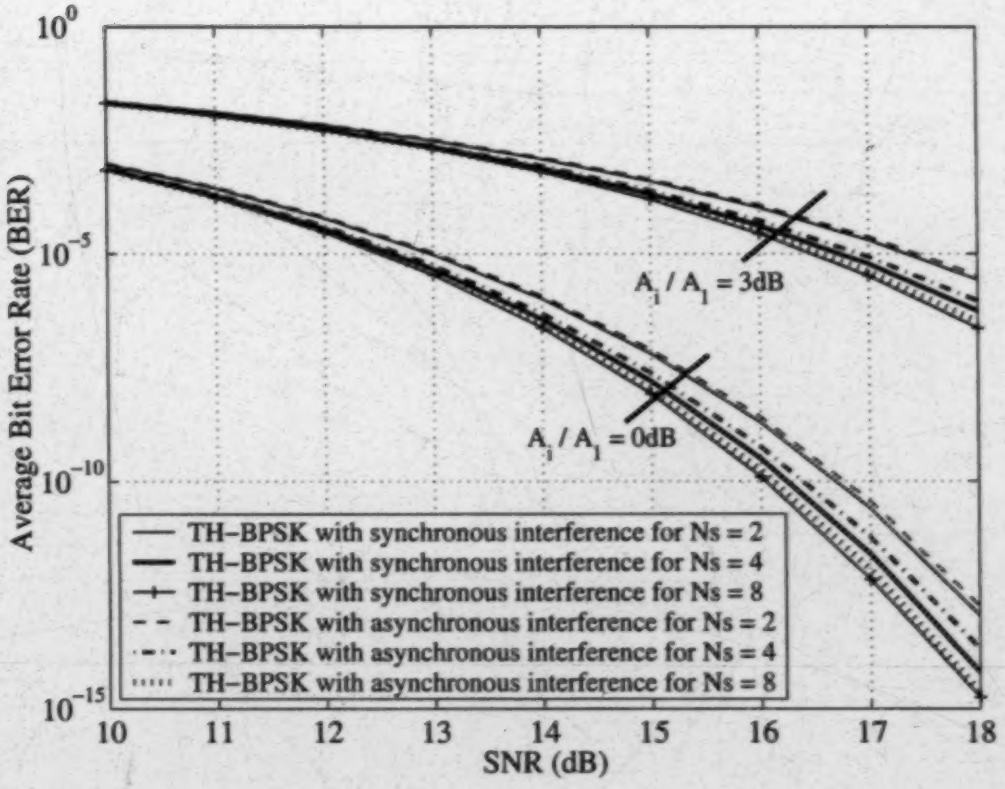

Fig. 5.4. Comparison of the TH-BPSK UWB system operating with synchronous and asynchronous OFDM interference.

5.4 for large values of N_s. In contrast to the behaviour of UWB systems in the presence of MAI as obtained in [71], increasing the length of the repetition code will not suppress more narrowband OFDM interference and the UWB system performance will not be improved, when the value of N_s or N_c is large enough that the Gaussian approximation can be used for predicting the error probability reliably.

In Fig. 5.6, bit error rates of TH-PPM, TH-BPSK and DS-BPSK corrupted by OFDM interference are compared. We observe that the TH-BPSK system outperforms the TH-PPM system for all values of SNR. The TH-BPSK system provides similar BER's to the DS-BPSK system for small SNR values, say SNR $\leq$ 8 dB. In contrast to the results obtained using the Gaussian approximation, which indicate that TH-BPSK achieves the same performance as DS-BPSK when both systems are operated in OFDM interference, the DS-BPSK system actually outperforms the TH-BPSK system for moderate and large SNR values when $N_s = 2$ or 4. Note that DS-BPSK and TH-BPSK achieve the same BER performance, when the interference closely follows the Gaussian distribution as N_s increases.

Finally, we compare the interference suppression capabilities of these UWB modulation schemes in the presence of both multiple access interference and narrowband OFDM interference. In Fig. 5.7, the performances of these three schemes operating in MAI and OFDM interference are compared in terms of the average probability of error. In this case, an error rate floor appears for all these systems because of the multiple access interference. It is seen that the BER performances for all schemes are significantly improved by using a longer repetition code. Our numerical examples also indicate that TH-BPSK and DS-BPSK outperform TH-PPM for all values of SNR. Although the Gaussian approximation provides the same BER estimates for TH-BPSK and DS-BPSK, the performance of DS-BPSK is much better than that of TH-BPSK for large SNR values.

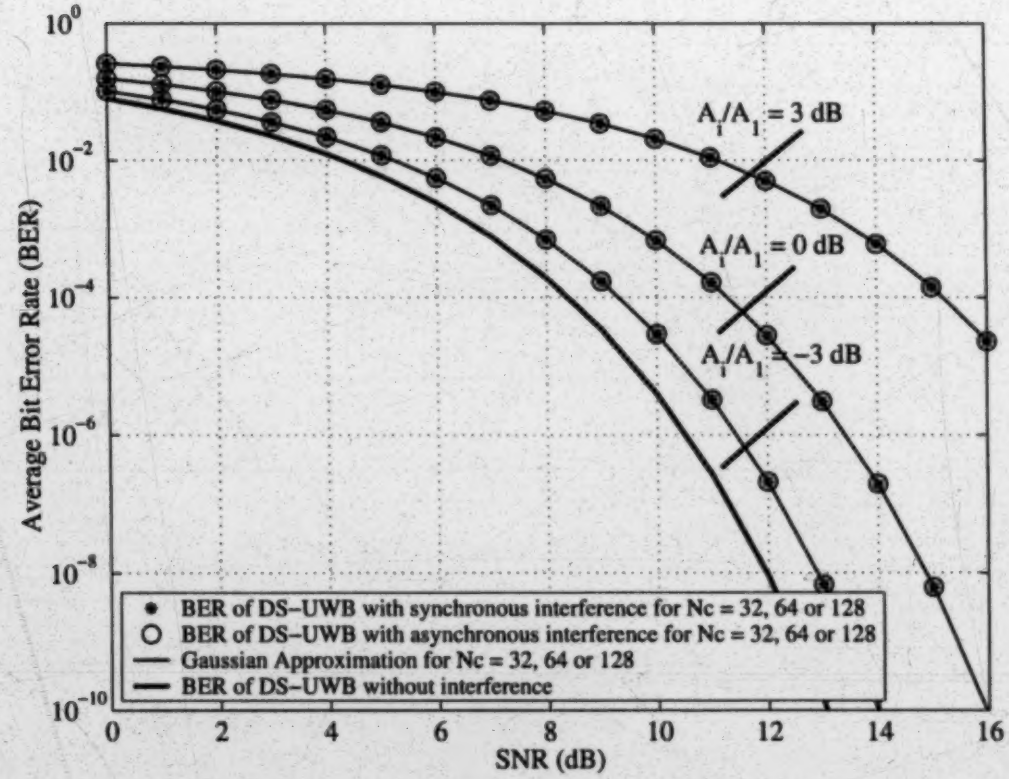

Fig. 5.5. The average BER versus SNR of the DS-BPSK UWB system operating with synchronous and asynchronous OFDM interference.

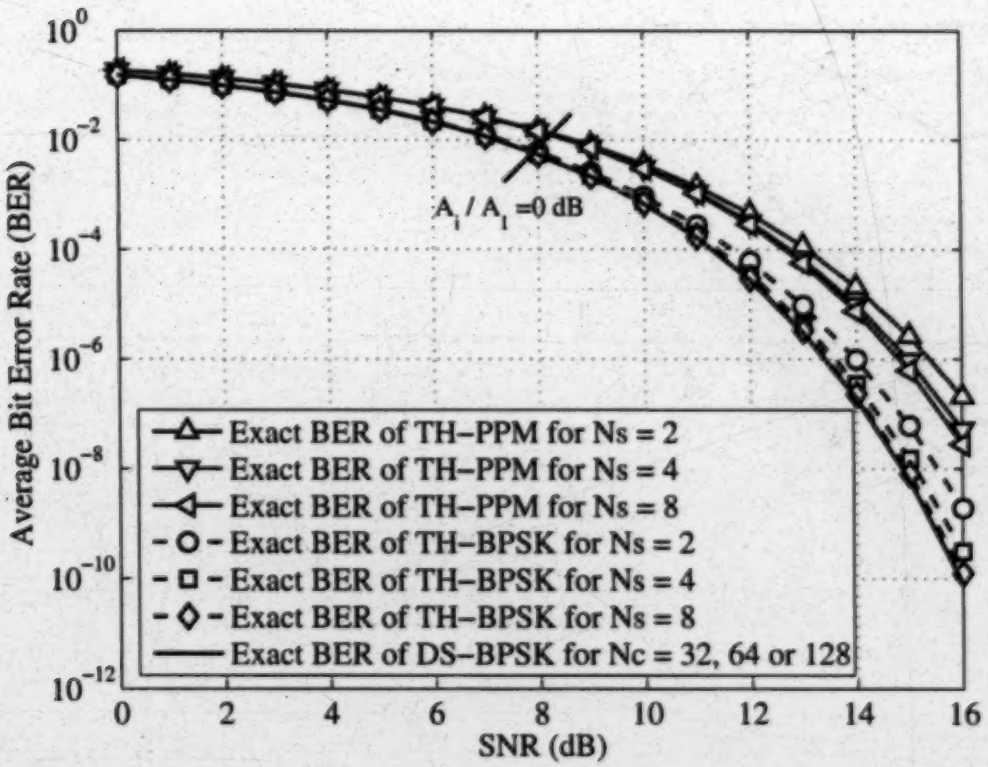
Average Bit Error Rate (BER)
SNR (dB)
A_i / A_1 =0 dB
Exact BER of TH–PPM for Ns = 2
Exact BER of TH–PPM for Ns = 4
Exact BER of TH–PPM for Ns = 8
Exact BER of TH–BPSK for Ns = 2
Exact BER of TH–BPSK for Ns = 4
Exact BER of TH–BPSK for Ns = 8
Exact BER of DS–BPSK for Nc = 32, 64 or 128

Fig. 5.6. Comparison of the TH-PPM, TH-BPSK and DS-BPSK systems with the same data rate operating in OFDM interference.

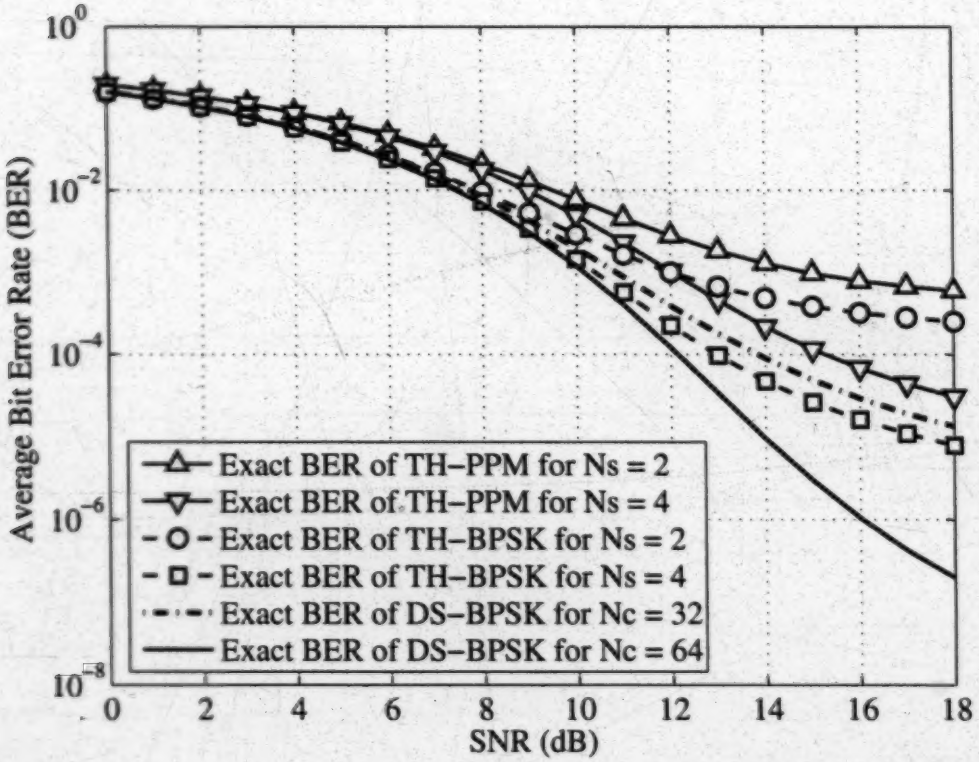
Average Bit Error Rate (BER)
SNR (dB)
Exact BER of TH–PPM for Ns = 2
Exact BER of TH–PPM for Ns = 4
Exact BER of TH–BPSK for Ns = 2
Exact BER of TH–BPSK for Ns = 4
Exact BER of DS–BPSK for Nc = 32
Exact BER of DS–BPSK for Nc = 64

Fig. 5.7. Comparison of the TH-PPM, TH-BPSK and DS-BPSK systems with the same data rate operating in OFDM interference and MAI.

5.6 Summary

In this chapter, we have derived accurate, analytical expressions for the average probability of bit error of time-hopping and direct-sequence UWB systems in the presence of IEEE 802.11a interference. Our precise analysis indicates that the Gaussian approximation for these UWB modulation schemes will overestimate the performance at large values of SNR when the length of the repetition code, N_s is not large enough. Compared with other methods used in the literature, our analysis provides a method for calculating precise BER's for arbitrary system parameters and values of SNR without any improper assumptions.

Our numerical results show that the narrowband interfering OFDM signal introduces more severe interference to UWB systems than the multiple access interference and that the BER performance of these UWB systems will be significantly deteriorated by the interfering OFDM signal with higher power levels. Considering the power levels regulated by IEEE standards, an OFDM signal may introduce much more interference to an UWB system than MAI.

Our comparisons of the performance of TH and DS UWB systems in the presence of OFDM interference indicate that TH-BPSK and DS-BPSK outperform TH-PPM for all values of SNR. Although the Gaussian approximation provides the same BER estimates for both TH-BPSK and DS-BPSK, the actual performance of TH-BPSK may be poorer than the actual performance of DS-BPSK depending on the UWB system parameters. We also compared the performances of different modulation schemes operating in OFDM interference and MAI. Overall, DS-BPSK provides the best performance. Therefore, we can conclude that the DS-UWB system can suppress more interference than the TH-UWB systems, and will be more preferable for commercial applications. An interesting observation was that, for practical values of N_s and N_c, increasing the length of the repetition code in a DS-UWB system does not reduce OFDM interference.

Chapter 6

Modulation Schemes and Rake Receiver Structures for UWB Systems on an Realistic UWB Indoor Channel

6.1 Introduction

Ultra-wideband communication systems are defined as of which the fractional bandwidth is greater than 25%, or the total bandwidth exceedes 500MHz. UWB radio signals employ the transmission of extremely short pulse that spread the energy of the signal from near DC to a few gigahertz. The fine delay resolution properties of UWB signals make UWB radio a valuable candidate for communications in dense multipath environments and the ultra-wide bandwidth makes the communications robust with respect to multipath fading. Meanwhile, the high ratio of the transmitted signal bandwidth to the information signal bandwidth makes UWB technology appealing for multiple access applications. Many multiple access techniques have been proposed. The most popular schemes are time-hopping [14], where different users are

distinguished by using time-hopping code sequences, and direct-sequence [58], where users are distinguished by using different spreading code sequences. As mentioned in Chapter 3, a new UWB radio system design, called direct-sequence impulse radio, was proposed in [61]. Unlike TH-UWB that only employs a time-hopping code or DS-UWB that only employs a direct spreading sequence, the DS-IR design in [61] employs both direct-sequence spreading and time-hopping codes. This DS-IR design gives more flexibility for multiple access designs. However, there is not enough information provided in [61] regarding the magnitude of the performance improvement achievable using DS-IR technology to justify the complexity incurred by using the combination of TH and DS codes over TH or DS UWB systems.

Much reported research has investigated UWB systems utilizing TH or DS techniques with PPM or BPSK modulation schemes for different channel models [72] - [78]. A Gaussian approximation for intersymbol interference and multiple access interference was employed in [51] and [74] to analyze the BER performance of TH and DS-UWB systems. In addition, [76] - [78] investigated the BER performance of TH or DS-UWB systems using semi-analytical methods. In this chapter, we fairly compare the multiple access performances of the TH-PPM, TH-BPSK, DS-BPSK and DS-IR BPSK systems on a realistic multipath fading channel. The comparisons indicate the actual BER performance differences between these UWB systems, superseding previous results obtained using the Gaussian approximation or semi-analytical methods, which both conclude that they have the same performance.

In order to fully utilize the channel diversity, a Rake receiver has to be used to capture and track the signal energy associated with a large number of multipaths. In [76] and [77], several Rake receivers including the all-Rake (ARake) receiver and selective-Rake (SRake) receiver were proposed for UWB reception and numerical results were provided to show the differences among these Rake receivers. In our work, we will show that the ARake structure does not always guarantee the best achievable performance for UWB systems operating on fading channels. The SRake receiver can achieve better performance than the ARake receiver when ISI exists in

the system. Further, the sensitivity of the performances of the Rake receivers to the number of Rake fingers is examined and the results show the importance of choosing suitable numbers of Rake fingers.

This chapter is organized as follows. In Section 6.2, the previously proposed UWB signal formats, the realistic fading channel model and the receiver structures are described. General methods for calculating the bit error probability are reviewed and briefly evaluated in Section 6.3 . The performances of different Rake receivers are compared and discussed in Section 6.4. Design comparisons of the BERs of TH-PPM and TH/DS/DS-IR BPSK systems are also made based on numerical results. Finally, conclusions are drawn in Section 6.5.

6.2 System Models

6.2.1 Fading Channel Model

Assuming N_u users are transmitting on a multipath fading channel, where $h^{(k)}$ represents the channel impulse response experienced by user k. The received signal is

$$r(t) = \sum_{k=1}^{N_u} s^{(k)}(t) * h^{(k)}(t) + n(t) \tag{6.1}$$

where $s^{(k)}(t)$ can be the TH-PPM, DS-BPSK, TH-BPSK or DS-IR signal as described in Chapter 3, and $n(t)$ is Gaussian additive noise with two-sided power spectral density $\frac{N_0}{2}$.

The multipath fading model we employ for UWB systems is recommended by the IEEE 802.15.3a standard based on the evolution of UWB physical submissions. This multipath indoor fading model is a modified Saleh-Valenzuela model where multipath components arrive in clusters [18]. A lognormal distribution rather than a Rayleigh distribution is employed for the multipath gain magnitude. Independent fading is assumed for each cluster as well as each ray within the cluster. Therefore, the multipath

model is mathematically described as

$$h(t) = X \sum_{l=0}^{L} \sum_{k=0}^{K} \alpha_{k,l} \delta(t - T_l - \tau_{k,l}) \tag{6.2}$$

where $\alpha_{k,l}$ is the multipath gain coefficient for cluster l and ray k, T_l is the delay of the lth cluster, $\tau_{k,l}$ is the delay of the kth ray relative to the arrival time of the lth cluster, and X represents lognormal shadowing. The number of clusters and rays in the multipath fading model is denoted by L and K, respectively, and are fixed for a given model. The interarrival time between two clusters, $T_{l+1} - T_l$, or between two rays within one cluster, $\tau_{k+1,l} - \tau_{k,l}$, is exponentially distributed. The amplitude of $\alpha_{k,l}$ has a lognormal distribution and the expected value $E(|\alpha_{k,l}|^2)$ is exponentially decayed according to $\exp(-T_l/\Gamma - \tau_{k,l}/\gamma)$, where Γ and γ denote a cluster decay factor and a ray decay factor, respectively.

In addition, reference [18] suggests four sets of parameters to represent the characteristics of multipath fading UWB channels. The parameter set CM1, CM2, CM3 and CM4 represents the model based on LOS (0-4m), NLOS (0-4m), NLOS (4-10m) and extreme NLOS (>10m) channel measurements, respectively. We focus our work on indoor fading scenarios with LOS and employ the CM1 model.

6.2.2 Rake Receiver Structure

If we assume that the channel estimation algorithm can provide the correlator template, together with the information of path delays and amplitudes for the desired user, a general coherent Rake receiver can be applied for receiving the UWB signals. If maximal ratio combining (MRC) is used in the receiver, in which each correlator output is weighted in terms of its signal amplitude-to-noise power ratio, the correlator template signal for TH-PPM systems can be written as

$$v_{PPM}(t) = \sum_{l \in S_N} \alpha_l^{(1)} \sum_{m=0}^{N_s-1} v\left(t - mT_f - c_m^{(1)} T_c - \tau_l^{(1)}\right) \tag{6.3}$$

where $v(t) = p(t) - p(t-\delta)$. For TH/DS-IR BPSK and DS-BPSK systems, the template signal is

$$v_{TH/DS-IR}(t) = \sum_{l \in S_N} \alpha_l^{(1)} \sum_{m=0}^{N_s-1} b_m^{(1)} p\left(t - mT_f - c_m^{(1)} T_c - \tau_l^{(1)}\right) \tag{6.4}$$

and

$$v_{DS}(t) = \sum_{l \in S_N} \alpha_l^{(1)} \sum_{m=0}^{N_c-1} b_m^{(1)} p\left(t - mT_c - \tau_l^{(1)}\right) \tag{6.5}$$

respectively. The set S_N represents a set of paths for the desired user. An estimate of the desired user's information bit can be obtained as

$$\hat{d}_j^{(1)} = \text{sgn}\left(\int_{-\infty}^{\infty} r(t)v(t)dt\right) \tag{6.6}$$

where $v(t)$ takes different forms as in (6.3), (6.4) and (6.5) for different modulation schemes.

Several Rake receiver combining structures have been investigated in [76] including the all-Rake, the selective-Rake and partial-Rake (PRake) structures. ARake, in general, combines all of the resolvable multipath components. Owing to the large bandwidth of UWB signals, the number of resolvable paths is quite large, typically, over one hundred. The number of Rake fingers to be used in a practical receiver design is a critical problem involving consideration of the system design complexity and the required channel estimation. It is not practical to implement a Rake receiver having a large number of correlators. SRake and PRake were proposed for reduced-complexity Rake receivers by combining only a subset of the available resolved multipath components with the consideration that most of the channel energy can be collected from a limited number of path components. Particularly, the SRake receiver selects the L_s strongest paths from the total L_r resolvable paths, which requires tracking all multipath components. The PRake receiver combines the first L_p arriving paths, which are not necessarily best. It is not necessary for PRake to sort all multipath components by magnitudes, and thus, much less channel estimation accuracy is required for PRake, which reduces the receiver complexity substantially. In this chapter, we consider ARake and SRake receivers.

6.3 Bit Error Probability

There are several methods for estimating the bit error rate performance of UWB systems on multipath fading channels. Here we briefly review these methods to indicate the differences among them and make our work self-contained.

The simplest analytical method is to use the Gaussian approximation as was done in [51] and [74]. In this method, the interference is modeled as a Gaussian distributed random variable. The SINR is then calculated, and the BER can be approximated as

$$P_e = Q\left(\sqrt{SINR}\right) \tag{6.7}$$

where $Q(\cdot)$ is the standard Q-function defined as

$$Q(x) = \frac{1}{\sqrt{2\pi}} \int_x^\infty e^{-t^2/2} dt, \quad x \geq 0.$$

Although the Gaussian approximation can provide closed-forms for estimating BER's, references [15] and [71] have shown that the Gaussian approximation is inaccurate for modeling the multiple access interference of UWB communication systems, rendering results based on the Gaussian approximation unreliable.

Semi-analytical methods were employed in some other work to improve the accuracy of BER estimates. One semi-analytical method was used in [76], in which the conditional BER $P_{e|\gamma_b}$ is computed conditioned on the received instantaneous SINR per bit, γ_b. The BER is then obtained by averaging $P_{e|\gamma_b}$ over the probability density function $p_{\gamma_b}(\cdot)$ of the instantaneous SINR at the output of the Rake receiver as

$$P_e = \int_0^\infty P_{e|\gamma_b}(x) p_{\gamma_b}(x) dx. \tag{6.8}$$

The instantaneous SINR depends on the channel parameters and the type of the Rake receiver used. The conditional BER $P_{e|\gamma_b}$ needs to be averaged over the channel ensemble.

Another semi-analytical method used in [77] is to model the interference as Gaussian distributed when conditioned on the channel parameters. The bit error proba-

bility conditioned on a particular channel realization is calculated as

$$P_{e|\mathbf{h}} = Q\left(\sqrt{SINR_0}\right) \tag{6.9}$$

where $\mathbf{h}$ is a vector of multipath components for the desired user, and $SINR_0$ represents the conditional SINR. Then, the average BER is obtained by averaging (6.9) over the number of channel realizations. Actually, these two semi-analytical methods are very similar to each other. First the conditional SINR is calculated based on the Gaussian approximation, then the BER is obtained by averaging over the channel ensemble. Although these semi-analytical methods were used to improve the accuracy of BER performance analysis, the conditional Gaussian approximation only uses the first and second moments of the interference, and does not utilize the full statistics of the interference in different modulation schemes. Therefore, some inaccuracy still exists in the results obtained. For example, as shown in [71], the conditional SINR's for TH/DS-IR BPSK and DS-BPSK systems are the same when estimated using the Gaussian approximation. Thus, the same multipath error rate performance will be obtained for these systems by averaging over the fading ensemble. However, we will show that the actual BER performances of these three schemes are different.

Recently, a different semi-analytical method was used in [78], in which the BER conditioned on the channel statistic and the information bits is expressed as

$$P_{e|\mathbf{h},d} = Q\left(\frac{S + I(d)}{\sigma}\right) \tag{6.10}$$

where $\mathbf{h}$ is one channel realization, d represents the information bits of the desired user, S is the signal component and I is the ISI component in the receiver decision statistic. By averaging across channel realizations and the information data sequences, the average BER is obtained. In this approach, the statistics of the intersymbol interference are considered and the inaccuracy introduced by the Gaussian approximation can be reduced. However, data sequence detection needs to be implemented for estimating the BER and it is difficult to obtain the decision statistic of UWB systems when operating with ISI and MAI, which limits the application of this semi-analytical method.

In our work, we use Monte-Carlo simulation to examine these proposed modulation schemes and Rake receivers for more general cases. More reliable information will be provided to evaluate these schemes and receiver structures, than has been previously published in the literature.

6.4 Simulation Results and Comparisons

In this section, simulation results are provided to compare different Rake receiver structures and evaluate proposed modulation schemes in terms of the average bit error rate performance in MAI environments and in ISI environments. The parameters of the example UWB systems are listed in Table 6.1. We consider uncoded UWB systems operating in an indoor environment. Fading delays and amplitudes are generated according to the IEEE 802.15.3a channel model [18]. Specifically, the CM1 model is considered, and the mean delay spread is 5 ns. Slow fading is assumed so that N successive symbols are transmitted in the coherence time of the channel. For multiple access applications, a different channel realization provided by IEEE 802.15.3 is assigned to each user. The BER curves are then obtained by averaging over at least 100 scenarios.

First, using the TH-BPSK system as example, we compare the BER performance of ARake and SRake receivers with MAI. The frame duration T_f is chosen to eliminate ISI. Later, a similar comparison will be provided for UWB systems operating with both ISI and MAI. These two comparisons of ARake and SRake will reveal interesting performance differences of the two Rake receivers for different fading scenarios. Furthermore, we evaluate and compare the BER performances of candidate UWB modulation schemes. The actual performances of these modulation schemes will be clearly indicated by our numerical examples.

Fig. 6.1 shows the BERs of the TH-BPSK system using ARake and SRake receivers. The frame duration T_f is set to be 48 ns to eliminate the effects of intersymbol interference. The ARake receiver combines more than 100 fingers. For SRake re-

TABLE 6.1

Parameters of the Example TH, DS and DS-IR UWB systems

Parameter	Notation	Gaussian monocycle
Time Normalization Factor	τ_p	0.2 ns
Frame Width	T_f	9.6 or 48 ns
Bit Duration	T_b	19.2 or 96 ns
PPM Delay	δ	0.108 ns
Chip Width	T_c	0.6 ns
Number of Users	N_u	8
Number of Hops per Frame	N_h	16 or 80
Repetition Code Length	N_s	2
Number of Chips per Frame	N_c	32 or 160

ceivers, the strongest 25 and 5 fingers are selected and the corresponding BER curves are plotted. It is seen that ARake provides the best performance as expected, and in agreement with previous observations in [76], though [76] did not consider MAI environments. Compared to the performance obtained using the ARake receiver, SRake receivers incur performance losses for 25 and 5 fingers. The smaller the number of Rake fingers, the poorer the BER performance. This can be explained as simply as that the smaller amount of energy captured by fewer Rake fingers leads to worse BER performance for the desired user. Fig. 6.1 shows that to improve the BER by an order of magnitude from 10^{-2} to 10^{-3} requires going to 25 fingers from 5 fingers in this case, and that the 25-finger SRake receiver performance is very close to the ARake receiver performance, which means the 25-finger SRake receiver can capture most energy of the transmitted signl.

In Fig. 6.2, we compare the BER's of the TH-BPSK system operating with ISI and MAI. The frame width, T_f, is set to be 9.6 ns. In this case, intersymbol interference

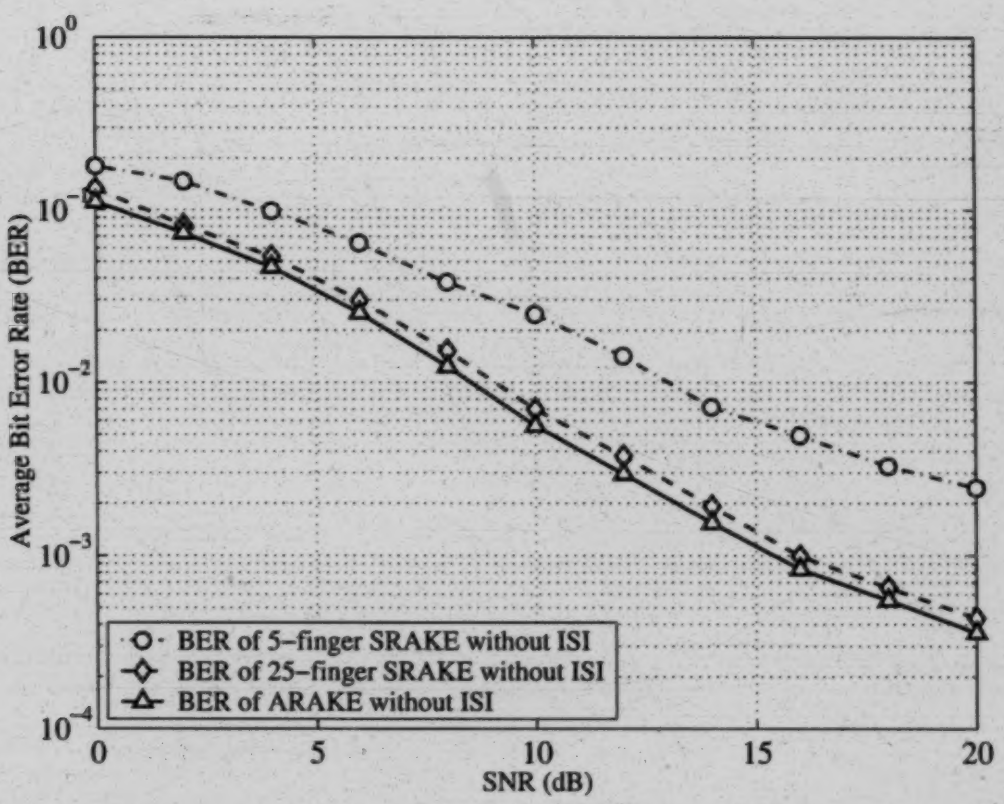
Average Bit Error Rate (BER)
SNR (dB)
BER of 5–finger SRAKE without ISI
BER of 25–finger SRAKE without ISI
BER of ARAKE without ISI

Fig. 6.1. The average BER of the TH-BPSK system in the presence of MAI for $N_s = 2$.

introduced by fading cannot be ignored. The BER performances of the example TH-BPSK system using ARake and SRake multipath combining are compared for this scenario. It is, perhaps, surprising to note that the SRake receiver using 25 fingers achieves better BER performance than the ARake receiver. Though ARake combining provides the upper limit of achievable performance when the multipaths are resolvable [76], it is not optimal when there is significant ISI in the system. Although ARake combining can capture all the energy of the desired information bit, it also captures the energy of the consecutive interfering bits of the desired user when ISI cannot be ignored. In this case, ARake receivers might introduce stronger intersymbol interference to the desired information bit, and thus deteriorate the BER performance. On the other hand, SRake combining using a suitable number of fingers can achieve better performance than ARake combining, as shown in Fig. 6.2. Fig. 6.2 also shows that the performance of SRake combining in ISI environments strongly depends on the number of fingers. When only the 5 strongest fingers are combined in SRake combining, the BER performance is deteriorated by using fewer fingers, as compared to the 25-finger SRake combiner. However, we note that the 5-finger SRake receiver achieves almost the same performance as the ARake receiver for large SNR values, where the ISI dominates the noise and determines the receiver performance. Although the 5-finger SRake receiver only captures part of the energy of the desired information bit, it also reduces the interference energy from the consecutive interfering bits. Therefore, the 5-finger SRake receiver can achieve almost the same BERs as the ARake receiver at large SNR values. We also observe that the 25-finger SRake receiver achieves better performance than the 15-finger SRake receiver for small SNR values, as expected. When the SNR increases, the performance of the 15-finger SRake receiver approaches and surpasses the performance of the 25-finger SRake receiver. In general, increasing the number of fingers will improve the BER performance of the SRake receiver. However, there is a "threshold" value of the number of fingers when significant ISI is present. When the number of Rake fingers combined is less than this threshold, the BER performance improves by combining more fingers; when

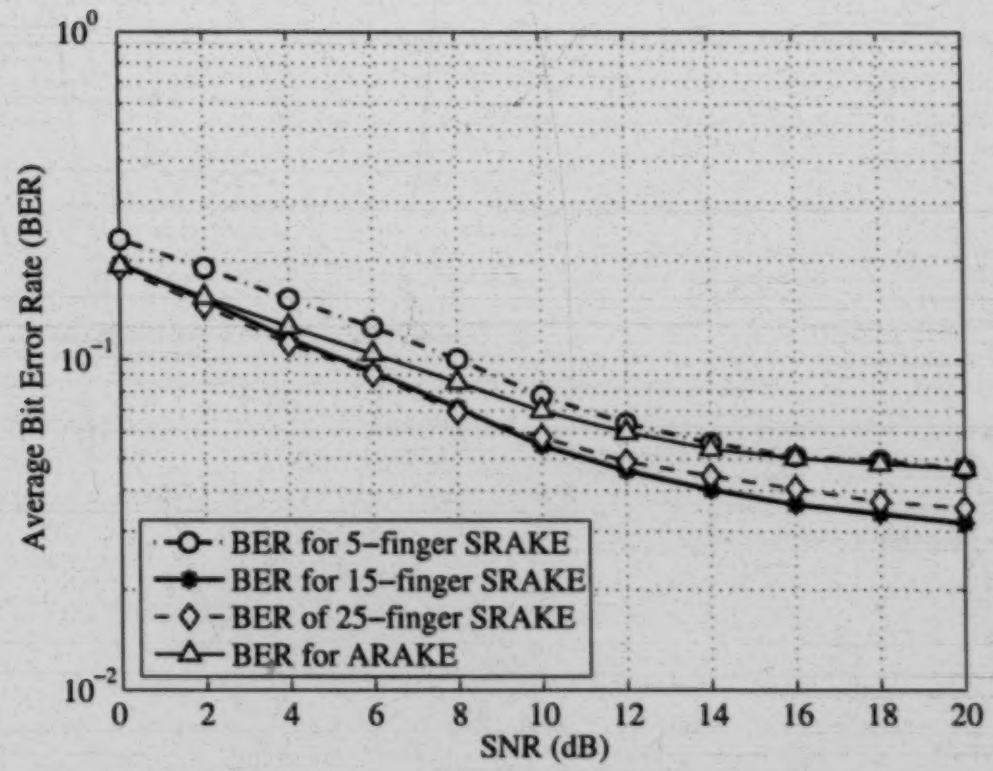

Fig. 6.2. The average BER versus SNR of the TH-BPSK system in the presence of ISI and MAI for $N_s = 2$.

the number of fingers selected is larger than this threshold value, the performance cannot be further improved, and can be deteriorated. Therefore, the number of fingers combined in SRake needs to be carefully chosen to ensure the "best" achievable performance in practical UWB systems that operate with ISI.

Although SRake and ARake receivers were compared in Figs. 6.1 and 6.2 using the TH-BPSK modulation format, similar observation were also obtained for other UWB modulation schemes. The comparisons of SRake and ARake give us more insight of Rake receptions for UWB systems. Based on this knowledge, we compare the error rate performance of different UWB schemes including TH, DS and DS-IR

UWB systems using PPM and BPSK modulations. In order to fairly compare these systems, we have carefully chosen the system parameters to normalize the energy of the information bit and to ensure the same data rate for all systems. According to the normalization, the same BER estimates for DS-BPSK, TH-BPSK and DS-IR BPSK will be obtained when predicted by using some analytical and semi-analytical methods based on the Gaussian approximation, highlighting its limitations. However, simulation results in our work indicate that the different schemes show different BER performances, in contrast to the conclusions drawn by using the Gaussian approximations.

In Fig. 6.3, we compare the single-user BER performances of these UWB systems, in which only ISI is considered and 25-finger SRake receivers are utilized for good reception. As seen, the TH-PPM achieves the poorest performance among these four systems for all SNR values. We also note that DS-IR BPSK and TH-BPSK achieve almost the same performance. The two BER curves are almost graphically indistinguishable. This means TH/DS-IR BPSK have similar ISI susceptibility. It is worth noting that DS-BPSK achieves the best performance, especially for large SNR values, which supercedes previous work that concludes that TH-BPSK and DS-BPSK have the same average bit error rates [51], [78].

For the ISI-free scenario, ARake reception is used for these modulation schemes. The BER curves of different UWB systems operating with 7 interfering users are plotted in Fig. 6.4. TH-PPM still provides the poorest performance for all SNR values. It is seen that the DS-IR BPSK system outperforms the TH-BPSK system for medium and large SNR values. The performance of DS-IR, however, is poorer than the performance of the DS-BPSK system. These observations confirm the conclusions obtained in [63], which compares the multiple access performances of different UWB systems on an AWGN channel based on exact analysis.

Based on Figs. 6.3 and 6.4, we conclude that DS-BPSK has the least susceptibility for either ISI or MAI. In order to investigate the total interference suppression of all these systems, we compare the BER performances of four UWB systems in

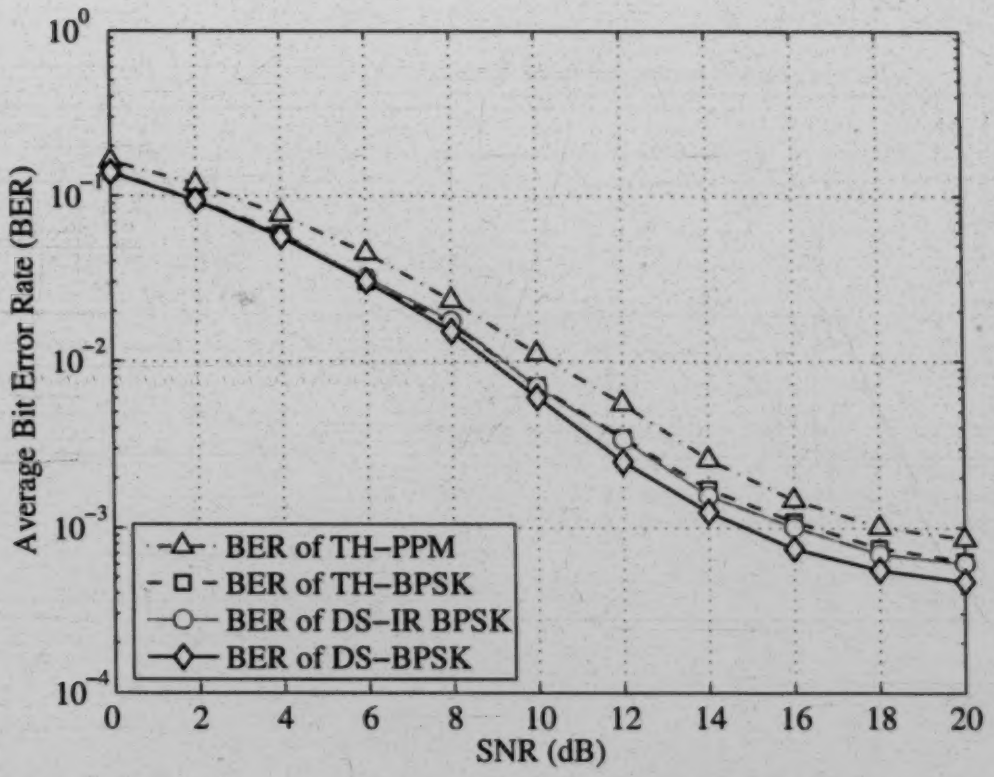

Fig. 6.3. Comparison of single-user UWB systems in the presence of ISI with $N_s = 4$.

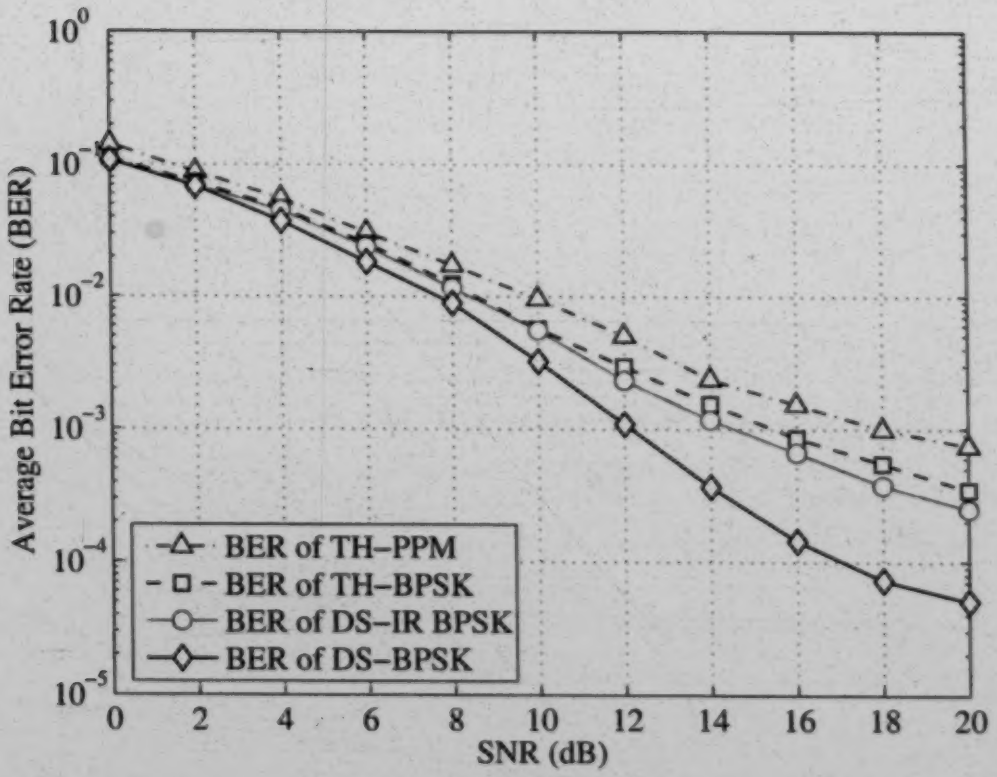

Fig. 6.4. Comparison of multiple access UWB systems without ISI for $N_s = 2$.

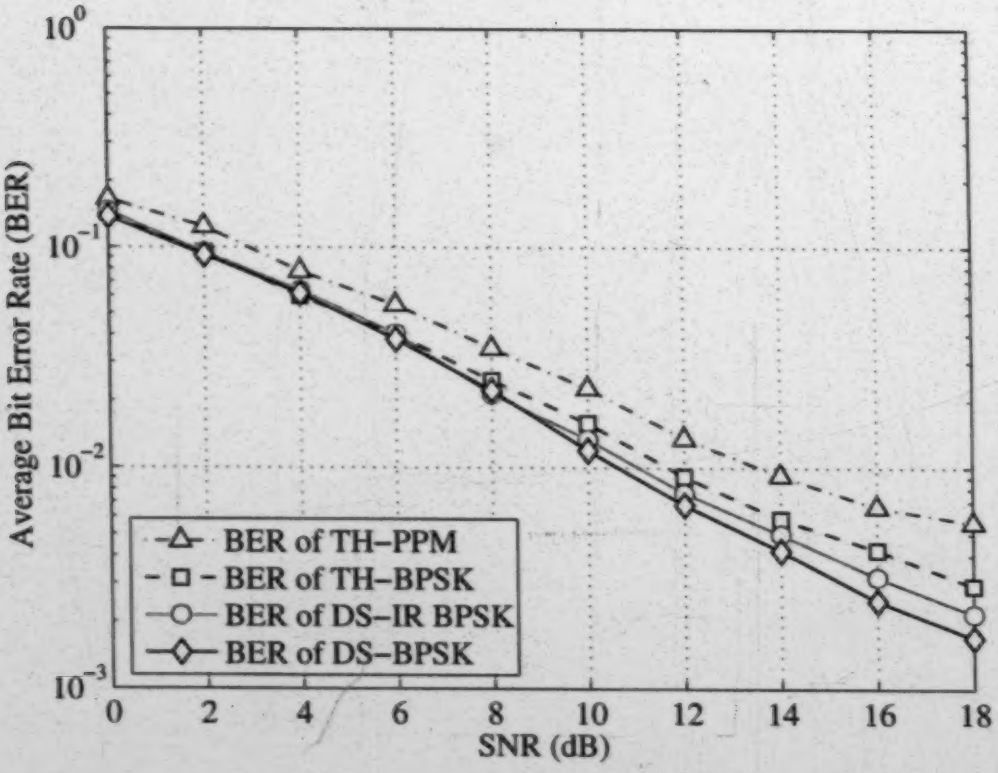

Fig. 6.5. Comparison of UWB systems in the presence of ISI and MAI with $N_s = 4$.

the presence of ISI and MAI in Fig. 6.5. We observe, from our numerical results, that the BER performance of TH-PPM is the poorest, DS-IR provides better BER performance than TH-BPSK, but poorer performance than DS-BPSK.

6.5 Summary

In this chapter, we have discussed ARake and SRake receivers for different transmission scenarios. In our work, we found that the ARake receiver doesn not necessarily guarantee the upper limit of the achievable performance and the SRake receiver can provide better performance than the ARake receiver when ISI is present.

We also evaluated and compared the interference susceptibilities of some proposed UWB modulation formats. Although the Gaussian approximation provides the same BER estimates for TH-BPSK, DS-BPSK and DS-IR BPSK systems, our performance comparisons of TH-PPM, TH-BPSK, DS-BPSK and DS-IR BPSK UWB systems for different fading scenarios show the actual performances of these systems are different. In particular, TH-PPM provides the poorest performance for either single-user or multi-user scenarios, while DS-BPSK achieves the best BER performance in the presence of ISI and MAI. The performances of TH-BPSK and DS-IR BPSK are almost the same for the single-user scenario and DS-IR outperforms TH-BPSK when operating only with MAI. Overall, we conclude that the DS-BPSK system is the best choice among these TH, DS and DS-IR systems, under consideration of the multiple access performances on fading channels and the complexity of the implementations. The newly proposed DS-IR system, with its more complicated transceiver design and poorer bit error rate performance, does not compete well with the DS-BPSK system for multiple access UWB communications.

Chapter 7

Conclusions and Suggestions for Future Work

In this chapter, we first highlight important findings of this thesis, and then suggest several topics for future research.

7.1 Conclusions

1. An analytical expression has been obtained for the characteristic function of the multiple access interference in TH-PPM UWB systems.

2. The average BER of a TH-PPM system with asynchronous users has been expressed in terms of a double-integral. The integrand is positive and well behaved. The exact BER for a TH-PPM system can be obtained with modest computational complexity.

3. The accuracy of the Gaussian approximation has been assessed. It has been shown that the Gaussian approximation is valid for predicting BER's with small SNR values, but inaccurate for medium and large SNR values. It has been seen that the Gaussian approximation improves for the longer repetition codes in the sense that it is accurate for a wider range of values of SNR.

4. We have shown that the time shift factor δ directly affects the performance of TH-PPM systems. Due to the sensitivity of the TH-PPM UWB system to the choice of the time shift, the optimal value of δ should be chosen according to the specific pulse and pulse width employed.

5. It has been shown numerically that higher-order Gaussian monocycles have better performance than lower-order Gaussian monocycles for a fixed pulse width.

6. An expression for predicting the BER of the TH-BPSK system has been derived. The TH-BPSK system has been shown to achieve better performance the TH-PPM system, as measured by the average BER.

7. A tractable analytical BER expression has been developed for the performance of DS-BPSK UWB systems. It has been shown that the Gaussian approximation substantially overestimates the performance of the DS-UWB system at large values of SNR.

8. A simple and accurate alternative analysis based on the simplified receiver decision statistic has also been presented. The simplified analytical method is shown to provide BER results essentially as accurate as the exact analysis and require much less computational complexity.

9. A newly proposed DS-IR modulation scheme has been investigated and the exact analysis has been obtained for assessing this modulation scheme.

10. We have shown that DS-BPSK outperforms TH-BPSK for medium and large values of SNR, which contradicts some previous results published using the Gaussian approximation.

11. It has been shown that the BER performance of the DS-IR system is better than that of the TH-BPSK system, but poorer than the performance of the DS-BPSK system, which cannot justify the usage of both TH and DS codes.

12. The previously proposed pulse shapes have been investigated in terms of the compliance with the FCC spectral emission constraints and the bit error rate. We have found that higher-order Gaussian monocycles and the prolate spheroidal function based pulses can meet the spectral emission masks without frequency shifting. The modified Hermite polynomial based pulses require frequency shifting and bandpass filtering to meet the spectral masks.

13. A novel paradigm for designing time-limited pulse shapes for UWB communication systems has been proposed. Pulse can be designed using our paradigm that not only conform to required spectral emission constraints, but also achieve good BER performance in MAI environments.

14. It has been shown that our design paradigm provides more degrees of freedom for adjusting the pulse spectrum to meet the mask and many more novel pulses can be obtained using this paradigm.

15. Accurate, analytical expressions for the average probability of bit error of time-hopping and direct-sequence UWB systems in the presence of narrowband OFDM interference have been derived.

16. We have found that the Gaussian approximation for these modulation schemes will overestimate the performance at large values of SNR when the length of the repetition code, N_s is not large enough.

17. Numerical results have shown that the narrowband interfering OFDM signal introduces more severe interference to UWB systems than the multiple access interference and the BER performance of UWB systems will be significantly deteriorated by interfering OFDM signals with higher power levels.

18. It has been shown that the actual performance of TH-BPSK may be poorer than the actual performance of DS-BPSK depending on the UWB system parameters.

19. We have also observed that for practical values of N_s and N_c, increasing the length of the repetition code in a DS-UWB system does not reduce OFDM interference.

20. ARake and SRake receivers have been investigated for different UWB transmission scenarios. It has been found that the ARake receiver does not necessarily guarantee the upper limit of the achievable performance and the SRake receiver can provide better performance than the ARake receiver when ISI is present.

21. It has been shown that TH-PPM provides the poorest performance for either single-user or multi-user scenarios, while DS-BPSK achieves the best BER performance in the presence of ISI and MAI.

22. Numerical results suggest that the actual performances of TH-BPSK, DS-IR BPSK and DS-BPSK UWB systems are different, although the Gaussian approximation and some semi-analytical methods provide the same BER estimates for these systems.

23. It has been shown that the newly proposed DS-IR system achieves poorer performance than the DS-BPSK system with more complicated transceiver design, which does not compete well with the DS-BPSK system for multiple access UWB transmission.

7.2 Suggestions for Future Research

1. It has been shown that multiple access interference is not Gaussian distributed. It is of interest to investigate the distribution of multiple access interference based on the characteristic function of MAI obtained in our work.

2. It has been shown that multiple access interference causes an error rate floor in UWB systems, which is undesirable in a UWB communication network. It is

therefore of interest to construct a new receiver structure to mitigate MAI based on the statistic of MAI obtained, and thus improve the BER performance.

3. Narrowband OFDM signals have been shown to introduce significant interference to UWB systems. It is worth investigating new receiver structures to suppress narrowband interference so as to improve the UWB system performance.

4. It has been shown that the proposed pulse design paradigm has superiority over other pulse design methods. Novel transceiver structures for UWB transmissions utilizing previous pulse shaping results should be considered.

5. Considering the Gaussian approximation cannot provide accurate BER estimates for UWB systems in multipath fading, while simulation is quite time-consuming, further investigation on the performance of UWB systems in frequency-selective fading is needed. It is of interest to extend our accurate analysis technique to practical fading models. However, challenges remain in doing such exact performance analysis since self-interference terms on different RAKE fingers are highly correlated as known.

6. Although the single-band impulse radio is the original proposal for UWB communications, multiband UWB systems have also attracted much interest because of their advantages. Particularly, multicarrier, multiband systems use OFDM techniques to transmit the information on each of the subbands gain more attention because of nice properties of OFDM. Several problems in multiband OFDM are worthy of investigation. OFDM's resistance to frequency-selective fading comes at the price of greater intercarrier interference (ICI) from its own subband transmissions, and greater sensitivity to dynamic range (thus requiring a higher peak-to-average power ratio (PAPR)). Therefore, PAPR needs to be carefully investigated with the consideration of the FCC emission regulations and the power consumption.

7. One of the main advantages of UWB transmission is the large amount of available frequency diversity. It is also known that multiband OFDM does not provide any frequency diversity, as a matter of fact OFDM converts a frequency-selective channel into several parallel flat fading channels. However, it is desirable for multiband OFDM systems to have frequency diversity in specific applications. It is of interest to design novel schemes to achieve this goal.

8. The performance analysis has been obtained for UWB systems with a perfect synchronization assumption. As known, UWB systems transmit information using extremely short pulses on hostile channels, for which perfect synchronization is very difficult to achieve. On the other hand, mis-synchronization of a UWB system will seriously deteriorate its performance. It is of interest to investigate the performance of UWB systems without perfect synchronization. In addition, different non-coherent receivers should be considered for UWB reception in terms of error rate performance.

References

[1] R. E. Ziemer and W. H. Tranter, *Principle of Communication*, New York: John Wiley & Sons, 2002.

[2] T. S. Rappaport, A. Annamalai, R. M. Buehrer and W. H. Tranter "Wireless communications: past events and a future perspective," *IEEE Communications Magazine*, 50th Anniversary Commemorative Issue, pp. 148–161, May 2002.

[3] G, C, Corazza, "Marconi's history," *Proc. IEEE*, vol. 86, pp. 1307–1311, Jul. 1998.

[4] K. Siwiak and D. Mckeown, *Ultra-wideband radio technology*, New York: John Wiley & Sons, 2004.

[5] T. W. Barret, "History of ultra-wideband (UWB) radar & communications: pioneers and innovators," in *Proc. of the Progress in Electromagnetics Symposium*, Cambridge, USA, Jul. 5-14, 2000.

[6] J. D. Taylor, "Ultra-wideband Radar Overview," CRC Press, 1995.

[7] J. Reed, R. M. Buehrer and D. S. Ha, "Introduction to UWB: Impulse radio for radar and wireless communications," Virginia Polytechnic Institute & State University.

[8] R. A. Scholtz and M. Z. Win, *Wireless Communications, TDMA versus CDMA: Impulse Radio.* Kluwer Academic Publishers, pp. 245-263, 1997.

[9] M. Z. Win and R. A. Scholtz, "Impulse radio: How it works," *IEEE Commun. Lett.*, vol. 2, pp. 51–53, Feb. 1998.

[10] R. A. Scholtz, "Multiple access with time-hopping impulse modulation," in *Proc. IEEE MILCOM 1998*, Boston, USA, Oct. 18-21, 1998.

[11] R. Ramírez-Mireles, "Multiple-access with ultra-wideand impulse radio modulation using spread spectrum time hopping and block waveform pulse position modulated signals," Ph.D. dissertation, Faculty of the Graduated School, University of Southern California, Los, Angeles, USA, 1998.

[12] M. L. Welborn, "System consideration for ultra-wideband wireless networks," in *Proc. IEEE Radio and Wireless Conference*, Boston, USA, Aug. 19-22, 2001, pp.5–8.

[13] I. Oppermann, M. Hämäläinen and J. Iinatti, *UWB Theory and Applications*, Chichester: John Wiley & Sons, 2004.

[14] M. Z. Win and R. A. Scholtz, "Ultra-wide bandwidth time-hopping spread-spectrum impulse radio for wireless multiple-access communications," *IEEE Trans. Commun.*, vol. 48, pp. 679–691, Apr. 2000.

[15] B. Hu and N. C. Beaulieu, "Accurate evaluation of multiple access performance in TH-PPM and TH-BPSK UWB systems," *IEEE Trans. Commun.*, vol. 52, pp. 1758–1766, Oct. 2004.

[16] L. B. Michael, M. Ghavami and R. Kohno, "Multiple pulse generator for ultra-wideband communication using Hermite polynomial based orthogonal pulses," in *Proc. IEEE Conf. on Ultra Wideband Systems and Technologies*, Baltimore, USA, May 20-23, 2002, pp. 47–51.

[17] P. Withington, R. Reinhardt and R. Stanley, "Preliminary results from ultra-wideband (impulse) scanning receivers," in *Proc. IEEE MILCOM'99*, Atlantic City, USA, 1999.

[18] J. Foerster, "Channel modeling sub-committee report final," *IEEE P802.15 Wireless Personal Area Networks, P802.15-02/490r1-SG3a*, Feb. 2003.

[19] M. Z. Win and R. A. Scholtz, "Characterization of ultra-wide bandwidth wireless indoor channels: A communcation-theoretic view," *IEEE J. Select. Areas Commun.*, vol. 20, pp. 1613–1627, Dec. 2003.

[20] A. Saleh and R. Valenzuela, "A statistical model for indoor multipath propagation," *IEEE J. Select. Areas Commun.*, vol. 5, pp. 128-137, Feb. 1987.

[21] W. C. Lee, "Overview of cellular CDMA," *IEEE Trans. Vehicular Technology*, vol. 40, pp. 291–302, May 1991.

[22] S. Verdú, "Minimum probability of error for asynchronous Gaussian multiple-access channels," *IEEE Trans. Information Theory*, vol. 32, pp. 85–96, Jan. 1986.

[23] Y. C. Yoon and R. Kohno, "Optimum Multi-user detection in ultra-wideband (UWB) multiple-access communication systems," in *Proc. ICC 2002*, New York, USA, Apr. 28-May 2, 2002, pp. 812–816.

[24] S. Verdú, *Multiuser Detection*, Academic University Press, Cambridge:UK, 1998.

[25] M. Hamalainen, R. Tesi, V. Hovinen, N. Laine and J. Iinatti, "On the UWB system performance studies in AWGN channel with interference in UMTS band," in *Proc. IEEE Conf. on Ultra Wideband Systems and Technologies*, Baltimore, USA, May 20-23, 2002, pp. 321–325.

[26] M. Hämäläinen, V. Hovinen, R. Tesi, J. Iinatti and M. Latva-aho, "On the UWB system coexistence with GSM900, UMTS/WCDMA, and GPS," *IEEE J. Select. Areas Commun.*, vol. 20, pp. 1712–1721, Dec. 2002.

[27] M. Hamalainen, R. Tesi, V. Hovinen, N. Laine and J. Iinatti, "Ultra wideband system performance studies in AWGN channel with intentional interference," in

Proc. International Workshop on Ultra Wideband Systems, Oulu, Finland, June 2-5, 2003.

[28] L. Zhao and A. M. Haimovich, "Performance of ultra-wideband communications in the presence of interference," *IEEE J. Select. Areas Commun.*, vol. 20, pp. 1684–1691, Dec. 2002.

[29] K. Eshima, Y. Hase, S. Oomori, F. Takahashi and R. Kohno, "Performance analysis of interference between UWB and SS signals," in *Proc. of the IEEE International Symposium on Spread Spectrum Techniques and Applications*, Prague, Czech Republic, Sept. 2-5, 2002, pp. 59–63.

[30] A. Swami, B. Sadler and J. Turner, "On the coexistence of ultra-wideband and narrowband radio systems," in *Proc. IEEE MILCOM 2001*, McLean, USA, Oct. 28-31, 2001, pp. 16–19.

[31] J. R. Foerster, "The performance of a direct-sequence spread ultrawide-band system in the presence of multipath, narrowband interference, and multiuser interference," in *Proc. IEEE Conf. on Ultra Wideband Systems and Technologies*, Baltimore, USA, May 20-23 2002, pp. 87–91.

[32] M. Hämäläinen, V. Hovinen and J. Iinatti, "Performance comparison between various UWB signals in AWGN channel in presence of multitone interference at the GSM downlink band," in *Proc. of the International Symposium on Wireless Personal Multimedia Communications*, Aalborg, Denmark, Sept. 9-12 2001, pp. 449–453.

[33] E. Baccarelli, M. Biagi and L. Taglione, "A novel approach to in-band interference mitigation in ultra wide band radio systems," in *Proc. IEEE Conf. on Ultra Wideband Systems and Technologies*, Baltimore, USA, May 20-23, 2002, pp. 297–301.

[34] B. Firoozbakhsh, T. G. Pratt and N. Jayant, "Analysis of IEEE 802.11a interference on UWB systems," in *Proc. IEEE Conf. on Ultra Wideband Systems and Technologies*, Reston, USA, Nov. 16-20, 2003, pp. 473–477.

[35] J. G. Proakis, *Digital Communications*. New York: McGraw-Hill, 1995.

[36] R. Price and P. E. Green, Jr., "A communication technique for multipath channels," *Proc. IRE*, vol. 46, 555-570, Mar. 1958.

[37] T. Eng and L. B. Milstein, "Coherent DS-CDMA performance in Nakagami multipath fading," *IEEE Trans. Commun.*, vol. 43, pp. 1134–1143, Apr. 1995.

[38] FCC, "First report and order in the matter of revision of part 15 of the commission's rules regarding ultra-wideband transmission systems," ET Docket 98–153, FCC 02-48, Tech. Rep., 2002.

[39] European Telecommunications Standards Institute (ETSI), "Ultra wideband for short range devices - task group ERM TG31A,".

[40] B. Huang, "UWB Regulatory Overview," Sony AWT Group, Oct. 3 2002.

[41] L. Zhao and A. M. Haimovich, "Multi-user capacity of M-ary PPM ultra-wideband communications," in *Proc. IEEE Conf. on Ultra Wideband Systems and Technologies*, Baltimore, USA, May 20-23, 2002.

[42] A. R. Forouzan, M. Nasiri-Kenari and J. A. Salehi, "Performance analysis of time hopping spread-spectrum multiple-access systems: uncoded and coded schemes," *IEEE Trans. Wireless Commun.*, vol. 1, pp. 671–681, Oct. 2002.

[43] K. A. Hamdi and X. Gu, "Bit error rate analysis for TH-CDMA/PPM impulse radio networks," in *Proc. WCNC'2003*, New Orleans, USA, Mar. 2003.

[44] G. Durisi and G. Romano, "On the validity of Gaussian approximation to characterize the multiuser capacity of UWB TH-PPM," in *Proc. IEEE Conf. on Ultra*

Wideband Systems and Technologies, Baltimore, USA, May 20-23, 2002, pp. 157–161.

[45] G. Durisi and S. Benedetto, "Performance evaluation of TH-PPM UWB systems in the presence of multiuser interference," *IEEE Commun. Lett.*, vol. 7, pp. 224–226, May 2003.

[46] J. Cheng and N. C. Beaulieu, "Accurate DS-CDMA bit error probability calculation in Rayleigh fading," *IEEE Trans. Wireless Commun.*, vol. 1, pp. 3–15, Jan. 2002.

[47] N. C. Beaulieu, "The evaluation of error probabilities for intersymbol and cochannel interference," *IEEE Trans. Commun.*, vol. 39, pp. 1740–1749, Dec. 1991.

[48] B. Hu and N. C. Beaulieu, "Exact bit error rate analysis of TH-PPM UWB systems in the presence of multiple access interference," *IEEE Commun. Lett.*, vol.7, pp. 572–574, Dec. 2003.

[49] J. R. Foerster, "The effects of Multipath Interference on the performance of UWB systems in an indoor wireless channel," in *Proc. IEEE 2001 VTC*, USA, May 2001, pp.1176–1180.

[50] G. Yue, L. Ge and S. Li, "Performance of UWB time-hopping spread-spectrum impulse radio in multipath environments," in *Proc. IEEE 2003 VTC*, Korea, Apr. 2003.

[51] A. Taha and K. M. Chugg, "A theoretical study on the effects of interference on UWB multiple access impulse radio," in *Proc. Asilomar Conference on Signals, Systems and Computers*, Nov. 3-6, 2002.

[52] V. S. Somayazulu, "Multiple access performance in UWB systems using time hopping vs. direct sequence spreading," in *Technical Papers in Intel Lab.*

[53] G. Durisi and S. Benedetto, "Performance evaluation and comparison of different modulation schemes for UWB multiaccess systems ," in *Proc. IEEE ICC 2003*, Alaska, USA, May 2003.

[54] X. Chen and S. Kiaei, "Monocycles shapes for ultra wideband system," in *Proc. IEEE Conf. on Ultra Wideband Systems and Technologies*, Baltimore, USA, May 20-23, 2002, pp. 597–600.

[55] J. Zhang, T. D. Abhayapala and R. A. Kennedy, "Performance of ultra-wideband correlator receiver using Gaussian monocycles ," in *Proc. IEEE ICC 2003.*, Alaska, USA, May 2003.

[56] J. S. Lehnert and M. B. Pursley, "Error probabilities for binary direct-sequence spread-spectrum communications with random signature sequences," *IEEE Trans. Commun.*, vol. 35, pp. 87–98, Jan. 1987.

[57] A. Papoulis, *The Fourier Integral and its Applications*. New York: McGraw-Hill, 1962.

[58] N. Boubaker and K. B. Letaief, "Ultra wideband DSSS for multiple access communications using antipodal signaling," in *Proc. IEEE ICC 2003*, Alaska, USA, May 2003, pp. 2197–2201.

[59] M. Sabattini, E. Masry and L. B. Milstein, "A non-Gaussian approach to the performance analysis of UWB TH-BPPM systems," in *Proc. IEEE Conf. on Ultra Wideband Systems and Technologies*, Reston, USA, Nov.16-20, 2003.

[60] G. Durisi, A. Tarable, J. Romme and S. Benedetto, "A general method for error probability computation of UWB systems for indoor multiuser communications," *Journal of Communications and Networks*, vol. 5, no. 4, pp. 354–364, Dec. 2003.

[61] L. Piazzo, "Performance analysis and Optimization for impulse radio and direct-sequence impulse radio in multiuser interference," *IEEE Trans. Commun.*, vol. 52, pp. 801–810, May 2004.

[62] F. E. Glave, "An upper bound on the probability of error due to intersymbol interference for correlated digital signals," *IEEE Trans. Inform. Theory*, vol. IT-18, pp. 356–363, May 1972.

[63] B. Hu and N. C. Beaulieu, "Comparison of direct-sequence impulse radio and direct-sequence UWB in multi-user interference," submitted.

[64] J. Cheng, "Performance analysis of digital systems with fading and interference," *Ph.D. dissertation*, Dept. Elect. and Comp. Eng., Univ. of Alberta, AB, Canada, 2002.

[65] B. Parr, B. Cho, K. Wallace and Z. Ding, "A novel ultra-wideband pulse design algorithm," *IEEE Commun. Lett.*, vol. 7, pp. 219–221, May 2003.

[66] M. Win, "Spectrum density of random time-hopping spread-spectrum UWB signals with uniform timing jitter," in *Proc. MILCOM'99*, Atlantic City, New Jersey, 1999, pp. 1196–1200.

[67] J. A. N. da Silva and M. L. R. De Campos, "Orthogonal pulse shape modulation for impulse radio," in *Proc. Int. Telecomm. Symp. 2002*, Natal, Brazil, Sept. 8-12, 2002.

[68] S. M. Kendall and A. Stuart, *The Advanced Theory of Statistics. Vol. 1 Distribution Theory*, London: Charles Griffin and Company Limited, 1977.

[69] L. B. Michael, M. Ghavami and R. Kohno, "Effect of timing jitter on Hermite function based orthogonal pulses for ultra wideband communication," in *Proc. WPMC'01*, Aalborg, Denmark, 2001, pp. 441–444.

[70] B. Hu and N. C. Beaulieu, "Pulse shapes for ultra-wideband communication systems," *IEEE Transactions on Wireless Communications*, vol. 4, pp.1789–1797, Jul. 2005.

[71] B. Hu and N. C. Beaulieu, "Accurate performance evaluation of time-Hopping and direct-sequence UWB systems in multi-user interference," *IEEE Trans. Commun.*, vol. 53, pp. 1053–1062, Jun. 2005.

[72] A. Taha and K. M. Chugg, "Multipath diversity reception of wireless multiple access time-hopping digital impulse radio," in *Proc. IEEE Conf. on Ultra Wideband Systems and Technologies*, Baltimore, USA, May 20-23, 2002.

[73] G. Durisi, J. Romme and S. Benedetto, "Performance of TH and DS UWB multiaccess systems in Presence of Multipath channel and narrowband interference, " in *Proc. IWUWBS2003*, Oulu, Finland, Jun. 2-4, 2003.

[74] G. Durisi, J. Romme and S. Benedetto, "A general method for SER computation of M-PAM and M-PPM UWB systems for indoor multiuser communications," in *Proc. IEEE GLOBECOM 2003*, San Francisco, USA, Dec. 2003, pp. 734–738.

[75] G. Durisi and S. Benedetto, "Performance of coherent and non-coherent receivers for UWB communications," in *Proc. IEEE ICC 2004*, Paris, France, Jun. 20-24, 2004, pp. 3429–3433.

[76] D. Cassioli, M. Z. Win, F. Vatalaro and A. F. Molisch, "Performance of low-complexity Rake reception in a realistic UWB channel," in *Proc. ICC 2002*, New York City, USA, Apr. 28-May 2, 2002, pp. 763–767.

[77] A. Rajeswaran, V. S. Somayazulu and J. R. Foerster, "Rake performance for a pulse based UWB system in a realistic UWB indoor channel," in *Proc. ICC 2003*, Alaska, USA, May 11-15, 2003, pp. 2879–2883.

[78] R. D. Wilson and R. A. Scholtz, "Comparisons of CDMA and Modulation Schems for UWB Radio in a Multipath Environment" in *IEEE GLOBECOM 2003*, San Francisco, USA, Dec. 2003, pp.754–758.

Vita

Bo Hu

EDUCATION

University of Alberta	Ph.D. Candidate	Electrical and Computer Engineering September 2001 – Present
Xi'an Jiaotong University	M.Sc. (Eng.)	Electrical and Computer Engineering September 1998 – June 2001
Xi'an Jiaotong University	B.Eng. (First Class)	Electrical and Computer Engineering September 1994 – July 1998

WORK EXPERIENCE

University of Alberta	Sessional Instructor	Jan. 2006 - Apr. 2006
University of Alberta	Research Assistant	Sept. 2001 - Jan. 2006
University of Alberta	Lab Instructor	Sept. 2005 - Dec. 2005
Gennux Microsystems Corp.	System Consultant	Jul. 2005 - Present
University of Alberta	Teaching Assistant	Sept. 2001 - Apr. 2005
China Kejian Info-tech, LTD, CO. (Advanced Wireless Technology)	Intern software engineer	Sept. 1999 - May 2001
Xi'an Jiaotong University	Research Assistant Teaching Assistant	Jan. 1998 - Aug. 1999

AWARDS

Alberta Ingenuity Studentship, Alberta, 2002-2006.

iCORE (Informatics Circle of Research Excellence) Graduate Scholarship, Alberta, 2003-2006.

J. Gordin Kaplan Graduate Student Award, University of Alberta, 2004.

Graduate Scholarship, Xi'an Jiaotong University, Xi'an, China, 1998-2000.

Best Graduation Project, Xi'an Jiaotong University, Xi'an, China, 1998.

Undergraduate Scholarship, Xi'an Jiaotong University, Xi'an, China, 1995-1998.

Excellent Student Leader, Xi'an Jiaotong University, Xi'an, China, 1996.

Freshman Scholarship, Xi'an Jiaotong University, Xi'an, China, 1994-1995.

PUBLICATIONS

Bo Hu and Norman C. Beaulieu, "Pulse shapes for ultra-wideband communication systems," *IEEE Transactions on Wireless Communications*, vol. 4, pp. 1789-1797, Jul. 2005.

Bo Hu and Norman C. Beaulieu, "Accurate performance evaluation of time-hopping and direct-sequence UWB systems in multi-user interference," *IEEE Transactions on Communications*, vol. 53, pp. 1053-1062, June 2005.

Bo Hu and Norman C. Beaulieu, "Accurate evaluation of multiple-access performance in TH-PPM and TH-BPSK UWB systems," *IEEE Transactions on Communications*, vol. 52, pp. 1758-1766, Oct. 2004.

Bo Hu and Norman C. Beaulieu, "Exact bit error rate of TH-PPM UWB systems in the presence of multiple access interference," *IEEE Communications Letters*, vol. 7, pp 572-574, Dec. 2003.

Norman C. Beaulieu and Bo Hu, "A pulse design paradigm for ultra-wideband communication systems," to appear in *IEEE Transactions on Wireless Communications.*

Bo Hu and Norman C. Beaulieu, "Performance of an ultra-wideband communication system in the presence of narrowband OFDM interference," accepted pending revisions for publication in *IEEE Transactions on Communications.*

Bo Hu and Norman C. Beaulieu, "Exact performance analysis of DS-UWB systems in the presence of multi-user interference," submitted.

Bo Hu and Norman C. Beaulieu, "Comparison of direct-sequence impulse radio and direct-sequence UWB in multi-user interference," submitted.

Norman C. Beaulieu and Bo Hu, "A novel receiver structure for time-hopping UWB in multiple access interference," submitted.

Bo Hu and Norman C. Beaulieu, "Multi-User Interference Performance Comparison of Direct-Sequence Impulse Radio and Direct-Sequence UWB in AWGN," *IEEE WCNC'06*, Las Vegas, USA, 2006.

Bo Hu and Norman C. Beaulieu, "Comparison of modulation schemes and Rake receiver structures for UWB systems on an IEEE 802.15.3a indoor channel," *IEEE GLOBECOM 2005*, St. Louis, USA, 2005.

Bo Hu and Norman C. Beaulieu, "Accurate BER of time-hopping and direct-sequence UWB systems in multi-user interference," *IEEE PacRim 2005*, Victoria, Canada, 2005.

Bo Hu and Norman C. Beaulieu, "Effects of IEEE 802.11a narrowband interference on a UWB communication system," *IEEE ICC 2005*, Seoul, Korea, 2005.

Bo Hu and Norma C. Beaulieu, "Effects of multi-user interference on the error rate of DS-UWB systems," *IEEE CCECE 2005*, Saskatoon, Canada, 2005.

Norman C. Beaulieu and Bo Hu, "A novel pulse design algorithm for ultra-wideband communications," *IEEE GLOBECOM 2004*, Dallas, Texas, 2004.

Bo Hu and Norman C. Beaulieu, "Pulse-shaping in UWB communication systems," *IEEE VTC-Fall 2004*, Los Angeles, 2004.

Bo Hu and Norman C. Beaulieu, "Accurate evaluation of multiple access performance in time-hopping UWB systems," *IEEE ICC 2004*, Paris, France, 2004.

Norman C. Beaulieu and Bo Hu, "Multiple access interference in time-hopping ultra-wideband radio," *SPIE Second International Symposium on Fluctuations and Noise 2004, Noise in Communications Conference*, vol 5473, Maspalomas, Spain, 2004. Keynote Invited Paper.

Bo Hu and Norman C. Beaulieu, "Precise bit error rate of TH-PPM UWB systems in the presence of multiple access interference," *IEEE UWBST 2003*, Virginia, USA, 2003.